Development of Nanocontainer-based Self-healing Coatings for Corrosion Protection of Magnesium Alloy AZ91D

Submitted in partial fulfillment of the requirements

for the award of the degree of

DOCTOR OF PHILOSOPHY

in

CHEMICAL ENGINEERING

by

Mr. ADSUL SWAPNIL HANMANT

(Roll No. 716168)

Supervisors:

Dr. SHIRISH HARI SONAWANE

Professor, Dept. of Chemical Engineering

NIT, Warangal

and

Dr. R. SUBASRI

Sci. 'G' and Head

Centre for Sol-Gel Coatings

ARCI, Hyderabad

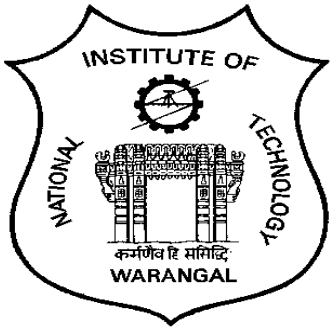

Department of Chemical Engineering

NATIONAL INSTITUTE OF TECHNOLOGY

Warangal-506 004, Telangana, India

June - 2021

Dedicated

to

My Parents

DECLARATION

This is to certify that the work presented in the thesis entitled *"**Development of Nanocontainer-based Self-healing Coatings for Corrosion Protection of Magnesium Alloy AZ91D**"* is a bonafide work done by me under the supervision of ***Prof. Shirish H. Sonawane*** (Internal Supervisor) and ***Dr. R. Subasri*** (External Supervisor) and was not submitted anywhere else for the award of any other degree.

I declare that this submission represents my ideas in my own words and wherever others' ideas or words have been included, I have adequately cited and referenced the original sources. I also declare that I have adhered to all the principles of academic honesty and integrity and have not misrepresented, fabricated or falsified any idea/data/fact/source in my submission. I understand that any violation of the above will be a cause for disciplinary action by the institute and can also evoke penal action from the sources which have thus not been properly cited or from whom proper permission has not been taken when needed.

Date: 24-06-2021

Mr. Adsul Swapnil Hanmant

Roll No. 716168

CERTIFICATE

NATIONAL INSTITUTE OF TECHNOLOGY- WARANGAL

Warangal – 506004, Telangana, INDIA.

This is to certify that the thesis entitled *"**Development of Nanocontainer-based Self-healing Coatings for Corrosion Protection of Magnesium Alloy AZ91D**"* being submitted by ***Mr. Adsul Swapnil Hanmant (Roll No.716168)*** for the award of the degree of Doctor of Philosophy (Ph.D.) in Chemical Engineering to the National Institute of Technology, Warangal, India is a record of the bonafide research work carried out by him under our supervision. The thesis has fulfilled the requirements according to the regulations of this institute and in our opinion has reached the standards for submission. The results embodied in the thesis have not been submitted to any other University or Institute for the award of any degree or diploma.

Date: 24-06-2021

Dr. Shirish Hari Sonawane
Professor
Internal Supervisor
Department of Chemical Engineering,
National Institute of Technology, Warangal.

Dr. R. Subasri
Sci. 'G' and Head
External Supervisor
Centre for Sol-Gel Coatings
ARCI, Hyderabad

ACKNOWLEDGEMENT

It is my pleasure to acknowledge the people who made this thesis possible.

First and foremost, I express my deepest gratitude to my supervisors, ***Dr. R. Subasri*** and ***Prof. Shirish Hari Sonawane*** for their constant encouragement, motivation, co-operation and guidance, since the day I started my research work. Their passion and dedication towards the research has always energized me to overcome the barriers in research, which helped me to develop the skills required for the research over time. Ever since, they supported me not only by sharing their valuable thoughts and ideas on my research work but also supported me in personal life through the rough road to complete this degree.

I would like to express my gratitude towards ***Director, ARCI, Hyderabad*** who gave me an opportunity to carry out the research work and other authorities from Administrative block, Finance section and Technical Information Centre who ensured the smooth procedure of research by providing background support. I would also like to thank members of Centre for Sol-Gel Coatings for their time to time support throughout my research work at ARCI. I would like to extend my sincere thanks to the members of other Centres of Excellence in ARCI Hyderabad and Chennai for extending their characterization facilities for my research work.

I would like to sincerely thank ***Director, NIT, Warangal*** and other authorities who gave me an opportunity to register for Ph.D. in the Department of Chemical Engineering. I would also like to thank ***Dr. S. Srinath***, Head, Department of Chemical Engineering for his valuable support for carrying out the entire research work. I would like to extend my thanks to Doctoral Scrutiny Committee (DSC) members ***Dr. S. Srinath*** (DSC Chairman and Head, Dept. of Chemical Engg.), ***Prof. Y. Pydi Setty*** (Former member, Dept. of Chemical Engg.), ***Dr. K. Raghu Raja Pandiyan*** (Member, Assistant Professor, Dept. of Chemical Engg.) and ***Dr. R. Satish Babu*** (Member, Associate Professor, Dept. of Biotechnology) for their valuable suggestions and generously sharing their ideas with me. Their critical inputs helped me in enriching the quality of my research work. I would like to extend my thanks to all the faculty members and supporting staff in Dept. of Chemical Engineering for their valuable suggestions and encouragement.

I take this opportunity to sincerely acknowledge the financial support from Science and Engineering Research Board (SERB) of Department of Science and Technology (DST),

Government of India. I would like to thank ARCI, Hyderabad for providing me financial support for remaining period after completion of tenure of the SERB project.

I am extremely thankful to my friends *S. Manasa, D. Nazeer Basha, Aarti Gautam and Dr. Anas N. S.* from ARCI, Hyderabad and *Dr. Uday Bagale, Dr. Prashant Suryawanshi, Dr. Abhay Lingayat, Dr. Gajanan Suryawanshi, Ganesh Gawale, Roshan Bodile, Dr. Harshal Patil, P. Narsimha, Upendra Mourya and Vikas Hakke* from NIT, Warangal who have been my continuous source of energy while carrying out the research.

Last but not least, I would like to thank my father ***Mr. Hanmant Adsul***, mother ***Mrs. Kamal Adsul*** and sister ***Mrs. Swapnali Mali*** for their unbelievable support, help, motivation and blessings that helped me to reach this stage.

Mr. Adsul Swapnil Hanmant

Abstract

The objective of the research work was development of nanocontainer-based self-healing coatings for corrosion protection of magnesium alloy AZ91D using sol-gel process. Mg alloys, owing to their very low standard electrode potential and easily deteriorating thin film of oxides/hydroxides, needs to be protected from the corrosive environments. Among the number of methodologies that have been used to protect Mg alloys, use of protective coatings has been found to be most efficient and cost effective approach which provides a barrier between substrate and corrosive medium. Various methodologies/coating techniques like conversion coatings, micro-arc oxidation, chemical/ physical vapor deposition, organic/inorganic and sol-gel coatings have been developed for corrosion protection of Mg alloys. Sol-gel coatings offer a great potential to be used as an eco-friendly alternative for carcinogenic chrome-based conversion coatings. They provide better adhesion to the substrates by chemical as well as physical bonding. However, only protective coatings cannot provide effective corrosion protection for longer durations as they may experience physical damage or deterioration after exposure to corrosive medium. Hence, active materials like corrosion inhibitors, catalysts, monomers, etc. are encapsulated into micro/nanocontainers, which are then dispersed into coating matrix. This will ensure controlled release of aforementioned active agents as a response to the change in localized pH whenever there is any defect in the coating. This facilitates prolonged corrosion protection to the substrates due to timely release of protective/inhibiting agents.

Based on this, an extended literature survey was conducted to formulate the research plan. The thesis work deals with four different types of self-healing coating systems. First system consists of generation of cationic corrosion inhibitors, Ce^{3+}-Zr^{4+} loaded halloysite clay nanotube (HNT) based self-healing coatings. A comparative study of this was carried out with hybrid organic-inorganic matrix sol (MAT) and as-received HNT nanoclay dispersed hybrid matrix sol (clay matrix, CM). Electrochemical measurements and weight loss studies were carried out to evaluate anticorrosion properties, whereas scanning vibrating electrode technique (SVET) and micro-Raman spectroscopic analysis were used for confirmation of self-healing ability. It was observed that, MAT sol and CM sol based coatings could give better barrier properties only up to 72 h of exposure to 0.6 M NaCl solution, whereas inhibitor loaded HNT based coatings could give better anticorrosion properties up to 120 h of exposure. SVET and micro-Raman spectroscopic analyses showed

the release of corrosion inhibitor in the scribed area after exposure to NaCl solution, which proved the self-healing ability of coatings.

Second system is based on cationic Ce^{3+}-Zr^{4+} intercalated layered montmorillonite (MMT) nanoclay based self-healing coatings. The cationic inhibitors were intercalated into layers of MMT clay by using two methods, i.e., by simple mixing and by vacuum evacuation where, MMT clay was mixed with inhibitor solution under constant stirring conditions and MMT clay dispersed inhibitor solution was evacuated under vacuum respectively. Both the inhibitor mixed MMT (IMM) and inhibitor evacuated MMT (IEM) were dispersed in hybrid matrix sol to synthesize IMM sol and IEM sol. The anticorrosion properties of coatings were evaluated using electrochemical studies and weight loss measurements, whereas self-healing ability was examined by using SVET and salt immersion tests in 0.6 M NaCl solution. IEM sol based coatings were found to give better barrier properties for prolonged duration of 120 h and also depicted self-healing ability by release of cations in the scribed area.

Third system deals with the comparison of corrosion inhibition ability of Ce^{3+}-Zr^{4+} based coatings with coatings based on organic corrosion inhibitors like 8-hydroxyquinoline (HQ) and 2-mercaptobenzothiazole (MBT). In this case, the lumen of HNTs was etched by using 1 M H_2SO_4 in order to accommodate higher amount of inhibitors. Further, these different corrosion inhibitors were loaded in as-received and etched HNTs (EHNTs). The release kinetics of the corrosion inhibitors from the lumen of HNT and EHNT was studied by measuring percentage release of the aforementioned three corrosion inhibitors at various pH conditions and the release data of Ce^{3+}-Zr^{4+} was further validated using various kinetic models. The corrosion protection ability of three inhibitors was compared using electrochemical studies and found that, Ce^{3+}-Zr^{4+} loaded HNT based coatings gave highest corrosion protection, whereas HQ based coatings depicted better anticorrosion properties when loaded in EHNTs after prolonged durations of exposure.

The fourth system comprised of study of effect of coating technique (spray coating and dip coating) on corrosion protection ability of the MAT sol, CM sol and Ce^{3+}-Zr^{4+} loaded HNT based coatings. As observed from electrochemical studies and accelerated corrosion tests, spray coated substrates gave higher corrosion resistance than dip coated substrates owing to the higher coating thickness. Further, 3 layer dip coatings with thickness similar to that of spray coatings based on Ce^{3+}-Zr^{4+} loaded HNTs were generated and found that, multilayer dip coatings showed better barrier properties than spray coating after prolonged durations of exposure in accelerated corrosion tests.

Table of Contents

List of Figures

List of Tables

Abbreviations and Nomenclatures

Abbreviation	Description
Mg	Magnesium
ASTM	American Society for Testing and Materials
SCE	Saturated Calomel Electrode
SCC	Stress Corrosion Cracking
UV- Vis	Ultraviolet Visible
PVD	Physical Vapour Deposition
EPD	Electrophoretic Deposition
NIR	Near Infrared Radiation
LDH	Layered Double Hydroxides
LBL	Layer-by-layer
HNT	Halloysite Nanotubes
MMT	Montmorillonite Nanoclay
SiC	Silicon Carbide
CCC	Chromate Conversion Coatings
EIS	Electrochemical Impedance Spectroscopy
MAO	Micro-arc Oxidation
SANP	Self-assembled Nanophase Particles
XPS	X-ray Photoelectron Spectroscopy
XRD	X-ray Diffraction
PEO	Plasma Electrolytic Oxidation
SVET	Scanning Vibrating Electrode Technique

EDS	Energy Dispersive Spectroscopy
EDXRF	Energy Dispersive X-ray Fluorescence
ICP-OES	Inductively Coupled Plasma Optical Emission Spectroscopy
MBT	2-mercaptobenzothaizole
Na-EDTA	Sodium-ethylenediaminetetraacetic acid
YSZ	Yttria stabilized zirconia
SEM	Scanning Electron Microscope
CTAB	Cetyltrimethyl ammonium bromide
SBF	Simulated Body Fluid
OCP	Open Circuit Potential
TEOS	Tetraethoxysilane
SKP	Scanning Kelvin Probe
GPTMS	3-Glycidoxypropyltrimethoxysilane
ORMOSIL®	Organically modified silicate
HQ	8-Hydroxoquinoline
BTA	Benzotriazole
CNT	Carbon Nanotube
EPMA	Electron Probe Micro-analyser
MAT	Matrix sol
CM	Clay Matrix sol
SH	Self-healing sol
PVA	Polyvinyl alcohol
TEM	Transmission Electron Microscope
FESEM	Field Emission Scanning Electron Microscope

BET	Brunauer Emmett Teller
DI	De-ionised
BIA	Benzamidazole
IEM	Inhibitor Evacuated montmorillonite
IMM	Inhibitor Mixed montmorillonite
SAXS	Small Angle X-ray Scattering
GO	Graphene oxide
EHNT	Etched halloysite nanotube
MAA	Methacrylic acid
SST	Salt Spray test

Chapter 1

INTRODUCTION

Chapter 1
Introduction

1.1 Principle of corrosion

Most of the natural processes have a tendency to flow towards lowest possible energy level. For example, metals like iron, aluminum, magnesium, etc. and their alloys also have a tendency to react and/or combine with other elements or environmental factors to attain their lowest energy state. Aforementioned elements react with oxygen and water in the surrounding in order to reach the lower energy level to form hydrated metal oxides whose composition is similar to that of original metal ore.

A chemical or electrochemical reaction of metal with its surrounding atmosphere, which results in degradation of metal and its properties is known as corrosion. Basically, corrosion is an electrochemical process where electric circuit is formed with cathode, anode and electrolyte. Here, electrolyte is nothing but corrosive medium to which the metal is exposed and where cathodic and anodic electrodes are constituted by phases of the metal. The factors constituting the environment that affect the material properties are physical state (gas, liquid and solid), chemical composition (constituents and concentration), temperature, relative velocity and mechanical load on the material. The corrosion behavior of material and the surrounding atmosphere are interdependent on each other because all materials get degraded in some amount and all environments are corrosive to some extent. From industrial point of view, inorganic materials are more corrosive than organic materials. Corrosion can be classified in number of ways such as temperature based (high temperature and low temperature), mechanism based (direct combination and electrochemical) and nature of corrosive media (dry and wet). Magnesium and its alloys are considered as lightest engineering material for automobile and aerospace application. However, their use is limited owing to its very high chemical reactivity. The various types of corrosion experienced by Mg and its alloys along with a schematic representation describing the detailed mechanism of corrosion will be elaborated in the following section [1].

1.2 Magnesium and Magnesium alloys

The name magnesium was derived from a Greek word Magnesia, a district of Eastern Thessaly in Greece. Joseph Black at Edinburgh first recognized magnesium as an element

in 1755. Further, Sir Humphry Davy isolated pure elemental form of magnesium by the electrolysis of magnesium oxide in 1808. Later, the French scientist Antoine-Alexandre-Brutus Bussy obtained metallic form of magnesium in 1831 by reacting magnesium chloride with potassium [2]. Magnesium has been widely distributed among 80 minerals, which contain more than 20 % of Mg in their crystals. The major sources of magnesium (Fig. 1.1) are carnallite, magnesite, seawater and dolomite [3, 4].

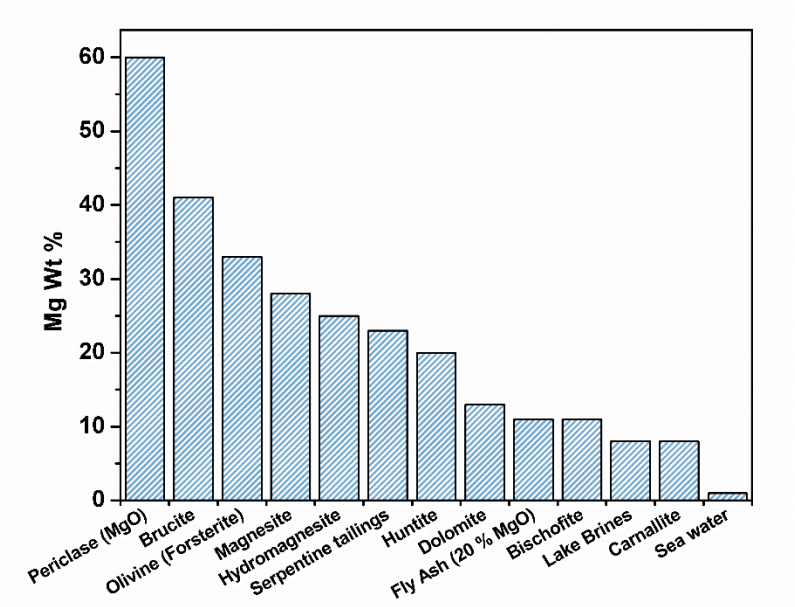

Figure 1.1: Availability of Mg in raw materials for Mg production [3] *(With permission from John Wiley and Sons, January 04, 2021, License No. 4981750269240)*

Magnesium is one of the lightest elements among the engineering materials with a density of 1.74 g/cm^3, which is 64.4 % that of aluminum (2.7 g/cm^3) and 22.1 % that of steel (7.86 g/cm^3). It has good ductility, good machining ability, better noise and vibration dampening characteristics, wide availability and excellent castability. Magnesium has the hexagonal close packed crystal structure [5].

Alloying of pure magnesium with different elements helps to improve its strength-to-weight ratio and makes it an important material for the applications where weight reduction and reduction of inertial forces are required. Theoretically, Mg can form solid solutions with 25 different elements because of analogous atomic size. However, electronic configuration, affinity towards chemicals, solubility limits, costs and potential applications limit the use of different elements. Following are some alloying elements and their effects of addition to Mg:

a) *Aluminum* has the most favourable effect on Mg. It improves the strength, hardness and castability. Adequate strength and ductility can be obtained with

addition up to 6 % (maximum 10 %). $Mg_{17}Al_{12}$ phase shows poor thermal stability that limits the creep resistance of alloy.

b) *Zinc* is considered as most effective and common alloying element after aluminum. It improves room temperature strength along with aluminum (with addition of 1 % or more, when Al is 7 % to 10 %). It gives increased alloying fluidity in casting. It enhances the corrosion resistance when added with iron and nickel impurities. Along with zirconium and rare earths, it produces precipitation hardenable alloys with better strength.

c) *Manganese* enhances yield strength and salt solution anticorrosion properties of Mg-Al and Mg-Al-Zn alloys. It reduces solubility of impurity metals by capturing them in intermetallic compounds, which can be removed during melting. It can be added up to 1.5 %.

d) *Rare earths* improve corrosion resistance, high temperature creep and strength. They enhance the casting ability by reducing the freezing range of alloy, thereby reducing the porosity.

e) *Iron* is the most harmful impurity as it reduces the anticorrosion property. The maximum limit is restricted at 0.005 % for maximum corrosion resistance.

f) *Nickel* improves the room temperature ultimate and yield strength but reduces ductility and anticorrosion properties. The maximum limit for Ni is 0.005 % for optimum corrosion protection [6].

Mg alloys are classified mainly based on designations such as alloy nomenclature and tempering conditions. In alloy designations, the alloying elements are given the abbreviations according to ASTM B275. The designation consists of letters that denote major alloying elements and then the numbers that denote the weight percentage of those elements. It is comprised of three parts. The first part consists of two abbreviation letters of main alloy elements specified in decreasing order of percentage or else in alphabetical order if percentages are similar. Percentages of the two main alloying elements are stated in second part. Part three differentiates alloys by mentioning a letter of the alphabet in the order of their improved purity. In temper designations, other fabrication conditions such as temperature conditions, hardening conditions, etc. are also included and separated from alloy designations using a dash such as AZ91E-T4 [7].

For example, in case of Mg alloy AZ91D:

AZ: Indicates Al and Zn as main alloying elements

91: Indicates percentages of Al and Zn rounded-off to whole numbers (9 and 1, respectively)

D: Indicates high purity alloy registered with ASTM.

1.3 Applications of magnesium and its alloys

Magnesium and its alloys are being implemented in enormous number of applications because of their lightweight, high strength-to-weight ratio, casting qualities, high damping capacity and ease of machining. Also, wide availability at lower prices results in an increased number of applications.

a) *Automotive applications:* Weight reduction of 22 % to 70 % is possible with the use of Mg alloys as automotive components, which results in low fuel consumption and CO_2 emissions. Most commonly used automotive components are engine blocks, wheel frame of steering, seat frames, instrument panels, rims of wheels, cylinder heads, etc. that have been used by car manufacturers like BMW, Toyota, GM, Audi, Honda, Isuzu, Ford, etc.

b) *Aerospace applications:* Weight reduction is one of the most focussed objective in aerospace industry as it aims in saving overall operational cost. Mg alloys are generally used to manufacture gearbox casings of helicopter. Mg alloys played an important role in World War-II with overall usage of around 5555 kg in B-36 bomber. Considerable amount of Mg alloy was used in ballistic missiles such as Titan, Agena and Atlas.

c) *Medical applications:* Mg alloys are good biocompatible materials and get biodegraded by corrosion with human body fluid. They have been used as orthopaedic biomaterials but the usage is restricted due to low corrosion resistance and hydrogen accumulation around the implant.

d) *Sports applications:* Higher specific strength, excellent damping characteristics and ease in formability makes Mg alloys useful in sports equipment. They are commonly used in chassis of in-line skates, golf club head, bicycle frames, tennis rackets and handles of archery bows.

e) *Electronics applications:* Magnesium alloys display great enhancement in heat transfer, strength, and property to shield radio frequency and electromagnetic interference as compared to its competitors. Hence, they are used for casings of computers, cell phones and media players [7].

Fig. 1.2 shows pictures of common applications where magnesium alloys have been used.

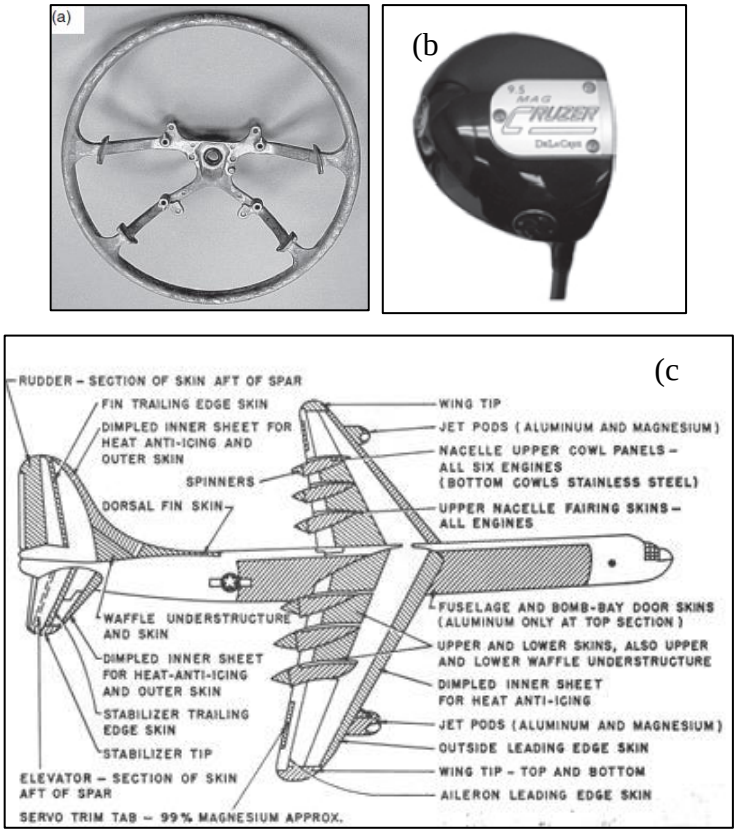

Figure 1.2: (a) Casing of steering wheel for Toyota Camry, (b) Golf club head [7] and (c) schematic of Mg components used in B-36 bomber [8] *(With permission from John Wiley and Sons, January 02, 2021, License No. 4980630835251)*

Among the various magnesium alloys, our studies were focused on AZ91D, which is a die-casted alloy of Mg-Al-Zn type. It comes with the alloying elements such as Al-9 %; Zn-0.7 %, Mn-0.33 %; Fe-0.005 % and Ni-0.002 %, along with Mg. This alloy exhibits good casting ability, better stability in atmosphere, high ductility and reasonably high yield strength at temperatures down to -120 ^{o}C. AZ91D alloy of Mg-Al-Zn series is considered as a high purity alloy with very low impurity levels of iron, copper and nickel and strictly controlled iron-manganese ratio. This highly pure alloy has much better mechanical and physical properties than the earlier grades. In this alloy, increase in aluminum content enhances the yield strength but results in reduced ductility. These alloys are generally easy to cast but exhibit microshrinkage with the sand casting [9].

Table 1.1: Physical properties of Mg alloy AZ91D [10] *(With permission from ASM International, January 04, 2021, License ID. 600032284)*

Property	Unit	Temp (°C)	AZ91D
Density	g/cm^3	20	1.81
Liquidus Temperature	°C	-	598.9
Incipient melting temperature	°C	-	420-435
Linear thermal expansion coefficient	µm/m	20-100	26
Specific heat of fusion	kJ/kg	-	370
Specific heat	kJ/kg °C	20	1.02
Thermal conductivity	W/m K	20	51
Electrical conductivity	MS/m	20	6.6

Table 1.2: Typical mechanical properties of Mg alloy AZ91D [10] *(With permission from ASM International, January 04, 2021, License ID. 600032284)*

Property	Unit	AZ91D
Ultimate tensile strength	MPa	240
Tensile yield strength (0.2 % offset)	MPa	160
Compressive yield strength	MPa	160
Fracture elongation	%	3
Elastic modulus, tension	GPa	45
Elastic modulus, shear	GPa	17
Brinell hardness	-	70
Impact strength, Charpy un-notched	J	6

1.4 Corrosion mechanism of magnesium alloy, AZ91D

Mg alloy usage in the above-mentioned applications is restricted due to their poor corrosion resistance properties. They exhibit a standard electrode potential of -2.37 V, which increases to -1.63 V (vs SCE) in 0.55 M NaCl solution. This could indicate that the thin film of oxides [MgO and $Mg(OH)_2$] are formed when the substrate is exposed to corrosive medium. The major aspects for poor corrosion resistance of magnesium alloys are (1) depletion of the passive thin film of oxides on exposure to corrosive medium and

(2) formation of galvanic couples due to impurities, flux contaminations, poor design and secondary phases such as $Mg_{17}Al_{12}$, AlMn, Al_8Mn_5, $Mg_{12}Nd$, Mg_2Pb, etc. [11].

Theoretically, potential-pH diagram can be used to predict the stability of Mg in water. The electrochemical thermodynamics of Mg can be understood with the help of potential-pH diagram (Pourbaix diagram) of the magnesium-water system as shown in Fig. 1.3. It shows that magnesium dissolves into ions, oxides and hydroxides over a broad range of pH and potential. The diagram depicts a small area of Mg, MgH_2 and H_2 at much more negative potentials as compared to the open circuit potentials of Mg in salt water solution. An area in the diagram shows more passiveness of potential at higher pH. This means that, at higher pH values, $MgO/Mg(OH)_2$ is more stable and forms a passive film, whereas at lower pH $MgO/Mg(OH)_2$ is unstable and dissolves in water to form Mg^{2+}. It can also be observed that, when corrosion takes place, the pH value is changed at localised area. The only drawback of this diagram is that, it can only predict thermodynamic stability or the tendency of Mg to get corroded in water and not the kinetic behaviour of corrosion mechanism [12, 13].

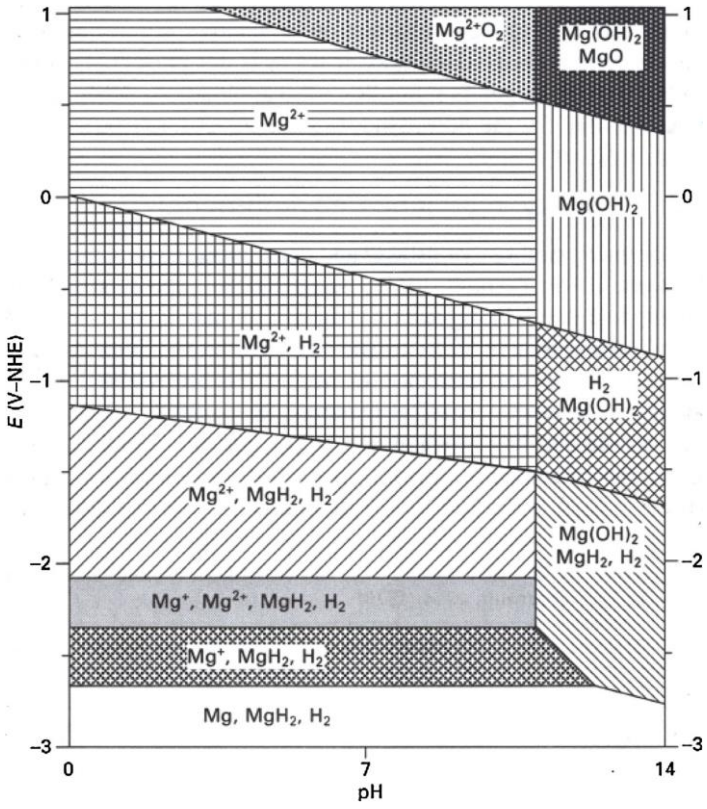

Figure 1.3: Potential-pH diagram of Mg in water [12] *(With permission from John Wiley and Sons, January 02, 2021, License No. 4980631006673)*

The mechanism of corrosion of magnesium and magnesium alloys can be understood by the reactions involved in dissolution of Mg in aqueous conditions to produce hydroxides

of Mg and hydrogen gas. This indicates that corrosion of Mg does not depend on oxygen concentration even though the presence of oxygen is crucial in atmospheric corrosion. The corrosion mechanism in aqueous conditions as shown in Fig. 1.4 is mainly associated with the micro-galvanic coupling of anodic and cathodic areas.

The overall reaction can be,

$Mg + 2\ H_2O \longrightarrow Mg(OH)_2 + H_2$

The intermediate reactions can be,

$Mg \longrightarrow Mg^{2+} + 2\ e^-$ (Anodic reaction)

$2H_2O + 2\ e^- \longrightarrow H_2 + 2\ OH^-$ (Cathodic reaction)

$Mg^{2+} + 2\ OH^- \longrightarrow Mg(OH)_2$ (Product formation)

The exact corrosion mechanism of Mg alloys has not yet been studied completely. However, it is expected that the overall corrosion reaction for Mg alloys will be similar to that of Mg, because during the dissolution of Mg-Al-Zn alloys, it was observed that, Mg and Al were the elements found dissolving but the Zn did not dissolve. This revealed that the above-mentioned corrosion reaction is applicable for Mg alloys as well [13].

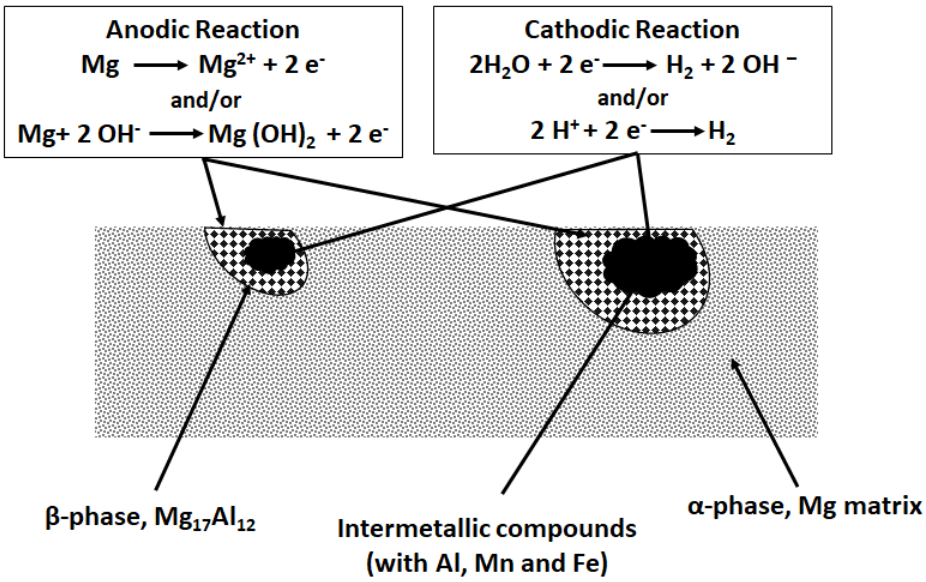

Figure 1.4: Corrosion mechanism of AZ91D [14] *(With permission from Elsevier, January 04, 2021, License No. 4981740648519)*

Most of the times, the oxide/hydroxide films formed on the Mg alloy surface gives considerable corrosion protection when exposed to the rural, industrial and marine environment. Hence, the corrosion rate of Mg alloys remains in between that of mild steel and Al alloys. Usually, Mg alloy corrosion initiates in localized form, which can be deep and widely spread. The nature of corrosion further depends upon the alloy chemistry and

exposure environments. Magnesium alloys can experience various types of corrosion (Fig. 1.5) as follows [11, 15].

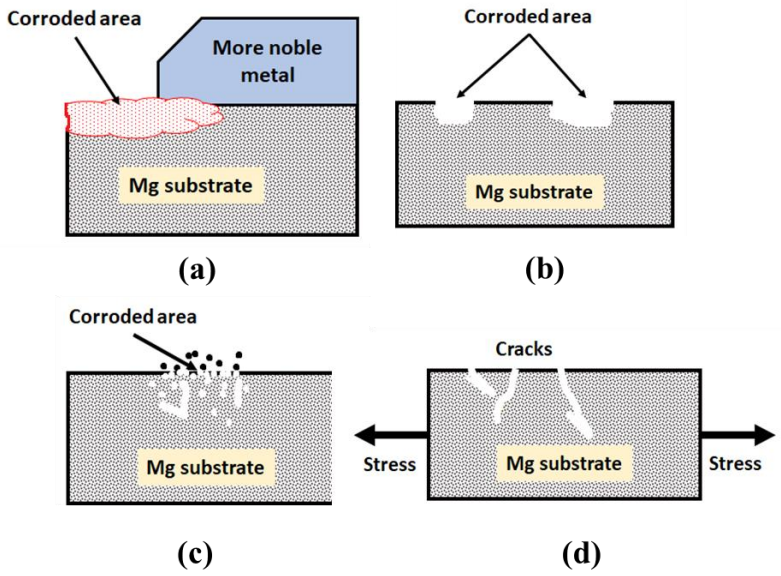

Figure 1.5: Schematic of various types of corrosion occurring with Mg alloy; (a) Galvanic corrosion, (b) Pitting corrosion, (c) Intergranular corrosion and (d) Stress corrosion cracking

a) *Galvanic corrosion:* Mg alloys are highly prone to galvanic corrosion due to contact with the cathode, which can be external metal or internal metal in the form of impurity or secondary phases. Metals such as Fe, Cu and Ni having low hydrogen overpotential forms a cathode and causes galvanic corrosion. On the other hand, when combined with metals having higher hydrogen overpotential such as Al, Zn and Sn, the galvanic corrosion is less. The corrosion rate is accelerated by medium with high conductivity, large anodic and cathodic potential difference, low polarizability of anode and cathode, large anodic to cathodic area ratio and less distance between anode and cathode.

b) *Localized or Pitting corrosion:* Being a natural passive metal, Mg experiences localized corrosion at its open corrosion potential after exposure to corrosive ions in oxygen-free medium, due to which pitting occurs in neutral or alkaline medium. It is examined that, pitting occurs adjacent to secondary phase particles like $Mg_{17}Al_{12}$ and AlMn, which in turn breaks the passive region. This results in formation of electrolytic cell constituting secondary phase as cathode and Mg matrix phase as anode.

c) *Intergranular corrosion:* Precipitation of secondary phase at the grain boundaries results in intergranular corrosion. Precipitation and segregation usually occurs at the grain boundaries. It is observed that, alloys with intermetallic phases or compounds suffer

highly with intergranular corrosion. During early stages of immersion in mild corrosive medium, localized corrosion occurs at the grain boundaries at the interface of secondary phase precipitates, which can be called as intergranular corrosion.

d) *Filiform corrosion:* Surfaces of Mg alloys are often vulnerable to filiform corrosion. This is caused by active galvanic cells across the metal/alloy surface where the head is anode and tail is cathode. Generally, it takes place under protective coatings and anodized layers. Uncoated Mg alloy is susceptible to filiform corrosion that further leads to pitting. This indicates that oxide film has formed on the surface, which is ruptured by H_2 evolution.

e) *Stress corrosion cracking (SCC):* SCC in Mg is mostly transgranular. $Mg_{17}Al_{12}$ precipitation along grain boundaries results in intergranular SCC. Mg alloys are highly resistant to SCC above pH 10.2. They are also resistant to SCC in neutral solutions with chlorides, distilled water and fluoride containing solutions. SCC in Mg alloys can be explained with two mechanisms, i.e., continuous or discontinuous crack propagation which takes place by anodic dissolution or by a series of mechanical fractures at crack tip respectively.

Microstructural studies of Mg alloy give more detailed information regarding initiation of corrosion at micro level. Fig. 1.6 shows microstructure of Mg alloy AZ91D. The corrosion resistance of AZ91D increases with increase in Al content due to the Al containing microconstituents such as β phase and eutectic phase. It is observed that, β phase acts as a barrier as well as a cathode for electrolytic cell. Lower concentration of β phase makes it to work as cathode and increases α matrix corrosion and vice versa.

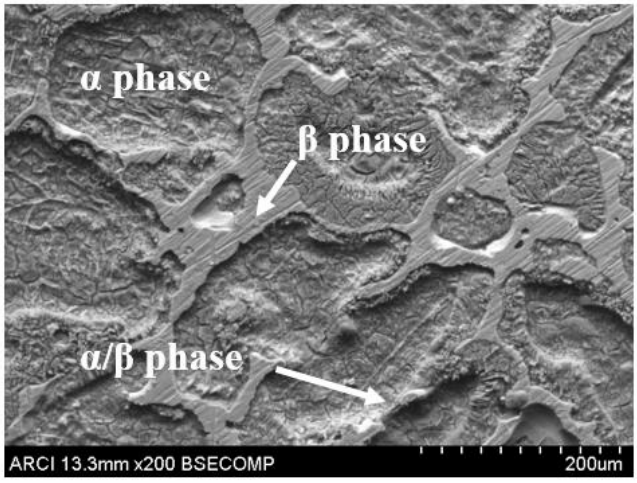

Figure 1.6: Typical microstructure of Mg alloy AZ91D

The atmospheric corrosion begins at the phases with low Al content, whereas better anticorrosion properties are observed where Al content is higher. In this case, initial corrosion attack occurs at α phase and continuation of α phase dissolution results in the formation of pits. The decrement in the corrosion rate takes place with dissolution of higher Al content phases after initial rapid α phase corrosion during which the pH is neutral. However, such phases are corroded further as the pH increases because higher pH acts as accelerator to Al containing phases [16].

Uncoated magnesium alloys are susceptible to corrosion under various atmospheric conditions and different exposure media. The effect of different exposure media on Mg alloys are given below [17]:

a) *Atmospheres:* Mg alloy forms a grey film of oxides/hydroxides in atmospheric conditions, which partially protects the surface from further corrosion attack. Mg alloys show better surface protection against uniform corrosion or atmospheric corrosion as compared to that in marine and industrial atmospheres unless have any joint that holds the water. The exposure of Mg alloy in rural atmosphere for shorter durations results in formation of hydroxides and hydrated carbonates of Mg in case of longer exposures.
b) *Freshwater:* In steady water, Mg will form a thin film of oxides, which breaks down with the salts present in water such as chlorides or heavy metal salts. Dissolved oxygen in fresh water does not contribute to corrosion. However, gentle agitation may break the thin film leading to the formation of pits. The pH increases with initial Mg ion dissolution resulting in the precipitation of insoluble $Mg(OH)_2$.
c) *Salt solutions:* Severe corrosion takes place when Mg alloys are exposed to neutral salt solutions of Fe, Cu and Ni, as these salts later behave as cathode. Fluorides results in formation of magnesium fluoride, which gives some resistance to corrosion. Oxidizing salts such as chlorides and sulphides are considered as more corrosive than non-oxidizing salts such as chromates, phosphates and vanadates.
d) *Acids and alkalis:* Mg alloys show some resistance to corrosion with exposure to hydrofluoric acid and chromic acid as compared to other mineral acids. However, at elevated temperatures Mg alloys are susceptible to corrosion with all acids. Mg alloys are resistant to basic pH solutions and 10 wt % NaOH solution is widely used for pretreatment of substrates.
e) *Organic compounds:* Mg alloys are not susceptible to corrosion with exposure to higher alcohols, ketones, ethers, aliphatic and aromatic compounds and glycols. Halogen based

compounds do not attack Mg alloys but in presence of water or at higher temperatures, they are prone to corrosion.

f) *Gases:* Anhydrous chlorine, bromine, iodine and fluorine results in low to negligible corrosion at room temperature. However, when these gases mix with water, the severity of corrosion enhances. The rate of oxidation of Mg alloys increases linearly with time and temperature.

1.5 Corrosion protection of magnesium alloys

Various methodologies have been researched and implemented for the protection of magnesium alloys from attack of corrosive species. This includes, lowering the heavy metal impurity level, eradicating bad design, flux involvements, surface contaminations, galvanic couples, use of protective coatings with corrosion inhibitors and electrochemical protection methods. Surface treatment/coatings are considered as most effective approach to protect the alloy by providing effective barrier between alloy surface and external aggressive environment. The coatings intended to protect the surface should be uniform, adherent, pore-free, possess sufficient mechanical resistance, flexibility towards deformation, self-healing if the coating experiences physical damage and should not be vulnerable to imperfections on surface during application. Being highly reactive and inherently alkaline surface, Mg alloys form oxide/hydroxide films in contact with air or water influencing the coating properties. Thus, the surface should be pre-cleaned/ pre-treated to make it more compatible with all types of coatings. In this context, several coating methodologies/techniques have been developed for Mg alloys, which include conversion coatings, micro-arc oxidation, ion beam treatment, chemical vapour deposition, physical vapour deposition, flame or plasma spray, sol-gel coatings and organic/inorganic coatings and details of some these processes are provided below [17, 18].

a) *Electrochemical Plating:*

Electroplating is one of the most widely used efficient and simple technique for generating metallic coatings on substrates. The electroplating process can be characterized into two parts such as electroless plating and electroplating. In both the parts, metal salt in the solution is reduced into its metallic form on the substrate. In electroplating, external source supplies electrons for reduction, whereas reducing agent in the solution supplies electrons for reduction in case of electroless plating. Magnesium is considered as most difficult for plating, being highly reactive. The formation of passive oxide layer makes it necessary to provide pretreatment to generate a thin film that prevents formation of oxide

layer. Zinc immersion and conversion coating with fluoride containing bath are most commonly used processes prior to plating. Formation of intermetallic species like Mg_xAl_y along the grain boundaries makes plating difficult on the alloys because of uneven charge along the substrate. Electroplating explores additional challenge because of intermittent supply of current density in electrolyte bath resulting in uneven coating on irregular shapes. Cu-Ni-Cr plating was found to have better anticorrosion properties in interior and mild external environments, whereas electroless Ni coating showed stable electronic contact, improved solderability and good wear and corrosion resistance for the components in electronics industry [17-20]. Number of components in automobile, electronics and aerospace industries that are coated with electroplating technique are mentioned in table 1.3.

Table 1.3: Commercialized electroplating coatings for components made up of Mg alloys [19]

Part	**Form**	**Requirement**	**Pre-treatment**	**Finish**
Automotive Parts				
Under hood parts (valve covers, fuel induction housing)	Die cast	Appearance, durability, resistance to salt splash, oils	Wet abrasion or alkaline clean plus chrome pickle or iron phosphate	Epoxy or epoxy-polyester Powder coat
Power train components (clutch housings, transfer cases)	Die cast	Resistance to salt splash	None	None
Engine brackets	Die cast	Resistance to heat, salt splash, oils	Wet abrasion of none	None
Wheels	Die cast	Appearance, resistance to UV exposure, brake dust, stone chipping, humidity	Chrome pickle or iron phosphate	E-coat, triglycidyl isocyanurate(TGIC) (a), polyester powder acrylic powder clear coat

Interior parts (hidden items)	Die cast	Humidity	Cut wire aluminum blast, wire brush or none	None
Exterior parts (visible items)	Die cast	Appearance, resistance to weather, brake dust, stone chipping, UV, salt splash	Chrome pickle or iron phosphate	E-coat, liquid acrylic coat and acrylic powder clear coat
Electronics/Computer				
Housings	Die cast	Mild interior, sales appeal, durability, adhesion	Chrome pickle or ion phosphate	Sprayed acrylic, polyester or urethane, exterior coating textured epoxy powder coat.
Disc drive activator arm	Die cast/extruded	Mild interior, limited temperature and humidity variations. No particle release is allowed	Dichromate No. 7 or chrome-pickle final dichromate or none on machined surfaces	E-coat on die-cast surfaces, none on external surfaces
Aerospace parts				
Aircraft auxiliary components and helicopter gear-box housing	Sand cast	Exterior severe marine and tropical	Sand blast and acid pickle, Dichromate No. 7	Backed epoxy primer, polyurethane exterior finish coat or silicate anodize and epoxy coat

b) Conversion coatings

Chemical or electrochemical treatment of metal surfaces with conversion coating solutions produce physical surfaces of chromates, metal oxides, phosphates or other electrolytic solutions that form chemical bond with surface of metal. Further, these are

capable of providing better corrosion resistance as well as adhesion properties to the paint. Earlier, hexavalent chrome based coatings were considered as most reliable conversion coatings (Fig. 1.7). In this case, as soon as Mg substrate is immersed in the chromate treatment bath, redox reaction (reaction 2) takes place with change in local pH. This results in the precipitation of oxides and hydroxides of Mg and Cr (reactions 1 and 3). Further, with the withdrawal of substrate from bath, hydroxides of Mg and Cr get dehydrated into their respective oxides (reactions 4 and 5). However, these coatings are carcinogenic in nature that limited their use according to new environmental regulations by European Union from June 2017.

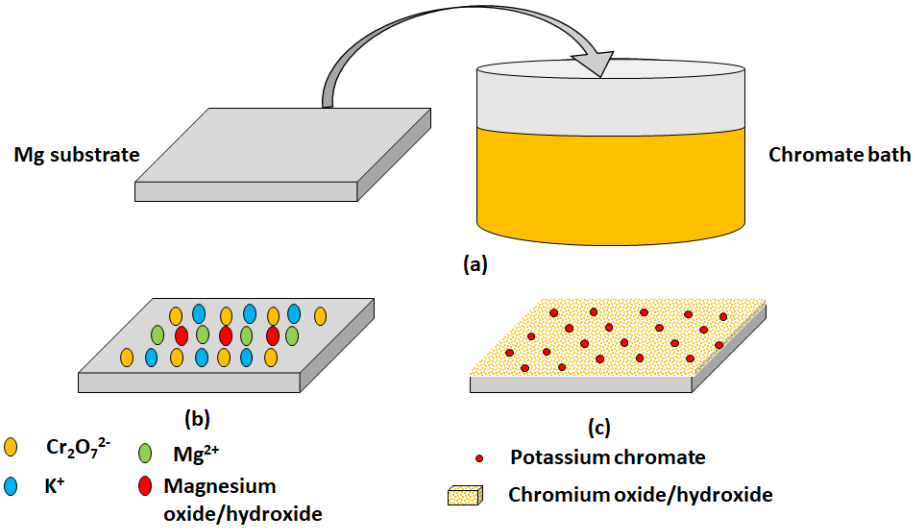

Figure 1.7: Schematic depicting the application of hexavalent chrome based coatings on Mg alloy; (a) substrate immersion in chromate bath, (b) redox reaction and (c) deposition of coating

$$2H_2O + Mg^{2+} \longrightarrow Mg(OH)_2 + 2H^+ \quad (1)$$

$$Cr_2O_7^{2-} + 14H^+ + 3Mg \longrightarrow 2Cr^{3+} + 7H_2O + 3Mg^{2+} \quad (2)$$

$$Cr^{3+} + 3H_2O \longrightarrow Cr(OH)_3 + 3H^+ \quad (3)$$

$$2Cr(OH)_3 \longrightarrow Cr_2O_3 + 3H_2O \quad (4)$$

$$Mg(OH)_2 \longrightarrow MgO + H_2O \quad (5)$$

Most of the conversion processes include series of steps such as, degreasing, water rinsing, alkaline cleaning, acid pickling, conversion treatment, post-treatment in organic chelating agents and heat treatment. Chemical conversion solutions are mainly composed of oxidants, promoters, corrosion inhibitors, wetting agents and pH buffer regulators. Oxidants (nitrate and perchlorate) are useful in increasing the OH^- concentration and enhance the dissolution of Mg and formation of conversion film. Promoters (Zr and V salts)

get precipitated on Mg alloy to form seeding nuclei for the generation of conversion film. Corrosion inhibitors slow down the dissolution of Mg^{2+}, being adsorbed on the Mg alloy surface by formation of solution stabilizing complexes. Precipitation of conversion film becomes easier by reduction of surface tension of Mg alloys using wetting agents. Controlling the pH of solution with pH regulators affects the formation and quality of conversion layer. Based on the main ingredient, the conversion coatings can be classified as chromate based, stannate based, rare earth oxide based, phosphate based, phosphate-permanganate based, fluoride based and based on compounds of V, Zr, Mo, W, Ti and Co [17-20].

c) Hydride coating

Magnesium hydride coatings have been developed using electrochemical methods as a replacement to hexavalent chrome based coatings. The process is carried out at basic pH with Mg substrate acting as cathode and electrolytic solution composed of quaternary ammonium salts, metal hydroxides or other alkaline materials. The solution resistance can be controlled by adding a supporting electrolyte. In a similar way as electroplating, the substrates are pre-treated with mechanical polishing, degreasing with acetone and acidic and alkaline etching. The corrosion rate of AZ91D with hydride coating is three times lesser than that of chromate-based coatings [20].

d) Anodization

Anodization is an electrochemical process used for generating uniformly thick and stable oxide layers on Mg alloys. The coatings are composed of thin films acting as a barrier at metal surface-coating interface and another layer with cell-like structure. Each cell consists of pores whose sizes are controlled by electrolyte concentration, temperature, current density and applied voltage. The sealing quality of anodized films is based on the pore size and density. The abrasion and anticorrosion properties of anodized film can be enhanced by sealing of porous film. Lowering temperature of electrolyte and increasing the current density can generate films with enhanced wear resistance and hardness. Generation of flaws and inclusions from mechanical pretreatment can affect the uniform deposition of coatings. This process fails to attain uniform throwing power in case of complex shapes to be coated. Coatings generated by anodization are in the form of ceramic like materials, which may not be suitable for all applications due to their mechanical strength [17-20].

e) Gas-phase deposition processes

Protective films generated from gas phase are typically composed of metallic coatings and organic coatings such as thermal spray coatings, chemical vapour deposition,

physical vapour deposition, diamond like carbon films, diffusion coatings and ion implantation. In case of thermal spray coatings, coating materials such as metals, ceramics or polymers are put up into spray gun after which they are heat treated beyond their melting temperature and the resultant droplets are forced towards substrate in gaseous stream. In chemical vapour deposition (CVD), solid particles are deposited on hot surface with a chemical reaction in gas phase. Physical vapour deposition (PVD) consists of deposition of atoms or molecules in a vapour phase on to the surface of substrate. It serves for generating coatings for wear and corrosion resistance or only with unique anticorrosion properties. PVD has limitations such as the deposition temperature should be lower than stability temperature of Mg (180 ^{o}C) and it is difficult to attain better adhesion and corrosion resistance at such lower temperature. The applications of aforementioned coating methods on Mg alloys for corrosion protection have been given in detail by Grey and Luan [20].

f) Surface cladding via Laser treatment

Surface cladding via laser treatment generates uniform solid solutions in which rapid solidification of modified metal surface takes place. In this case, high power laser is used to melt metallic coating material and substrate followed by rapid melting, mixing and solidification. Cu, Cr and Al coatings have been found to give more positive potentials and better corrosion protection for Mg-Li, Mg-Zr and other commercial alloys such as AZ91. It has advantages such as, capability to treat complex objects and control the concentration of modified film with lower operational cost [20].

g) Organic coatings

Organic coatings are generally used to enhance anticorrosion, abrasion and wear resistance properties or for decorative applications at any stage of coating system. They are incorporated with binders, additives and pigments like dryers, hardening agents, surface activating compounds, corrosion inhibitors, dispersing agents and stabilizing agents. These coatings systems can be generated with number of approaches such as plasma polymerization, sol-gel coating, powder coatings, E-coating, and painting. These coatings are based on resins such as acrylic, butyrate, cellulose acetate, nylon, epoxies, alkyd, polyesters, polypropylene, polyethylene, rubber resins, polyurethanes and vinyls. Generally, organic coatings are solvent based. However, due to environmental concern, they can be completely water- based or based on mixture of water and organic solvent, where 70-80% is water and remaining is the organic solvent used for dissolving water insoluble compounds. The main objective of these coatings is to work as barrier between the substrate and surrounding environment as well as hindering the transport of ions,

oxygen and water. Organic coatings face various difficulties during application such as, uneven film, uneven crosslink density in film, unevenness in various additives concentration and changes in polymer appearance with disclosure to number of atmospheric conditions. These limitations are overcome by the use of multilayer coating system comprised of aforementioned layers of organic coatings.

The most important aspect in painting is choosing proper primer that can be resistant to alkali and based on polymers like polyurethane, polyvinyl butyral, vinyl epoxy and acrylic. The anticorrosion properties of paint can be enhanced by addition of pigments like chromate, titanium dioxide and conducting polymers. Polymeric systems that are suitable for aluminum alloys and steels cannot be used for Mg alloys because of their low steadiness in alkaline exposure, brittleness, low UV hindrance and lower adhesion strength.

In powder coating, pigmented powdered resin is placed on the substrate and heat treated to melt the polymer together to form even, non-porous coating. Usually, electrostatic spraying, fluidised bed or flame spraying of thermoplastic powders generates coating. This process is preferred over other processes because of eco-friendly nature, solvent free, even thicker coatings can be obtained and less spillage of material during coating generation. However, it comes with disadvantages such as use of completely dry powder, thin coatings cannot be obtained, limitations in coatings discontinuous areas and requirement of higher curing temperature (~200 ℃), which may not be compatible to all substrates.

E-coating or electrophoretic deposition is a colloidal process, which involves migration of suspended charged particles in a stationary electrolyte towards oppositely charged electrode in presence of applied electric field and gets deposited there. It is categorised into two types based on the potential applied such as anodic and cathodic electrophoretic deposition. For example, deposition of positively charged particles takes place at cathode and vice versa as shown in Fig. 1.8. This process is considered more versatile as compared to its counterparts since the deposition can be made on any kind of conducting substrate, flexibility achieved in control over thickness, cost effective, requires less formation time, needs simple apparatus and mass production of films is possible using suspensions with low concentration (< 1 g/L). There are number of factors that need to be considered while synthesizing the suspension for EPD like size of particle, liquid dielectric constant, conductivity of suspension, viscosity, stability and zeta potential [17-20].

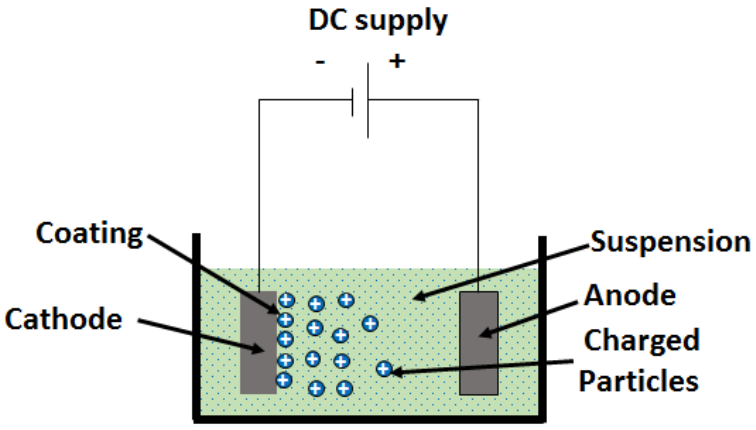

Figure 1.8: Schematic of cathodic electrophoretic deposition

h) Sol-Gel coatings

Sol-gel coatings offer a great potential to be used as an eco-friendly alternative to chromate based and other types of coatings. Sol-gel coatings are capable of providing better adhesion to metallic substrates by chemical bonding as well as good physical bonding to organic top coats, thereby reducing number of pretreatment processes. They offer several others advantages such as, i) lower curing temperature that prevents thermal volatilization and degradation of additives like corrosion inhibitors, ii) use of liquid precursors which makes it possible to produce coatings of variable thickness on any complex shapes and iii) the films are formed by green coating technologies and does not form any impurity after coating generation. These coatings are considered as more versatile as number of additives such as corrosion inhibitors, dyes, catalysts, monomers, etc. can be included in the coating matrix to improve functionality of coatings. The coatings can be generated with aqueous and/or non-aqueous processes in organic or aqueous solvents [18].

After comparing all above processes for generation of coatings on Mg alloy AZ91D, sol-gel process was chosen for our further studies considering the above-mentioned advantages. The basics of sol-gel process are discussed below in detail.

1.6 Sol-Gel Process

The sol-gel process is comprised of the synthesis of a colloidal solution through generation of organic-inorganic hybrid sol or only inorganic sol, which proceeds with the gelation to form continuous polymer network, gel via aqueous or non-aqueous processes. The non-aqueous process involves synthesis of colloidal solution followed by its gelation via precursor molecule condensation, whereas the hydrolytic approach involves hydrolysis followed by condensation of metal alkoxides. Typical sol-gel process mainly consists of

two stages, i.e., hydrolysis as well as condensation reactions of metal alkoxides ($M(OR)_n$) which can readily react with water. Alkoxides of silica, titanium, zirconium, tin, cerium and aluminum are generally used in generation of corrosion protection coatings using sol-gel route. Among them, silicon alkoxides are mostly preferred due to their moderate rate of reaction and stability. The generalised reaction scheme based on silica based alkoxides followed in sol-gel process is as follows:

Hydrolysis

$$Si\text{-}(OR)_4 + H_2O \longrightarrow (OR)_3\text{-}Si\text{-}OH + R\text{-}OH$$

Alcohol condensation

$$(OR)_3\text{-}Si\text{-}OH + Si\text{-}(OR)_4 \longrightarrow (OR)_3\text{-}Si\text{-}O\text{-}Si\text{-}(OR)_3 + R\text{-}OH$$

Water condensation

$$(OR)_3\text{-}Si\text{-}OH + (OR)_3\text{-}Si\text{-}OH \longrightarrow (OR)_3\text{-}Si\text{-}O\text{-}Si\text{-}(OR)_3 + H_2O$$

Hydrolysis of alkoxides with water results in the exchange of alkoxides groups (-OR) and hydroxyl groups (-OH). Further, two -OH groups or –OH group and –OR group condense to generate bonds of M-O-M with alcohol or water. In this case, the hydrolysis rate is usually higher than the condensation rate and condensation process starts before hydrolysis comes to end. Another important factor that affects the kinetics of process is the addition of mutual solvents such as alcohols. Alcohols are required to achieve homogeneity of reaction system, as silicon alkoxides and water are not miscible. The amount and type of alcohol also influences on the thickness and structure of sol-gel based coatings. Considering the faster reaction rates of titanium, zirconium or cerium alkoxides, usage of complexing agents is compulsory. The condensation reaction is inhibited by using carboxylic acids, β-Diketones, β-ketoesters, or other complexing agents. The chemical reactivity of some of the alkoxides is as shown:

$$Ce(OR)_4 > Zr(OR)_4 > Ti(OR)_4 > Sn(OR)_4 > Si(OR)_4$$

Due to low reactivity of silicon alkoxides, addition of catalysts such as acid or base is required in order to accelerate the process. Use of base as a catalyst results in the formation of highly branched silica network, whereas linear or randomly branched network is formed with acid catalyst.

Sol-Gel process based corrosion protection coatings can be deposited using techniques such as spraying, dipping, spinning and electrophoretic deposition. Dip coating and spin coating can be used only for flat substrates, whereas electrodeposition can be used for complex shaped substrates to obtain uniform coatings.

Heat treatment of the sol-gel coatings can be carried out in two ways such as high temperature (around 900 ^{o}C) annealing and low temperature (< 200 ^{o}C) drying. However, high temperature curing under atmospheric conditions results in lowered corrosion resistance of coatings due to the cracks generated. Hence, low temperature curing is generally preferred as it gives crack-free coatings. Along with the temperature, heating rate also plays a major role in structural and anticorrosion properties of coatings. More compact coatings with better barrier properties are obtained with lower rate of heat treatment.

Low curing temperatures of sol-gel process allows inducing organic groups into inorganic groups to produce novel hybrid systems containing both organic and inorganic parts where, organic part renders improved flexibility and functional compatibility with top coats and inorganic part enhances mechanical properties. Fig. 1.9 shows improved chemical bonding of paint system based on epoxy resin with hybrid sol-gel coating based on silica by functionalization of organic group of hybrid coating with epoxy groups [18, 20-22].

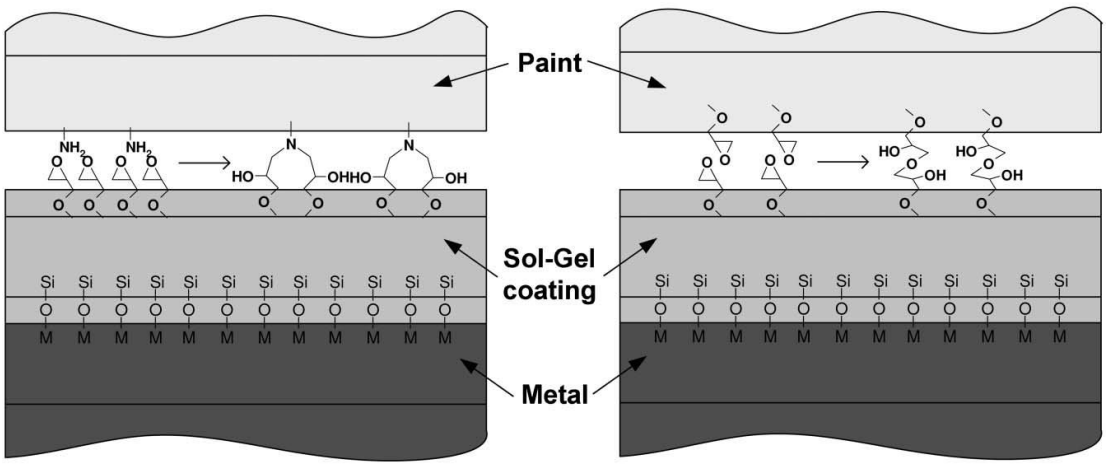

Figure 1.9: Schematic representation of bond formation of epoxy based paint system with silica based hybrid sol-gel coating [22] *(With permission from Royal Society of Chemistry, January 02, 2021, License ID. 1087667-1)*

Hybrid sol-gel coatings are well known to provide dense coatings with better properties. However, a coating alone cannot provide a better protection to the substrate because of inbuilt micropores, low cross-link density areas and in situations where mechanical damage occur to the coatings, which give access to diffusion of corrosive media like water, oxygen, chloride/fluoride ions to the coating-substrate interface. This brings two possible trends of improving anticorrosion properties of sol-gel coatings; direct inclusion of active materials for corrosion prevention into the coating matrix or encapsulation of these active materials into nanocontainers, nanoporous layers and oxide nanoparticle reservoirs. The active

materials generally used are corrosion inhibitors (phosphates, vanadates, borates, cerium and molybdate compounds), catalysts, monomers and dyes. Encapsulating the active materials (to provide controlled release and to avoid unwanted interaction of these materials with coating matrix) is the best possible way to give prolonged corrosion protection. This approach is named as self-healing and corresponding coatings are self-healing coatings, which release the corrosion inhibitors and/or polymerizing agents in a controlled manner as soon as the defect occurs in the coating. This will result in use of corrosion inhibitor only when required and increase the corrosion protection ability of coatings for a longer period. The principle and types of self-healing approach is further discussed below [22, 23].

1.7 Self-healing coatings

The term self-healing has come from the natural tendency of living organisms to heal any injury automatically. For example, when a damage occurs on the blood vessels, it cuts the layer of epidermis and dermis and blood starts to come out (Fig. 1.10). Further, a scab is generated from blood components to prevent further blood loss and heals the damage by joining broken layers of dermis and epidermis. This results in the healing of wounds naturally, which inspired scientists to generate the self-healing ability in the coatings [24].

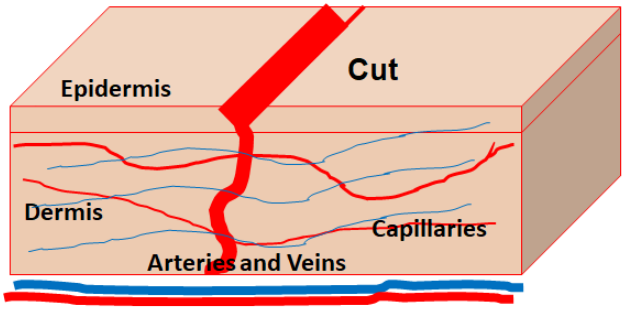

Figure 1.10: Healing mechanism of injury on skin

Self-healing coatings are the one which can heal the damage on the surface and recover the original coating properties. In this case, the coatings restore their barrier properties by sealing the defect through polymerizing agents or by inhibiting the corrosive actions at defective site using corrosion inhibitors. The self-healing can be classified into two types as autonomous and non-autonomous.

a) Autonomous/Extrinsic self-healing mechanism:

Autonomous self-healing systems have the ability to heal the damage to regain their integrity and functional properties without any external trigger. This involves encapsulating the monomer into microcapsules and embedding them in coating matrix that contains the

catalyst for polymerization. When any defect occurs on the coating surface, the microcapsules are ruptured and the monomer is polymerized to generate a passive film, thus retaining the protective properties of coating. In this mechanism, the mechanical damage to coatings introduces polymerizable agent in the damaged area, which polymerizes in presence of catalyst embedded in coating matrix or with air or moisture in environment to form passive film, thereby restoring the coating barrier properties. White and Sottos [25] gave a typical example, where dicyclopentadiene monomer is encapsulated in urea-formaldehyde microcapsules and microcapsules are then embedded in coating matrix along with Grubbs catalyst (transition metal carbene complexes). The monomer gets released in the crack due to rupture of microcapsules and is polymerized with catalyst to heal the crack by passive polymeric film as shown in Fig. 1.11.

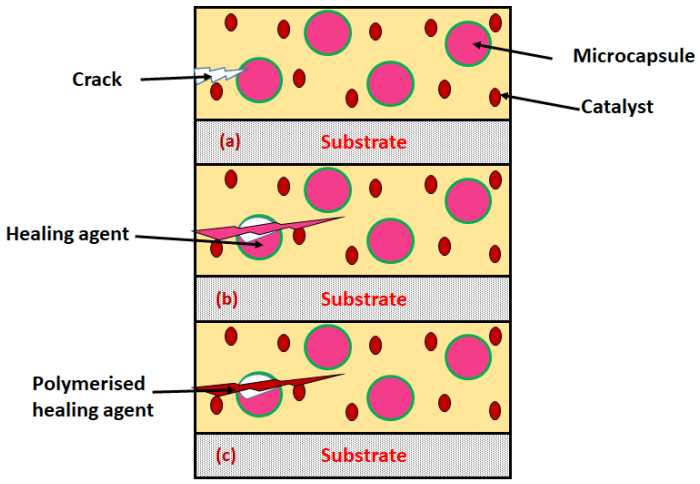

Figure 1.11: a) Monomeric healing agent embedded in microcapsules and catalyst in coating matrix, b) healing agent releases into crack and c) polymerization of monomer in presence of catalyst [25]

Microcapsule-based self-healing approach comes with the limitation of complete or multiple healing due to limited amount of healing agent. In order to overcome this limitation, thin capillaries and/or hollow glass fibers (30-100 μm diameter) were used to load the low viscosity healing agents (Fig. 1.12). These hollow fibers have advantages such as loading of higher volume of healing agents, damaged site can be easily inspected and can be activated with different methods or types of resins. This approach has some limitations such as multistep fabrication is required, resins must have low viscosity and fibers must be broken with external triggering.

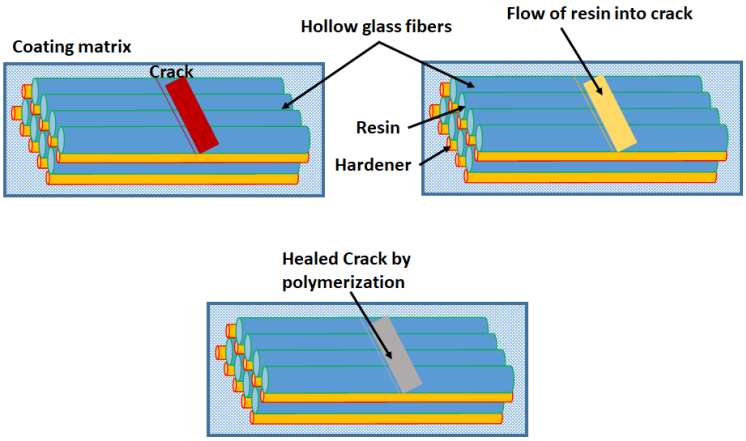

Figure 1.12: Schematic representation of self-healing mechanism by hollow glass fibers [28] *(With permission from John Wiley and Sons, January 03, 2021, License ID. 1087810-1)*

Microvascular systems are capable of continuous release of healing materials for extending the functional life of self-healing coatings. In such continuous self-healing systems, the coating matrix is composed of catalysts and interconnected microchannels for storage and delivery of healing agents as shown in Fig. 1.13. In this case, when a defect/crack propagates through the microchannels, the healing agent flow into the crack and gets polymerized to heal the crack in presence of catalyst. If in case, the crack reopens, the microchannels allows release of more healing agent and heal the damage again.

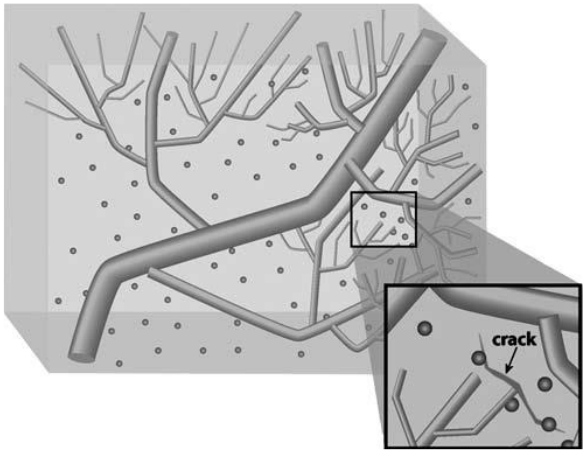

Figure 1.13: Schematics of self-healing mechanism with microvascular system [28] *(With permission from John Wiley and Sons, January 03, 2021, License ID. 1087810-1)*

Another approach involves use of corrosion inhibitor to inhibit the corrosion reactions taking place at defective site. However, this approach requires external triggering conditions such as ions, oxygen, water and pH, which are available when corrosion takes place at defect site. The corrosion inhibitor can be embedded directly in the coating matrix or can be encapsulated in the micro/nanocontainers. However, direct embedment of

inhibitor in coating matrix [26] induces limitations such as incompatibility of inhibitor with coating matrix, inhibitor aggregation, and improper and untimely leaching of inhibitor. In order to avoid these circumstances, inhibitors are loaded in micro/nanocontainers. This will result in supply of inhibitor at the damaged area only when it is supposed to enhance the durability and barrier properties of coating. In this approach, corrosion inhibitor restricts the anodic dissolution and cathodic reactions. Inhibitors having an ability to enhance the passivity of oxide film on substrate control the anodic dissolution, whereas formation of precipitates of oxides and hydroxides at cathodic site by inhibitors retards cathodic reactions. Some of the corrosion inhibitors suppress both cathodic and anodic activities by physical / chemical adsorption, or chemical complexation / reaction in substrates. Hence, corrosion inhibitor encapsulated coatings are most widely used because of their simple design and their healing ability directly inhibits corrosion process.

b) Non-autonomous/ Intrinsic self-healing mechanism:

Anticorrosion properties of coatings can also be restored manually using external trigger not available at corrosion site such as light and heat, which can be easily applicable in corrosive environment. Recovery of physical conformation of networks of polymer and non-autonomous chemical bonds are major factors that are responsible for healing of damaged coatings. External stimuli are used to supply the activation energy needed for separation or reformation of bonds. Triggering with heat improves the flowability of polymers, which brings the broken bonds together by enhancing the reaction rate. The heat stimulus used can be artificial such as heat gun or naturally obtained from surrounding environments such as abrasion and sunlight. Commonly used light stimuli for this approach are UV light, NIR radiation or sunlight.

Such approaches can be developed by dynamic covalent bonds, ionic interactions and hydrogen bonds. For example, rise in temperature decomposes thermally reversible bonds, allows polymer to reach the crack and re-crosslink to heal it. The major advantage of this mechanism is that, the healing processes can be repeated a number of times without requirement of another healing agent.

Shape memory polymers are materials, which can regenerate their original shape using heat and light from a temporary deformation. In self-healing approaches, shape memory polymers have been used to heal the cracks in polymer composites. Viscoelastic transformations are responsible for shape transitions of polymers when they are processed at glass transition temperature or melting temperature. However, self-healing coatings also come with some limitations such as cost of precursors and catalyst along with cost incurred

for synthesis of capsules or containers. Further, there can be limitation in stability or uniform distribution of capsules/containers in coating matrix [27-29].

In spite of the aforementioned shortcomings, self-healing coatings have potential to provide better barrier properties and corrosion protection for longer duration when damage occurs on the coated surface to expose the substrate. The active materials such as catalysts, corrosion inhibitors and monomers can be encapsulated in various micro/nanocontainers in order to provide controlled release when there is change in local environment or due to physical damage to the coating. The next section will discuss about different micro-nanocontainers used for synthesis of smart self-healing coatings.

1.8 Capsules and/or containers for encapsulation of active materials

The principal approach of designing self-healing coatings is to load active materials into containers/capsules with a shell capable of controlled permeability or release and then embedding them into the coating matrix. Thus, these containers/capsules are evenly distributed in the coating matrix, thereby avoiding the interaction of active material with coating matrix. When there is a change in surrounding environment or because of external impact, the containers/capsules respond to these stimuli and release the active material according to requirement [30].

These micro/nanocapsules are containers of sizes ranging from several nm to few mm, composed of core (solid, liquid or gases) surrounded by a shell. The performance of self-healing coatings is mainly based on design of these capsules. The word nanocontainers was differentiated from capsules as the nanocontainers have more wide structure, more loading capacity with similar sizes and other properties than capsules for drug delivery [30]. The nanocontainers to be synthesized should be, i) chemically and mechanically stable, ii) compatible with coating material, iii) with enough loading capability, iv) able to prevent leakage of active materials from shell wall, v) able to sense the corrosion immediately and vi) capable of releasing the active materials as per requirement. Various nanocontainers that have been studied earlier are discussed below:

a) *Polymeric microcapsules* are most preferred containers for loading active agents in self-healing coatings. Number of methods have been used for synthesis of polymeric microcapsules such as sol-gel methods, extrusion and interfacial polymerization. *In situ* polymerization of oil-in-water emulsion is most widely preferred method for encapsulating active materials because of its convenience and easy preparation methods. Fig. 1.11 shows self-healing mechanism with polymeric microcapsules.

b) *Layered double hydroxides (LDH) (anionic clays or hydrotalcite)* are well known anionic exchanging materials that are composed of stacks of cationic multiple metal hydroxide species intercalated between anions and solvent/water molecules. LDH is expressed with general molecular formula $[M_{1-x}^{2+}, M_x^{3+} (OH)_2]^{x+} (A_{x/m}^{m-}. n H_2O)^{x-}$, where, the cations M^{2+} and M^{3+} stay in the octahedral voids in brucite-like layers and the water based interlayer spacing occupy the anion A^{m-} as shown in Fig. 1.14. Intercalation of organic anion inhibitors is possible because of the potential of supplying anions. The anion exchange containers are capable of exchanging harmful chlorides and release inhibiting species in case of corrosive attack. They have been widely used as supercapacitors, polymer additives, anion exchangers, adsorbents, drug delivery, catalysts and corrosion inhibitive carriers.

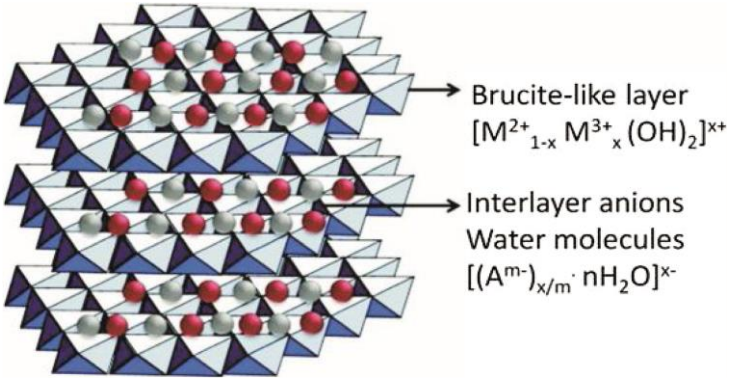

Figure 1.14: Schematic representation of LDH structure and composition [32] *(With permission from Elsevier, January 02, 2021, License No. 4980640619116)*

c) *Polyelectrolyte multilayer based nanocapsules*

Polyelectrolyte layers have potential to release corrosion inhibitors embedded in multilayers in a controlled manner with a change in pH at local corrosion site and mechanical damage to the coating. Layer-by-layer (LBL) approach is used to assemble polyelectrolytes over the surface of nanoparticles. In this approach, oppositely charged species are assembled in stepwise manner under the influence of electrostatic force on the surface of nanoparticles with an accuracy of nanometer scale and forms the coatings with several functionalities. Number of deposition cycles and the type of polyelectrolyte used, control the coating properties. The formation of polyelectrolyte layers is correlated to their nature and adsorption conditions irrespective of substrate type and substrate surface charge density. Fig. 1.15 depicts the polyelectrolyte assembly formation [33,34].

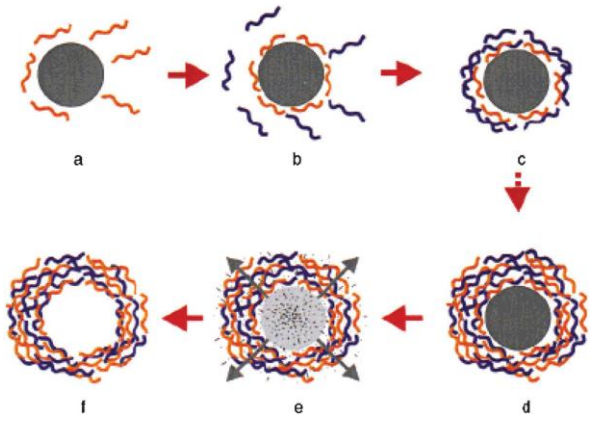

Figure 1.15: Schematic representation of formation of polyelectrolyte capsule, a–d) assembly of polyelectrolyte with LBL approach; e–f) formation of hollow capsules of polyelectrolyte [31] *(With permission from John Wiley and Sons, January 02, 2021, License No. 4980640464376)*

d) Carbon nanotubes as reservoirs for active materials

Carbon nanotubes are well known because of their attractive electrical, mechanical and thermal properties. They have tubular morphology with high specific area, light weight and high strength. These tubes are made with several concentric shells of carbon with each shell separated by 0.34 nm distance. They can be loaded with active materials for synthesis of anticorrosion coatings. The mechanism of self-healing with carbon nanotubes is schematically represented as shown in Fig. 1.16 [35].

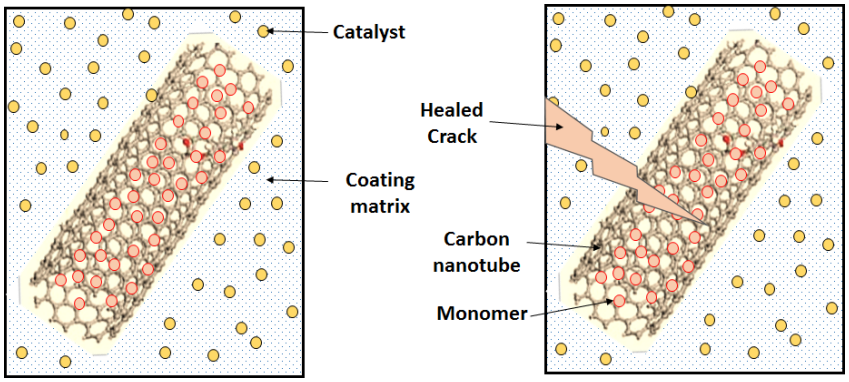

Figure 1.16: Schematic representation of self-healing mechanism with carbon nanotubes [35]

e) Clay based nanocontainers

Long term self-healing can be carried out with the containers that have higher encapsulating capacity with slower release rate of corrosion inhibitors. These features are available with nanotubes or ion exchange clays with higher surface area or volumes with small opening ends. Aluminosilicate clays such as halloysite and montmorillonite (also

referred as bentonite) clays are some of the organic clays that are used as nanocontainer for anticorrosion coatings.

Halloysite nanoclay is a dioctahedral clay mineral in kaolin group consisting of two basal surfaces, i.e., inner lumen of octahedral alumina (Al_2O_3) and outer layer of tetrahedral silica (SiO_2). Generally, length of halloysite nanotubes (HNT) ranges between few microns to around 30 µm, while the external diameter is around 30-190 nm and internal diameter is 10-100 nm as shown in Fig. 1.17. The molecular formula of HNT is $Al_2Si_2O_5(OH)_4 .nH_2O$ where, for hydrated HNT (Halloysite- 10 A^o) n=2 and for dehydrated HNT (Halloysite- 7 A^o) n=0. The outer layer being SiO_2 has weak negative charge and inner Al_2O_3 carries strong positive charge below pH 8.5. HNT with length of around 0.5-1 µm, external diameter of 50-70 nm and lumen diameter of 15 nm, are considered as chemically inert.

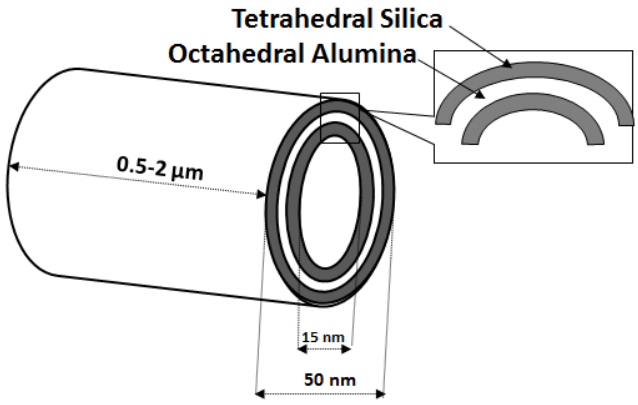

Figure 1.17: Schematic representation of halloysite nanotube

The lumen is hydrophobic and outer surface is hydrophilic because of presence of covalent bonds. In general, both hydrophilic and hydrophobic compounds can be loaded in lumen of HNT with appropriate pre-treatment. The cationic compounds can be easily loaded owing to the active surface and tubular structure. The HNT lumen is only about 10 %, which can be increased up to 40 %-50 % of total volume by acid treatment. However, the acid etching is dependent on factors such as acid concentration, temperature and time of process. HNTs comes with several advantages such as, non-toxic, biocompatible and naturally occurring; good dispersion ability and high surface area; ability to hold release if not stimulated and during processing; ability to encapsulate number of additives; can be implemented in number of forms like gels, powders, lotions, creams and sprays; has fast adsorption rate, high capacity and a high rate of loading; and is highly porous with high aspect ratio, which increases its effectiveness [36, 37].

Montmorillonite clay, a phyllosilicate mineral also referred as bentonite clay, a layered clay belonging to smectite group is widely used in the field of anticorrosion coatings owing to

number of merits like particle size <10 µm, larger surface area (~100 m^2/g) and ion exchange properties. Cation exchange capacity and the surface area can be enhanced by pillaring of MMT clay. The crystal structure of MMT clay is composed of tetrahedral sheets of silica coalesced with an edge shared octahedral sheet of alumina in 2:1 ratio as depicted in Fig. 1.18. The length of diffusion pathways of oxygen, water and aggressive ions can be increased by embedding montmorillonite in the coating matrix. Montmorillonite clay containing interlayer cations undergoes isomorphic substitution with metals having lower valence and leads to negative charge imbalance compensated by other exchangeable metal cations. Therefore, cationic corrosion inhibitors can be exchanged with cations of MMT nanoclay and effectively used for corrosion protection.

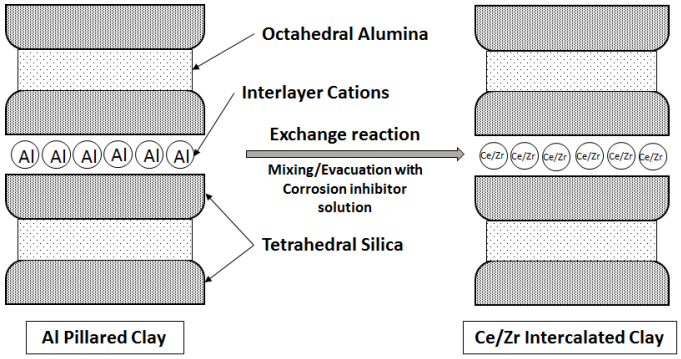

Figure 1.18: Schematic mechanism of intercalation of corrosion inhibitors into MMT clay

Considering the advantages and limitations of all the nanocontainers, halloysite and montmorillonite clays were chosen as nanocontainers in the present study for loading of different corrosion inhibitors. However, it would also be useful to study the role of corrosion inhibitors and mechanism of their inhibition before loading them into nanocontainers for corrosion protection studies.

1.9 Role and mechanism of corrosion inhibitors

A corrosion inhibitor can be defined as a chemical substance or mixture of substances that effectively mitigates corrosion in a corrosive atmosphere even with addition of very low concentrations without a considerable reaction with the environment components. Inhibitors are added in very low concentrations of 0.0001 to 1.5 wt %. Corrosion prevention or control can be effectively and efficiently carried out by corrosion inhibitors. They are used in petroleum refineries, oil and gas exploration and production, heavy manufacturing, water treatment, product additive industries and chemical manufacturing. They have

always been investigated as first choice for mitigation of corrosion, in the oil refineries and chemical industries [38].

Mechanism of action for corrosion inhibitors:

a) Inhibitors are adsorbed on the surface of metal or alloy by chemisorption by forming a barrier providing passive film with an effect of inhibitor or by bond formation of inhibitor with metal ions.
b) The inhibitor forms an oxide layer by sealing the pores and repairing the damaged metal oxide for protection of metal surface.
c) A complex is formed in aqueous media with the reaction of inhibitor with corrosion component.

Classification of corrosion inhibitors:

The corrosion inhibitors are artificial or natural and are categorized based on nature of chemical as inorganic or organic; on the action mechanism as cathodic, anodic or both cathodic-anodic and by action of adsorption as oxidants or not oxidants. The organic inhibitors can act as both, anodic and cathodic, whereas inorganic inhibitors show either cathodic or anodic activity only.

a) Inorganic inhibitors

Anodic inhibitors also referred as passivating inhibitors, prevents the anodic reaction, forms protective film on the metal surface and supports natural passivation of metal surface. In short, insoluble and cohesive film is formed on the surface of metal because of reaction between corrosion inhibitors and the corrosion products formed. These inhibitors can result in pitting corrosion if the concentration is below critical value for oxidation. Non-oxidizing and oxidizing anions are the two types of passivating inhibitors used to inhibit corrosion. Passivation of metals can be carried out by non-oxidizing anions such as molybdate, phosphate and tungstate in presence of oxygen. Organic non-oxidizing inhibitors are sodium cinnamate, sodium benzoate and polyphosphate. Some of anodic inorganic inhibitors commonly used are sodium chromates, molybdates, hydroxides, phosphates, and silicates. Metallic ions Me^{n+} at anode reacts with anodic inhibitor to form insoluble hydroxide layer on the substrate surface, which is impermeable to the metallic ions. Further, hydrolysis of inhibitor results in the release of OH^- ions as shown in Fig. 1.19.

Cathodic inhibitors prevents or reduces cathodic reaction. These inhibitors produce cathodic reaction in alkaline conditions due to the presence of metal ions, resulting in the formation of insoluble precipitates at the cathodic sites. This compact film prevents the

diffusion of reducing species in these areas. They also reduce the corrosion currents by inhibiting cathodic polarization. The phenomenon of release of hydrogen ions, where

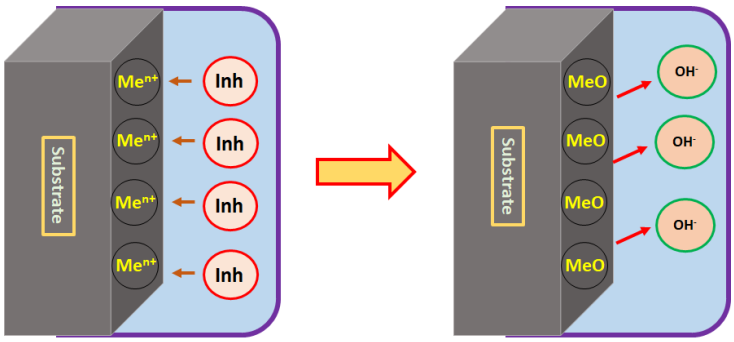

Figure 1.19: Schematic representation of mechanism of action of anodic inorganic corrosion inhibitor [39]

hydrogen is discharged and also known as overvoltage, is minimized by these type of corrosion inhibitors. Cathodic inhibitors prevent contact of metal with surrounding environment by forming a barrier film of insoluble precipitates. Cathodic inhibitors are considered as safer than anodic inhibitors as they are independent of concentration. Commonly used inorganic cathodic inhibitors include the ions of zinc, calcium, magnesium and nickel; cerium, zirconium, bismuth, arsenic and antimony oxides and salts; and polyphosphates, phosphonates, tannins and lignins. Additionally, inorganic compounds such as nitrates, nitrites and chromates also have been used as inhibitors. Fig. 1.20 shows schematic representation of mechanical effect of cathodic inhibitors to prohibit the corrosion process.

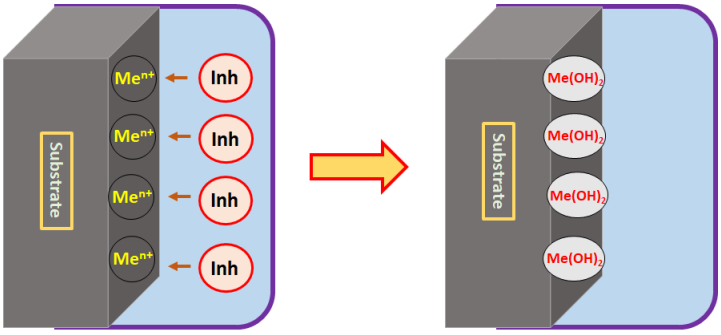

Figure 1.20: Schematic representation of mechanism of action of cathodic inorganic corrosion inhibitor [39]

b) Organic inhibitors

Organic heterocyclic compounds containing polar groups and compounds containing sulfur, nitrogen, or oxygen atoms are preferred over inorganic inhibitors because of less toxicity. Organic compounds work as either anodic, cathodic or both as cathodic and anodic inhibitors via surface adsorption by formation of covalent bonds with the metal. Organic

inhibitors generate a thick layer of monolayers and modify the double layer structure at the metal interface by decreasing depolarization rate, thereby covering the corrosion affected area on the substrate surface. These inhibitors form protective film by suppressing anodic and cathodic activities or decreasing transport of electroactive species towards or away from the metal substrate surface. Lowering the concentration of inhibitor works effectively, if the rate of adsorption is strong. The adsorption of positively or negatively charged soluble organic compounds are responsible for the formation of passive film. Inhibitors such as imidazolines, amines and acetylenic alcohols form passive films by adsorption. Various amines, amides and polyethoxylated compounds work as anodic inhibitors, whereas cathodic inhibitors are sulfonates. Polar groups such as hydroxyl, nitrogen, sulfur, phosphorous, or selenium can act as organic inhibitors [39, 40]. Fig. 1.21 shows mechanism of organic inhibitors by forming barrier film on metal substrate by adsorption.

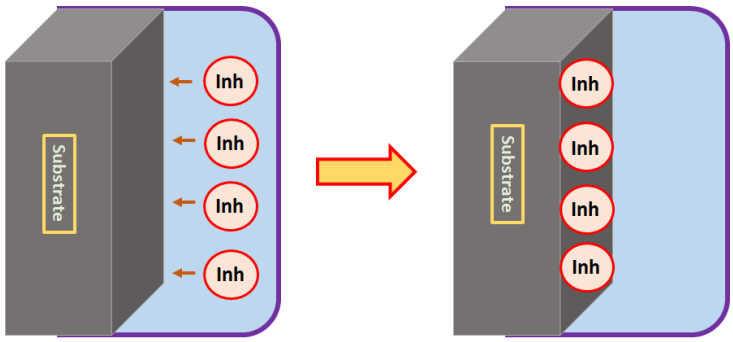

Figure 1.21: Schematic representation of mechanism of action of organic corrosion inhibitor [39]

After understanding the background of magnesium and their alloys, Mg alloy AZ91D was chosen for generation of coatings and studying their self-healing ability followed by elucidating their corrosion protection mechanism. Being susceptible to various forms of corrosion as mentioned in this chapter, various corrosion protection methods have been studied along with the use of containers for encapsulating corrosion inhibitors. Hence, based on the advantages, durability and availability, sol-gel process was selected for generating barrier coatings and halloysite and montmorillonite clays were chosen for achieving self-healing functionality in the coatings. Further, the mechanism and types of corrosion inhibitor were studied for selection of corrosion inhibitor. In next chapter, we will discuss about the investigations carried out for various corrosion protection coatings along with the one giving self-healing ability using various nanocontainers and corrosion inhibitors for Mg alloy AZ91D.

1.10 Aim and Objectives of Study

a) Aim: Development of nanoclay based self-healing corrosion protection coatings on magnesium alloy, AZ91D.

b) Objectives:

i. Generating the coatings with self-healing functionality on Mg alloy, AZ91D. Coatings comprised of corrosion inhibitor (Ce^{3+}-Zr^{4+}) loaded nanoclays such as halloysite and montmorillonite clays, where open ends of the HNTs were capped using polymeric microcapsules.

ii. Evaluation of self-healing ability of coatings by various characterization techniques.

iii. Comparing corrosion protection abilities of different corrosion inhibitors such as Ce^{3+}-Zr^{4+}, 8-hydroxyquinoline and 2-mercaptobenzothiazole

iv. Evaluating release rate of different corrosion inhibitors from halloysite clay and validation of release data using various kinetic models

v. Analysing effect of coating techniques on corrosion protection ability

1.11 Thesis Organization

- *Chapter 1* gives details about background of magnesium and magnesium alloys with the information about the alloying of Mg. Further, various applications have been discussed, where Mg and its alloys are widely used. The detailed corrosion mechanism has been discussed considering the type of corrosion experienced along with the microstructure and factors responsible for corrosion of Mg alloys. This chapter also includes detailed discussion about corrosion protection methodologies implemented for Mg alloys. It also includes role and mechanism of different corrosion inhibitors for corrosion protection of Mg alloys.
- *Chapter 2* gives details of literature review of corrosion protection coatings on Mg alloys. Further, it discusses the literature on self-healing coatings on Mg alloys based on different types of micro/nanocontainers. It also includes literature on different corrosion inhibitors used for corrosion protection of Mg alloys.
- *Chapter 3* confers about self-healing halloysite nanoclay based corrosion protection coatings generated on Mg alloy AZ91D. In this, as-received and Ce^{3+}-Zr^{4+} loaded halloysite nanotubes were analysed for their morphology and inhibitor loading by various characterization techniques. The corrosion protection ability of coatings was analysed by weight loss analysis and electrochemical measurements. The self-

healing functionality of coatings was confirmed by scanning vibrating electrode technique and micro-Raman spectroscopy.

- *Chapter 4* describes about Ce^{3+}-Zr^{4+} intercalated montmorillonite nanoclay dispersed self-healing coatings developed on AZ91D. The morphological and intercalation studies were analysed by transmission electron microscopy and X-ray diffraction analysis, respectively. Electrochemical measurements, weight loss analysis and immersion tests were performed to evaluate the corrosion protection ability of coatings. Further, scanning vibrating electrode technique was used for confirmation of the self-healing ability of coatings.
- *Chapter 5* gives comparison of corrosion protection ability of different corrosion inhibitors loaded into as-received and etched halloysite clay nanotubes. Etched halloysite clay and inhibitor loaded etched halloysite clay were characterized for their morphology and loading ability by transmission electron microscopy, X-ray diffraction and BET analyses. The release rate of corrosion inhibitors from as-received and etched halloysite nanoclay was analysed and was fitted with various kinetic models. The corrosion protection ability of different corrosion inhibitor based coatings was assessed by electrochemical studies and salt spray tests.
- *Chapter 6* shows the effect of coating technique on corrosion protection properties of AZ91D. Coatings with same thickness were generated by using dip coating and spray coating techniques. The corrosion mitigation properties were analysed by using salt spray tests and electrochemical measurements.
- *Chapter 7* provides a conclusion of the work carried out with a glimpse of the scope for future work

1.12 References

[1] J. R. Davis, Corrosion- Understanding the basics, ASM International, USA (2000), pp. 1-20.

[2] https://www.rsc.org/periodic-table/element/12/magnesium

[3] Edward Ghali, Properties, use and performance of magnesium and its alloys, in: Corrosion resistance of aluminum and magnesium alloys: understanding, performance and testing, John Wiley & Sons (2010) pp. 321-347.

[4] George J. Simandl, Hagen Schultes, Jana Simandl, & Suzanne Paradis, Magnesium - Raw Materials, Metal Extraction and Economics - Global Picture, Proceedings of the Ninth Biennial SGA Meeting, Dublin (2007) pp. 827-830.

[5] Mustafa Kemal Kulekci, Magnesium and its alloy applications in automotive industry, Int. J. Adv. Manuf. Technol. 39 (2008) 851-865.

[6] Ken Savage, Magnesium and magnesium alloys, in: Casting, ASM Handbook, ASM International, 15 (2008) pp. 1100-1113.

[7] Manoj Gupta, Nai Mui Ling Sharon, Magnesium alloys, in: Magnesium, Magnesium Alloys and Magnesium Composites, John Wiley and Sons (2011) pp-42-43.

[8] S.N. Mathaudhu, E.A. Nyberg, Magnesium Alloys in U.S. Military Applications: Past, Current and Future Solutions, in: S.N. Mathaudhu, A.A. Luo, N.R. Neelameggham, E.A. Nyberg, W.H. Sillekens, Essential Readings in Magnesium Technology, Springer, Cham (2016) pp. 71-76.

[9] J.R. Davis, Selection and applications of magnesium and magnesium alloys, in: Metals Handbook Desk Edition, ASM Handbook (1998) pp. 559-570.

[10] Susan Housh, Barry Mikucki, Properties of magnesium alloys, in: Properties and selection: Nonferrous alloys and special purpose materials, ASM Handbook 2 (1990) pp. 480-516.

[11] Zeng Rong-chang, Zhang Jin, Huang Wei-jiu, W. Dietzel, K.U. Keiner, C. Blawert, K.E. Wei, Review of studies on corrosion of magnesium alloys, Trans. Nonferrous Metals Soc. China 16 (2006) s763–s771.

[12] Andrej Atrens, Guang-Ling Song, Ming Liu, Zhiming Shi, Fuyong Cao, Matthew S. Dargusch, Review of recent developments in the field of magnesium corrosion, Adv. Eng. Mater. 17 (4) (2015) 400-453.

[13] Barbara A. Shaw, Ryan C. Wolfe, Corrosion of magnesium and magnesium-base Alloys, in: S. D. Cramer, B. S. Covino, Corrosion: Materials, ASM Handbook 13B

(2005) pp. 205-227.

[14] B. L. Luan, D. Yang, X. Y. Liu, G. L. Song, Corrosion protection of magnesium alloys using conversion and electrophoretic deposition, in: G. L. Song, Corrosion of magnesium alloys, Woodhead Publishing (2011) pp. 541-564.

[15] Guang Ling Song, Andrej Atrens, Corrosion mechanisms of magnesium alloys, Adv. Eng. Mater. 1 (1) (1999) 11-33.

[16] Martin Jonsson, Dan Persson, The influence of the microstructure on the atmospheric corrosion behavior of magnesium alloys AZ91D and AM50, Corros. Sci. 52 (2010) 1077-1085.

[17] Lénia M. Calado, M. F. Montemor, Corrosion protection of magnesium alloys by functional coatings, in: Lisa Klein, Mario Aparicio, Andrei Jitianu, Handbook of Sol-Gel science and technology, Springer Nature (2018) pp. 2473-2505.

[18] Rong-Gang Hu, Su Zhang, Jun-Fu Bu, Chang-Jian Lin, Guang-Ling Song, Recent progress in corrosion protection of magnesium alloys by organic coatings, Prog. Org. Coat. 73 (2012) 129-141.

[19] Stephen Abela, Protective coatings for magnesium alloys, in: Frank Czerwinski, Magnesium alloys-Corrosion and surface treatments, InTech Croatia (2011) pp. 195-220.

[20] J. E. Gray, B. Luan, Protective coatings on magnesium and its alloys-a critical review, J. Alloys. Comp. 336 (2002) 88-113.

[21] C. J. Brinker, G. Scherrer, Sol-Gel Science: The Physics and Chemistry of Sol-Gel Processing, Academic Press, San Diego (1990) pp. 1-20.

[22] M.L. Zheludkevich, I. Miranda Salvado, M.G.S. Ferreira, Sol-gel coatings for corrosion protection of metals, J. Mater. Chem. 15 (2005) 5099-5111.

[23] Xiankang Zhong, Qing Li, Junying Hu, Shiyan Zhang, Bo Chen, Shuqiang Xu, Fei Luo, A novel approach to heal sol-gel coating system on magnesium alloy for corrosion protection, Electrochim. Acta 55 (2010) 2424-2429.

[24] Akihiro Yabuki, Indra W. Fathona, Self-healing corrosion protective coatings in transportation industries, in: Abdel Salam Hamdy Makhlouf, Nedal Y. Abu-Thabit, Advances in smart coatings and thin films for future industrial and biomedical engineering applications, Elsevier (2020) pp. 99-133.

[25] E. N. Brown, M. R. Kessler, N. R. Sottos and S. R. White, In situ poly(urea-formaldehyde) microencapsulation of dicyclopentadiene, J. Microencapsulation 20

(2003) 719-730.

[26] X. Zhong, Q. Li, J. Hu, Y. Lu, Characterization and corrosion studies of ceria thin film based on fluorinated AZ91D magnesium alloy, Corr. Sci. 50 (2008) 2304-2309.

[27] Fan Zhang, Pengfei Ju, Mengqiu Pan, Dawei Zhang, Yao Huang, Guoliang Li, Xiaogang Li, Self-healing mechanisms in smart protective coatings- a review, Corros. Sci. 144 (2008) 74-88.

[28] Swapan Kumar Ghosh, Self-healing materials: fundamentals, design strategies and applications, Willey-VCH Verlag GmbH and Co. (2009) pp. 1-28.

[29] M. Abdolah Zadeh, S. van der Zwaag, S. Garcia, Self-healing corrosion-protective sol–gel coatings based on extrinsic and intrinsic healing approaches, in: Self-healing Materials, Springer, (2016) pp. 185–218.

[30] Dmitry Shchukin, Helmuth Mohwald, Self-repairing coatings containing active nanoreservoirs, Small (Willey-VCH) 3 (6) (2007) 926-943.

[31] Dmitry Grigoriev, Elena Shchukina, and Dmitry G. Shchukin, Nanocontainers for self-healing coatings, Adv. Mater. Inerfaces 4 (1) (2017) 1600318, 1-11.

[32] Lian Guo, Wei Wu Yongfeng Zhou, Fen Zhang, Rongchang Zeng, Jianmin Zeng, Layered double hydroxide coatings on magnesium alloys-a review, J. Mater. Sci. Technol. 34 (2018) 1455-1466.

[33] Huige Wei, Yiran Wang, Jiang Guo, Nancy Z. Shen, Dawei Jiang, et al, Advanced micro/nanocapsules for self-healing smart anticorrosion coatings, J. mater. Chem. A. 3 (2015) 469-480.

[34] Dmitry G. Shchukin, Container-based multifunctional self-healing polymer coatings, Polym. Chem. 4 (2013) 4871-4877.

[35] R Subasri, Swapnil H. Adsul, S. Manasa, Smart nanocontainers for anticorrosion applications, in: Phuong Nguyen-Tri, Trong-On Do, Tuan Anh Nguyen, Smart Nanocontainers, Elsevier (2020) pp. 399-412.

[36] K.A. Zahidah, S. Kakooei, M.C. Ismail, P.B. Raja, Halloysite nanotubes as nanocontainer for smart coating application: a review, Prog. Org. Coat. 111 (2017) 175–185.

[37] E. Joussein, S. Petit, J. Churchman, B. Theng, D. Righi, B. Delvaux, Halloysite clay Minerals- a review, Clay Miner. 40 (2005) 383–426.

[38] L.S. Van Delinder, Corrosion Inhibitors Basics: An Introduction, NACE International, (1984).

[39] C. G. Dariva, A.F. Galio, Corrosion inhibitors- Principles, mechanisms and applications, in: Mahmood Aliofkhazraei, Developments in Corrosion Protection, InTech Open (2014) pp. 365-379.

[40] Branko N. Popov, Corrosion Inhibitors, In: Corrosion Engineering, Elsevier (2015) pp. 581-597.

Chapter 2

LITERATURE REVIEW

Chapter 2
Literature Review

2.1 Corrosion protection coatings for Mg alloy, AZ91D

In the first chapter, the need for corrosion protection and various methods to mitigate the corrosion of Mg alloy, AZ91D was explored. One of the most effective approaches among them is to provide a dense barrier between substrate and the surrounding environment using protective coatings. The principles of operation of various coating techniques such as conversion coatings, hydride coatings, anodization, organic coatings, etc. were also discussed. This chapter includes a review of earlier studies, which have been carried out most widely for corrosion protection of Mg alloys using the aforesaid techniques.

In order to provide good adhesion and better anticorrosion properties to the coatings, the substrate surface must be cleaned or activated by chemical and mechanical methods prior to coating deposition. Each step of pretreatment stage has some impact on the elemental composition of substrates and morphology of surface. In case of mechanical cleaning, emery papers (SiC sheets) of different grits are used to grind the surface for removing the impurities that have got accumulated during processing or other contaminations. The chemical cleaning of Mg alloys is usually carried out in three steps such as solvent cleaning, alkaline cleaning and acid cleaning. Solvent cleaning is performed to eliminate the solid particles, all the oils, compounds generated or accumulated during polishing and other types of waxes/greases used to protect the surface. Alkaline washing is carried out for the removal of residual contaminants and for dissolution of Al phases on the substrate surface wherein, Al is dissolved above pH 9 and Mg matrix phase remains unaffected. At the end, acid treatment is essential to remove contaminants bounded to the surface and other oxide films not removed during earlier stages. Fig. 2.1 depicts a schematic representation of substrate cleaning steps of Mg alloys [1-5].

2.1.1 Conversion coatings

Among the various coating techniques used for corrosion protection, chemical conversion coatings are considered to have better potential of protection due to the advantages such as speed of operation, ease of application along with low capital and operating costs due to low consumption of energy, high efficiency, short processing time

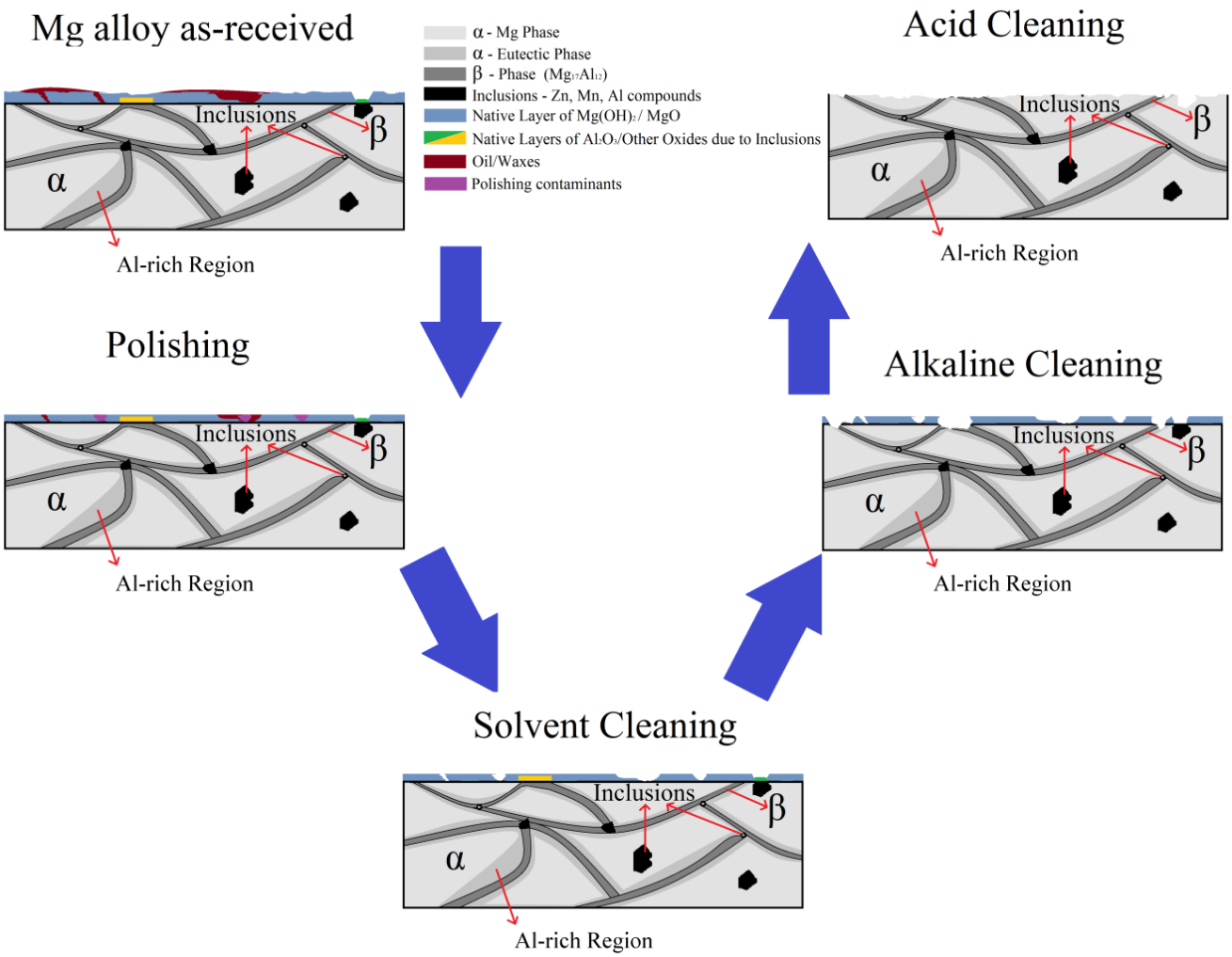

Figure 2.1: Schematic representation of substrate cleaning stages of Mg alloys [6]

and being a low temperature process. The coatings are generated by complex interaction of metal dissolution along with precipitation in an aqueous solution. The coatings are generally composed of oxides or hydroxides of magnesium and of other metals that arise from aqueous metal ions in the solution. In Mg alloys, conversion coatings play an important role in corrosion protection and provide improved adhesion for the topcoat. The most preferred conversion coatings include chromates, permanganates, phosphates, molybdates and rare earths based compounds [7].

The chromate conversion coatings (CCC) are considered to be generated because of dissolution of surface of metal followed by reduction of oxygen or water to form OH^- resulting in the increased pH at interface of liquid-metal. This results in the precipitation of a thin film consisting of both hexavalent and trivalent chromate compounds [8]. CCC constitutes dense films of hydroxides of Mg^{2+} and Cr^{3+} with porous outer layer of $Cr(OH)_3$ over Mg substrate. This outer layer is generated from $Mg(OH)_2$ selective dissolution,

increased thickness of which gives better corrosion protection in chloride medium [9]. Magnesium alloys such as AZ31C, AZ63A and AZ91C with CCC have shown significant reduction of corrosion in salt spray tests [10]. Sharma [11] developed CCC on Mg-Li alloys with the thickness around 8-11 μm with better adhesion, optical and paint-base properties under thermal cycling and humidity tests. Ono et al. [12] discussed substrate/coatings interface morphology and mechanism of film growth by applying the mixture of $Na_2Cr_2O_7$ and MgF_2 on pure Mg and AZ91D substrates. A number of chemical conversion coatings such as cerium oxide, stannate, galvanized black anodizing and chromate were generated on Mg alloy AZ31B and their performance was evaluated for environmental stability (humidity, thermo vacuum performance and thermal cycling), optical properties (solar absorbance and infrared emittance) and corrosion resistance. The anticorrosion properties of coatings were observed in the order as: galvanized black anodizing > chromating > cerium oxide > stannate coating [13]. Pommiers-Berlin et al. [14] have carried out several pre-treatments on Mg alloy EV31A followed by CCC and the detailed study of mechanism of chromate based coatings was carried out using electrochemical and spectroscopic techniques. However, since 2017, the usage of Cr (VI) compounds is restricted under the Registration, Evaluation, Authorization and Restriction of Chemicals (REACH) regulation due to their carcinogenic nature to living beings.

Most widely used conversion coatings as a replacement to hexavalent chrome-based coatings on Mg alloy are phosphates, permanganates, rare earth-based compounds and molybdates. Saji [7], Gray and Luan [8], Hornberger et al. [15], Chen et al. [16] and Pommiers et al. [17] have reviewed wide number of articles based on aforesaid conversion coatings. Eco-friendly vanadate solution based conversion coatings were generated on Mg alloy AZ31 with variable concentration and pH conditions. Electrochemical impedance spectroscopic (EIS) and cyclic voltammetry studies revealed that, the localized anticorrosion properties of coatings were improved with 50 g/L concentration of vanadate [18]. HCl pre-treatment was carried out on pure Mg and Mg alloys, AZ91D and AM50 substrates followed by generation of conversion coating in bath containing solution of cerium salts and hydrogen peroxide. The coatings were found to be more homogeneous, adherent, diffused and having more corrosion resistance with acid treatment than the one without acid treatment [19]. Hu et al. [20] pretreated AZ91D substrates with molybdate conversion coatings followed by generation of a three-layered composite sol-gel coating stack. The molybdate conversion coatings were developed with variation in parameters such as pH, immersion time and bath temperature. Anticorrosion properties of coatings

were evaluated using EIS and polarization studies and it was found that the conversion coating with 7.3 g/L concentration of molybdate solution at pH 5 for 30 min at 30 ^{o}C gave better protection. Saji [21] has reviewed conversion coatings based on eco-friendly, economic and biodegradable organic compounds. These organic conversion coatings are classified based on phytic acid; polyphenols, hydroxy benezene/benzoic acids; aliphatic carboxylic acid (oxalates, citrates, etc.) and other approaches where organic compounds are used as additives in inorganic conversion coatings, chitosan-based and silane-based coatings. Jian et al. [22] developed Ce/Mn conversion coatings on Mg alloy EV31 with $Ce(NO_3)_3$ as corrosion inhibitor and $KMnO_4$ as oxidizing agent. Electrochemical studies and salt spray analysis for shorter (48 h) and prolonged durations (336 h) showed that conversion coating generated with 30 s of exposure gave better barrier and self-healing properties due to the formation of passive cerium oxide film with thickness of around 200-400 nm. Cai et al. [23] have generated micro-arc oxidation (MAO) coating over Mg alloy AZ91D pretreated with Ce-based conversion film. Electrochemical measurements have revealed that, MAO coating with Ce-based conversion layer gave better corrosion resistance than only MAO coating and only Ce-based conversion coating due to high Pilling-Bedworth ratio, which is between 1 and 2 that corresponded to protective oxide film of Ce. Several other conversion coatings have been implemented for protecting Mg alloys with number of additives, additional topcoat of sol-gel coating and variations in operating parameters [24-30].

2.1.2 Anodization

Anodization is carried out by applying higher voltage to the substrate immersed in an electrolytic bath such as electrolytic solutions of silicate, fluoride or phosphate similar to that in conversion coatings. In this case, substrate surface is forced to react with the electrolyte, which results in the formation of complex coating in various steps. After generation of thick metal oxide film, arc formation takes place at substrate-solution interface, when dielectric strength of the oxide layer is equal to the applied voltage. The resultant heat of arc formed, decomposes additive precursors in the electrolyte, thereby forming oxide layer deposition of these precursor elements. These coatings are considered as more eco-friendly than conversion coatings, but with higher capital and running costs [31, 32].

Various commercial processes such as Anomag, Dow 17, HAE (developed by Harry A. Evangelides), Magoxid-coat, Tagnite surface treatment, galvanic anodizing and Cr-22

treatment have been used to generate anodized coatings [8]. Barbosa et al. [33] have generated oxides and hydroxides films of Mg by anodization in NaOH solutions of various concentrations (0.1, 1 and 4 M) with variation in applied voltage (30-90 V) and current density (20-1500 mA/cm^2). The coatings are comprised of thin inner barrier layer and outer crystalline porous layer of hydroxides and oxides of Mg, respectively. A bilayer coating consisting of anodized film generated in electrolytic solution of sodium silicate and sodium borate and self-assembled nanophase particles (SANP) film was generated on Mg alloy AZ31B by Guo and An [34]. It was observed that the bilayer film consists of loose layer of SANP with Mg-O-Si covalent bonds and Si-O-Si bonds having high density and dense layer of MgO and magnesium silicate. This bilayer withstood for 354 h of exposure to 0.029 wt % NaCl solution as analysed from EIS studies. Lopez et al. [35] developed protective film by anodization on Mg alloy AZ91D in sodium molybdate solution (0.05-0.25 M) under inert atmosphere with pH 9 at 20 ^oC. The coatings were comprised of hydroxides and oxides of Mg and Mo with traces of alumina as observed from X-ray Photoelectron Spectroscopy (XPS) and X-ray Diffraction (XRD) analyses. Electrochemical measurements indicated that coatings were found to give better corrosion protection for 12 h in Ringer solution (consists of MoO_4^{2-}) with 0.25 M concentration of molybdate at 1 V for 45 min. Alkaline electrolytic solution comprised of silicate and borate along with 1H-benzotriaole as a corrosion inhibitor (0-10 g/L) was used by Guo et al. [36] to generate anodized coatings on AZ31B substrates. It was observed that, the anodized surface became more uniform and compact (with decrease in pore diameter and number of pores) with increase in benzotriazole concentration from 0 to 5 g/L. However, further increase in concentration increases the pore diameter and surface became uneven again. Further, electrochemical and weight loss measurements indicated that anodized coatings with 5 g/L benzotriazole gave better anticorrosion properties owing to the uniform, compact and thick film. A number of studies have been carried out with anodization in various electrolytic solutions, by variation in operating parameters and with several additives [37- 40].

2.1.3 Plasma Electrolytic Oxidation (PEO)

PEO also referred to as MAO or spark anodizing is a technique wherein anodization is carried out at applied voltages exceeding the dielectric breakdown potentials of the oxide films formed. The higher voltages applied during the processing results in the microscopic discharges at the interface of substrate and electrolyte, thereby changing the structure of oxide film formed. PEO is generally performed in electrolytic solutions containing

phosphates, silicates or aluminate with generated coatings consisting of amorphous and crystalline phases of corresponding Mg compounds. The thickness of the coatings can be increased up to 50-100 μm at a growth rate of 1-5 μm/min. A thin barrier film generated at substrate-coating interface is composed of two to three-layered structure of few hundreds of nanometres. PEO coatings have limitations such as uncontrolled porosity, poor adhesion strength and reduced mechanical properties [32, 41].

Srinivasan et al. [42] have developed PEO coatings on AM50 substrates with 30 mA/cm^2 current density for 15 min at 10 ^oC in two different electrolytic solutions of KOH; Na_3PO_4 and $Ca(OH)_2$; Na_3PO_4. EIS measurements in 0.1 M NaCl solution have shown that, after half an hour, the corrosion resistance of both coatings was almost similar but with the increase in exposure durations up to 50 h, KOH based coatings were completely degraded, whereas $Ca(OH)_2$ based coatings did not exhibit any significant degradation. In another approach, PEO coatings were developed by Mohedano et al. [43] on AM50 Mg alloy using alkaline silicate solutions at constant voltage for 10 min. Post-treatment was carried out on PEO coatings with $Ce(NO_3)_3$ solutions of different concentrations (3 and 10 g/L) for different durations of time (20 and 180 min). EIS results in 0.5 wt % NaCl for 3 days have shown that higher immersion time in $Ce(NO_3)_3$ solutions (180 min) and higher concentration (10 g/L) lead to better corrosion resistance. MA8 Mg alloy substrates were used by Gnedenkov et al. [44] for generating PEO coatings using sodium orthosilicate and sodium fluoride which were then post-treated with 8-hydroxyquinoline (HQ) (3 g/L) and NaOH solution at pH 12-12.5. The comparative study of bare substrates, PEO coatings, and PEO coatings with HQ using electrochemical measurements in 3 wt % NaCl indicated that coating with inhibitor has shown enhanced anticorrosion properties. Chen et al. [45] have generated composite coatings of PEO and sol-gel matrix on Mg alloy AZ91. PEO coated substrates were exposed to the solutions of sodium-based salts of glycolic acid, 4-aminosalicylic acid and 2, 6-pyridinedicarboxylic acid at basic pH followed by coating with hybrid sol-gel matrix. EIS and Scanning Vibrating Electrode Technique (SVET) measurements have revealed that all three salts have shown barrier property and self-healing ability for long-term exposure to corrosive medium. MAO coatings generated on AZ31 substrates by Guo et al. [46] were immersed in gel solution comprised of $Ce(NO_3)_3$ and acrylamide monomer under vacuum. Electrochemical studies and salt spray tests have shown that the coatings provided self-healing ability in the scribed area and restricted the pit formation owing to the inhibition effect of Ce^{3+} ions and adsorption of polyacrylamide gels. MAO coatings with and without inclusion of nanoparticles (ZrO_2, TiO_2 and Al_2O_3)

were generated by Mandelli et al. [47] on AM60B Mg alloy followed by sealing with organo-functional silane coating. The adhesion strength and scratch hardness was found to be better for MAO coatings comprised of ZrO_2 and Al_2O_3 nanoparticles. Composite coatings with silane post treatment provided better corrosion protection as observed from immersion tests and electrochemical studies. Zhang et al. [48] have dispersed cationic Ce^{3+} loaded sodium zeolite microparticles in epoxy resin and then coated on AZ31 substrates treated with PEO. Energy dispersive spectroscopy (EDS) and energy dispersive X-ray fluorescence (EDXRF) was used to evaluate exchange capacity of Na-zeolite with Ce^{3+}, whereas the release profiles of Ce^{3+} were examined at different pH for 20 h using inductively coupled plasma optical emission spectrometer (ICP-OES). EIS studies depicted that, Ce^{3+} exchanged zeolite has shown self-healing ability in 0.5 M NaCl solution after 7 days. Liu et al. [49] have loaded corrosion inhibitors such as $Ce(NO_3)_3$, Na_3PO_4 and $NaVO_3$ into MAO coatings generated on AM60 by atmospheric and vacuum impregnation. This was followed by topcoat of water-based paint mixed with epoxy coating. It was observed that vacuum impregnation gave higher inhibitor loading efficiency, thereby showing better self-healing ability for Na_3PO_4 as compared to other inhibitors. Liu et al. [50] generated MAO coatings vacuum impregnated with Na_3PO_4 followed by topcoat of 2-mercaptobenzothiazole (MBT) dispersed water-based paint on Mg alloy AM60. Electrochemical studies have revealed that coatings consisting of dual corrosion inhibitor gave highest corrosion resistance owing to the absorption of MBT on the hydroxide and phosphate films of Mg formed after exposure to corrosive medium. Li et al. [51] have generated MAO coating on AZ31 substrates followed by development of Na-EDTA based nanosheet-structured Mg-Al LDH coating at very high pH of 13.76. Electrochemical measurements revealed four orders of magnitude higher current density than that of composite coatings of LDH and MAO while the coating remained crack-free with stable nanosheet like structure of LDH after prolonged exposure. Number of other studies [52-57] based on PEO have been carried out by variation of operating parameters and studied their effect on coating properties, post-treatment with another coating technique or by sealing with rare earth elements and monomers.

2.1.4 Electrophoretic deposition or E-coatings

Electrophoretic deposition (EPD) is a colloidal process based on the suspension of particles and the driving force for the process is charge on the particle and particle mobility under the influence of applied potential or current. This technique has been implemented

for nanosize zeolite membrane, silica thick film, metal substrates coated with hydroxyapatite in biomedical applications, gas diffusion sensors and electrodes, multilayer composites, carbon nanotubes films, oxide nanorods, etc. The major disadvantage of this process is that the aqueous electrolytic solution cannot be used as hydrogen and oxygen evolution at the electrodes affects the coating quality [58].

A. Shahriari [59] used EPD for generating alumina interlayer on AZ91D using alumina particles and then for topcoat of 3 mol % yttria stabilized zirconia (YSZ). In this case, voids in the aluminum interlayer were filled by YSZ particles provided barrier film that prohibits dissolution of Mg and permeation of corrosive media. Being denser coating, YSZ coating provided better anticorrosion properties in 0.6 M NaCl with Al interlayer than without Al interlayer, as observed from EIS studies. SiO_2 and TiO_2 nanoparticles dispersed in 0.08 M iodine and acetone as a solvent were deposited on AZ91D by EPD. The coated samples were then anodized in alkaline Na_2SiO_3 solution containing SiO_2 and TiO_2 nanoparticles. Scanning Electron Microscopy (SEM) and XPS analyses showed that the coatings are composed of composite oxides of Ti-Si-Mg, which play a vital role in corrosion protection of AZ91D as observed from polarization results in 0.1 M KCl [60]. Fluoride conversion treatment on AZ91 was carried out by Rojaee et al. [61] followed by MAO in alkaline Na_2SiO_3 solution for 30 min. Further, EPD was conducted by dispersing 50 g/L hydroxyapatite powder in methanol in two steps; first deposition at 50 V/cm^2 for 3 min and second one at 30 V/cm^2 for 5 min. The coated substrates were dried at room temperature for 30 min after each step, to ensure formation of dense coatings without cracks during drying. Polarization studies in simulated body fluid (SBF) for 1 h revealed that hydroxyapatite based coatings showed higher corrosion resistance. AZ91D substrates were coated with EPD in a suspension consisting of YSZ and stabilizing agents such as polyvinyl alcohol and cetyltrimethyl ammonium bromide (CTAB) by Amiri et al. [62]. Changes in thickness and bonding strength were observed with variation in YSZ particle concentration, current density and deposition time. EIS, polarization studies (30 min) and immersion tests (7 days) in SBF have shown that coatings were capable of providing barrier to corrosive ions. A number of other composite coatings have been generated on Mg alloy using EPD in conjunction with other methods in order to improve biocompatibility in implants and corrosion resistance [63-68].

2.1.5 Epoxy coatings

Generation of water borne coatings or coatings with low content of volatile solvents has been considered as important factor in industrial sector. One of the most widely used eco-

friendly coating technique is epoxy coatings in which the epoxy resins acts as binder to the organic coatings. Epoxy coatings generally use hardeners such as polyamines or polyamides, which form coatings with rigid network because of resin chain cross-linking. These coatings have great potential to protect metallic substrates due to their low permeability to corrosive medium and better resistance to abrasion and erosion. The major limitations of epoxy coatings is balancing the mechanical performance, barrier properties and aesthetic property after aging [69, 70].

Epoxy coatings have been widely used for hindering corrosion of steel and Al alloys in offshore industries and aerospace industries, respectively. However, epoxy coatings does not meet industrial demands very effectively for protecting Mg alloys from corrosion. Hence, the important aspect to use them for corrosion protection of Mg alloys is to improve their mechanical and barrier properties by using various additives [32]. Lu et al. [71] generated Mg-rich epoxy coating by addition of pure Mg particles into epoxy coating on AZ91D. These coatings have shown better corrosion resistance as compared to epoxy coating without Mg particles as observed from EIS results. The Open Circuit Potential (OCP) measurements have shown that higher anticorrosion properties are attributed to cathodic protection effect of the Mg-rich coatings. Further, Lu et al [72] generated silane pretreatment film on AZ91D substrates before applying Mg-rich epoxy coating. Si-O-Mg covalent bond formed between silane film and Mg substrate improved adhesion properties of coatings. The Macho test and EIS studies revealed that Mg-rich epoxy coating prohibited diffusion of electrolyte to the substrates and better corrosion resistance up to 3800 h. Anti-corrosion coatings based on epoxy-resin dispersed with Fe_2O_3 nanopowders (2.5 wt %, 5 wt % and 7.5 wt %) were developed by Jin et al. [73] on AZ91D substrates and cured at room temperature. Immersion and potentiodynamic polarization measurements in 0.6 M NaCl solution for 25 days indicated that 5 wt % nanopowder induced coatings have shown more positive potential and least weight loss after 25 days. Chen et al. [74] generated MAO coatings on AZ31 substrates using alkaline silicate solutions, pre-treated with bis-silane and top coated with epoxy coatings. In this case, bis-silane is expected to react with substrate and the epoxy, resulting in the formation of more dense and hydrophobic films. Electrochemical measurements and immersion tests for 644 h and 120 h in 0.6 M NaCl solution indicated that, silane pretreated substrates have shown better anticorrosion properties. Yan et al. [75] have used eco-friendly methionine as green corrosion inhibitor intercalated into Mg-Al LDH to generate epoxy-based self-healing coatings on AZ91 substrates at different pH conditions (pH 5, 7 and 9). The inhibition efficiency of

methionine was evaluated by exposing bare substrates to LDH extraction solution using electrochemical measurements in 0.06 M NaCl solution for 60 h. The self-healing ability of epoxy coatings comprising of methionine intercalated LDH was examined by electrochemical measurements for 38 days in 0.6 M NaCl solution and found that, the anticorrosion ability of coatings enhanced with the exposure durations because of adsorption of methionine released from LDH on the AZ91 surface. Considering the biocompatibility of Mg alloys, Li et al. [76] have summarised recent development on polymeric coatings based on their strategy of synthesis, anticorrosion properties and biocompatibility. The polymeric coatings were mainly based on synthetic and natural polymers like polylactic acid, poly (lactide-co-glycolic) acid, polycaprolactone, polydopamine, chitosan and collagen. It was observed that most of the studies were focussed on one or two properties, whereas in order to provide better adhesion, lower permeability and controlled degradation rate, multifunctional composite coatings are required. Extensive research has been carried out on corrosion protection of Mg alloys using epoxy coatings [77-83]. It has been observed that, additives such as nanoparticles have been found useful for improving mechanical and barrier properties of coatings. However, negligible research has been found regarding addition of corrosion inhibiting additives with their effectiveness for Mg alloys and compatibility with epoxy coatings.

2.1.6 Sol-Gel Coatings

Being a chemical synthesis method, sol-gel process is widely utilised in synthesis of inorganic materials such as ceramics and glass because of its low operating temperature. In 1842, French chemist J. J. Ebelmen carried out heating of hydroxide of uranium for the synthesis of uranium oxide. However, the approach could not last long due to lengthy heating and aging process [84]. Later, in 1950s, R. Roy et al. [85] manufactured sol-gel silicate powders by changing conventional sol-gel process into new ceramic oxides synthesis. In 1971, synthesis of low bulk density silica was patented which involves hydrolysis of tetraethoxysilane (TEOS) with cationic surfactants. During 1980s, hybrid organic-inorganic materials were synthesized using sol-gel process, which gained attention in fields of polymer chemistry, ceramics, inorganic-organic chemistry and development of many other hybrid materials [86].

The sol-gel process can be divided into three types based on the precursors like metal alkoxides, metallic salt aqueous solutions and organically modified silanes. The use of

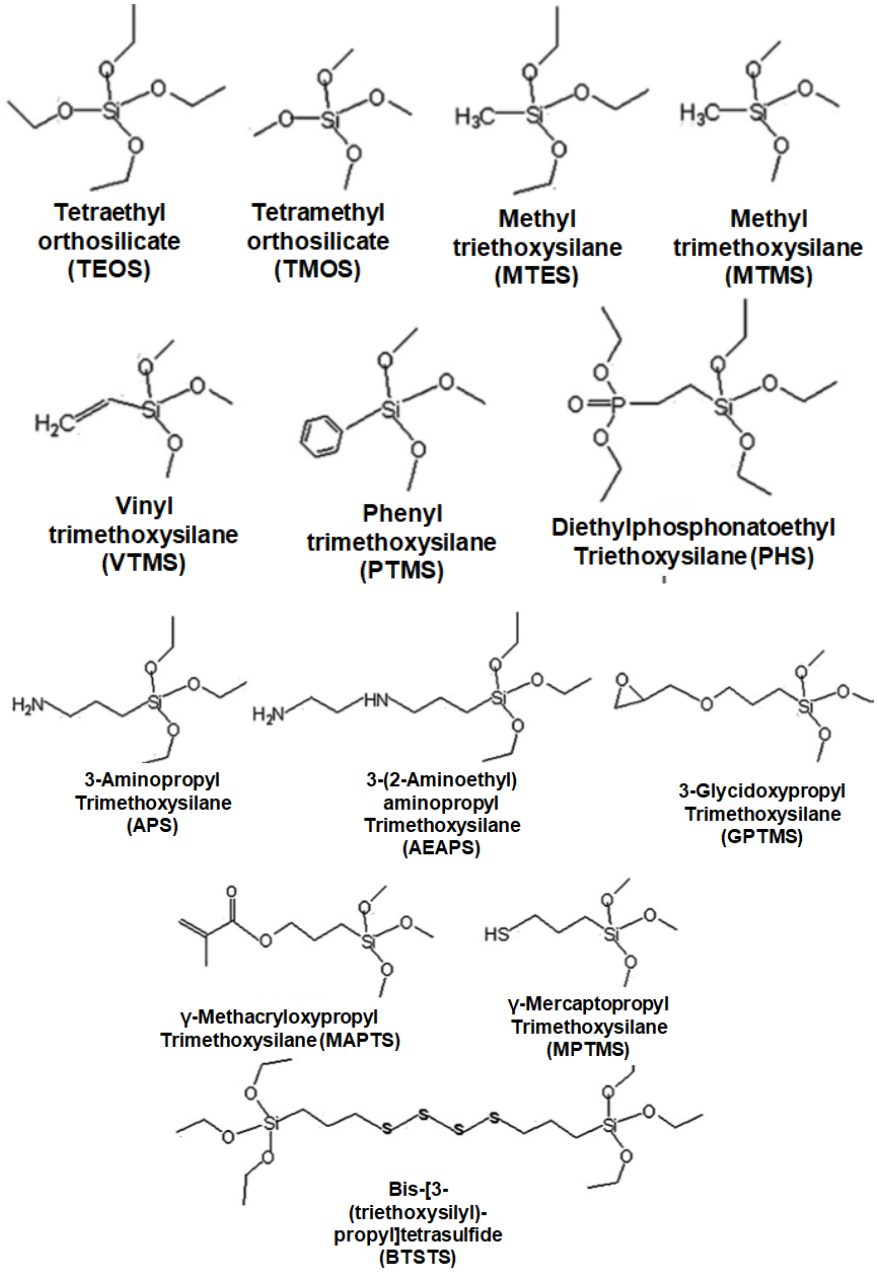

Figure 2.2: Commonly used alkoxy silane precursors for development of sol-gel coatings

metal salts precursors is limited due to the complex procedure. As mentioned in chapter-1, hydrolysis and condensation processes of sol-gel are dependent on parameters such as pH, temperature, hydrolysis and condensation rate of precursors, rate of oxidation, mixing method, concentration and nature of anions, etc. Wide number of precursors have been used for coating generation on Mg alloys as shown in Fig. 2.2.

In general, sols are synthesized by two methods; organic and inorganic. The organic approach involves alcoholic or organic solvent-based solutions of metal or metalloid alkoxides, whereas inorganic approach includes network evolution through the synthesis

of colloidal solutions of oxides. These dense sol-gel coatings with highly cross-linked structure show better barrier properties against corrosion attack. They induce better adhesion properties to metal substrates with covalent bond formation and attain better organic topcoat compatibility [32].

As mentioned in chapter-1, three coating techniques like dip coating, spray coating and spin coating have been widely used for generation of coatings. In case of dip coating technique (Fig. 2.3.a), the substrate is immersed in the sol and then taken out at a specified withdrawal speed. The coating thickness is dependent on viscosity of sol, withdrawal speed and the solid content of sol. The coatings experiences six forces during withdrawal: (i) gravity, (ii) viscous drag force by substrate on liquid, (iii) surface tension force, (iv) boundary layer liquid inertial force, (v) gradient of surface tension and (vi) conjoining or disjoining pressure (for films with thickness less than 1 μm). Organic lacquer industries widely use spray coating technique (Fig. 2.3.b). The coatings can be generated by manual spray gun or by automated conveyor. The coating thickness can be varied by number of spray passes and distance between spray nozzle and substrate. In spin coating technique (Fig. 2.3.c), the substrate rotates around the axis perpendicular to the coating area with continuous drops of sol falling from top at the centre of substrate. In this, centrifugal draining makes the deposited film thinner and becomes uniform by the balancing of centrifugal force and viscous force [87].

Sol-gel coatings have been broadly classified into three types as metal oxide coatings, hybrid organic-inorganic coatings and composite sol-gel coatings.

a) Metal oxide coatings:

Metal oxides such as ZrO_2, SiO_2, TiO_2, CeO_2, Al_2O_3, etc. are well known to provide better chemical stability and effective barrier properties to the coatings. SiO_2 is capable of improving oxidation and corrosion resistance under acidic conditions with variation of temperatures because of its high chemical and thermal resistance. ZrO_2 with its high thermal expansion coefficient, reduce formation of cracks during high temperature curing and its higher hardness and better chemical stability, gives better anticorrosion properties.

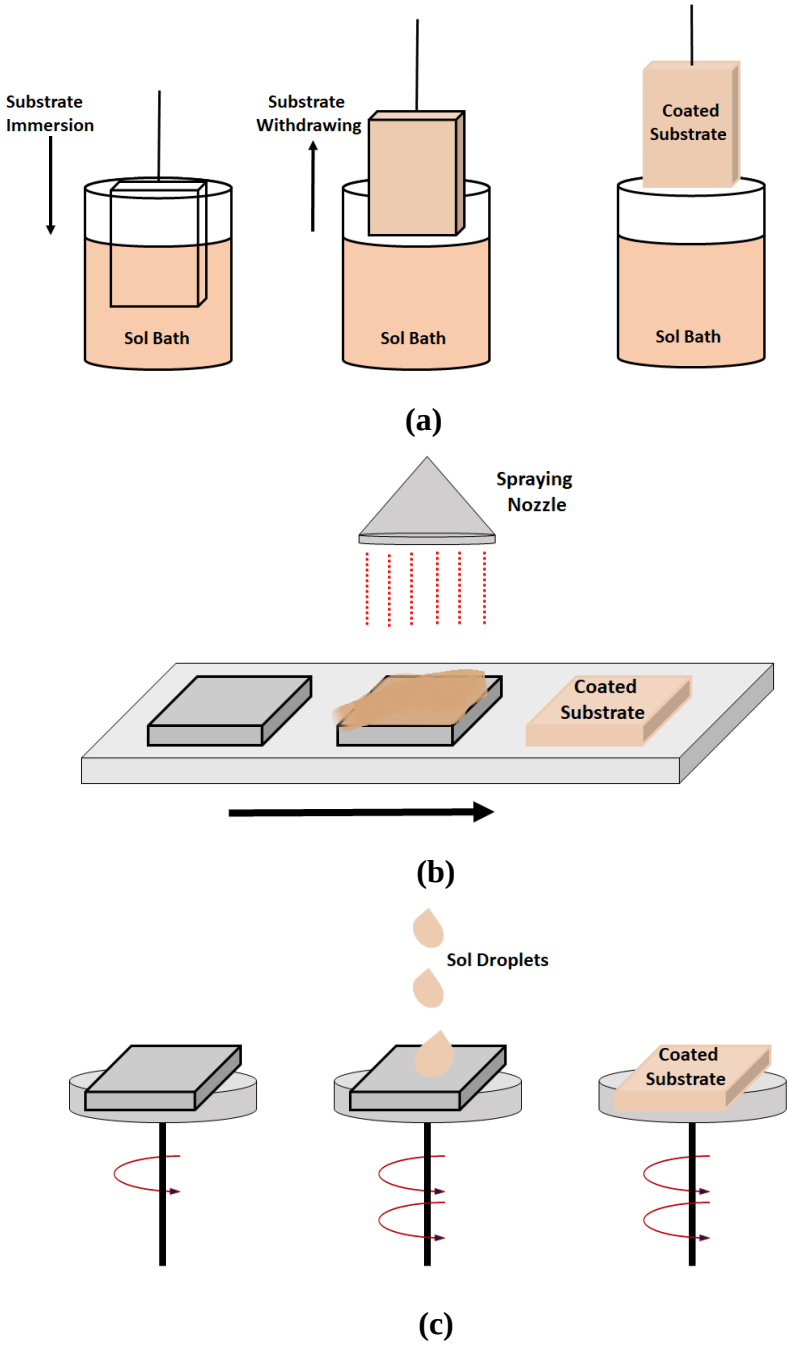

Figure 2.3: Graphical representation of coating techniques; (a) dip coating, (b) spray coating and (c) spin coating

Al_2O_3 is considered as an ideal material for anticorrosion coatings because of its insulating property with low conductivity for transmitting electrons. Low electron conductivity, better chemical stability and better heat resistance makes TiO_2 an ideal material for corrosion protection coatings. However, TiO_2 based sols have low pH resulting in poor adhesion properties on Mg alloys, as Mg alloys gets eroded at acidic pH [86].

The sol-gel coatings based on CeO_2 and ZrO_2 were prepared by Phani et al. [88] on magnesium alloys AZ91D (machined, as-casted and sand-blasted) and AZ31 (rolled and

machined) with multiple dip coatings layers along with intermediate heating at 125 ^{o}C for 15 min and final annealing at 180 ^{o}C for AZ91D and 140 ^{o}C for AZ31. The annealed coatings were observed to have dense, continuous and amorphous structure with better adhesion properties. Annealed coated AZ91D (as-casted and machined) and AZ31 (machined) substrates have shown better corrosion resistance as observed from salt spray tests of 96 h. Ceria-based sol-gel coatings were prepared by Han et al. [89] on AZ91 substrates with variation in parameters such as fluorinating pretreatment, inter-layer heat treatment, number of coating layers and sintering temperature. It was observed that, fluorinated triple layer coating without inter-layer heat treatment sintered at 350 ^{o}C was found to give least corrosion current as observed from polarization results. Sol-gel based ceramic film comprising nanocrystalline ZrO_2 has been developed on AZ91D by Li et al. [90] using dip coating technique. The results have shown that the coatings were found to give better corrosion resistance and more positive potential owing to tetragonal phase of ZrO_2 as observed from EIS and polarization results. Zhong et al. [91] have generated phytic acid conversion coatings followed by alumina based silane coatings on AZ91D substrates. The coatings were sintered at various temperatures from 120 ^{o}C to 380 ^{o}C. It was observed that, at 280 ^{o}C coatings have shown transformation from amorphous to crystalline phase and showed better corrosion resistance with sintering at 380 ^{o}C. Composite ceria/titania based sol-gel coatings were developed by Fan et al. [92] on AZ91D substrates with inner layer of CeO_2 in order to avoid direct contact of acidic pH TiO_2 sol with substrate. Multiple layers of each of CeO_2 and TiO_2 were generated to evaluate effect on hydrophilicity and corrosion resistant properties of coatings. EIS and polarization studies in 0.6 M NaCl revealed better anticorrosion ability and hydrophilicity with two layers of TiO_2 and single layer of CeO_2. Several research groups have generated metal oxide based sol-gel coatings on various Mg alloys such as AZ91D, ZE41 and AZ80 [93-97].

b) Hybrid organic-inorganic coatings:

Pure inorganic coatings come with the limitations like brittle and thick films, formation of cracks, requirement of high temperature for curing, etc. Hence, incorporation of organic species into the inorganic networks to generate hybrid coatings can overcome these limitations.

Hybrid organic-inorganic coatings comprised of phosphonate functionalities were generated by Khramov et al. [98] for corrosion protection of Mg alloy AZ31B by dip

coating technique. TEOS along with diethyl phosphonatoethyl-triethoxysilane (PHS) were used in different molar ratios (1:1 to 4:1) for synthesis of hybrid sol. EIS and polarization measurements in dilute Harrison's solution (0.35 wt % $(NH_4)_2SO_4$ and 0.05 wt % NaCl) indicated that, the anticorrosion performance of coatings improved with addition of PHS into TEOS with 1:1 ratio. However, with the increase in molar ratio, the anticorrosion property of coatings decreased as revealed from Scanning Kelvin Probe (SKP) analysis. Crack-free hybrid sol-gel coatings were developed by Qian et al. [99] on Mg alloy AZ31B using dip coating technique owing to the addition of cross-linking agent. EIS and polarization studies in Harrison's solution after 96 h revealed that, the barrier property of coatings decreased because of hydrolysis of Mg-O-Si bond under aqueous conditions at the interface of substrate and coating. Mg alloy AZ31 substrates were coated with hybrid sol consisting of TEOS and GPTMS in a molar ratio of 3:1 by Hernandez-Barrios [100]. The barrier property of coating was evaluated based on the variation of parameters such as catalyst concentration (acetic acid; 2.5, 5 and 10 vol %), immersion time (15, 30, 60 and 120 s) and aging time of sol (0 to 28 days). Potentiodynamic polarization measurements in 0.6 wt % NaCl solution for 1 h have shown that, catalyst concentration of 5 vol % or lower with immersion time of 30 s or less gave homogeneous and continuous coatings free of corrosion products at interface. Further, aging time of 3 and 6 days resulted in denser SiO_2 network, lower corrosion product formation and better adhesion strength of substrate and coating. Mg alloys AZ31 and AZ61 were thermally treated by Diaz et al. [101] at 200 ^oC for 1 h prior to generation of coatings with hybrid sol of MAPTS and TMOS (4:1 molar ratio) by dip coating technique. Surface morphology of heat treated and coated substrates have shown dense, crack-free and homogeneous coatings as compared to those without heat treatment in case of AZ61. Lower O: Si atomic ratio observed from EDS analysis in case of heat treated and coated AZ61 indicated that, SiO_2 network formed on the substrate is not hydrolysed even after increase in local pH. This resulted in better barrier properties of coatings on heat treated AZ61 as observed from EIS measurements. However, this phenomenon was not observed on coated and non-heated AZ61 and on coated, heated and non-heated AZ31 substrates. Four different coating systems consisting of hybrid organic-inorganic, inorganic, zirconium containing and cerium containing coatings were generated by Barranco et al. [102] on Mg alloy AZ91 with precursors such as TMOS, diethoxydimethylsilane (DEDMS), zirconium tetrabutoxide and cerium nitrate hexahydrate. One set of substrates were directly characterized, whereas other set was characterized with additional topcoat of organic coating. EIS measurements in Na_2SO_4

solution for 7 days have shown that, hybrid coatings gave better barrier properties than inorganic coatings alone. Hybrid coatings incorporated with Ce^{3+} imparted better corrosion resistance with topcoat and localised EIS (LEIS) studies revealed that the protection continues for 7 days even after generation of defects into the coatings. Eco-friendly hybrid silane-based coatings were developed by Dalmoro et al. [103] on AZ91 substrates using co-monomers; TEOS and MTMS; and phenyl phosphonic acid (PhPA) & ethylenediamine tetramethylenephosphonic acid (EDTPO) as adhesion promoters. Some of the substrates were pretreated with alkaline phosphate solution, acetic acid and hydrofluoric acid for providing good and stable passivating hydroxide film. EIS measurements in 0.29 wt % NaCl solution for 72 h indicated that addition of EDTPO and PhPA molecules has shown catalytic effect to cover the complete substrate and remove the defects generated by pretreatment. The improved barrier properties of EDTPO based coatings corresponded to multiple bonds formed with phosphonic group, silica network and oxide/hydroxide layer. Pagliaro et al. [104] have reviewed many articles corresponding to hybrid sol-gel coatings with organically modified silicates (ORMOSIL®), silica/polymer composites and nanomaterials. Two types of hybrid coatings were generated on Mg alloy AZ31B substrates by Lamaka et al. [105] with GPTMS as organic precursor and zirconia and titania based inorganic precursors. Tris(trimethylsilyl) phosphate (tTMSPh) is bi-functional compound which forms chemical bonds with substrate, thereby improving the adhesion properties and gets polymerized with organic component without destroying its barrier properties, was added to hybrid sol. EIS studies have shown that titania based coatings with tTMSPh, imparted better barrier properties for 2 weeks in 0.029 wt % NaCl solution. Samadianfard et al. [106] have dispersed oxidised fullerene (OF) in hybrid sol-gel matrix that was coated on Mg alloy AM60B. EIS measurements showed significant enhancement in the anticorrosion properties of coatings with OF nanoparticle concentrations between 200-500 mg/L. Ashraf et al. [107] have generated hybrid sol-gel coating dispersed with TiO_2 nanoparticles and various amino acids such as serine, alanine, cysteine and arginine for corrosion protection of AZ91. EIS and polarization studies have shown that, presence of cysteine, alanine and serine along with TiO_2 nanoparticles in the coating have revealed enhanced corrosion protection. Fernández-Hernán et al. [108] have developed multilayer coatings for corrosion protection of AZ31B, which are composed of primary layer of sol-gel coating and secondary film of sol-gel coating dispersed with multiwall carbon nanotubes and functionalised graphene nanoplatelets. Electrochemical studies and hydrogen evolution tests have revealed that, multilayer coating system consisting of

functionalised graphene nanoplatelets have shown best corrosion protection with lowest release of hydrogen. Rosero-Navarro [109] and El-Hadad [110] also generated hybrid sol-gel coatings on Mg alloys and evaluated their barrier properties.

c) Composite sol-gel coatings:

Sol-gel coatings are widely used as composite coatings, where they are combined in the form of topcoat and pretreatment layer with conversion coatings [20, 26] and epoxy coatings [72, 77, 79-81, 111], respectively. Being porous in nature, MAO and anodized coatings are generally top coated with sol-gel coatings or nanoparticles synthesized using sol-gel process for enhancing the anticorrosion ability of coatings. This also increases the shelf life of coatings by addition of number of active materials in sol-gel coatings.

Lamaka et al. [112] have anodized Mg alloy ZK30 substrates in alkaline phosphate solution and then immersed in 0.005 M aqueous solutions of $Ce(NO_3)_3$ and HQ for 30 min. The substrates were then dip coated with hybrid sol made up of GPTMS and titanium iso-propoxide (2:1 by volume). The EIS and SVET measurements in 0.29 wt % and 0.029 wt % NaCl solution revealed that, anticorrosion properties of composite film with HQ were equivalent to that with only anodized film, whereas the composite film with Ce^{3+} showed enhanced barrier properties owing to the formation of passive and insoluble cerium hydroxides. Ivanou et al. [113] used an alkaline silicate-fluoride solution to generate an oxide layer using PEO followed by immersion in 0.069 wt % aqueous inhibitor solution of 1,2,4-triazole for 15 sec. The sol synthesized using GPTMS, PTMS and titanium iso-propoxide was used to coat the PEO coated substrates and some non-PEO, acid etched substrates. EIS and SVET measurements in 0.51 M NaCl solution for 30 days have shown better corrosion protection with corrosion inhibitor impregnated coatings. These coatings behave as effective self-healing coatings, as PEO layer act as inhibitor reservoir in which inhibitor is secured closer to the substrate, where corrosion initiates and top layer of sol-gel coatings controls its leaching. MAO coatings were developed by Shang et al. [114] on Mg alloy AZ91D substrates in alkaline aluminate solutions consisting of small quantities of montmorillonite clay particles and acacia gum. Further, a top coat comprising three layers of sol-gel film containing SiO_2-ZrO_2 composite was generated. Electrochemical measurements have shown that effective barrier properties were achieved with sol-gel films that can be used to block the pores of MAO coatings. Laleh et al. [115] used alkaline aluminate solution to generate MAO coatings on AZ91D substrates followed by dip coating of sol-gel matrix synthesized from tetra-n-butyl orthotitanate for sealing the pores of MAO

coating. The effect of curing temperature was analysed for the three-layered sol-gel coating at 150 ^{o}C and 350 ^{o}C. The coatings heat treated at 350 ^{o}C have shown nano-structure morphology with less porosity and found to give more corrosion resistance than coatings with amorphous morphology. Apart from this, sol-gel coatings are widely used for generating coatings for biomedical implants because of their less toxicity and biocompatibility [61, 64, 116].

The above-mentioned conventional coating methods provide barrier properties that restrict or delay the contact between the substrate and corrosive environment. Adding various functionalities into these coatings by dispersing corrosion inhibitors, generating top coats with another coating method, sealing with corrosion inhibitor solution and/or generating multiple layers for increased thickness can impart a more active corrosion protection that prohibits progress of corrosion. In spite of these additives, coatings cannot provide corrosion protection, if there is a mechanical damage to the coated surface or diffusion of corrosive media through porous coatings. In short, such coatings cannot provide prolonged corrosion protection to impart longer shelf life to metallic substrates. In order to overcome these drawbacks or limitations, the concept of self-healing coatings has come into picture.

2.2 Self-healing coatings for Mg alloys

Self-healing coatings are smart protective coatings, where the active materials like corrosion inhibitors, monomers, catalysts, dyes, etc. are confined into the containers/carriers for storage to avoid disadvantages such as uncontrolled release, compatibility with coating matrix, leaching of inhibitors, etc. The active agents encapsulated in the carriers are released in response to an external trigger like mechanical stress, change in local pH, exposure to aggressive ions or UV radiation. In this context, limited studies have been carried out so far in the development of self-healing coatings on Mg alloy, which will be discussed in this section.

2.2.1 Conversion coatings with self-healing ability

Eco-friendly vanadate solution based conversion coatings were generated by Hamdy et al. [18] on Mg alloy AZ31 with variable concentrations and pH conditions. EIS and cyclic voltammetry measurements in 0.6 M NaCl solution for 7 days explored that, the localized anticorrosion properties of coatings were improved with 50 g/L concentration of vanadate. Hamdy et al. [27] used diluted tin oxide solution of various concentrations to generate

conversion coatings on AZ91D at pH 12.9. Some of the substrates were pretreated with acidic pickling and alkaline etching to evaluate the effect of surface modification. Electrochemical measurements in 0.6 M NaCl solution revealed that, stannate concentration above 50 g/L has shown adverse effect on corrosion resistance and surface pretreatment did not offer enhanced effect on anticorrosion properties of coatings. Stannate concentration of 50 g/L has shown better hindrance to localised corrosion and microcracks. Molybdate intercalated hydrotalcite coating was generated by Zeng et al. [117] on AZ31 substrates by co-precipitation and hydrothermal process at 125 ^{o}C for 36 h in Teflon-lined autoclave. The hydrogen evolution rate of coated substrates (2.2E-2 ml/cm^2.h) after 144 h in 0.6 M NaCl solution was found to be much lower than that of bare substrates (4.2E-3 ml/cm^2.h). Polarization studies indicated that the corrosion current of coated substrates was two orders lower than that of bare substrates, which may be attributed to inhibiting activity of molybdate ions. Molybdate intercalated hydrotalcite has the capacity to exchange Cl^- ions by inhibiting MoO_4^{2-} ions, thereby showing high stability and self-healing ability as observed from EIS measurements. Jiang et al. [118] pretreated AZ31 substrates with 0.8 vol % HNO_3 and 16 vol % HF followed by generation of conversion coatings in electrolytic bath consisting of 19.7 mM $NaVO_3$ and $Ce(NO_3)_3.6H_2O$ (0.92 mM - 46.1 mM). In this case, the self-healing ability of vanadia based conversion coatings was evaluated with addition of various concentrations of cerium salt. Optimum concentration of ceria salt which gives better corrosion protection was evaluated by EIS studies in 0.6 M NaCl solution for 4 h followed by evaluation of self-healing ability using EIS and scratch immersion for 168 h. It was observed that, the anticorrosion properties of coatings enhanced with the increase in exposure durations and SEM-EDS analysis has shown progressive increase in appearance of vanadates in the form of flakes in scratched area. Chen et al. [119] used phytic acid as a corrosion inhibitor to modify hydrotalcite film by intercalation into hydroxide sheets using decarbonation and by adsorption onto external surface. Hydrotalcite films were generated on AZ31 substrates followed by immersion in phytic acid solutions of pH 6.5 and 11. EIS and polarization measurements in 0.59 wt % NaCl solution for 48 h indicated that, alkaline solution of phytic acid provided better barrier property and self-healing ability as compared to the one at pH 6.5, which could be attributed to formation of microcracks due to CO_2 release and residual stress. Nezamdoust et al. [120] have developed composite coating on AM60B, which was composed of primary layer of conversion coatings of Ti-Zr and secondary layers of hybrid organic-inorganic coating and phenyl trimethoxysilane (PTMS). Electrochemical measurements have shown that composite

coatings provided much better barrier properties than only hybrid sol-gel coatings and PTMS coatings wherein, only sol-gel coatings were relatively more uniform and defect-free.

2.2.2 Container-based self-healing coatings

Ordered mesoporous silica nanocontainers were manufactured by Qiao et al. [83] using sol-gel method, loaded with MBT and then dispersed into epoxy matrix. Effect of loading of nanocontainers was evaluated with 2 wt % and 4 wt % coating formulations. Coatings consisting of 4 wt % MBT loaded nanocontainers have shown better anticorrosion properties in 0.6 M NaCl solution for 168 h and showed self-healing ability in artificial defect with 96 h of exposure to 0.59 wt % NaCl solution, as observed from EIS studies. MBT loaded porous hollow SiO_2 nanocontainer dispersed electroless Ni coating was generated by Xie et al. [121] on Mg alloy AZ31. In this case, AZ31 substrates were pretreated with phosphoric acid and hydrofluoric acid solutions followed by immersion in fluoride-containing solution and then in nanocontainer dispersed fluoride-containing solution. Initially, the inhibition ability of benzotriazole (BTA), HQ and MBT was evaluated by measuring H_2 evolution rate after 5 h of exposure to 0.6 M NaCl solution and found that, MBT has shown least release of H_2, thereby confirming its better inhibition ability for AZ31. EIS and polarization measurements in 0.6 M NaCl solution for 12 h revealed that, MBT loaded nanocontainer based coatings have shown better anticorrosion properties than the one without corrosion inhibitor. Xie et al. [122] used sodium fluoride as a corrosion inhibitor, encapsulated in mesoporous silica nanocontainers which are then dispersed in Ni coatings generated on AZ31. XPS studies have revealed the release of fluoride ions from nanocontainers and formation of protective layer of magnesium fluoride at the localised corroded area. EIS and polarization studies have shown that the introduction of fluoride loaded nanocontainers have decreased the corrosion rate in 0.06 M NaCl solution for 24 h. Paeonol was used as corrosion inhibitor by Ding et al. [123], loaded in mechanized silica nanoparticles consisting of mesoporous silica nanoparticles and supramolecular nanovalves and then dispersed into self-assembled nanophase particle coating matrix. Further, the superhydrophobic functionality was developed by adding 1H, 1H, 2H, 2H-Perfluorodecyltriethoxysilane to the coating matrix. EIS (0.29 wt % NaCl solution for 15 days) and SVET (0.059 wt % NaCl solution for 72 h) measurements have revealed that silica nanoparticles respond to localised corrosion by releasing entrapped

corrosion inhibitor under the influence of alkaline environment resulting in the formation of barrier film.

Cerium molybdate nanocontainers were synthesized by Kartsonakis et al. [77] owing to the inhibiting action of cationic cerium and anionic molybdate and MBT, which is a widely used organic corrosion inhibitor was encapsulated inside the cerium molybdate nanocontainers. These nanocontainer dispersed hybrid coatings generated on Mg alloy ZK10 were composed of organically modified silane and cross-linked polymers. Coatings have shown enhanced corrosion protection in 0.5 M NaCl for 4 months and revealed self-healing ability in artificial defect after exposure to 0.001 M NaCl for 73 h, as observed from EIS measurements. Song et al. [124] coated AZ91D substrates with cerium-based conversion coatings containing various concentrations of $La(NO_3)_3$ loaded gelatin-chitosan microcapsules which were synthesized using complex coacervation method. Electron Probe Micro-analyser (EPMA) has shown appearance of lanthanum content in the defect area with the help of elemental mapping with 24 h of exposure to 0.6 M NaCl solution, thereby showing the self-healing ability. EIS and polarization measurements for 7 days have revealed that, coatings with 20 % microcapsules have depicted better anticorrosion properties, which lasted for 4 days. Montemor et al. [125] oxidised carbon nanotubes (CNT) in concentrated HNO_3 and H_2SO_4 solutions for 24 h and then treated with aqueous solutions (0.001 M) of $La(NO_3)_3$ and $Ce(NO_3)_3$. The modified CNTs were then dispersed into 5 vol % of bis-[triethoxy amino] silane solution at neutral pH followed by immersion of AZ31 substrates in silane solution for 60 sec. The anticorrosion properties of coatings were examined by SVET in 0.29 wt % NaCl solution for 48 h and found the suppressed anodic and cathodic activity at the substrate. Chen et al. [126] encapsulated poly(lactic-co-glycolic) acid (PLGA, 5-20 wt %) porous particles with BTA (10-20 wt % loading) in dichloromethane solvent and electro-sprayed on Mg alloy AMlite followed by spray coating with epoxy resin. The amount of PLGA was fixed to 20 wt % considering the shape and size of spheres obtained with other concentrations. EIS and polarization measurements in 0.59 wt % NaCl solution illustrated that, BTA loaded PLGA based coatings have shown best corrosion protection which could be attributed to rapid response of PLGA to water, change in pH and formation of nanopores after evaporation of solvent for release of BTA. Kartsonakis et al. [127] loaded TiO_2 nanocontainers with MBT and polypyrrole were dispersed in hybrid coating matrix consisting of epoxy resin and organically modified silane. The above coating matrix was dip coated for 6 times on HF and NaOH pretreated Mg alloy ZK10. EIS measurements in 5 mM NaCl solution for 12 days indicated that

coatings consisting of polypyrrole and MBT loaded TiO_2 have shown better anticorrosion properties as S or N atoms of released MBT interacts with Mg of the substrate and change the electron density at local site, thereby reducing the anodic and cathodic activity. PEO coatings were developed by Sun et al. [128] on Mg alloy AM50 with alkaline silicate solution consisting of BTA (10 g/L) loaded halloysite nanotubes (HNT). Electrochemical studies in 0.6 M NaCl solution have depicted that PEO coatings with HNT did not give active corrosion protection after 4 h of exposure, whereas the coatings with BTA loaded HNT have shown higher corrosion resistance against the pit formation.

Guo et al. [129] have reviewed biocompatible, self-healing and self-cleaning Layered Double Hydroxide (LDH) based composite coatings on Mg alloys. The review gave details about synthetic methods of single LDH coatings and composite LDH coatings on Mg alloy. Single LDH coatings are synthesized by *in situ* growth methods, co-precipitation, electrochemical deposition, spin coating and anion exchange, whereas composite LDH-based coatings are mostly self-healing, biocompatible, self-cleaning and sealing LDH-based coatings. Among the above methods, though in-situ growth methods have been widely used, it comes with some disadvantages as the other methods have. Extensive research has been carried out on LDH based coatings for corrosion protection of Mg alloys; some of them have been briefly mentioned in Table 2.1.

Table 2.1: Different LDH based coatings on Mg alloys [129] *(With permission from Elsevier, January 04, 2021, License No. 4981840751427)*

Method	**Substrate**	**LDH Coating**	**Ref.**
One-step in situ growth method	AZ91D	MgAl-CO_3^{2-}	130
One-step in situ growth method	Pure Mg	MgFe-CO_3^{2-}	131
Two-step in situ growth method	AZ31	MgAl-CO_3^{2-}	132
Hydrothermal treatment	AZ91D	MgAl-CO_3^{2-}	133
Hydrothermal treatment	JDBM	MgAl-CO_3^{2-}	134
Urea hydrolysis	AZ31	MgAl-CO_3^{2-}	135
Urea hydrolysis	Pure Mg	MgAl-CO_3^{2-}	136
Steam coating	AZ31	MgAl-CO_3^{2-}	137
Steam coating	AZ31	MgAl-CO_3^{2-}	138

Hydrothermal crystallisation method	AZ31D	MgAl-CO_3^{2-}	139
Co-precipitation and hydrothermal method	AZ31	MgAl-CO_3^{2-}	140
Co-precipitation and hydrothermal method	AZ31	MgAl-MoO_4^{2-}	141
Electrochemical deposition	AZ31	LiAl-CO_3^{2-}	142
Electrochemical deposition	AZ91D	ZnAl-NO_3^-	143
Spinning coating	AZ31	MgAl-CO_3^{2-}	144
Anion-exchange	AZ91D	ZnAl-Cl^-	145
Anion-exchange	AZ91D	ZnAl-VO_x^-	146

2.2.3 Other self-healing coatings

Calado et al. [147] pretreated Mg alloy AZ31 substrates with alkali, dip coated with hybrid sol consisting of phytic acid and 3-aminopropyltrimethoxysilane at pH values of 5, 6.5 and 8 followed by rinsing in water. Immersion test was performed in SBF at pH 7.4 for 14 days and subsequently cleaned with chromic acid prior to weight loss measurements. Immersion tests and EIS analysis have shown that, hybrid coatings at pH 8 have least mass loss and better corrosion resistance, respectively. Hybrid epoxy-silane coating dispersed with CeO_2 nanoparticles were generated on Mg alloy AZ31 by Galio et al. [148] using dip coating with multiple layers. The coatings were examined for their barrier properties and self-healing ability by various electrochemical techniques such as EIS (0.29 wt % NaCl for 29 days), Localised EIS (0.029 wt % NaCl for 50 h), SVET (0.29 wt % NaCl for 22 h) and Scanning Ion-Selective Electrode Technique (SIET, 0.29 wt % NaCl for 25 h). Electrochemical analyses revealed that, the localised corrosion was delayed with the presence of CeO_2 and the cathodic/anodic activities are suppressed because Ce^{3+} showed self-healing and inhibitory activities after coming in contact with OH^- during initiation of corrosion and forms stable cerium hydroxides. Hybrid organic-inorganic sol synthesized using GPTMS and zirconium (IV) propoxide was coated on AZ31 substrates by Jiang et al. [149]. HQ was added before and after hydrolysis of hybrid sol. Initially EIS studies were carried out in 5 mM NaCl for 14 days to evaluate inhibiting activity of HQ by immersing AZ31 substrates in inhibitor solutions. Further, EIS measurements for coated substrates revealed that, coatings based on HQ added after hydrolysis have shown better anticorrosion properties. This could be attributed to interaction of HQ with the components

(organic/inorganic) of coatings as there would be less interaction of HQ with the silane after hydrolysis. Zhao et al. [150] have modified surface of AZ31 substrate with polyethylene amine solution to introduce positive charge followed by generation of multilayers of polyacrylic acid modified SiO_2 nanoparticles and 3-aminopropyl trimethoxysilane modified CeO_2 nanoparticles using spin-spray layer-by-layer assembly. Electrochemical studies and hydrogen evolution tests of 360 h showed that multilayer assembly imparted better barrier and self-healing ability due to SiO_2 and CeO_2 nanoparticles respectively. Calado et al. [151] have used tri(bis(2-ethylhexyl)phosphate) ($Ce(DEHP)_3$) as a novel inhibitor dispersed in hybrid epoxy-silane coating matrix for corrosion protection of AZ31 substrates. EIS studies have shown that addition of small concentrations of $Ce(DEHP)_3$ gave long term protection, whereas localised electrochemical measurements have confirmed that the inhibitor hinders the localised corrosion progress with change in pH. Zhao et al. [152] have prepared self-healing superamphiphobic coatings composed of compact epoxy coating and porous superamphiphobic coating (based on TEOS and 1H,1H,2H,2H-perfluorodecyltriethoxysilane dispersed with silica nanoparticles) for corrosion protection of Mg alloy AZ31B. The two-layer coating comprised of fluorosilane provides excellent superamphiphobicity, better barrier and self-healing properties as compared to that of alkyl silane based coatings, even after generating artificial defect into the coating as observed from immersion test and salt spray tests. Li et al. [153] used alkali pretreated Mg alloy AZ31 substrates for dip coating with hybrid sol consisting of phytic acid and 3-aminopropyltrimethoxysilane at pH values of 5, 6.5 and 8. Immersion tests and EIS analysis in SBF at neutral pH have shown that, hybrid coatings at pH 8 have least mass loss and better corrosion resistance, respectively. Yao et al. [154] have reviewed a number of strategies used to develop superhydrophobic coatings with corrosion protection ability on Mg alloys. They have classified different kinds of methodologies for the development of hierarchical micro/nano structures on Mg alloy surfaces such as solution immersion, electrochemical machining, electrodeposition, micro-arc oxidation, hydrothermal processes and spraying. They also discussed about the improvement in the properties of coatings by stability of the air pockets and hierarchical structures, inducing self-healing ability with corrosion inhibitors and generation of slippery liquid-infused porous surfaces. Soliman et al. [155] have developed HQ based coatings incorporated with nano-graphene oxide (GO) particles on oxidized and phosphate treated AZ31 substrates. EIS and immersion tests in SBF for 3 days indicated that, polymerized HQ-GO hybrid films on pretreated substrates have shown self-healing ability along with

excellent barrier properties. Wu et al. [156] have generated Mg-M LDH layer (M-Al, Cr & Fe) on anodized AZ31 substrates by in-situ growth method. The electrochemical studies and weight loss measurements have revealed that Mg-Al based LDH has depicted higher corrosion resistance and lowest weight loss. This could be attributed to the adsorption of Cl^- and release of NO_3^- from LDH along with the formation of passive and stable film of $Mg(OH)_2$, thereby inhibiting the pitting corrosion. A number of other studies, which examine the self-healing ability of coatings consisting of different inhibitors and coating formulations have been carried out on Mg alloys [157,158].

2.3 Corrosion inhibitors for corrosion protection of Mg alloys

In chapter-1, different types of corrosion inhibitors based on their chemical nature along with examples were discussed. The mechanism of inhibition of corrosion using these corrosion inhibitors has also been discussed. According to inhibiting mechanism, the corrosion inhibitors can be classified as passivation, precipitation and adsorption type. Passivating inhibitors such as nitrite, chromate and phosphate forms a passive film on substrates, thereby giving better barrier properties. The stability and inhibition efficiency of adsorptive inhibitors greatly depend on the interaction of inhibitor molecules with the substrate/solution interface. The commonly used adsorptive inhibitors are amines, carboxyls, phosphonates, sulphonates, etc. Precipitating inhibitors form insoluble compounds on substrate by reacting/combining with ions of solution. Inhibitors that form precipitation film on the substrate are zinc sulphate, calcium bicarbonate, sodium tripolyphosphate, etc. [159]. This section gives an account of various inhibitors, which were used in earlier studies for corrosion protection of Mg alloys.

Lamaka et al. [160] have carried out systematic screening of 151 different compounds, which have been evaluated for their inhibiting effects towards three grades of pure Mg and Mg alloys like AZ31, AZ91, AM50, WE43, ZE41 and Elektron 21. The analysis was based on ability of inhibitor to form stable, soluble complexes with Fe^{2+}/Fe^{3+} and then hydrogen evolution tests. The hydrogen evolution tests were carried out using eudiometers in 0.5 wt %, 0.29 wt % and 0.029 wt % NaCl solution with 0.5 g of chips of Mg/ alloy substrates for 22-78 h. In this study, new as well as earlier studied inhibitors have been listed based on their inhibition efficiency and compared with that of Cr (VI) as a reference. The sodium salt derivatives of salicylic acid and pyridinedicarboxylic acid were found to have better inhibition efficiencies for pure Mg and Mg alloys containing Al and rare earths. Umoren et al. [161] have evaluated seven natural polymers such as chitosan, dextran, carboxymethyl

cellulose, sodium alginate, pectin, hydroxyethyl cellulose and gum arabic for their inhibiting properties against Mg alloy AZ31 in 0.6 M NaCl using mass loss, hydrogen evolution, EIS, potentiodynamic polarization and scanning electrochemical microscopy (SECM). For evaluation of anticorrosion property, 1.0 g/L of natural polymer solutions were taken in 0.6 M NaCl solution. Weight loss and electrochemical studies have shown that 1 g/L of sodium alginate and hydroxyethyl cellulose were found to give efficiencies of 64.13% and 58.27%, respectively. Further, the detailed studies with two inhibitor formulations at different concentrations (0.5, 1.0 and 2.0 g/L) along with potassium iodide and date palm seeds oil were carried out. The electrochemical measurements have shown that, formulations of sodium alginate and hydroxyethyl cellulose gave 77.43 % and 80.56 % efficiencies respectively. Liu et al. [162] have analysed inhibition effect of sodium citrate (SC), sodium dodecylbenzenesulphonate (SDBS), diammonium phosphate ($(NH_4)_2HPO_4$) and sodium vanadate ($NaVO_3$) on Mg alloy AM60 in 0.59 wt % NaCl for 10 days by immersion and electrochemical measurements. Fig. 2.4 shows the inhibition mechanisms of four different corrosion inhibitors and substrate without inhibitor.

Further, it was observed that all four corrosion inhibitors (0.01 M) have shown corrosion protection after 10 days of immersion. However, only $(NH_4)_2HPO_4$ cannot provide protection against localized corrosion. Among all four inhibitors, SDBS has shown 93 % inhibition efficiency, which could be attributed to adsorption ability of S on Mg, insoluble film of Mg-SDBS and long alkyl chain. Kartsonakis et al. [163] have evaluated corrosion inhibitive properties of ammonium phosphate dibasic, calcium fluoride, HQ, SDBS, zinc nitrate and sodium fluoride towards Mg alloy ZK30 in 5 mM and 50 mM NaCl solution with 5 g/L concentration of each inhibitor except HQ (up to solubility limit).

Electrochemical measurements were carried for 144 h (5 mM NaCl) and 10 days (50 mM NaCl). In 5 mM NaCl, HQ, ammonium phosphate dibasic and calcium fluoride, whereas in 50 mM NaCl, HQ, SDBS, ammonium phosphate dibasic and sodium fluoride have shown better corrosion protection which corresponded to the generation of insoluble complexes of MgQ_2, MgF_2, $Mg_3(PO_4)_2$. 22 H_2O and Mg-SDBS. Sorkhabi et al. [164] have pretreated Mg alloy AZ91 substrates with cerium-lanthanum-permanganate (CLP) conversion coatings to protect the substrate from corrosion in acidic conditions of sol. The pretreated substrates were then dip coated with hybrid organic-inorganic sol dispersed with various amino acids such as L-alanine, L-glutamine, L-methionine and L-aspartic with concentrations of 0.1, 0.5, 1.0 and 0.5 wt % respectively. EIS measurements were carried

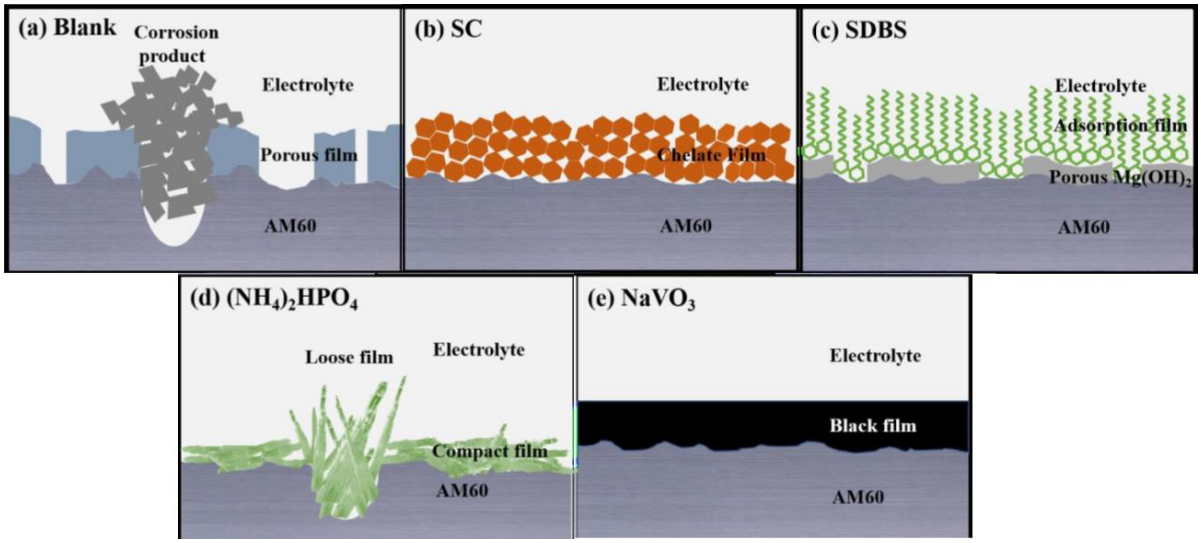

Figure 2.4: Schematic representation of inhibition mechanism of (a) blank, (b) SC, (c) SDBS, (d) ($(NH_4)_2HPO_4$) and (e) $NaVO_3$ [162]

out for various concentrations of all amino acids for different durations up to 48 h and found that L-aspartic gave better corrosion protection among all amino acids. As shown in Fig. 2.5, the heteroatoms of L-aspartic are closer to substrate surface as compared to other amino acids, resulting in its higher adsorption energy and these replace Mg atoms on substrate, thereby showing better inhibitive properties. Sorkhabi et al. [165] have added salts such as sodium gluconate ($NaC_6H_{11}O_7$), potassium hypophosphite (KH_2PO_2), and manganese (II) acetate (Mn $(CH_3CO_2)_2$) with concentrations of 0.1, 0.5 and 0.1 wt % respectively along with 0.5 wt % cloisite 20A nanoparticles to the hybrid sol-gel coatings generated on AZ91 substrates pretreated with CLP conversion coatings. EIS studies for 48 h in 0.6 M NaCl have revealed that, all the three salts can be used as corrosion inhibitors due to the presence of heteroatoms like O and P which makes the salts to get adsorbed on substrate surface and protect the substrate with addition of cloisite nanoparticles acting as surface modifier. Further, it was observed that, manganese (II) acetate and potassium hypophosphite could give better corrosion protection for longer and shorter durations respectively. Gao et al. [166] exposed AZ91D substrates to the ASTM D1384-87 corrosive medium (Na_2SO_4-148 mg/L, $NaHCO_3$-138 mg/L, NaCl-165 mg/L, pH 8.2) mixed with corrosion inhibitors such as SDBS (1.16 mM) and HQ (saturated solution). EIS and polarization measurements for 72 h in ASTM D1384-87 solution revealed that the inhibition ability of SDBS was limited, whereas HQ has shown effective corrosion protection owing to the development of stable film of $Mg(Q)_2$. However, combined use of SDBS and HQ has shown synergistic behaviour with inhibition efficiency of 98 % which could be observed because of adsorption of negative ions of dodecylbenzenesulphonate on the porous layer of $Mg(Q)_2$.

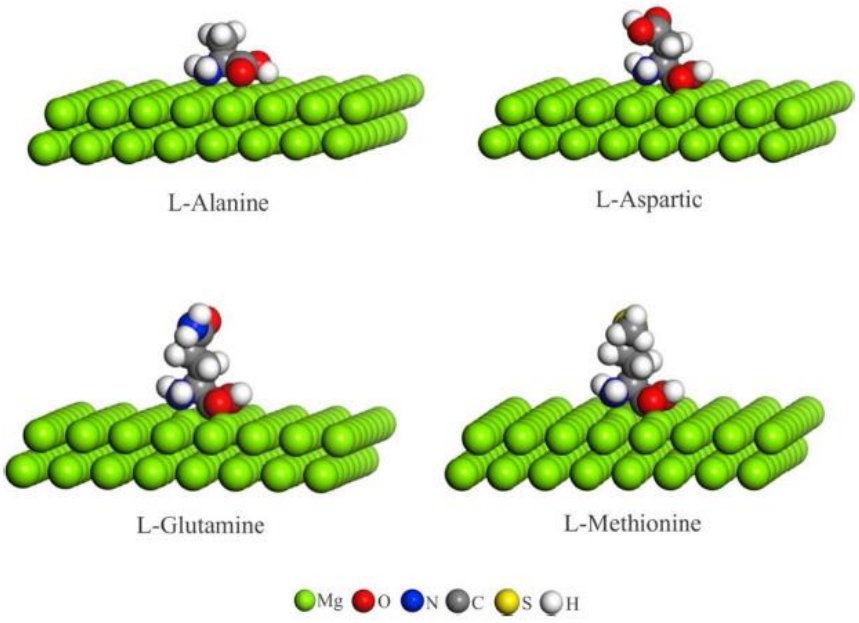

Figure 2.5: Adsorption behaviour of amino acids on AZ91 [164] *(With permission from Elsevier, January 04, 2021, License No. 4980641338179)*

2.4 Conclusion

- Owing to the very low standard electrode potential, Mg alloys are prone to the generation of thin oxide/hydroxide film, which may affect the adhesion properties of coating layers. Hence, surface cleaning by mechanical and chemical methods is essential to provide better anticorrosion and adhesion properties.
- A number of approaches have been attempted to develop corrosion protection coatings on Mg alloys, while most number of studies have been focused on conversion coatings, MAO/PEO coatings and sol-gel coatings. However, conversion and PEO coatings come with various limitations such as unable to provide long term protection, the requirement of pretreatment layer, high operating temperature, high porosity, poor adhesion strength etc. Epoxy coatings and EPD have also been used but they were generated as composite coatings with conversion or sol-gel coatings.
- Owing to eco-friendly nature, low curing temperature, versatility to number of additives and compatibility with other coating methods, sol-gel coatings have great potential to provide prolonged protection for enormous number of applications. Self-healing functionality could be achieved effectively by encapsulating the inhibiting/ active species into the containers or incorporating them into an additional layer of coating.

Various coating methods have been used to generate the self-healing ability in the coatings to provide long-term corrosion protection to Mg alloys.

- Being an inevitable part of corrosion protection coatings, species/compounds having corrosion inhibition ability have gained a lot of research interest. Large number of corrosion inhibitors have been examined for their corrosion inhibition ability towards Mg alloys, which included organic/inorganic compounds, naturally occurring species/polymers, etc.
- It was observed that not many studies have been carried out on HNT and MMT based self-healing coatings on Mg alloy though they have been extensively investigated for use on Al alloys. Also, the corrosion inhibition activity of cationic inhibitors like Ce^{3+} and Zr^{4+} has not been evaluated earlier on Mg alloys. Hence, the present work is focused on the evaluation of anticorrosion properties of cationic inhibitor encapsulated (HNT)/intercalated (MMT) based sol-gel coatings on AZ91D substrates.

2.5 References

[1] X. B. Chen, N. Birbilis, T.B. Abbott, Review of corrosion resistant conversion coatings for magnesium and its alloys, Corrosion 67 (2011) 035005.

[2] K. Brunelli, M. Dabalà, I. Calliari, M. Magrini, Effect of HCl pre-treatment on corrosion resistance of cerium-based conversion coatings on magnesium and magnesium alloys, Corros. Sci. 47(4) (2005) 989-1000.

[3] J. E. Hillis, Surface engineering of magnesium alloys, in: ASM Handbook, ASM International 5 (1996) pp. 819-834.

[4] G. L. Song, Z. Q. Xu, The Surface, microstructure and corrosion of magnesium alloy AZ31 sheet, Electrochim. Acta, 55 (2010) 4148-4161.

[5] G. M. Abady, N. H. Hilal, M. E. Rabiee, W. A. Badawy, Effect of Al content on the corrosion behaviour of Mg-Al alloy in aqueous solutions of different pH, Electrochim. Acta, 55(2010) 6651-6658.

[6] Carlos E. Castano, Cerium-based conversion coatings on magnesium alloys, Ph.D. Thesis, Missouri University of Science and Technology, Scholars' Mine (2014).

[7] Viswanathan S. Saji, Review of rare-earth-based conversion coatings for magnesium and its alloys, J. Mater. Res. Technol. 8 (5) (2019) 5012-5035.

[8] J.E. Gray, B. Luan, Protective coatings on magnesium and its alloys- a critical review, J. Alloys. Comp. 336 (2002) 88-113.

[9] A. U. Simaranov, S. L. Marshakov, Yu. N. Mikhailovskii, Protection of Metals, 28 (1992) 576.

[10] J.B. Mohler, Metal Finishing 73 (1974) 30.

[11] A.K. Sharma, Chromate conversion coatings for magnesium-lithium alloys, Metal Finishing 87 (1989) 73.

[12] S. Ono, T. Osaka, K. Asami, N. Masuko, Oxide films formed on magnesium and magnesium alloys by anodizing and chemical conversion coating. Corros. Rev. 16 (1998) 175.

[13] A. R. Shashikala, R. Umarani, S. M. Mayamma, A. K. Sharma, Chemical conversion coatings on magnesium alloys-a comparative study, Int. J. Electrochem. Sci. 3 (2008) 993-1004.

[14] Sebastien Pommiers-Belin, Jerome Frayret, Arnaud Uhart, JeanBernard Ledeuil, Jean-Charles Dupin, Alain Castetbon, Martine Potin-Gautier, Determination of the chemical mechanism of chromate conversion coating on magnesium alloy EV31A, Appl. Surf. Sci. 298 (2014) 199-207.

[15] H. Hornberger, S. Virtanen, A. R. Boccaccini, Biomedical coatings on magnesium alloys-a review, Acta Biomaterialia 8 (2012) 2442-2455.

[16] X. B. Chen, N. Birbilis, T. B. Abbott, Review of corrosion-resistant conversion coatings for magnesium and its alloys, Corrosion 67 (3) (2011) 035005.

[17] Sébastien Pommiers, Jérôme Frayret, Alain Castetbon, Martine Potin-Gautier, Alternative conversion coatings to chromate for the protection of magnesium alloys, Corros. Sci. 84 (2014) 135-146.

[18] Abdel Salam Hamdy, I. Doench, H. Mohwald, Assessment of one-step intelligent self-healing vanadia protective coatings for magnesium alloys in corrosive media, Electrochim. Acta. 56 (2011) 2493-2502.

[19] Katya Brunelli, Manuele Dabala, Irene Calliari, Maurizio Magrini, Effect of HCl pre-treatment on corrosion resistance of cerium-based conversion coatings on magnesium and magnesium alloys, Corros. Sci. 47 (2005) 989-1000.

[20] Junying Hu, Qing Li, Xiankang Zong, Liang Zhang, Bo Chen, Composite anticorrosion coatings for AZ91D magnesium alloy with molybdate conversion coating and silicon sol-gel coatings, Prog. Org. Coat. 66 (2009) 199-205.

[21] V. S. Saji, Organic conversion coatings for magnesium and its alloys, J. Ind. Eng. Chem. 75 (2019) 20-37.

[22] Shun-Yi Jian, Chi-Yu Yang, Jun-Kai Chang, Robust corrosion resistance and self-healing characteristics of a novel Ce/Mn conversion coatings on EV31 magnesium alloys, App. Surf. Sci. 510 (2020) 145385.

[23] Jingshun Cai, Fahe Cao, Linrong Chang, Junjun Zheng, Jianqing Zhang, Chunan Cao, The preparation and corrosion behaviours of MAO coating on AZ91D with rare earth conversion precursor film, Appl. Surf. Sci. 257 (2011) 3804-3811.

[24] Hélène Ardelean, Isabelle Frateur, Philippe Marcus, Corrosion protection of magnesium alloys by cerium, zirconium and niobium-based conversion coatings, Corros. Sci. 50 (2008) 1907-1918.

[25] Liping Wu, Zhongdong Yang, EIS study of molybdate conversion coatings formed on AZ91D magnesium alloy, Adv. Mater. Res. 189-193 (2011) 279-285.

[26] N.V. Murillo-Gutiérrez, F. Ansart, J-P. Bonino, M-J. Menu, M. Gressier, Protection against corrosion of magnesium alloys with both conversion layer and sol–gel coating, Surf. Coat. Technol. 232 (2013) 606-615.

[27] Abdel Salam Hamdy, D. P. Butt, Novel smart stannate based coatings of self-healing functionality for AZ91D magnesium alloy, Electrochim. Acta. 97 (2013) 296-303.

[28] Jie Sun, Gang Wang, Preparation and corrosion resistance of cerium conversion coatings on AZ91D magnesium alloy by a cathodic electrochemical treatment, Surf. Coat. Technol. 254 (2014) 42-48.

[29] Jithu Jayaraj, Amruth Raj S., A. Srinivasan, S. Ananthakumar, U. T. S Pillai, Nanda Gopala Krishna Dhaipule and U. Kamachi Mudali, Composite magnesium phosphate coatings for improved corrosion resistance of magnesium AZ31 alloy, Corros. Sci. 113 (2016) 104-115.

[30] I. L. Lehr, S. B. Saidman, Corrosion protection of AZ91D magnesium alloy by a cerium-molybdenum coating-The effect of citric acid as an additive, J. Magnesium Alloys 6 (2018) 356-365.

[31] Stephen Abela, Protective coatings for magnesium alloys, in: Frank Czerwinski, Magnesium alloys-Corrosion and surface treatments, InTech Croatia (2011) pp. 195-220.

[32] Lénia M. Calado, M. F. Montemor, Corrosion protection of magnesium alloys by functional coatings, in: Lisa Klein, Mario Aparicio, Andrei Jitianu, Handbook of Sol-Gel science and technology, Springer Nature (2018) pp. 2473-2505.

[33] D. Peixoto Barbosa, G. Knörnschild, Anodization of Mg-alloy AZ91 in NaOH solutions, Surf. Coat. Technol. 203 (2009) 1629-1636.

[34] Xinghua Guo, Maozhong An, Experimental study of electrochemical corrosion behaviour of bilayer on AZ31B Mg alloy, Corros. Sci. 52 (2010) 4017-4027.

[35] A.D. Forero Lopez, I.L. Lehr, S.B. Saidman, Anodisation of AZ91D magnesium alloy in molybdate solution for corrosion protection, J. Alloys Compd. 702 (2017) 338-345.

[36] Xinghua Guo, Maozhong An, Peixia Yang, Haixian Li, Caina Su, Effects of benzotriazole on anodized film formed on AZ31B magnesium alloy in environmental-friendly electrolyte, J. Alloys. Comp. 482 (2009) 487-497.

[37] Yongjun Zhang, Chuanwei Yan, Fuhui Wang, Wenfang Li, Electrochemical behaviour of anodized Mg alloy AZ91D in chloride containing aqueous solution, Corros. Sci. 47 (2005) 2816-2831.

[38] Luca Pezzato, Katya Brunelli, Enrico Napolitani, Maurizio Magrini, Manuele Dabalà, Surface properties of AZ91 magnesium alloy after PEO treatment using molybdate salts and low current densities, App. Surf. Sci. 357 (2015) 1031-1039.

[39] L. Li, Y. Cheng, H. Wang, Z. Zhang, Anodization of AZ91 magnesium alloy in alkaline solution containing silicate and corrosion properties of anodized films, Trans. Nonferrous Met. Soc. China (English Ed.) 18(3) (2008) 722–7.

[40] M. C. L. de Oliveira, V. S. M. Pereira, O. V. Correa, R. A. Antunes. Corrosion performance of anodized AZ91D magnesium alloy: effect of the anodizing potential on the film structure and corrosion behaviour. J. Mater. Eng. Perform. 23(2) (2014) 593–603.

[41] R. Arrabal, E. Matykina, T. Hashimoto, P. Skeldon, G.E. Thompson, Characterization of AC PEO coatings on magnesium alloys, Surf. Coat. Technol. 203 (2009) 2207-2220.

[42] P. Bala Srinivasan, J. Liang, C. Blawert, M. Stormer, W. Dietzel, A preliminary study of calcium containing plasma electrolytic oxidation coatings on AM50 magnesium alloys, J. Mater. Sci. 45 (2010) 1406-1410.

[43] M. Mohedano, C. Blawert, M. L. Zheludkewich, Cerium-based sealing of PEO coated AM50 magnesium alloy, Surf. Coat. Technol. 269 (2015) 145-154.

[44] A. S. Gnedenkov, S.L. Sinebryukhov, D.V. Mashtalyar, S.V. Gnedenkov, Protective properties of inhibitor-containing composite coatings on a Mg alloy, Corros. Sci. 102 (2016) 348-354.

[45] Y. Chen, X. Lu, S. V. Lamaka, P. Ju, C. Blawert, T. Zhang, F. Wang, M.L. Zheludkevich, Active protection of Mg alloy by composite PEO coating loaded with corrosion inhibitors, Applied Surface Science. 504 (2020) 144462.

[46] Jingjing Guo, Xianfeng Liu, Keqin Du, Quanzhong Guo, Yong Wang, Yunyan Liu, Li Feng, An anti-stripping and self-healing micro-arc oxidation/acrylamide gel composite coating on magnesium alloy AZ31, Mater. Lett. 260 (2020) 126912.

[47] A. Mandelli, M. Bestetti, A. Da Forno, N. Lecis, S. P. Trasatti, M. Trueba, A composite coating for corrosion protection of AM60B magnesium alloy, Surf. Coat. Technol. 205 (2011) 4459-4465.

[48] Gen Zhang, Liang Wu, Aitao Tang, Xingxing Ding, Bin Jiang, Andrej Atrens, Fusheng Pan, Smart epoxy coating containing zeolites loaded with Ce on a plasma electrolytic oxidation coating on Mg alloy AZ31 for active corrosion protection, Prog. Org. Coat. 132 (2019) 144-147.

[49] Dan Liu, Yingwei Song, Dayong Shan, En-Hou Han, Self-healing coatings prepared by loading interphase inhibitors into MAO coating of AM60 Mg alloy, J. Electrochem. Soc. 175 (7) (2018) C412-C421.

[50] Dan Liu, En-Hou Han, Yingwei Song, Dayong Shan, Enhancing the self-healing property by adding the synergistic corrosion inhibitors of Na_3PO_4 and 2-mercapto benzothiazole into the coating of Mg alloy, Electrochim. Acta 323 (2019) 134796.

[51] Chang-Yang Li, Ling Gao, Xiao-Li Fan, Rong-Chang Zeng, Dong-Chu Chen, Ke-Qian Zhi, In vitro degradation and cytocompatibility of a low temperature in-situ grown self-healing Mg-Al LDH coating on MAO-coated magnesium alloy AZ31, Bioact. Mater. 5 (2020) 364-376.

[52] S.V. Gnedenkov, S.L. Sinebryukhov, D.V. Mashtalyar, K.V. Nadaraia, D.P. Kiryukhin, G.A. Kichigina, P.P. Kushch, V.M. Buznik, Composite coatings formed on the PEO-layers with the use of solutions of tetrafluoroethylene telomers, Surf. Coat. Technol. 346 (2018) 53–62.

[53] A. Ghasemi, V.S. Raja, C. Blawert, W. Dietzel, K.U. Kainer, Study of the structure and corrosion behavior of PEO coatings on AM50 magnesium alloy by electrochemical impedance spectroscopy, Surf. Coat. Technol. 202 (2008) 3513-3518.

[54] Hongping Duan, Keqin Du, Chuanwei Yan, Fuhui Wang, Electrochemical corrosion behavior of composite coatings of sealed MAO film on magnesium alloy AZ91D, Electrochim. Acta. 51 (2006) 2698-2908.

[55] Weiping Li, Mingqi Tang, Liqun Zhu, Huicong Liu, Formation of microarc oxidation coatings on magnesium alloy with photocatalytic performance, App. Surf. Sci. 258 (2012) 10017-10021.

[56] J. Liang, P. Bala Srinivasan, C. Blawert, W. Dietzel, Influence of pH on the deterioration of plasma electrolytic oxidation coated AM50 magnesium alloy in NaCl solutions, Corros. Sci. 52 (2010) 540-547.

[57] M. Laleh, Farzad Kargar, A. Sabour Rouhaghdam, Investigation of rare earth sealing of porous micro-arc oxidation coating formed on AZ91D magnesium alloy, J. Rare Earths. 30 (11) (2012) 1293-1297.

[58] Laxmidhar Besra, Meilin Liu, A review on fundamentals and applications of electrophoretic deposition (EPD), Prog. Mater. Sci. 52 (2007) 1-61.

[59] A. Shahriari, H. Aghajani, Electrophoretic deposition of 3YSZ coating on AZ91D using aluminum interlayer, Prot. Metals. Phys. Chem. Surf. 53 (3) (2017) 518-526.

[60] Haruto Fukuda, Yasumichi Matsumoto, Formation of Ti-Si composite oxide films on Mg-Al-Zn alloy by electrophoretic deposition and anodization, Electrochim. Acta. 50 (2005) 5329-5333.

[61] Ramin Rojaee, Mohammadhossein Fathi, Keyvan Raeissi, Electrophoretic deposition of nanostructured hydroxyapatite coating on AZ91 magnesium alloy implants with different surface treatments, App. Surf. Sci. 285P (2013) 664-673.

[62] Hamed Amiri, Iman Mohammadi, Abdollah Afshar, Electrophoretic deposition of nano-zirconia coating on AZ91D magnesium alloy for bio-corrosion control purposes, Surf. Coat. Technol. 311 (2017) 183-190.

[63] Mehdi Razavi, Mohammadhossein Fathi, Omid Savabi, Daryoosh Vashaee and Lobat Tayebi, Micro-arc oxidation and electrophoretic deposition of nano-grain merwinite ($Ca_3MgSi_2O_8$) surface coating on magnesium alloy as biodegradable metallic implant, Surf. Interface. Anal. 46 (6) (2014) 1-6.

[64] Y. W. Song, D. Y. Shan, E. H. Han, Electrodeposition of hydroxyapatite coating on AZ91D magnesium alloy for biomaterial application, Mater. Lett. 62 (2008) 3276-3279.

[65] Congjie Wang, Bailing Jiang, Ming Liu, Yanfeng Ge, Corrosion characterization of micro-arc oxidization composite electrophoretic coating on AZ31B magnesium alloy, J. Alloys Compd. 621 (2015) 53-61.

[66] Luis Cordero-Arias, Aldo R. Boccaccini, Sannakaisa Virtanen, Electrochemical behavior of nanostructured TiO2/alginate composite coating on magnesium alloy AZ91D via electrophoretic deposition, Surf. Coat. Technol. 265 (2015) 212-217.

[67] Guang-Ling Song, "Electroless" deposition of a pre-film of electrophoresis coating and its corrosion resistance on a Mg alloy, Electrochim. Acta. 55 (2010) 2258-2268.

[68] Changjun Wu, Zhaohui Wen, Changsong Dai, Yinxiao Lu, Feixia Yang, Fabrication of calcium phosphate/chitosan coatings on AZ91D magnesium alloy with a novel method, Surf. Coat. Technol. 204 (2010) 3336-3347.

[69] P. A. Schweitzer, Corrosion-resistant linings and coatings, Marcel Dekker, Inc, New York, (2001) pp. 301-329.

[70] A. S. Khanna, Key issues in applying organic paint coatings, In: A. S. Khanna, High performance organic coatings, Woodhead Publishing Limited, Cambridge, UK (2008) pp. 3-26.

[71] Xiangyu Lu, Yu Zuo, Xuhui Zhao, Yuming Tang, Xingguo Feng, The study of a Mg-rich epoxy primer for protection of AZ91D magnesium alloy, Corros. Sci. 53 (2011) 153-160.

[72] Xiangyu Lu, Yu Zuo, Xuhui Zhao, Yuming Tang, The improved performance of a Mg-rich epoxy coating on AZ91D magnesium alloy by silane pretreatment, Corros. Sci. 60 (2012) 165-172.

[73] Tao Jin, Fan-mei Kong, Rui-qin Bai, Ru-liang Zhang, Anti-corrosion mechanism of epoxy-resin and different content Fe_2O_3 coatings on magnesium alloy, Front. Mater. Sci. 10 (4) (2016) 367-374.

[74] M. A. Chen, Y. C. Ou, C. Y. Yu, C. Xiao, S. Y. Liu, Corrosion performance of epoxy/BTESPT/MAO coating on AZ31 alloy, Surf. Eng. 32 (1) (2016) 38-46.

[75] Dashui Yan, Yanli Wang, Jialing Liu, Dalei Song, Tao Zhang, Jingyuan Liu, Fei He, Meng Zhang, Jun Wang, Self-healing system adapted to different pH environments for active corrosion protection of magnesium alloy, J. Alloys. Comp. 824 (2020) 153918.

[76] Ling-Yu Li, Lan-Yue Cui, Rong-Chang Zeng, Shuo-Qi Li, Xiao-Bo Chen, Yufeng Zheng, M. Bobby Kannan, Advances in functionalised polymer coatings on biodegradable magnesium alloys- a review, Acta Biomater. 79 (2018) 23-36.

[77] I.A. Kartsonakis, A.C. Balaskas, E.P. Koumoulos, C.A. Charitidis, G. Kordas, Evaluation of corrosion resistance of magnesium alloy ZK10 coated with hybrid organic–inorganic film including containers, Corros. Sci. 65 (2012) 481-493.

[78] Do Yeon Jung, Abdalla Abdal-hay, Seok Geun Park, Jae Kyoo Lim, Study on corrosion protection of nanocomposite layers (epoxy resin/ MWCNTs) based dip-coating on Mg alloy AM50, 15th European Conference on Composite Materials, Venice, Italy (2012).

[79] Fabiola Brusciotti, Darya V. Snihirova, Huibin Xue, M. Fatima Montemor, Svetlana V. Lamaka, Mario G.S. Ferreira, Hybrid epoxy–silane coatings for improved corrosion protection of Mg alloy, Corros. Sci. 67 (2013) 82-90.

[80] S.V. Lamaka, H.B. Xue, N.N.A.H. Meis, A.C.C. Esteves, M.G.S. Ferreira, Fault-tolerant hybrid epoxy-silane coating for corrosion protection of magnesium alloy AZ31, Prog. Org. Coat. 80 (2015) 98-105.

[81] N. V. Murillo-Gutiérrez, F. Ansart, J-P. Bonino, S. R. Kunst, C. F. Malfatti, Architectural optimization of an epoxy-based hybrid sol–gel coating for the corrosion protection of a cast Elektron21 magnesium alloy, App. Surf. Sci. 309 (2014) 62-73.

[82] Junjie Yang, Carsten Blawert, Sviatlana V. Lamaka, Darya Snihirova, Xiaopeng Lu, Shichun Di, Mikhail L. Zheludkevich, Corrosion protection properties of inhibitor containing hybrid PEO-epoxy coatings on magnesium, Corros. Sci. 140 (2018) 99-110.

[83] Yingjie Qiao, Wengpeng Li, Guixiang Wang, Xiaohong Zhang, Nana Cao, Application of ordered mesoporous silica nanocontainers in anticorrosive epoxy coating on magnesium alloy surface, RSC Adv. 59 (5) (2015) 47778-47787.

[84] J.J. Ebelmen, Ann. Chem. Phys. 5 (1842) 199.

[85] R. Roy, E.F. Osborn, Am. Miner. 39 (1954) 853.

[86] Duhua Wang, Gordon P. Bierwagen, Sol-gel coatings on metals for corrosion protection, Prog. Org. Coat. 64 (2009) 327-338.

[87] Q. Li, Sol-gel coatings to improve the corrosion resistance of magnesium (Mg) alloys, In: Guang-Ling Song, Corrosion prevention of magnesium alloys, Woodhead Publishing Ltd, NY (2013) pp. 469-488.

[88] A. R. Phani, F. J. Gammel, T. Hack, H. haefke, Enhanced corrosion resistance by sol-gel-based ZrO_2-CeO_2 coatings on magnesium alloys, Mater. Corros. 56(2) (2005) 77-82.

[89] Huimin Han, Dantong Wang, Huaqian Yu, min Zuo, Lihong Wang, Degang Zhao, Ceria coatings prepared by sol-gel approach on AZ91 magnesium alloy, Mater. Sci. For. 898 (2017) 1369-1380.

[90] Q. Li, B. Chen, S. Q. Xu, H. Gao, L. Zhang, C. Liu, Structural and electrochemical behaviour of sol-gel ZrO_2 ceramic film on chemically pre-treated AZ91D magnesium alloy, J. Alloys Compd. 478 (2009) 544–553 .

[91] X. K. Zhong, Q. Li, B. Chen, J. P. Wang, J. Y. Hu, W. Hu, Effect of sintering temperature on corrosion properties of sol-gel based Al_2O_3 coatings on pre-treated AZ91D magnesium alloy, Corros. Sci. 51 (2009) 2950–2958.

[92] J. M. Fan, Q. Li, W. Kang, S. Y. Zhang, B. Chen, Composite cerium oxide/ titanium oxide thin films for corrosion protection of AZ91D magnesium alloy via sol-gel process, Mater. Corros. 60 (2009) 438–443.

[93] S. Y. Zhang, Q. Li, B. Chen, X. K. Yang, Preparation and corrosion resistance studies of nanometric sol-gel-based CeO_2 film with a chromium-free pretreatment on AZ91D magnesium alloy, Electrochim. Acta 55 (2010) 870–877.

[94] X. K. Zhong, Q. Li, J. Y. Hu, Y. H. Lu, Characterization and corrosion studies of ceria thin film based on fluorinated AZ91D magnesium alloy, Corros. Sci. 50 (2008) 2304–2309.

[95] S. Y. Zhang, Q. Li, J. M. Fan, W. Kang, W. Hu, X. K. Yang, Novel composite films prepared by sol-gel technology for the corrosion protection of AZ91D magnesium alloy, Prog. Org. Coat. 66 (2009) 328–335.

[96] A. J. López, E. Otero, J. Rams, Sol-gel silica coatings on ZE41 magnesium alloy for corrosion protection, Surf Coat Technol. 205(7) (2010) 2375–2385.

[97] Y. Harada, S. Kumai, Effect of ceramics coating using sol-gel processing on corrosion resistance and age hardening of AZ80 magnesium alloy substrate, Surf. Coat. Technol. 228 (2013) 59–67.

[98] A. N. Khramov, V. N. Balbyshev, L. S. Kasten, R. A. Mantz, Sol-gel coatings with phosphate functionalities for surface modification of magnesium alloys, Thin Solid Films 514 (2006) 174-181.

[99] Zhiqiang Qian, Shidong Wang, Zhijian Wu, Corrosion behavior study of AZ31B magnesium alloy by sol-gel silica-based hybrid coating, Int. J. Electrochem. Sci. 12 (2007) 8269-8279.

[100] C. A. Hernández-Barrios, C. A. Cuao, M. A. Jaimes, A. E. Coy, F. Viejo, Effect of the catalyst concentration, the immersion time and the aging time on the morphology, composition and corrosion performance of TEOS-GPTMS sol-gel coatings deposited on the AZ31 magnesium alloy, Surf. Coat. Technol. 325 (2017) 257-269.

[101] L. Diaz, F. R. Garcia-Galvan, I. Llorente, A. Jimenez-Morales, J. C. Galvan, S. Feliu Jr, Effect of heat treatment of magnesium alloy substrates on corrosion resistance of a hybrid organic-inorganic sol-gel film, RSC Adv. 5 (2015) 105735-105746.

[102] V. Barranco, N. Carmona, J. C. Galván, M. Grobelny, L. Kwiatkowski, M. A. Villegas, Electrochemical study of tailored sol–gel thin films as pre-treatment prior to organic coating for AZ91 magnesium alloy, Prog. Org. Coat. 68 (2010) 347-355.

[103] Viviane Dalmoro, Denise S. Azambuja, Carlos Alemán, Elaine Armelin, Hybrid organophosphonic-silane coating for corrosion protection of magnesium alloy AZ91: The influence of acid and alkali pre-treatments, Surf. Coat. Technol. 357 (2019) 728-739.

[104] Mario Pagliaro, Rosaria Ciriminna, Giovanni Palmisano, Silica-based hybrid coatings, J. Mater. Chem. 19 (2009) 3116-3126.

[105] S.V. Lamaka, M.F. Montemor, A.F. Galio, M.L. Zheludkevich, C. Trindade, L.F. Dick, M.G.S. Ferreira, Novel hybrid sol–gel coatings for corrosion protection of AZ31B magnesium alloy, Electrochim. Acta. 53 (2008) 4773-4783.

[106] R. Samadianfard, D. Seifzadeh, A. Habibi-Yangjeh, Y. Jafari-Tarzanagh, Oxidized fullerene/sol-gel nanocomposite for corrosion protection of AM60B magnesium alloy, Surf. Coat. Technol. 385 (2020) 125400.

[107] M.A. Ashraf, Z. Liu, W.X. Peng, N. Yoysefi, Amino acid and TiO2 nanoparticles mixture inserted into sol-gel coatings: An efficient corrosion protection system for AZ91 magnesium alloy, Prog. Org. Coat. 136 (2019) 105296.

[108] J.P. Fernández-Hernán, A.J. López, B. Torres, J. Rams, Silicon oxide multilayer coatings doped with carbon nanotubes and graphene nanoplatelets for corrosion protection of AZ31B magnesium alloy, Prog. Org. Coat. 148 (2020) 105836.

[109] N. C. Rosero-Navarro, M. Curioni, Y. Castro, M. Aparicio, G. Thompson, A. Durán, Glass-like CexOy sol-gel coatings for corrosion protection of aluminium and magnesium alloys, Surf. Coat. Technol. 206 (2011) 257–264.

[110] A. A. El-Hadad, V. Barranco, A. Samaniego, I. Llorente, F. R. García-Galván, A. Jiménez-Morales, J. C. Galván, S. Feliu Jr, Influence of substrate composition on corrosion protection of sol-gel thin films on magnesium alloys in 0.6 M NaCl aqueous solution, Prog. Org. Coat. 77 (11) (2014) 1642–1652.

[111] D. K. Ivanou, M. Starykevich, A. D. Lisenkov, M. L. Zheludkevich, H. B. Xue, S. V. Lamaka, M. G. S. Ferreira, Plasma anodized ZE41 magnesium alloy sealed with hybrid epoxy-silane coating, Corros. Sci. 73 (2013) 300-308.

[112] S.V. Lamaka, G. Knörnschild, D.V. Snihirova, M.G. Taryba, M.L. Zheludkevich, M.G.S. Ferreira, Complex anticorrosion coating for ZK30 magnesium alloy, Electrochim. Acta. 55 (2009) 131-141.

[113] D. K. Ivanou, K. A. Yasakau, S. Kallip, A. D. Lisenkov, M. Starykevich, S. V. Lamaka, M. G. S. Ferreira, M. L. Zheludkevich, Active corrosion protection coating for ZE41 magnesium alloy created by combining PEO and sol-gel techniques, RSC Adv. 6 (15) (2016) 12553-12560.

[114] Wei Shang, Baizhen Chen, Xichang Shi, Ya Chen, Xiang Xiao, Electrochemical corrosion behavior of composite MAO/sol–gel coatings on magnesium alloy AZ91D using combined micro-arc oxidation and sol–gel technique, J. Alloys Compd. 474 (2009) 541-545.

[115] M. Laleh, Farzad Kargar, A. Sabour Rouhaghdam, Improvement in corrosion resistance of micro arc oxidation coating formed on AZ91D magnesium alloy via applying a nano-crystalline sol–gel layer, J. Sol-Gel Sci. Technol. 59 (2011) 297-303.

[116] P. Amaravathy, S. Sowndarya, S. Sathyanarayanan, N. Rajendran, Novel sol gel coating of Nb_2O_5 on magnesium alloy for biomedical applications, Surf. Coat. Technol. 244 (2014) 131–141.

[117] Rong-Chang Zeng, Zhen-Guo Liu, Fen Zhang, Shuo-Qi Li, Hong-Zhi Cui, En-Hou Han, Corrosion of molybdate intercalated hydrotalcite coating on AZ31 magnesium alloy, J. Mater. Chem. A. 2 (2014) 13049-13057.

[118] Xiao Jiang, Ruiguang Guo, Shuqin Jiang, Evaluation of self-healing ability of Ce-V conversion coating on AZ31 magnesium alloy, J. Magnesium Alloys. 4 (3) (2016) 230-241.

[119] Jun Chen, Yingwei Song, Dayong Shan, En-Hou Han, Modifications of the hydrotalcite film on AZ31 Mg alloy by phytic acid: The effects of morphology, composition and corrosion resistance, Corros. Sci. 74 (2013) 130-138.

[120] S. Nezamdoust, D. Seifzadeh, Z. Rajabalizadeh, Application of novel sol–gel composites on magnesium alloy, Journal of Magnesium and Alloys. 7 (2019) 419–432.

[121] Zhi-Hui Xie, Shiyao Shan, Nanocontainers-enhanced self-healing Ni coating for corrosion protection of Mg alloy, J. Mater. Sci. 53 (2018) 3744-3755.

[122] Zhi-Hui Xie, Dan Li, Zakiya Skeete, Anju Sharma, Chuan-Jian Zhing, Nanocontainer-enhanced self-healing for corrosion-resistant Ni coating on Mg alloy, ACS Appl. Mater. Interfaces 9 (2017) 36247-36260.

[123] ChenDi Ding, Ying Liu, MingDong Wang, Ting Wang, JiaJun Fu, Self-healing, superhydrophobic coating based on mechanized silica nanoparticles for reliable protection magnesium alloy, J. Mater. Chem. A. 4 (2016) 8041-8052.

[124] Jiahui Song, Xiufang Cui, Zhe Liu, Guo Jin, Erbao Liu, Dan Zhang, Zonghong Gao, Advanced microcapsules for self-healing conversion coatings on magnesium alloy in $Ce(NO_3)_3$ solution with microcapsules containing $La(NO_3)_3$, Surf. Coat. Technol. 307 (2016) 500-505.

[125] M. F. Montemor, M. G. S. Ferreira, Analytical characterisation and corrosion behaviour of bis-aminosilane coatings modified with carbon nanotubes activated with rare-earth salts applied on AZ31 magnesium alloy, Surf. Coat. Technol. 202 (2008) 4766-4774.

[126] Jing-Yu Chen, Xiao-Bo Chen, Jing-Liang Li, Bin Tang, Nick Birbilis, Xungai Wang, Electrosprayed PLGA smart containers for active anti-corrosion coating on magnesium alloy AMlite, J. Mater. Chem. A. 2 (2014) 5738-5743.

[127] I. A. Kartsonakis, A. C. Balaskas, E. P. Koumoulos, C. A. Charitidis, G. Kordas, ORMOSIL-epoxy coatings with ceramic containers for corrosion protection of magnesium alloys ZK10, Prog. Org. Coat. 76 (2013) 450-470.

[128] M. Sun, A. Yerokhin, M. Ya. Bychkova, D. V. Shtansky, E. A. Levashov, A. Matthews, Self-healing plasma electrolytic oxidation coatings doped with benzotriazole loaded halloysite nanotubes on AM50 magnesium alloy, Corros. Sci. 111 (2016) 753-769.

[129] Lian Guo, Wei Wu, Yong Feng Zhou, Fen Zhang, Rong Chang Zeng, Jianmin Zeng, Layered double hydroxide coatings on magnesium alloys: A review, J. Mater. Sci. Technol. 34 (2018) 1455-1466.

[130] J. K. Lin, J. Y. Uan, Formation of Mg, Al-hydrotalcite conversion coating on Mg alloy in aqueous HCO_3^-/CO_3^{2-} and corresponding protection against corrosion by the coating, Corros. Sci. 51 (5) (2009) 1181-1188.

[131] J. K. Lin, J. Y. Uan, C. P. Wu, H. H. Huang, Direct growth oriented Mg-Fe layered double hydroxide (LDH) on pure Mg substrates and *in vitro* corrosion and cell adhesion testing of LDH-coated Mg samples, J. Mater. Chem. 21 (2011) 5011–5020.

[132] J. Chen, Y. W. Song, D. Y. Shan, E. H. Han, Study of the corrosion mechanism of the in situ grown Mg-Al-CO_3^{2-} hydrotalcite film on AZ31 alloy, Corros. Sci. 65 (2012) 268–277.

[133] L. Wang, K. Zhang, W. Sun, T. Wu, H. He, G. Liu, Hydrothermal synthesis of corrosion resistant hydrotalcite conversion coating on AZ91D alloy, Mater. Lett. 106 (2013) 111–114.

[134] F. Peng, H. Li, D. Wang, P. Tian, Y. Tian, G. Yuan, D. Xu, X. Liu, Enhanced corrosion resistance and biocompatibility of magnesium alloy by Mg-Al-layered double hydroxide, Adv. Mater. Interfaces 8 (2016) 35033–35044.

[135] R. C. Zeng, Z. G. Liu, F. Zhang, S. Q. Li, Q. K. He, H. Z. Cui, E. H. Han, Corrosion resistance of in-situ Mg-Al hydrotalcite conversion film on AZ31 magnesium alloy by one-step formation, Trans. Nonferrous Met. Soc. China 25 (2015) 1917–1925.

[136] S. Li, Y. Shen, D. Liu, L. Fan, X. Zheng, J. Yang, One-step fabrication of oriented Mg/Al layered double hydroxide film on magnesium substrate with urea hydrolysis and its corrosion resistance, Compos. Interfaces 19 (2012) 489–498.

[137] T. Ishizaki, S. Chiba, H. Suzuki, In situ formation of anticorrosive Mg-Al layered double hydroxide-containing magnesium hydroxide film on magnesium alloy by steam coating, ECS Electrochem. Lett. 2 (2013) C15–C17.

[138] N. Kamiyama, G. Panomsuwan, E. Yamamoto, T. Sudare, N. Saito, T. Ishizaki, Effect of treatment time in the $Mg(OH)_2$/Mg-Al LDH composite film formed on Mg alloy AZ31 by steam coating on the corrosion resistance, Surf. Coat. Technol. 286 (2016) 172–177.

[139] J. Wang, D. Li, X. Yu, X. Jing, M. Zhang, Z. Jiang, Hydrotalcite conversion coating on Mg alloy and its corrosion resistance, J. Alloys Compd. 494 (2010) 271–274.

[140] F. Zhang, Z. G. Liu, R. C. Zeng, S. Q. Li, H. Z. Cui, L. Song, E. H. Han, Corrosion resistance of Mg-Al-LDH coating on magnesium alloy AZ31, Surf. Coat. Technol. 258 (2014) 1152–1158.

[141] R. C. Zeng, Z. G. Liu, F. Zhang, S. Q. Li, H. Z. Cui, E. H. Han, Corrosion of molybdate intercalated hydrotalcite coating on AZ31 Mg alloy, J. Mater. Chem. A. 2 (2014) 13049–13057.

[142] J. H. Syu, J. Y. Uan, M. C. Lin, Z. Y. Lin, Optically transparent Li-Al-CO_3 layered double hydroxides thin films on an AZ31 Mg alloy formed by electrochemical deposition and their corrosion resistance in a dilute chloride environment, Corros. Sci. 68 (2013) 238–248.

[143] F. Wu, J. Liang, Z. Peng, B. Liu, Electrochemical deposition and characterization of Zn-Al layered double hydroxides (LDHs) films on magnesium alloy, Appl. Surf. Sci. 313 (2014) 834–840.

[144] F. Zhang, M. Sun, S. Xu, L. Zhao, B. Zhang, Fabrication of oriented layered double hydroxide films by spin coating and their use in corrosion protection, Chem. Eng. J. 141 (2008) 362–367.

[145] M. Zhou, L. Yan, H. Ling, Y. Diao, X. Pang, Y. Wang, K. Gao, Design and fabrication of enhanced corrosion resistance Zn-Al layered double hydroxides films based anion-exchange mechanism on magnesium alloys, Appl. Surf. Sci. 404 (2017) 246–253.

[146] Yan Li, Shu Cai, Sibo Shen, Guohua Xu, Feiyang Zhang, Fengwu Wang, Self-healing hybrid coating of phytic acid/silane for improving the corrosion resistance of magnesium alloy, J. Coat. Technol. Res. 15 (3) (2018) 571-581.

[147] Lénia M. Calado, Maryna G. Taryba, Maria J. Carmezim, M. Fátima Montemor, Self-healing ceria-modified coating for corrosion protection of AZ31 magnesium alloy, Corros. Sci. 142 (2018) 12-21.

[148] A. F. Galio, S. V. Lamaka, M. L. Zheludkevich, L. F. P. Dick, I. L. Müller, M. G. S. Ferreira, Inhibitor-doped sol–gel coatings for corrosion protection of magnesium alloy AZ31, Surf. Coat. Technol. 204 (2010) 1479-1486.

[149] Dan Jiang, Xianchao Xia, Jian Hou, Xinxin Zhang, Zehua Dong, Enhanced Corrosion Barrier of Micro arc-Oxidized Mg Alloy by Self- Healing Superhydrophobic Silica Coating, Ind. Eng. Chem. Res. 58 (2019) 165-178.

[150] Yanbin Zhao, Zhao Zhang, Liqian Shi, Fen Zhang, Shuoqi Li, Rongchang Zeng, Corrosion resistance of a self-healing multilayer film based on SiO_2 and CeO_2 nanoparticles layer-by-layer assembly on Mg alloys, Mater. Lett. 237 (2019) 14-18.

[151] Lenia M. Calado, Maryna G. Taryba, Yegor Morozov, Maria J. Carmezim, M. Fatima Montemor, Novel smart and self-healing cerium phosphate-based corrosion inhibitor for AZ31 magnesium alloy, Corros. Sci. 170 (2020) 108648.

[152] Xia Zhao, Jinfei Wei, Bucheng Li, Sibei Li, Ning Tian, Lingyun Jing, Junping Zhang, A self-healing superamphiphobic coating for efficient corrosion protection of magnesium alloy, J. Colloid Interface Sci. 575 (2020) 140-149.

[153] Y. Li, S. Cai, S. Shen, G. Xu, F. Zhang, F. Wang, Self-healing hybrid coating of phytic acid/silane for improving the corrosion resistance of magnesium alloy, J. Coat. Technol. Res. 15 (2018) 571–581.

[154] Wenhui Yao, Liang Wu, Guangsheng Huang, Bin Jiang, Andrej Atrens, Fusheng Pan, Superhydrophobic coatings for corrosion protection of magnesium alloys, J. Mater. Sci. Technol. 52 (2020) 100-118.

[155] Hanaa Soliman, Junyu Qian, Shuai Tang, Peng Xian, Yingqi Chen, Abdel-Salam Makhlouf, Guojiang Wang, Hydroxyquinoline/nano-graphene oxide composite coating of self-healing functionality on treated Mg alloys AZ31, Surf. Coat. Technol. 385 (2020) 125395.

[156] Liang Wu, Danni Yang, Gen Zhang, Zhi Zhang, Sheng Zhang, Aitao Tang, Fusheng Pan, Fabrication and characterization of Mg-M layered double hydroxide films on anodized magnesium alloy AZ31, Appl. Surf. Sci. 431 (2018) 177-186.

[157] R. N. Peres, E. S. F. Cardoso, M. F. Montemor, H. G. de Melo, A. V. Benedetti, P. H. Suegama, Influence of the addition of SiO_2 nanoparticles to a hybrid coating applied on an AZ31 alloy for early corrosion protection, Surf. Coat. Technol. 303 (B) (2016) 372-384.

[158] Fen Zhang, Changlei Zhang, Liang Song, Rongchang Zeng, Shuoqi Li, Hongzhi Cui, Fabrication of the superhydrophobic surface on magnesium alloy and its corrosion resistance, J. Mater. Sci. Technol. 13 (11) (2015) 1139-11443.

[159] X. P. Guo, G. L. Song, J. Y. Hu, D. B. Huang, Corrosion inhibitors of magnesium (Mg) alloys, in: G. L. Song (Ed.), Corrosion Prevention of Magnesium Alloys, Woodhead Publishing (2013) pp. 61–84.

[160] S. V. Lamaka, B. Vaghefinazari, Di Mei, R. P. Petrauskas, D. Höche, M. L. Zheludkevich, Comprehensive screening of Mg corrosion inhibitors, Corros, Sci. 128 (2017) 224-240.

[161] Saviour A. Umoren, Moses M. Solomon, A. Madhankumar, Ime B. Obot, Exploration of natural polymers for use as green corrosion inhibitors for AZ31 magnesium alloy in saline environment, Carbohydr. Polym. 230 (2020) 115466.

[162] Dan Liu, Yingwei Song, Dayong Shan, En-Hou Han, Comparison of inhibition effect of four inhibitors on the corrosion behaviour of AM60 magnesium alloy, Int. J. Electrochem. Sci. 13 (2018) 2219-2235.

[163] I. A. Kartsonakis, S. G. Stanciu, A. A. Matei, E. K. Karaxi, R. Hristu, A. Karantonis, C. A. Charitidis, Evaluation of the protective ability of typical corrosion inhibitors for magnesium alloys towards the Mg ZK30 variant, Corros. Sci. 100 (2015) 194-208.

[164] Habib Ashassi-Sorkhabi, Saleh Moradi-Alavian, Mehdi D. Esrafili, Amir Kazempour, Hybrid sol-gel coatings based on silanes-amino acids for corrosion protection of AZ91 magnesium alloy: Electrochemical and DFT insights, Prog. Org. Coat. 131 (2019) 191-202.

[165] Habib Ashassi-Sorkhabi, Saleh Moradi-Alavian, Amir Kazempour, Salt-nanoparticle systems incorporated into sol-gel coatings for corrosion protection of AZ91 magnesium alloy, Prog. Org. Coat. 135 (2019) 475-482.

[166] H. Gao, Q. Li, Y. Dai, F. Luo, H. X. Zhang, High efficiency corrosion inhibitor 8-hydroxyquinoline and its synergistic effect with sodium dodecylbenzenesulphonate on AZ91D magnesium alloy, Corros. Sci. 52 (2010) 1603-1609.

Chapter 3

COATINGS BASED ON HALLOYSITE NANOTUBES LOADED WITH Ce^{3+}-Zr^{4+}

Chapter 3

Coatings based on halloysite nanotubes loaded with Ce^{3+}-Zr^{4+}

3.1 Introduction

As discussed in Chapter-1, magnesium (Mg) alloys are prone to corrosion very quickly, owing to their extremely low standard electrode potential of -1.63 V in 0.55 M NaCl (-2.37 V in atmospheric exposure), which limits their use in structural parts of automobile and aerospace industries. The poor anticorrosion properties of Mg alloys could be attributed to (a) dissolution of thin film of oxides/hydroxides with increase in pH after corrosive medium exposure and (b) occurrence of galvanic corrosion due to poor design, flux contaminations, impurities and secondary phases like $Mg_{l7}Al_{12}$, AlMn, Al_8Mn_5, $Mg_{12}Nd$, Mg_2Pb, etc. [1-3]. Various methodologies have been investigated for enhancing the anticorrosion properties of Mg alloys, which include decreasing the amount of Fe, Cu and Ni impurities, generating more homogeneous microstructure, increasing content of alloying elements that retards corrosion and applying protective coatings. Among these methodologies, use of protective coatings is the most promising strategy in which, methods such as anodization, electrophoretic deposition, plasma electrolytic oxidation (PEO) and sol-gel processing have been found to be more promising [4] as discussed in chapter 2.

Hybrid sol-gel coatings are considered as an eco-friendly alternative to chromate conversion coatings with an ability to generate crack-free coatings; having versatility to accommodate a number of additives and can be processed at low curing temperatures. Several pathways have been developed to enhance the corrosion protection ability of silane-based coatings, which includes direct dispersion of corrosion inhibiting agents into the coating matrix and/or loading them into containers, which avoid direct contact of inhibitor with coating matrix and prevent detrimental effect on anticorrosion properties of coatings [5-8]. Owing to the controlled release of inhibitors at the localised area only after occurrence of defect, encapsulation of corrosion inhibitor could provide prolonged corrosion protection. Use of naturally occurring nanoclay is considered as a cost-effective approach for encapsulation of corrosion inhibitors rather than synthesizing artificial containers. Halloysite nanotubes ($Al_2Si_2O_5$ $(OH)_4$. n H_2O, HNTs) are naturally occurring inorganic clays belonging to the alumino silicate clays of kaolin group having dioctahedral crystal structure with 10-100 nm internal diameter and length of 0.5-2 µm. HNTs are

composed of outer layer of tetrahedral silica with negative charge and inner layer of octahedral alumina with positive charge below pH 8.5 (Fig. 3.1) [9].

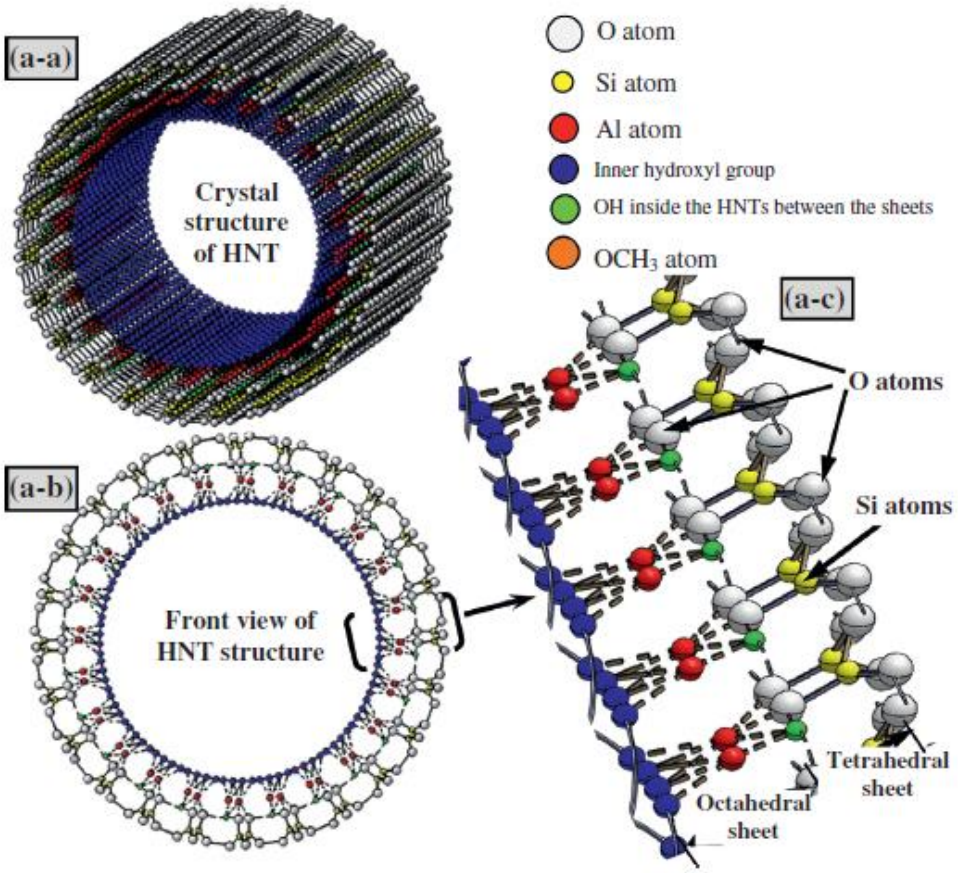

Figure 3.1: Morphological and molecular **s**tructure of HNT [10] *(With permission from Elsevier, January 02, 2021, License No. 4980620445121)*

Shchukin et al. [11] and Fix et al. [12] have loaded corrosion inhibitors such as 2-mercaptobenzothiazole (MBT) and benzotriazole (BTA); 8-hydroxyquinoline (HQ) respectively into lumen of HNTs and then dispersed them into hybrid sol-gel matrix that was coated on Al alloy substrates. Zahidah et al. [13] have loaded benzimidazole into HNTs and then dispersed them into epoxy matrix, which was coated on carbon steel for evaluation of corrosion protection ability of coatings. 10 wt % of dodecylamine loaded HNTs were doped in alkyd primer coated on carbon steel by Falcon et al. [14]. Shuchukina et al. [15] have generated polyester powder coating comprising of HQ loaded HNT and mesoporous silica nanoparticles on low carbon steel. Sun et al. [16] have loaded HNTs with BTA and then dispersed into electrolytic bath of PEO coatings generated on Mg alloy AM50. Mahmoudi et al. [17] have etched lumen of HNTs in order to accommodate higher amount of praseodymium as a corrosion inhibitor and encapsulated with polymeric microcapsules. The encapsulated HNTs were dispersed into organic-inorganic silane matrix and epoxy

silane matrix, which were dip coated on AZ31 substrates. As observed from electrochemical studies and salt spray tests, encapsulated inhibitor based silane and epoxy silane coatings showed long-term corrosion protection in 0.6 M NaCl solution with better barrier properties. Asadi et al. [18] have functionalized HNTs with 3-aminopropyltriethoxysilane (APTES) for enhanced loading of cationic Zn^{2+} as a corrosion inhibitor and then dispersed the inhibitor loaded as-received and modified HNTs into epoxy ester coating matrix. Initially the inhibition ability of inhibitor was examined with electrochemical studies by exposing bare steel substrates to Zn^{2+} cations released from as-received HNTs in NaCl solution and observed that corrosion current density was suppressed when substrates were exposed to Zn^{2+} cations released from modified HNTs. Further, electrochemical studies of scribed coatings exposed to NaCl solution for 48 h indicated better barrier properties owing to the release of Zn^{2+} cations in the scribed region. Number of other recent studies [19-22] have been performed by encapsulating different corrosion inhibitors into HNTs for corrosion protection of steel substrates.

As observed from literature survey, there are very few reports on corrosion protection of Mg alloys using inhibitor loaded HNTs. This chapter includes detailed explanation of our studies where, cationic Ce^{3+}-Zr^{4+} inhibitors were loaded in HNTs and then 2 wt % of them were dispersed in hybrid sol-gel matrix, to generate self-healing coatings on Mg alloy AZ91D. For comparison purpose, the effect of addition of as-received HNTs on barrier properties of coatings was also evaluated by dispersing as-received HNTs in hybrid matrix sol. In the following sections, the methodology used to synthesize the hybrid matrix sol (MAT), as-received HNT dispersed matrix sol (Clay matrix, CM sol) and self-healing (SH) sol followed by characterization of generated coatings by various electrochemical methods will be discussed.

3.2 Materials and Methods

3.2.1 Substrate preparation

Mg alloy AZ91D flat coupons with chemical composition in wt % by wet analysis: Al-9.14; Zn-0.86; Mn-0.30; Cu-0.09; Si-0.08; Fe-0.01; Ni-0.01 and rest Mg and of dimensions 2.5 cm x 2.0 cm x 0.6 cm were used as substrates. The substrates were mechanically cleaned by polishing with 1000 grit emery (silicon carbide) sheets followed by repeated degreasing with acetone for 30 min and then drying in atmospheric air.

3.2.2 Synthesis of hybrid matrix sol

100 ml of organic-inorganic matrix sol (MAT) was synthesized by hydrolysis of 3-glycidyloxypropyltrimethoxysilane (GPTMS) with tetraethoxysilane (TEOS), both supplied by Sigma Aldrich, USA in the molar ratio of 3.5:1 in presence of 0.1 N hydrochloric acid (HCl, Fisher Scientific, USA, 36.4 %) as a catalyst. Deionised (DI) water was added to the turbid solution under constant stirring conditions for 1 h until a transparent solution of matrix sol is obtained.

3.2.3 Synthesis of polymeric microcapsules

Polymeric microcapsules were synthesized by using *in situ* polymerization in an oil-in-water emulsion. 10 ml of 5 wt % aqueous solution of polyvinyl alcohol (PVA, Alfa Aesar, USA) was mixed with 260 ml of DI water under constant stirring conditions. 5 g urea (Sigma Aldrich, USA), 0.5 g ammonium chloride (NH_4Cl, Fisher Scientific, India) and 0.5 g resorcinol (Fisher Scientific, India) were added simultaneously to the above solution. pH of the solution was maintained at ~3.5 using 0.1 N HCl. 25 ml of hydrolysed GPTMS (Gelest Inc., USA, 98 %) was added dropwise to form an emulsion followed by stabilization for 10 min with constant stirring conditions. 12.67 g of 37 wt % formaldehyde (Fisher Scientific, India) was added to the stabilized emulsion. The emulsion was heated slowly and maintained at 55 ^oC under constant stirring for 4 h that was cooled at ambient temperature thereafter. Microcapsules were recovered from suspension by filtration under vacuum followed by repeated washing with DI water and then dried under vacuum [23-25].

3.2.4 Loading of HNTs with corrosion inhibitor

5 g of HNTs (Sigma Aldrich, USA) were used as-received without any pretreatment for loading of corrosion inhibitors such as cerium nitrate hexahydrate (Ce^{3+}, Loba Chemie, India, 99.9 %) and zirconium n-propoxide (Zr^{4+}, Gelest Inc., USA, 70 % in propanol) in a molar ratio of 1:23. 0.029 moles of methacrylic acid (MAA, ABCR GmbH & Co., Germany) was used as a complexing agent with Zr-n-propoxide. The corrosion inhibitors and complexing agent were loaded in HNTs by repeated vacuum evacuation for 3 h in vacuum desiccator as specified by Abdullayev et al. [26]. The inhibitor loaded HNTs were then separated from inhibitor solution using 10 min of centrifugation at 6500 rpm followed by repeated washing with 2-propanol in order to remove any adsorbed inhibitor. The inhibitor loaded HNTs (Fig. 3.2) were then dried in hot air oven at 60 °C for 1 h.

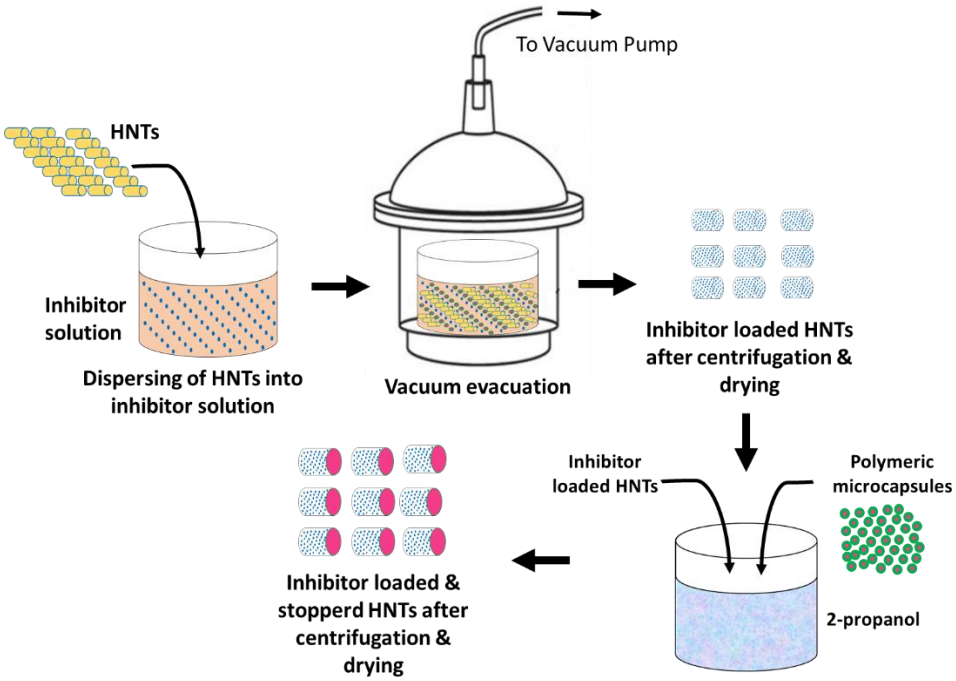

Figure 3.2: Schematic representation of inhibitor loading and stoppering of HNTs

3.2.5 Preparation of self-healing sol and coating deposition

In order to examine the effect of addition of HNTs, 2 g of as-received HNTs were dispersed in 98 g MAT sol to obtain clay matrix (CM) sol. 2 g of aforementioned inhibitor loaded HNTs were stoppered at the ends with 25 ml of polymeric microcapsules (dispersed in 2-propanol) and then dispersed in MAT sol to synthesize self-healing (SH) sol under constant stirring for 3 h.

Dip coating technique was used to generate coatings on AZ91D substrates at a withdrawal speed of 1 mm/s and then thermally cured at 130 ^{o}C for 1 h. A non-destructive coating thickness measurement gauge (PosiTector$^{®}$6000, DeFelsko Corporation, USA) was used to measure coating thickness which was found to be in the range of 3-5 µm.

3.3 Characterization Techniques

3.3.1 Morphological analysis of as-received and inhibitor loaded HNTs

The length and diameter of the HNTs was verified with a transmission electron microscope (TEM, Tecnai 220 G2, FEI, Netherlands). The length of the HNTs was ascertained with field emission scanning electron microscope (FESEM, ZEISS Gemini SEM 500) having a hot Schottky field emission (FE) gun. Scanning Electron Microscope-Energy Dispersive Spectroscopic (SEM-EDS, Hitachi S3400N) analysis was carried out for confirming the presence of corrosion inhibitors.

X-ray diffraction (XRD) measurements of as-received and inhibitor loaded HNTs were carried out using Bruker AXS D8 Advance, USA for phase analysis. The diffraction analysis was carried out in the 2-theta (2θ) range of 2-80^{o}, in a step scan mode with step size of 0.1^{o}. The instrument was fitted with a vertical goniometer on which Cu source and a high speed 1D Lynx Eye detector were mounted and the XRD profiles were acquired in symmetric geometry.

BET surface area and pore volume measurements were carried out for inhibitor loaded and unloaded HNTs by using a Micromeritics ASAP 2020 surface area and porosimetry analyser. Nitrogen adsorption-desorption was carried out at 77 K during the analysis. Adsorption experiments were carried out after degassing all the samples at 300 °C for 6 h under vacuum. Brunauer–Emmett–Teller procedure was employed to evaluate the specific surface area. The nitrogen adsorption volume was used to obtain the pore volume at a relative pressure (P/P_0).

3.3.2 Adhesion Test

The adhesion strength of MAT, CM and SH sol based coatings on AZ91D substrates was evaluated as per ASTM D3359-17 test procedure [27] by using cross-hatch cutter. Scribes were made on the surfaces in the form of 1 mm^2 grid lines. A pressure sensitive scotch adhesive tape was applied over the grid and pulled off rapidly at an angle close to 180^0. Optical microscope (Olympus BX51M) was used to examine the samples for any removal of the coating and then classified as 0B to 5B based on percentage of coating removed.

3.3.3 Weight loss measurements

Weight loss measurements of bare and coated AZ91D substrates with dimensions of 2.5 cm x 2 cm were carried out according to ASTM G31 [28]. AZ91D substrates were immersed in 200 ml of 0.6 M NaCl solution for different durations like 24 h, 72 h and 120 h. The substrates were washed with DI water and ethyl alcohol to clear away any loosely adhered salt and then exposed to chromic acid (200 g/L) solution for 2 min for eliminating the corrosion products accumulated on the surface. The traces of chromic acid were removed from the substrate surface by repeated washing with DI water and ethanol. The substrates were weighed prior and after immersion in NaCl solution and the corrosion rates were calculated using the weight difference. The repeatability of corrosion rates was examined by obtaining the weight losses of uncoated and coated substrates for three substrates each.

$$\text{Corrosion rate} = \frac{8.76 \times 10^4 \times w}{t \times A \times \rho}$$

Where, w is weight loss in grams (g), t is exposure time in hours (h), A is exposed area in cm^2 and ρ is density of the alloy in g/cm^3.

3.3.4 Electrochemical measurements

Electrochemical analyser (CH Instruments, Model 600E Series) was used for carrying out electrochemical impedance spectroscopy (EIS) and potentiodynamic polarization measurements. The three electrode configured system was composed of saturated calomel electrode (SCE) as reference electrode, platinum electrode as counter electrode and the substrate as working electrode with an exposure area of 1 cm^2. The EIS experiments were performed over a frequency range of 1 MHz to 0.01 Hz using an AC signal of 10 mV amplitude. The potentiodynamic polarization measurements were carried out on Mg alloy AZ91D after exposure to 0.6 M NaCl solution for various durations by applying potentials with reference to OCP over a range of ± 0.3 V with 0.8 mV/s scan rate.

3.3.5 Scanning Vibrating Electrode Technique (SVET) Measurements

SVET with Biologic SCV 470 control unit was used to evaluate the self-healing ability of uncoated and coated AZ91D substrates. The measurements were performed on substrates with dimensions 10 mm x 10 mm and a scan area of 4 mm x 4 mm with 64 x 48 points along X and Y axes. Uncoated and coated substrates were immersed in 0.6 M NaCl solution after generation of artificial defects having size in the range of 0.1 to 0.3 mm^2 with a depth of 30±1.0 µm and a width of 180 µm. Scans were started within 5 min of exposure to the electrolytic solution and the data were collected for various durations of exposure. Each scan comprised of 400 data points on a 20 x 20 grid with 1s per point integration time. 30 min are required for each complete scan with 5 min rest period between two scans. Vibrating electrode was used at a frequency of 100 Hz. Open circuit potential (OCP) was considered as a reference potential for all experiments. Current density data was obtained after various durations of exposure. 3D current density maps are used to depict cathodic and anodic regions denoted by negative and positive current densities, respectively for each scan area.

3.3.6 Micro-Raman spectroscopic analysis

Micro-Raman spectroscopic analysis was performed for confirmation of self-healing mechanism. The measurements were carried out in the scribed areas of uncoated and SH

sol coated substrates immediately after scribing and after 120 h of exposure of scribed area to 0.6 M NaCl solution. The data was acquired using Horiba Jobin Yvon-Lab Ram HR-800 Raman spectrometer with Argon ion laser of 514 nm as the light source over the scan range of 100–1000 cm $^{-1}$.

3.4 Results and Discussion

3.4.1 Morphological analysis of as-received and inhibitor loaded HNTs

Morphological analysis of as-received and inhibitor loaded and end-capped HNTs was performed by FESEM and TEM analysis for measurement of tube length and lumen diameter. SEM-EDS analysis was performed to examine the appearance of corrosion inhibitors after loading into HNTs. The surface morphology and SEM-EDS analysis of inhibitor unloaded and loaded HNTs is depicted in Fig. 3.3. The as-received HNTs showed tubular nature with lengths varying in the range of 0.1-2 µm and lumen diameters in the

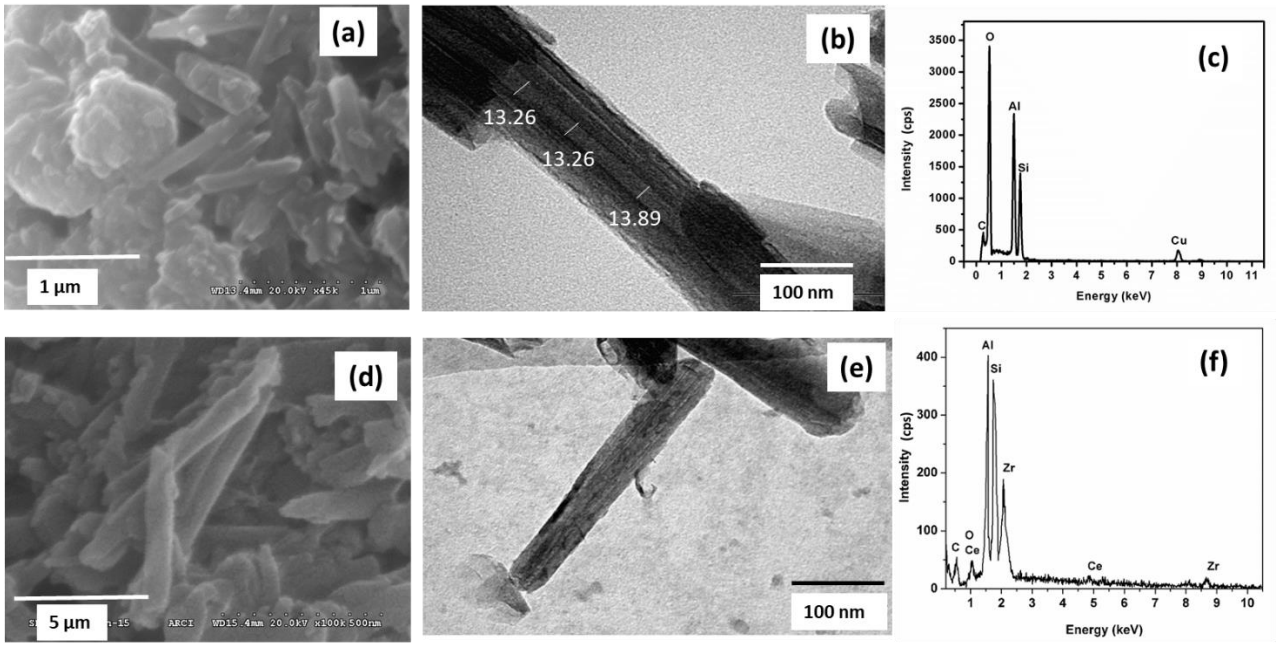

Figure 3.3: FESEM images (a), (d); TEM images (b), (e) and EDS spectra (c), (f) of as-received HNTs and inhibitor loaded HNTs

range of 10-15 nm as shown in Fig. 3.3 (a) & (b). Elemental analysis of as-received HNTs confirmed the composition to be aluminosilicate as shown in Fig. 3.3 (c). The as-received HNTs were loaded with cationic Ce^{3+}-Zr^{4+} corrosion inhibitors by vacuum evacuation and end stoppered using polymeric microcapsules to prevent the untimely release of inhibitors. FESEM and TEM images of inhibitor loaded HNTs shown in Fig. 3.3 (d) and (e) respectively, depicted that the corrosion inhibitors have covered the surface of HNTs,

which was confirmed by EDS analysis in Fig.3.3 (f) indicating appearance of Ce^{3+}-Zr^{4+}. The morphology of polymer-based microcapsules used for stoppering the ends of encapsulated HNTs was observed using FESEM as shown in Fig. 3.4. The diameter of microcapsules was found to be in the range of 0.5-1.5 µm.

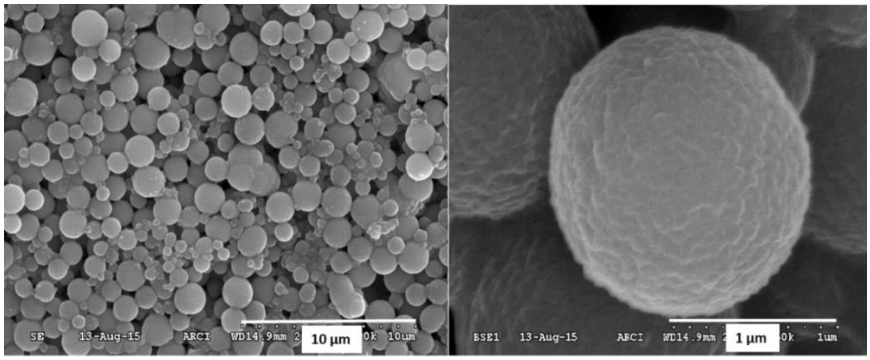

Figure 3.4: FESEM images of polymeric microcapsules

3.4.2 XRD analysis

XRD profiles of as-received and inhibitor encapsulated and end capped HNTs are as shown in Fig. 3.5. The XRD patterns of as-received and inhibitor encapsulated and end capped HNTs were found to be similar having no shift in 2θ values of (001) and (020) peaks. The peaks (001) and (020) corresponded to multilayer wall packing and tubular nature of HNTs, respectively. Hence, it could be concluded that corrosion inhibitors were encapsulated inside the lumen of HNTs and did not intercalate in the interlayer spacing of HNTs, as there was no shift in (001) & (020) peak positions [29].

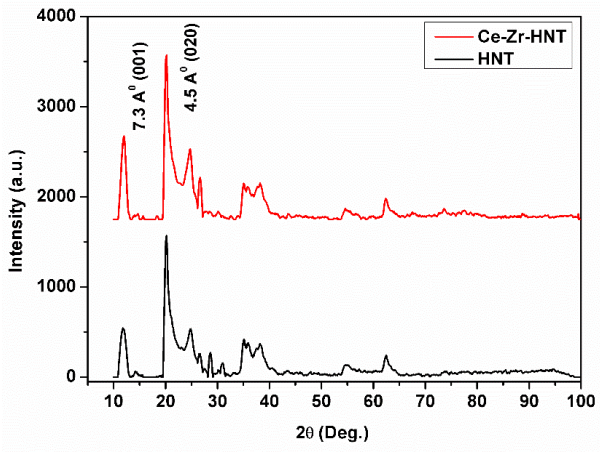

Figure 3.5: XRD profiles of as-received and inhibitor encapsulated HNTs

3.4.3 BET pore volume and surface area analysis

The encapsulation of corrosion inhibitors into the lumen of HNTs was ascertained with BET pore volume and surface area analysis. The variation in pore volume with respect to

pore diameter in case of as-received and inhibitor encapsulated and stoppered HNTs is depicted in Fig. 3.6.

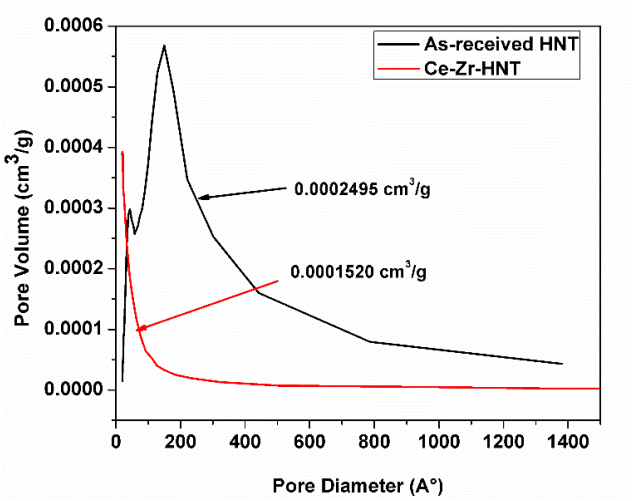

Figure 3.6: Pore volume analysis of as-received and inhibitor encapsulated and stoppered HNT

The surface area of as-received and inhibitor encapsulated HNTs was found to be 48.93 m^2/g and 14.51 m^2/g, respectively, which indicated that the inhibitor may have either got loaded into the lumen of HNTs or got adsorbed on their surface. The loading of inhibitor into the lumen was further verified from pore volume measurements, which was determined to be 0.0002495 cm^3/g and 0.0001520 cm^3/g for as-received and inhibitor encapsulated HNTs, respectively, which confirmed that the corrosion inhibitor encapsulation has taken place inside the lumen.

3.4.4 Thickness and adhesion strength of coatings

SEM cross sectional analysis was used to measure the thickness of SH coatings based on inhibitor loaded and stoppered HNTs. The thickness of SH coating was found to be around 4.20 µm as observed from SEM cross sectional image shown in Fig. 3.7.

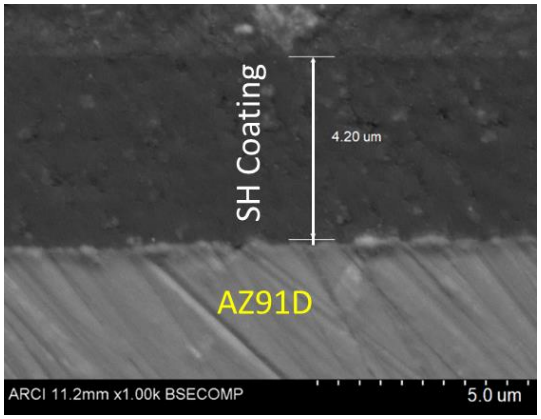

Figure 3.7: SEM cross sectional morphology of SH coating

The adhesion strength of coatings was evaluated by using tape adhesion test according to ASTM D3359-17 and the results are classified as shown in Fig. 3.8 [29]. The optical microscopic images for adhesion test of coated substrates carried out using cross-hatch cutter are as shown in Fig. 3.9. Very smooth edges of cut were observed with MAT sol coatings on AZ91D (Fig. 3.9a, 3.9b) after peeling off the tape. Hence, the coating adhesion was considered as rank 5B, which denoted best adhesion property as per ASTM D3359-17. Similarly, in case of SH sol coatings (Fig. 3.9e, 3.9f), no removal of coating around the edges was observed and the adhesion was ranked as 5B. However, around 35 % of the coated area was detached after the removal of tape in case of CM sol coatings (Fig.3.9c, 3.9d) and the coating adhesion was ranked as 2B.

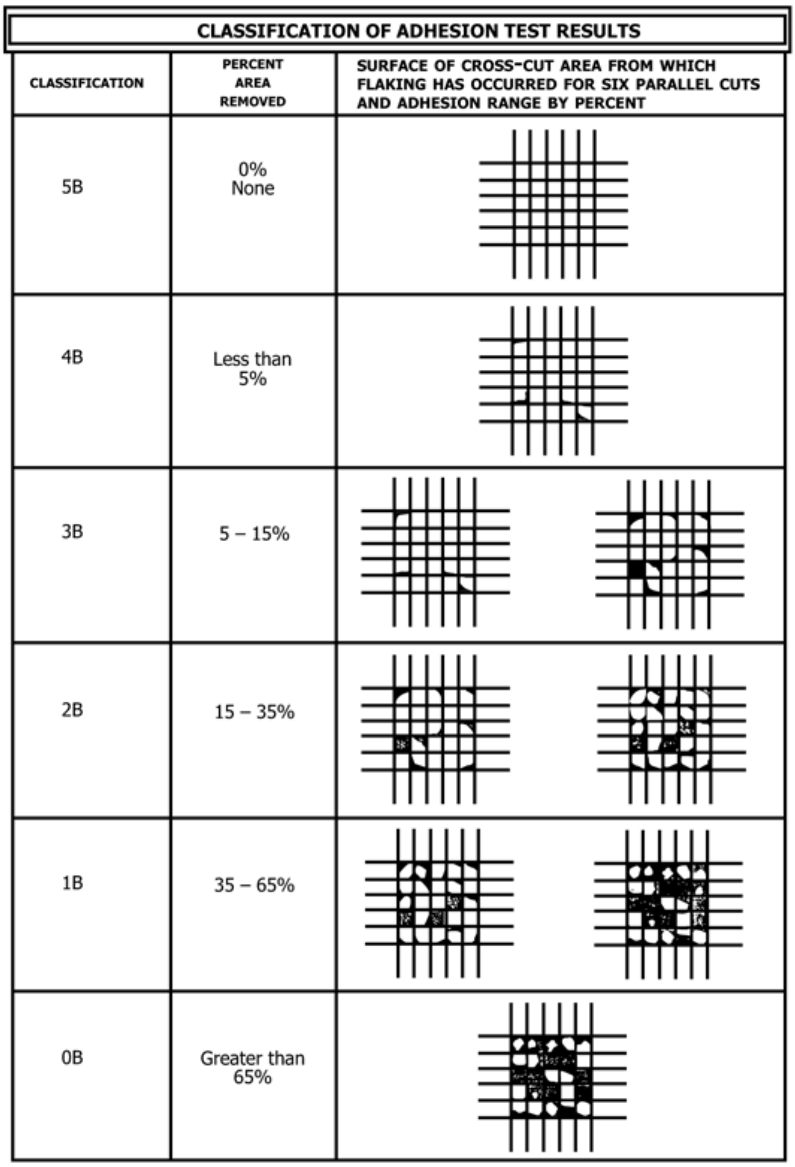

Figure 3.8: Classification of adhesion test results as per ASTM D3359-17

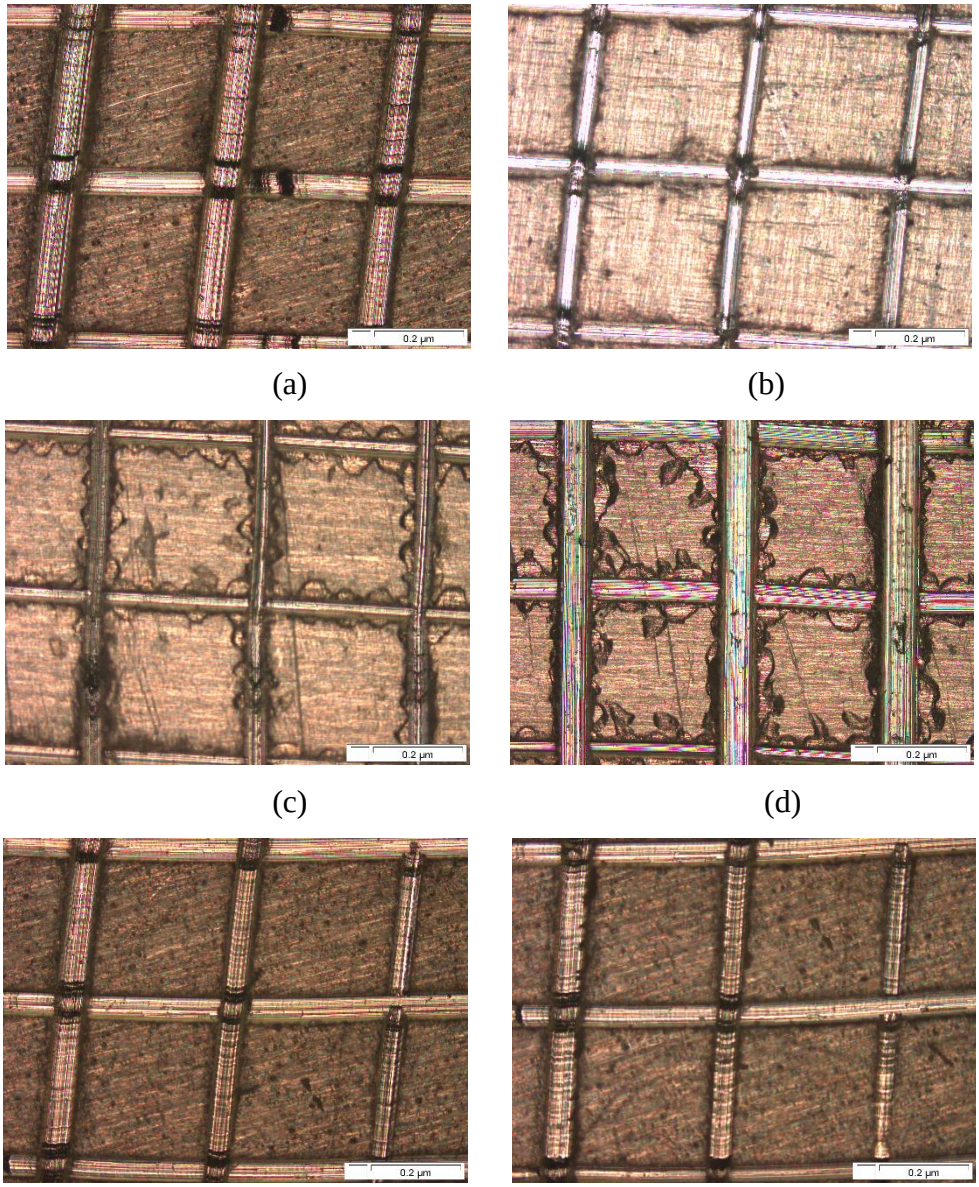

Figure 3.9: Optical microscopic images of adhesion test of MAT sol coated (a, b), CM sol coated (c, d) and SH sol coated (e, f) substrates before putting on tape and after removal of tape

3.4.5 Weight loss experiments

Corrosion resistance evaluation by weight loss measurements lend more practical data on the durability and corrosion resistance of uncoated and coated substrates. Here, rate of corrosion (Fig. 3.10) was evaluated for uncoated and coated AZ91D substrates after 24 h, 72 h and 120 h of exposure to 0.6 M NaCl solution. It can be observed that, the barrier property of MAT sol and SH sol coated substrates remained intact up to 24 h of exposure, thereby showing least corrosion rate. However, with increased durations of exposure to corrosive medium, the corrosion rate increases owing to the depletion of barrier property.

Until 72 h of exposure, bare substrates have shown decreased corrosion rate owing to the formation of thin oxide/hydroxide layer that restricts the corrosive attack on the surface. After 120 h, it can be ascertained that SH sol coated substrates showed least corrosion rate, implying that inclusion of inhibitor encapsulated clay nanotubes provided better barrier properties than CM sol coated specimen where corrosion rate was very high for all durations of exposure.

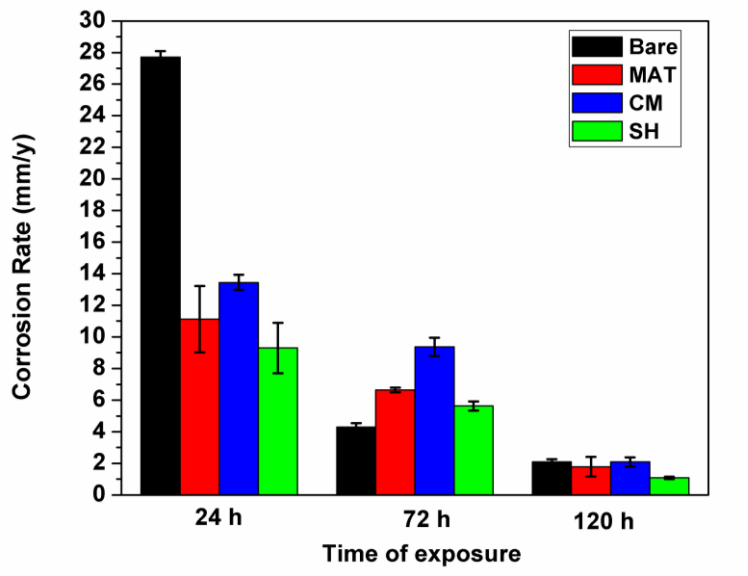

Figure 3.10: Comparison of corrosion rates of bare and coated substrates after various durations of exposure to 0.6 M NaCl solution

3.4.6 EIS and potentiodynamic polarization measurements

EIS and potentiodynamic polarization measurements were performed for evaluation of the anticorrosion properties of bare and coated (MAT, CM and SH) AZ91D samples after exposure to 0.6 M NaCl solution for various durations such as 24 h, 72 h and 120 h.

The Nyquist plots and bode plots for uncoated and coated substrates exposed to 0.6 M NaCl solution for different durations are depicted in Fig. 3.11 and Fig. 3.12 respectively. As observed from Table 3.1, after 24 h of exposure, SH sol coated substrates showed lower corrosion resistance because of reduced barrier property with the dispersion of HNTs, which could be confirmed from higher capacitance values. After 72 h of exposure, SH coated substrates showed higher impedance values because of generation of passive layer of oxides of cerium and zirconium after the corrosion inhibitor release from HNTs. The corrosion resistance of SH sol based coatings was found to increase with prolonged exposure of 120 h owing to the controlled release of corrosion inhibitors from lumen of HNTs. CM sol coated substrates showed lowest corrosion resistance after 72 h as HNTs do

not have favourable aspect ratio for dispersion in matrix sol as evaluated by Huttunen-Saarivirta et al. [30] who showed that the HNTs were distributed randomly into the coating matrix. After prolonged exposure of 120 h, though the corrosion resistance is on the higher side, the double layer capacitance is also higher for CM sol based coatings as compared to that of SH sol based coatings. This could indicate that CM sol based coatings have higher permeability to corrosive ions due to the porous nature of coatings. After 24 h of exposure, MAT sol coated substrates displayed highest impedance values in high frequency region, thereby showing higher corrosion resistance for MAT coated substrates owing to the better

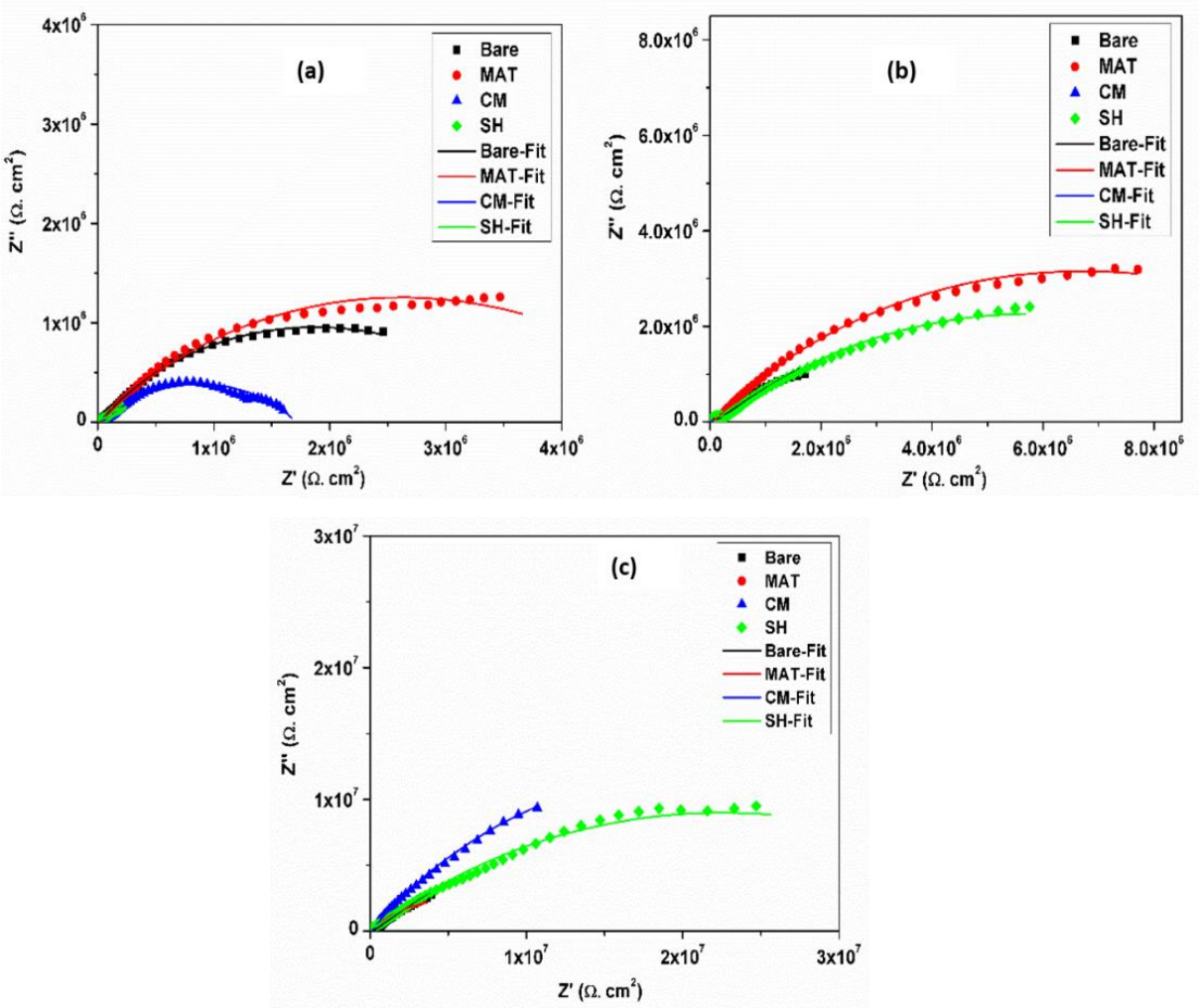

Figure 3.11: Nyquist plots for uncoated and coated AZ91D substrates after (a) 24 h, (b) 72 h and (c) 120 h exposure to 0.6 M NaCl solution

barrier properties. However, the corrosion resistance of MAT sol coated substrates decreased with the exposure of 120 h, which may have arised because of depletion of barrier properties of coatings. Bare substrates have shown considerable amount of corrosion resistance after 24 h of exposure due to thin film of oxides/hydroxides present on the

surface. However, it could be observed that, with the increase in exposure durations, the capacitance of this film was also increased indicating the increase in porosity of film and hence lower corrosion resistance.

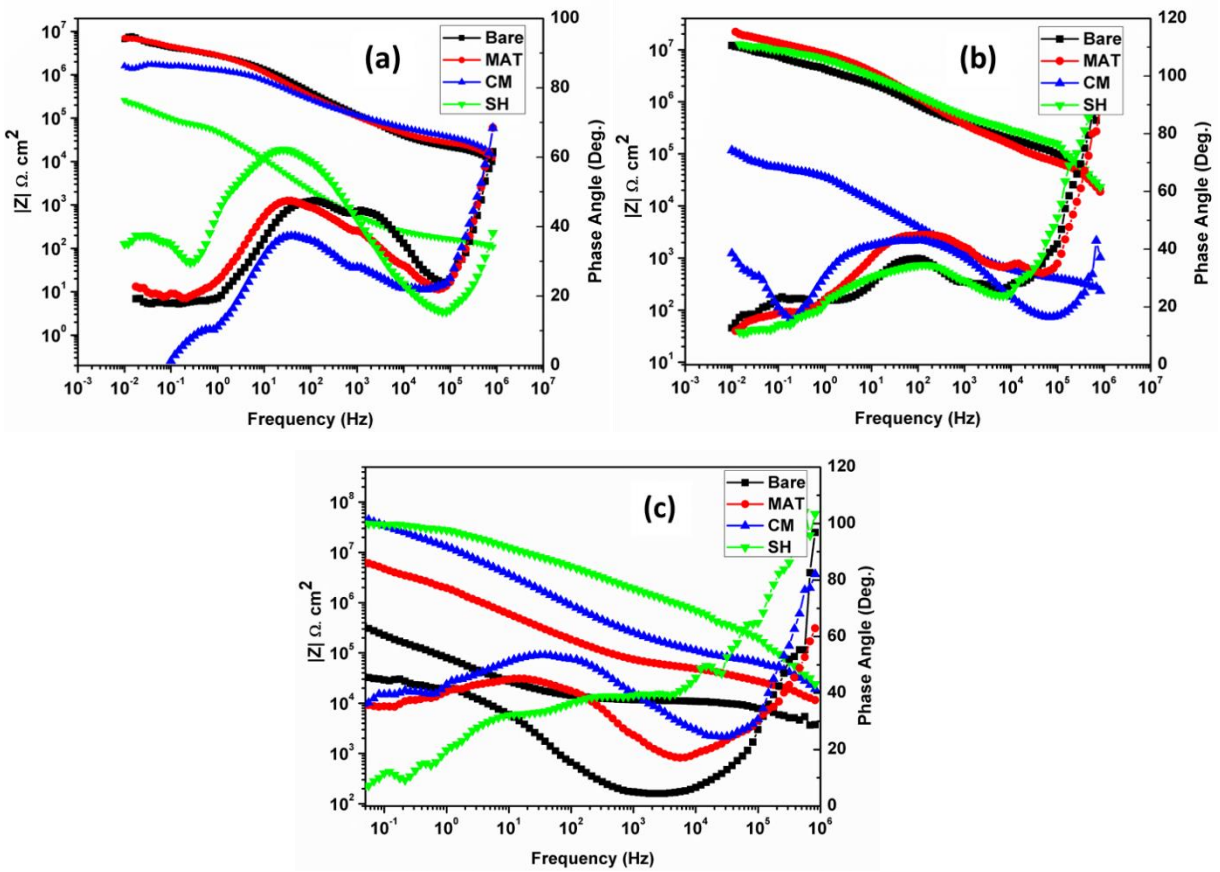

Figure 3.12: Bode plots for uncoated and coated AZ91D substrates after (a) 24 h, (b) 72 h and (c) 120 h exposure to 0.6 M NaCl solution

In case of EIS studies, best suited electrical equivalent circuit was preferred for analysing the impedance data of coated and bare substrates as depicted in Fig. 3.13.

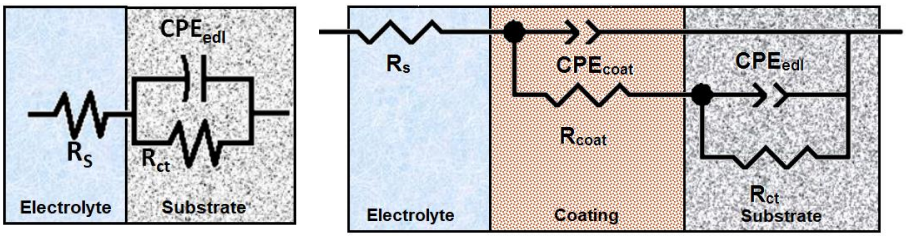

(a) (b)

Figure 3.13: Equivalent electric circuits used to fit EIS data of (a) bare and (b) coated substrates

In case of bare substrates (Fig. 3.13a), very thin porous oxide/hydroxide film is formed after exposure to corrosive medium which provides negligible corrosion resistance. Further, this thin film was removed during pretreatment of substrates. Hence, the results

were fitted with one-time constant circuit for bare substrates where, the charge transfer resistance (R_{ct}) is in parallel with electrical double layer capacitance (CPE_{edl}) which is in series with solution resistance. For coated substrates, two-time constant circuit was used in which the charge transfer resistance (R_{ct}) is in parallel with electrical double layer capacitance (CPE_{edl}) which is in series with coating resistance (R_{coat}) with C_{coat} corresponding to coating capacitance. Here, constant phase element is preferred over pure capacitor as the Nyquist plots are deviating from ideal semi-circle behaviour. This non-ideal frequency response could be associated with the inhomogeneity of the surface of metal originating from interfacial phenomena or surface roughness. The magnitude of pseudo capacitance was evaluated using following expression:

$$C = (Q_0 \times R)^{(1 \div n)} (1 \div R) \qquad (1)$$

Where, C is pseudo capacitance in F/cm^2; Q_0 is Constant Phase Element in $S\text{-}sec^n/cm^2$; n is frequency factor and R is resistance in **Ω**.

Table 3.1: EIS fit data for bare and coated substrates exposed to 0.6 M NaCl solution for various durations

Sl. No.	Exposure Time	Substrate	R_s Ω.cm^2	R_{coat} Ω.cm^2	R_{ct} Ω.cm^2	C_{coat}/ CPE F/cm^2	C_{edl}/CPE F/cm^2	χ^2
01	**24 h**	**Bare**	291.5	-	3.7E6	-	1.5E-8	0.001
		MAT	234.9	2.6E4	5.2E6	1.5E-11	3.5E-8	0.0023
		CM	106	4.3E4	1.7E6	1.4E-11	2.4E-8	0.0072
		SH	159.3	1.3E5	3.2E5	4.1E-6	4.5E-5	0.028
02	**72 h**	**Bare**	632.4	-	1.5E7	-	5.6E-8	0.0037
		MAT	765.6	7.3E4	1.3E7	9.8E-12	7.8E-9	0.0038
		CM	269.3	351.3	7.6E4	5. 7E-10	4.3E-6	0.0012
		SH	230.1	2.0E5	1.1E7	8.3E-12	3.4E-8	0.0038
03	**120 h**	**Bare**	731.6	-	1.9E5	-	2.2E-10	0.0016
		MAT	645.7	4.4E4	9.5E6	2.5E-11	2.3E-7	0.0027

		CM	458.9	7.4E4	4.8E7	9.9E-12	2.1E-8	0.0023
		SH	307.0	3.5E5	4.5E7	7.3E-12	2.7E-9	0.0061

Tafel plots obtained from potentiodynamic polarization studies for bare and coated AZ91D after 24 h, 72 h and 120 h of exposure to 0.6 M NaCl solution are shown in Fig. 3.14. The polarization results showed similar behaviour of corrosion protection of bare and coated substrates as obtained that from EIS studies. The corrosion currents and corrosion potentials obtained by Tafel extrapolation method are mentioned in Table 3.2.

The bare substrates have shown lower corrosion current after 24 h of exposure owing to the formation of thin film of oxides/hydroxides. However, this film tends to get deteriorated with the increase in exposure durations thereby showing increase in corrosion currents after 72 h and 120 h. Matrix sol coated substrates have shown lower corrosion current after 24 h due to the better barrier properties. In this case also, the barrier properties get deteriorated after 72 h of exposure resulting in increased corrosion current. The corrosion current decreases after 120 h due to the formation of oxides/hydroxides film after deterioration of barrier properties of matrix sol based coatings. CM sol coated substrates have shown lowest corrosion current owing to the barrier properties of matrix sol and dispersion of HNTs into it. According to Huttunen-Saarivirta et al.[30], the HNTs are randomly distributed in the coating matrix, which affects the barrier properties and porosity of coatings. The corrosion potential of these coatings increases after 72 h of exposure due to formation of oxide layer underneath the coating after diffusion of NaCl through the coatings. After prolonged exposure of these coatings, the thin film of oxides gets deteriorated and the corrosion potential decreases rapidly. SH sol coated substrates have shown higher corrosion current after 24 h due to dispersion of inhibitor loaded HNTs into matrix sol. The corrosion currents for SH sol coated substrates were found to be decreasing with the increasing durations of exposure and observed to be least after 120 h of exposure owing to the release of corrosion inhibitors loaded into the HNTs after change in localised pH. The corrosion potential also becomes more positive due to the formation of passive layers of hydroxides of the corrosion inhibitors Ce^{3+} and Zr^{4+}.

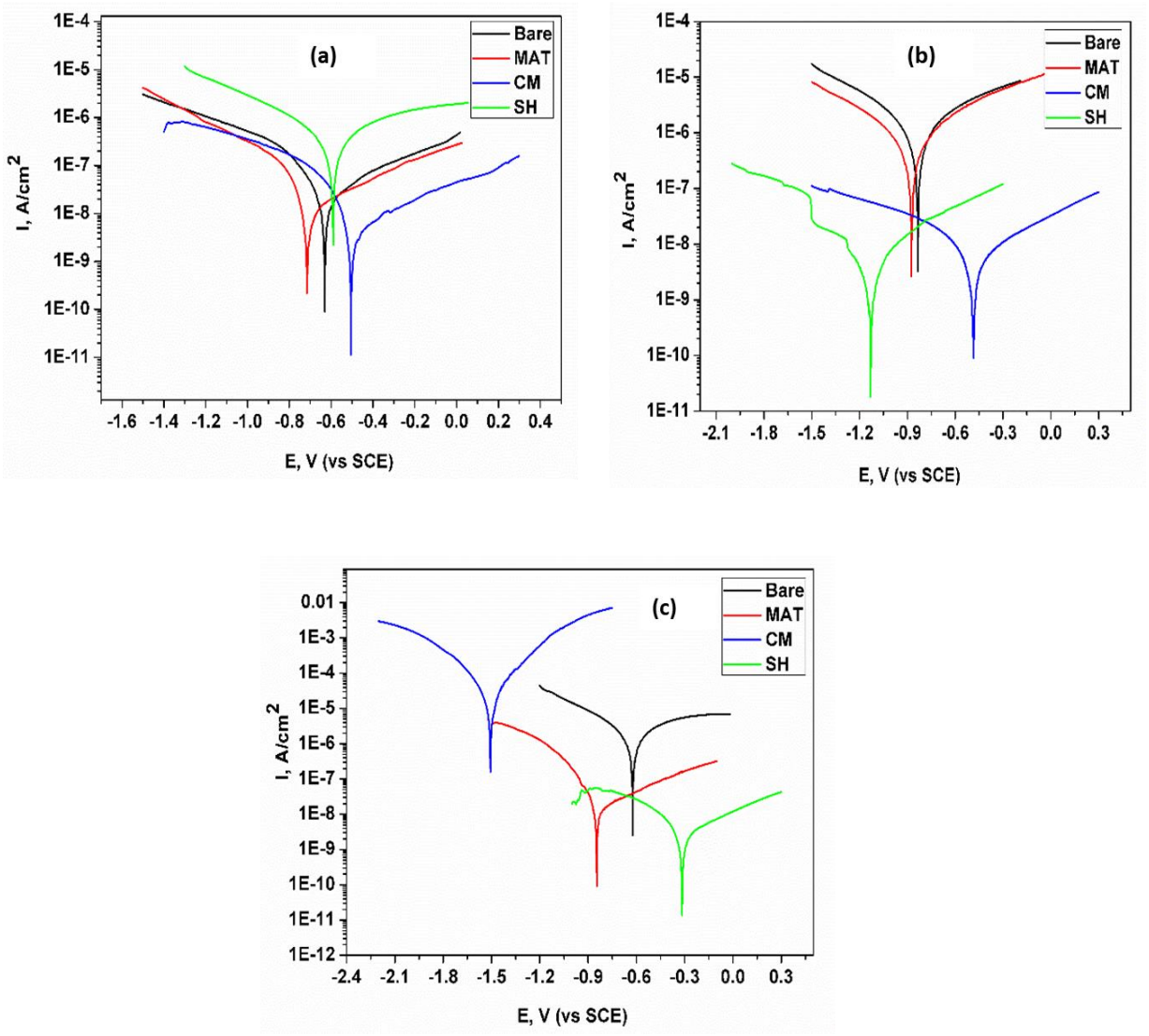

Figure 3.14: Polarization plots of uncoated and coated substrates exposed to 0.6 M NaCl solution after (a) 24 h, (b) 72 h and (c) 120 h

This could reveal that coatings have exhibited the self-healing property by releasing the corrosion inhibitors from nanotubes, thereby providing long-term protection. These results are further corroborated with SVET analysis.

Table 3.2: Tafel fitting parameters for uncoated and coated substrates exposed to 0.6 M NaCl solution for various durations

Sl. No.	Exposure Time	Substrate	E_{corr}, V (vs SCE)	I_{corr}, A/cm^2	R_p Ω.cm^2
01	24 h	**Bare**	-0.613	2.3E-8	1.9E6
		MAT	-0.715	1.5E-8	2.9E6
		CM	-0.505	6.3E-9	7.8E6

		SH	-0.590	2.1E-7	2.1E5
02	**72 h**	**Bare**	-0.834	5.2E-7	8.2E4
		MAT	-0.875	3.3E-7	1.4E5
		CM	-0.486	3.9E-9	1.2E7
		SH	-1.131	2.5E-9	1.6E7
03	**120 h**	**Bare**	-0.662	1.0E-6	1.1E5
		MAT	-0.846	2.5E-8	1.7E6
		CM	-1.506	1.2E-5	2.6E3
		SH	-0.316	2.7E-9	1.8E7

3.4.7 SVET analysis

The SVET results of uncoated and coated (MAT and SH) AZ91D substrates immersed in 0.6 M NaCl solution for various durations of time are depicted in Fig. 3.15. High anodic current flow depicted by red colour indicated the increased corrosion rate at the localised defect area because of small anode large cathode configuration. This revealed that the surface of substrate is exposed to the corrosive medium due to the depletion of passive oxide film.

In case of MAT sol coated substrates, the anodic current at the defect area was found to be higher after initial durations of exposure, which got decreased after 24 h because of restoration of barrier property of coatings. Current density maps of Ce^{3+}-Zr^{4+} loaded HNT based SH sol coated substrates have shown that anodic current density at the defect area was observed to decrease consistently with the increase in exposure durations. After 24 h, the current density was decreased drastically, due to self-healing activity and hence, SH sol based coatings have shown very low corrosion rates. The SVET data emphatically confirmed that the corrosion protection takes place because of release of corrosion inhibitors from the lumen of clay nanotubes. These coatings exhibited barrier property due to the matrix sol and self-healing property from the inhibitor-encapsulated HNTs, which plays an active role after depletion of barrier property with the localised pH change. Thus, SVET measurements confirmed that under the influence of localised pH, SH sol coated

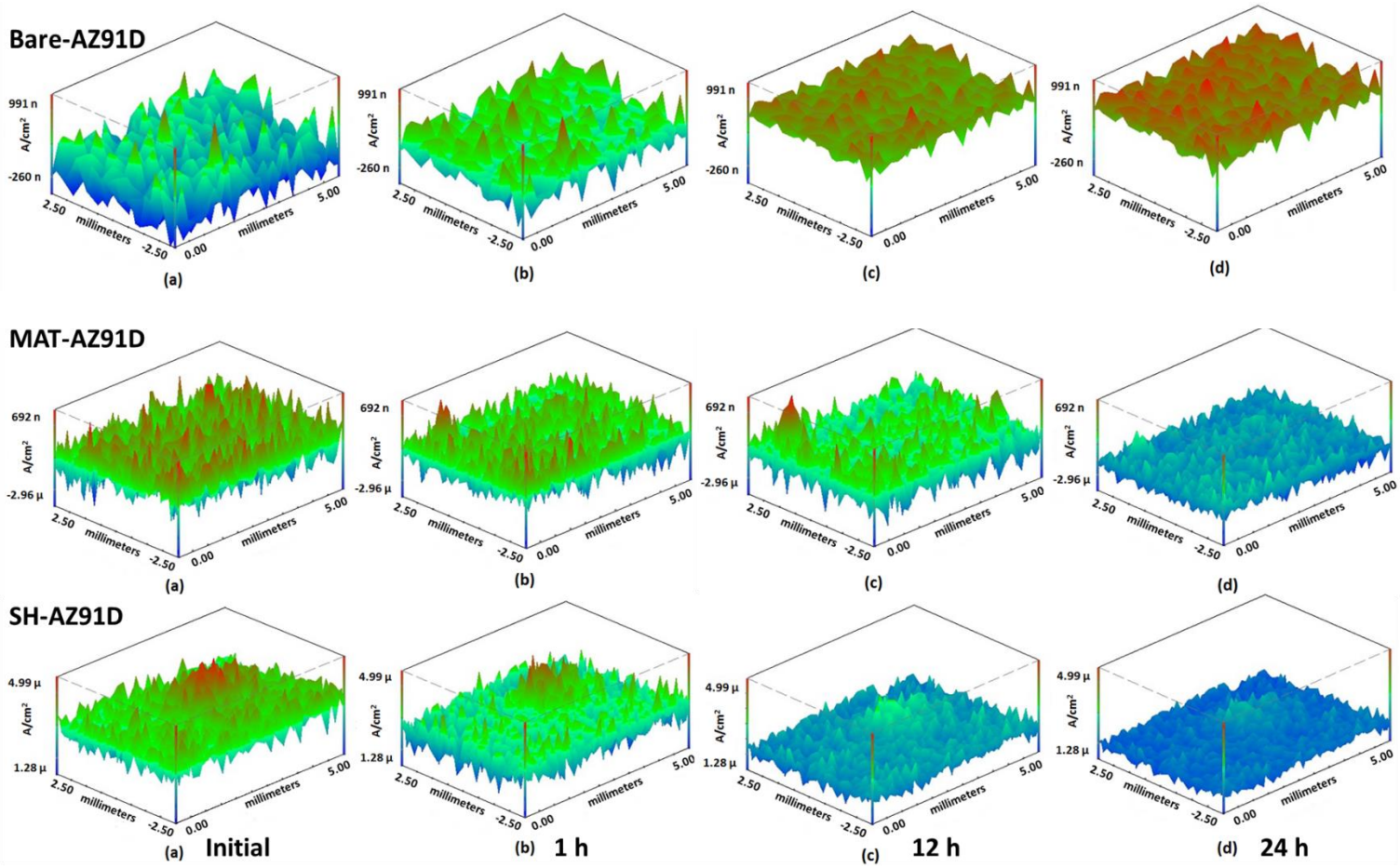

Figure 3.15: Current density maps for the bare, MAT sol coated and SH sol coated AZ91D after exposure to 0.6 M NaCl: (a) Initial, (b) after 1h, (c) after 12 h and (d) after 24 h

AZ91 substrate could heal the damaged coatings without external intervention because of self-healing mechanism. This results in decrease of current densities even after longer durations of exposure to the corrosive medium, unlike the bare substrate. The current density of bare substrates at the defect area was found to be increasing with the increase in exposure durations to the corrosive medium. The self-healing ability of Ce^{3+}-Zr^{4+} loaded HNT based coatings would be further confirmed with Micro-Raman spectroscopic analysis and will be discussed in next section.

3.4.8 Micro-Raman spectroscopic analysis

The scribed area on uncoated and SH sol coated AZ91D substrates was analysed before and after 120 h exposure to 0.6 M NaCl solution using Micro-Raman spectroscopic analysis. The spectra of bare and coated substrates obtained under both the conditions are depicted in Fig. 3.16. Bare substrates have shown the spectrum with broad peaks at 254 cm^{-1} and 446 cm^{-1}, which are due to MgO and $Mg(OH)_2$ before exposure to 0.6 M NaCl

solution. As depicted in Fig. 3.16 (a), peaks of Al_2O_3 and ZnO also have been observed on the scribed area at 633 cm^{-1}; 752 cm^{-1} and 380 cm^{-1} respectively. Spectrum has depicted broad nature of peak, which could correspond to the formation of thin porous layer of oxides on the surface of substrates. However, the spectrum has shown sharp and high intensity peak at 254 cm^{-1} after 120 h of exposure to 3.5 % NaCl on scribed area which revealed that the oxides with crystalline phase have formed (Fig. 3.16 (b)) [31].

Spectrum of SH sol coated substrates (Fig. 3.16 (c)) showed the presence of MgO, $Mg(OH)_2$ at 254 cm^{-1} and ZnO at 393 cm^{-1} before exposure to NaCl solution in scribed area. After 120 h of exposure (Fig. 3.16 (d)), sharp peaks at 233 cm^{-1} and 560 cm^{-1} conform to ZrO_2; peak at 277 cm^{-1} corresponds to MgO, whereas peak at 449 cm^{-1} corresponds to CeO_2 in scribed area [32,33]. This confirms the self-healing ability of coatings owing to the release of corrosion inhibitors into the scribed area. The photographs of bare and scribed SH sol coated AZ91D substrates before and after exposure to 0.6 M NaCl solution for 120 h are depicted in Fig. 3.17.

EIS and polarization measurements precisely confirmed that the inhibitor encapsulated HNT-based self-healing coatings could deliver enhanced anticorrosion properties as compared to the hybrid matrix sol-based coatings after prolonged exposure to corrosive medium. The coatings represent a potential to heal the damage by the release of corrosion inhibitor from HNTs, thereby providing the corrosion protection by two ways. First one is by development of a protective passive film of oxides and second by generation of barrier layer of polyethylene oxide (PEO) because of polymerization of epoxy functional group from the hybrid matrix sol as depicted in below equation.

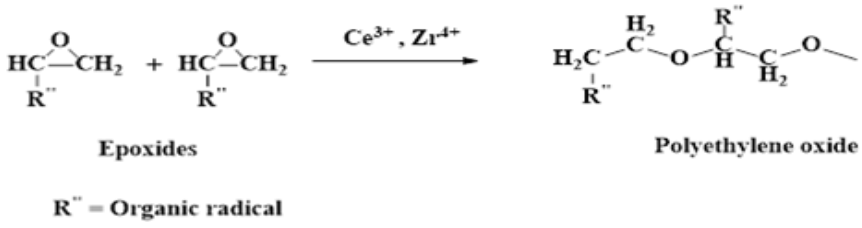

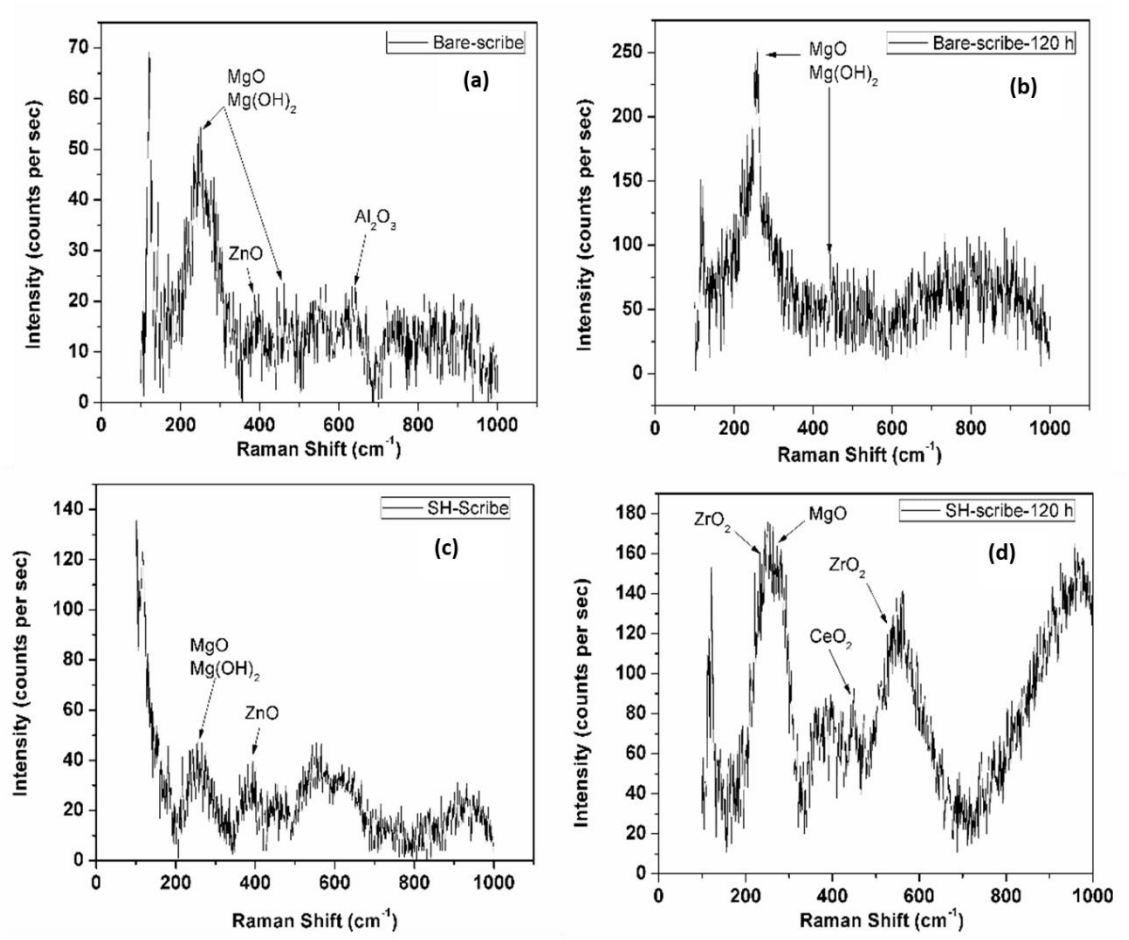

Figure 3.16: Micro-Raman spectroscopic analysis of uncoated AZ91D (a) before exposure; (b) after exposure and SH sol coated AZ91D (c) before exposure; (d) after exposure to 0.6 M NaCl solution for 120 h

Cationic corrosion inhibitors initiate both these mechanisms, thereby rendering better barrier properties. The autonomic-healing phenomenon as mentioned earlier could be confirmed by SVET analysis and electrochemical measurements. Micro-Raman spectroscopic analysis could confirm the phase compositions to be CeO_2 and ZrO_2 on the scribed area after exposure to NaCl solution. Hence, it could be concluded that micro-Raman spectroscopy can also be used as an analytical tool along with scanning electrochemical techniques to confirm the self-healing ability of the coatings. A schematic representation showing stages of self-healing phenomena of coating such as crack initiation and autonomic-healing of crack after generation of passive film along with development of a PEO layer in presence of catalysts is depicted in Fig. 3.18.

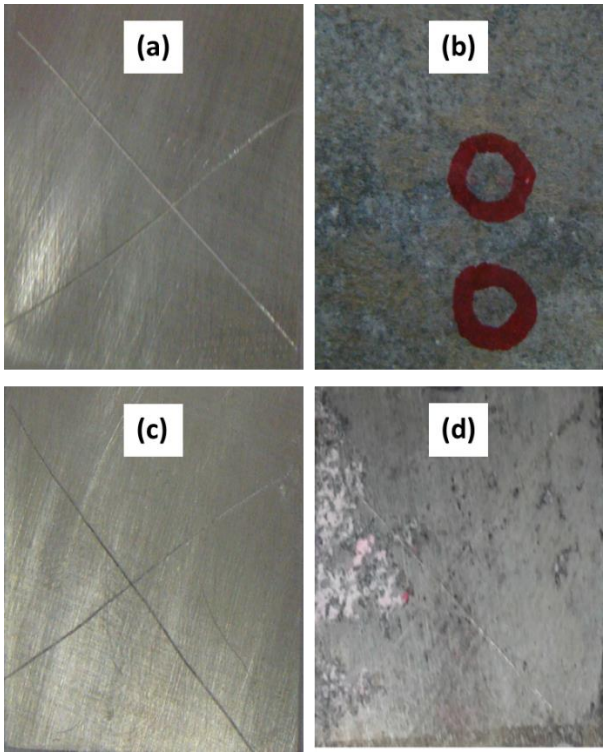

Figure 3.17: Photographs of (a), (b) bare and (c), (d) SH sol coated scribed substrates before and after 120 h of exposure to 0.6 M NaCl solution

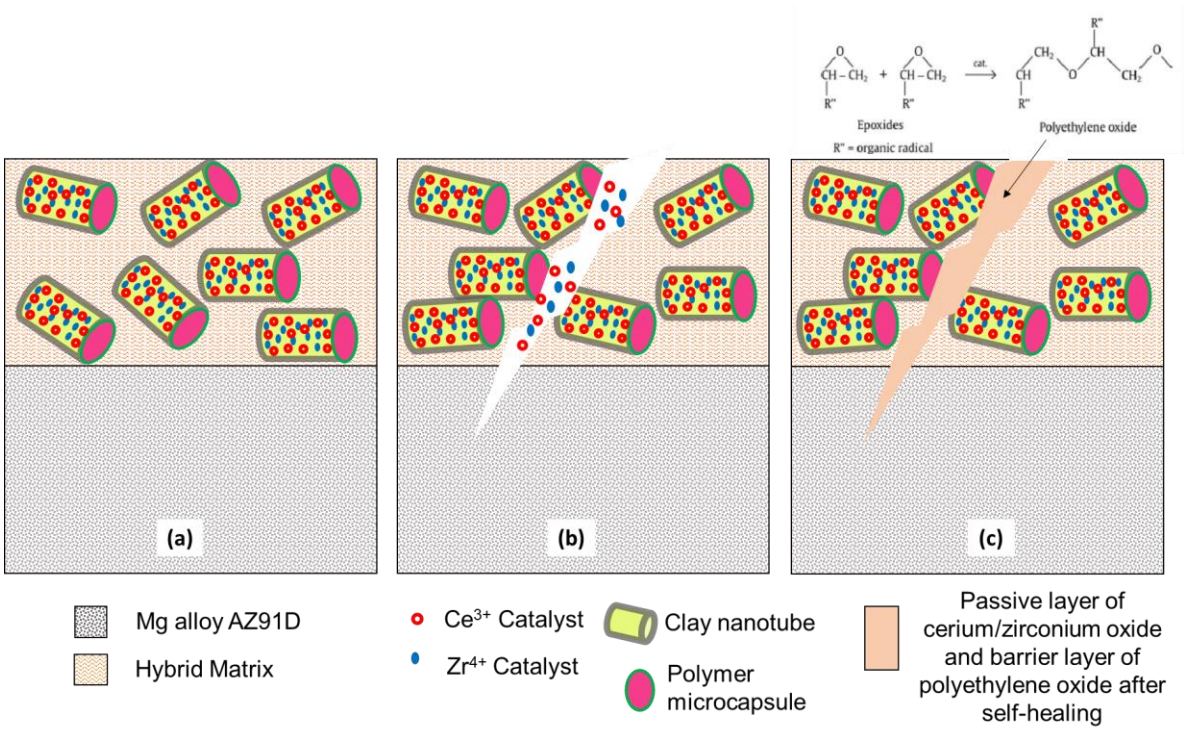

Figure 3.18: Schematic representation of self-healing mechanism of coating: (a) as-generated coating; (b) after crack initiation and (c) self-healing layer formation

3.5 References

[1] Rong-chang Zeng, Jin Zhang, Wei-jiu Huang, W. Dietzel, K. U. Keiner, C. Blawert, K. E. Wei, Review of studies on corrosion of magnesium alloys, Trans. Nonferrous Metals Soc. China 16 (2006) s763–s771.

[2] G. L. Song, A. Atrens, Corrosion mechanisms of magnesium alloys, Adv. Eng. Mater. 1 (1999) 11–33.

[3] B. L. Mordike, T. Ebert, Magnesium-properties, applications and potential, Mater. Sci. Eng. A302 (2001) 37–45.

[4] J. E. Gray, B. Luan, Protective coatings on magnesium and its alloys- a critical review, J. Alloys. Comp. 336 (2002) 88-113.

[5] X. Zhong, Q. Li, J. Hu, S. Zhang, B. Chen, S. Xu, F. Luo, A novel approach to heal the sol-gel coating system on magnesium alloy for corrosion protection, Electrochim. Acta 55 (2010) 2424–2429.

[6] M. L. Zheludkevich, S. K. Poznyak, L. M. Rodrigues, D. Raps, T. Hack, L. F. Dick, Active protection coatings with layered double hydroxide nanocontainers of corrosion inhibitor, Corros. Sci. 52 (2) (2010) 602-611.

[7] J. Tedim, S. K. Poznyak, A. Kuznetsova, D. Raps, T. Hack, M. L. Zheludkevich, Enhancement of active corrosion protection via combination of inhibitor-loaded nanocontainers, ACS Appl. Mater. Interfaces. 2(5) (2010) 1528-1535.

[8] D. Shchukin, H. Mohwald, Surface-Engineered Nanocontainers for Entrapment of Corrosion Inhibitors, Adv. Funct. Mater. 17 (2007) 1451-1458.

[9] Khairina Azmi Zahidah, Saeid Kakooei, Mokhtar Che Ismail, Pandian Bothi Raja, Halloysite nanotubes as nanocontainer for smart coating application: A review, Prog. Org. Coat. 111 (2017) 175-185.

[10] M. T. Albdiry, B. F. Yousif, Role of silanized halloysite nanotubeson structural, mechanical properties and fracture toughness of thermoset nanocomposites, Mater. Des. 57 (2014) 279-288.

[11] D. G. Shchukin, S. V. Lamaka, K. A. Yasakau, M. L. Zheludkevich, M. G. S. Ferreira, H. Möhwald, Active anticorrosion coatings with halloysite nanocontainers, J. Phys. Chem. C112 (2008) 958–964.

[12] D. Fix, D. V. Andreeva, Y. M. Lvov, D. G. Shchukin, H. Möhwald, Application of inhibitor- loaded halloysite nanotubes in active anti-corrosive coatings, Adv. Funct. Mater. 19 (2009) 1720–1727.

[13] Khairina Azmi Zahidah, Saeid Kakooei, Massoud Kermanioryani, Hamed Mohebbi, Mokhtar Che Ismail, Pandian Bothi Raja, Benzimidazole-loaded halloysite nanotube as a smart coating application, Int. J. Eng. Technol. Inn. 7 (4) (2017) 243-254.

[14] Jesus Marino Falcón, Tiago Sawczen, Idalina Vieira Aoki, Dodecylamine-loaded halloysite nanocontainers for active anticorrosion coatings, Front. Mater. 2 (69) (2015) 1-13.

[15] Elena Shchukina, Dmitry Shchukin, Dmitry Grigoriev, Effect of inhibitor-loaded halloysites and mesoporous silica nanocontainers on corrosion protection of powder coatings, Prog. Org. Coat. 102 (2017) 60-65.

[16] M. Sun, A. Yerokhin, M. Ya. Bychkova, D. V. Shtansky, E. A. Levashov, A. Matthews, Self-healing plasma electrolytic oxidation coatings doped with benzotriazole loaded halloysite nanotubes on AM50 magnesium alloy, Corros. Sci. 111 (2016) 753-769.

[17] R. Mahmoudi, P. Kardar, A. M. Arabi, R. Amini, P. Pasbakhsh, The active corrosion performance of silane coating treated by praseodymium encapsulated with halloysite nanotubes, Prog. Org. Coat. 138 (2020) 105404.

[18] Najmeh Asadi, Reza Naderi, Mohammad Mahdavian, Doping of zinc cations in chemically modified halloysite nanotubes to improve protection function of an epoxy ester coating, Corros. Sci. 151 (2019) 69-80.

[19] Dong Xu, Chang Lou, Jian Huang, Xin Lu, Zhong Xin, Changlu Zhou, Effect of inhibitor-loaded halloysite nanotubes on active corrosion protection of polybenzoxazine coatings on mild steel, Prog. Org. Coat. 134 (2019) 126-133.

[20] Duo Zhang, Haoqiang Zhang, Song Zhao, Zhaogang Li, Suoxia Hou, Electrochemical impedance spectroscopy evaluation of corrosion protection of X65 carbon steel by halloysite nanotube-filled epoxy composite coatings in 3.5 % NaCl solution, Int. J. Electrochem. Sci. 14 (2019) 4659-4667.

[21] A. R. Hoseinzadeh, S. Javadpour, Investigation of loaded halloysite nanotubes with novel inhibitor as a smart anticorrosion epoxy coating, Mater. Res. Express. 6 (2019) 115703.

[22] Yanling Jia, Teng Qiu, Longhai Guo, Jun Ye, Lifan He, Xiaoyu Li, Preparation of pH responsive smart nanocontainer via inclusion of inhibitor in graphene/halloysite nanotubes and its application in intelligent anticorrosion protection, Appl. Surf. Sci. 504 (2020) 144496.

[23] E. N. Brown, S. R. White, N. R. Sottos, Microcapsule induced toughening in a self-healing polymer composite, J. Mater. Sci. 39 (2004) 1703–1710.

[24] S. R. White, N. R. Sottos, P. H. Guebelle, J. S. Moore, M. R. Kessler, S. R. Sriram, E. N. Brown, S. Viswanathan, Autonomic healing of polymer composites, Nature 409 (2001) 794–797.

[25] C. Suryanarayana, K. C. Rao, D. Kumar, Preparation and characterization of microcapsules containing linseed oil and its use in self-healing coatings, Prog. Org. Coat. 63 (2008) 72–78.

[26] Elshad Abdullayev, Yuri Lvov, Clay nanotubes for corrosion inhibitor encapsulation: release control with end stoppers, J. Mater. Chem. 20 (2010) 6681-6687.

[27] ASTM D3359-17, Standard Test Methods for Rating Adhesion by Tape Test (2009) 1-9.

[28] ASTM G31-72, Standard Guide for Laboratory Immersion Corrosion Testing of Metals, 03-02, 2004.

[29] A. Joshi, E. Abdullayev, A. Vasiliev, O. Volkova, Y. Lvov, Interfacial modification of clay nanotubes for the sustained release of corrosion inhibitors, Langmuir 29 (2013) 7439–7448.

[30] E. Huttunen-Saarivirta, G.V. Vaganov, V. E. Yudin, J. Vuorinen, Characterization and corrosion protection properties of epoxy powder coatings containing nanoclays, Prog. Org. Coat. 76 (2013) 757-767.

[31] K. Ishikawa, N. Fujima, H. Komura, First order Raman scattering in MgO microcrystals, J. Appl. Phys. 57 (3) (1983) 973-975.

[32] P. Barberis, T. Merle-Mejean, P. Quintard, On Raman spectroscopy of zirconium oxide films, J. Nucl. Mater. 246 (1997) 232-243.

[33] G. Balakrishnan, C. M. Raghavan, C. Ghosh, R. Divakar, E. Mohandas, Jung Il Song, S. I. Bae, Tae Gyu Kim, X-ray diffraction, Raman and photoluminescence studies of nanocrystalline cerium oxide thin films, Ceram. Int. 39 (2013) 8327-8333.

Chapter 4

Ce^{3+}-Zr^{4+} INTERCALATED MONTMORILLONITE NANOCLAY-BASED COATINGS

Chapter-4

Ce^{3+}-Zr^{4+} intercalated montmorillonite nanoclay-based coatings

4.1 Introduction

In chapters 1 and 2, the use of naturally occurring nanoclay as a cost-effective approach for encapsulation of corrosion inhibitors and application in corrosion protection coatings was discussed and reviewed. In Chapter 3, one of the naturally occurring nanoclay, halloysite nanotubes (HNT) was found to be efficient for prolonged corrosion protection of Mg alloy when cationic Ce^{3+}-Zr^{4+} corrosion inhibitors are loaded into it.

Layered nanoclay materials having ion exchanging capability are also emerging smart materials for corrosion protection of metals and alloys. These nanoclays come with an ability to intercalate the cationic or anionic corrosion inhibitors in their structure. Layered aluminosilicate clays such as bentonite and montmorillonite (MMT) belonging to smectite group are widely used cationic exchange compounds in the field of corrosion protection owing to their beneficial properties like particle size <10 µm, ion exchanging ability and large surface area (~100 m^2/g) [1]. Literature studies have evaluated that the pillaring of MMT clay particles with cations results in increased surface area and cation exchange capacity [2]. The crystal structure of layered MMT clay is comprised of tetrahedral silicate layer coalesced with an edge shared octahedral aluminate layer as shown in Fig. 4.1.

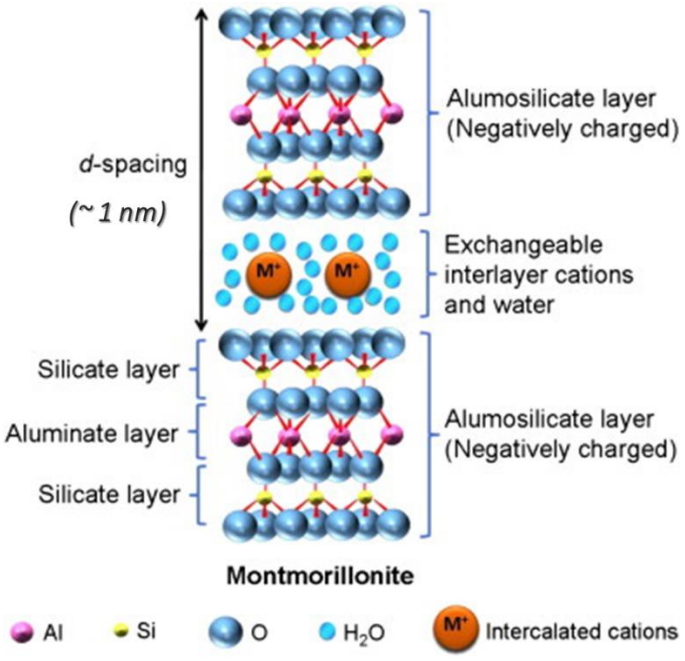

Figure 4.1: Structural representation of MMT clay [3]

The natural chemical components of MMT clay can be represented with the molecular formula as, $(Na, Ca)_{0.33}(Al, Mg)_2(Si_4O_{10})(OH)_2.nH_2O$. Usually, the metal cations such as Na^+, Ca^{2+}, Al^{3+}, etc. are intercalated between the layers of silica and alumina, which can be exchanged with the cations of corrosion inhibitors [4].

Sorkhabi et al. [5] have generated hybrid sol-gel coatings dispersed with MMT nanoclay (cloisite® Na^+, cloisite® 20A, and cloisite® 30B) and amino acids as corrosion inhibitors (L-glutamine, L-methionine and L-alanine) on AZ91 substrates pretreated with cerium-lanthanum permanganate (CLP) conversion coatings. The number of parameters such as molar ratio of silane precursors, withdrawal speeds of dip coating, residence time, number of exposure durations to 0.6 M NaCl solution and different concentrations of montmorillonite clays and amino acids were optimised. Danaee et al. [6-9] added various concentrations of MMT clay and cerium nitrate hexahydrate into epoxy matrix to generate nanocomposite coatings on carbon steel. It was examined that nanocomposite coatings without clay particles included some microcracks and perforations, whereas the one with clay particles showed improved corrosion protection. Electrochemical Impedance Spectroscopic (EIS) and Energy Dispersive Spectroscopic (EDS) analyses showed that the coatings provided better barrier properties when scribed, due to the migration of cationic Ce^{3+} into the damaged area. Izadi et al. [10] have evaluated the inhibition efficiency of Ocimum Basilium (basil leaf extract) intercalated into Na-MMT and examined the corrosion protection ability of inhibitor intercalated MMT dispersed silane coating on mild steel. Electrochemical studies in 0.6 M NaCl solution for different durations of exposure revealed that 10 g/l concentration of inhibitor intercalated MMT showed enhanced corrosion resistance for longer durations owing to the formation of Fe^{2+} basil chelates at the coating-metal interface.

Zou et al. [11] have generated hydrothermal coatings comprised of Zn^{2+} intercalated MMT clay on AZ31 Mg alloy. Electrochemical and immersion studies were carried out in Dulbecco's modified eagle medium (DMEM) with 10% calf serum to evaluate the barrier property, cytocompatibility, degradation behaviour and antibacterial activity of the coatings for longer durations of exposure. Ghazi et al. [12] dispersed 3 wt % of cationic benzamidazole (BIA) and Zn^{2+} intercalated Na-MMT into nanocomposite epoxy ester coatings which were then generated on steel panels. EIS studies for 1 day and 25 days in 0.6 M NaCl solution revealed that coatings based on BIA- MMT and BIA-MMT + Zn-MMT showed enhanced corrosion resistance as compared to blank, Zn-MMT and Na-MMT based coatings. FE-SEM analysis showed that cationic corrosion inhibitors have

released into scribed area during salt immersion test for 11 h, thereby showing the self-healing ability of coatings. Thai et al. [13] dispersed Ce^{3+} intercalated Na-MMT into hybrid sol, which was deposited on Al alloy AA2024. Electrochemical measurements and salt spray tests revealed that Ce-MMT gave enhanced barrier and self-healing properties after exposure to 0.59 wt % NaCl solution owing to the 60 % release of Ce^{3+} as observed from UV-visible spectroscopic measurements. Mo et al. [14] have pretreated Na-MMT with chitosan, intercalated with Ce^{3+} and further dispersed into waterborne polyurethane coating. EIS studies and salt spray tests for 14 days and 32 days revealed that coatings comprised of chitosan modified Ce-MMT did not show appearance of any corrosion product and significantly showed highest impedance. Mohammadi et al. [4] have generated epoxy coatings dispersed with cationic Ce^{3+} intercalated Na-MMT on mild steel substrates. Electrochemical studies showed enhanced corrosion inhibition property of Ce^{3+} on mild steel panels after 48 h of exposure to 0.6 M NaCl solution. The barrier properties of epoxy coatings with Ce-MMT were evaluated using electrochemical studies and salt spray tests for 60 days and observed that epoxy coatings with Ce-MMT showed enhanced corrosion protection as compared to that with Na-MMT and neat epoxy coating. Truc et al. [15] modified Na-MMT with 8-hydroxyquinoline (HQ) which was further incorporated in epoxy matrix and deposited on carbon steel substrates. The inhibition ability of HQ was evaluated using electrochemical studies in 0.59 wt % NaCl for 20 h. The corrosion protection ability of HQ-MMT dispersed epoxy coatings was compared with quaternary ammonium salt modified MMT using EIS and salt spray tests for 21 days and 240 h respectively.

Santana et al. [16] pretreated AISI 1010 mild steel substrates with phosphoric acid and then dip coated with hybrid sol-gel matrix dispersed with 0.5 wt % of both laponite layered nanoclay and Ce(III) as corrosion inhibitor. Electrochemical measurements in 0.06 M NaCl solution for 24 h revealed that the dispersion of nanoclays into coating matrix retarded the diffusion of corrosive medium into the substrate and Ce (III) inhibited the corrosion process in case of damage to the coating. Naderi et al. [17] generated hybrid sol-gel coatings on alkali pretreated pure Al substrates. The coatings matrix was dispersed with various concentrations of Ce $(NO_3)_3$ as corrosion inhibitor and Na-MMT nanoparticles. The coatings with 100 ppm and 5000 ppm of Ce $(NO_3)_3$ and Na-MMT, respectively imparted superior corrosion protection than the coatings with either Ce $(NO_3)_3$ or Na-MMT owing to the formation of insoluble passive film at cathodic site. Hybrid silane coatings were developed on hot dip galvanized steel by Deflorian et al. [18], which were dispersed with

various concentrations of Na-MMT nanoparticles and 5 wt % of ceria enriched MMT nanoparticles. It was observed from electrochemical studies that, coatings dispersed with Na-MMT were better protective and dispersion of ceria enriched MMT did not enhance the anticorrosive properties of silane coatings. Number of other studies [19-24] have been carried out by dispersing MMT clay into sol-gel matrix and polymer matrix to generate nanocomposite coatings on metals and alloys substrates.

As observed from literature survey, there are very few reports [1, 5, 25] on corrosion protection of Mg alloys by dispersing MMT clay into coating matrix as an additive, whereas only one article has been reported [11] for intercalation of cations into layered structure of MMT. This chapter includes detailed explanation of our studies where, cationic Ce^{3+}-Zr^{4+} inhibitors were intercalated into MMT and then 2 wt % of them were dispersed in hybrid sol-gel matrix, to generate self-healing coatings on Mg alloy AZ91D. In order to delineate the effect of MMT alone on the protective properties of coatings, as-received MMT was dispersed in hybrid matrix sol and coatings generated were subjected to the same set of investigations as the coatings derived from sols with inhibitor intercalated MMT. In the following sections, the methodology used to synthesize the as-received MMT dispersed matrix sol (Clay matrix, CM sol) and MMT clay based self-healing (SH) sol followed by characterization of generated coatings by various electrochemical methods will be discussed.

4.2 Materials and Methods

4.2.1 MMT clay modification methodology

Aluminum pillared MMT clay (Sigma Aldrich, USA) was modified with the cationic corrosion inhibitors, Ce^{3+}-Zr^{4+} using two different ways, namely (a) physical mixing of MMT clay with corrosion inhibitor solution under constant stirring conditions and (b) addition of MMT clay into corrosion inhibitor solution followed by evacuation in vacuum desiccator. This could result in intercalation of cationic inhibitor into the interlayer spacing of MMT as depicted in Fig. 4.2. The synthesis of hybrid sol and corrosion inhibitor solution was carried out as per procedures mentioned in section 3.2 of Chapter 3. In the first approach (a), 5 g of aluminum pillared MMT clay was mixed with corrosion inhibitor solution under constant stirring conditions for 30 min. The inhibitor mixed MMT clay (IMM) was centrifuged at 5000 rpm for 10 min to separate it from inhibitor solution, washed repeatedly with 2-propanol and water to remove any adsorbed inhibitor and thermally treated in hot air oven at 80 ^{o}C for 1 h. In another approach (b), the pillared MMT

clay was dispersed into inhibitor solution and then evacuated multiple times under vacuum for 3 h. The aforementioned procedure for separating the clay from inhibitor solution was implemented to obtain inhibitor evacuated MMT clay (IEM).

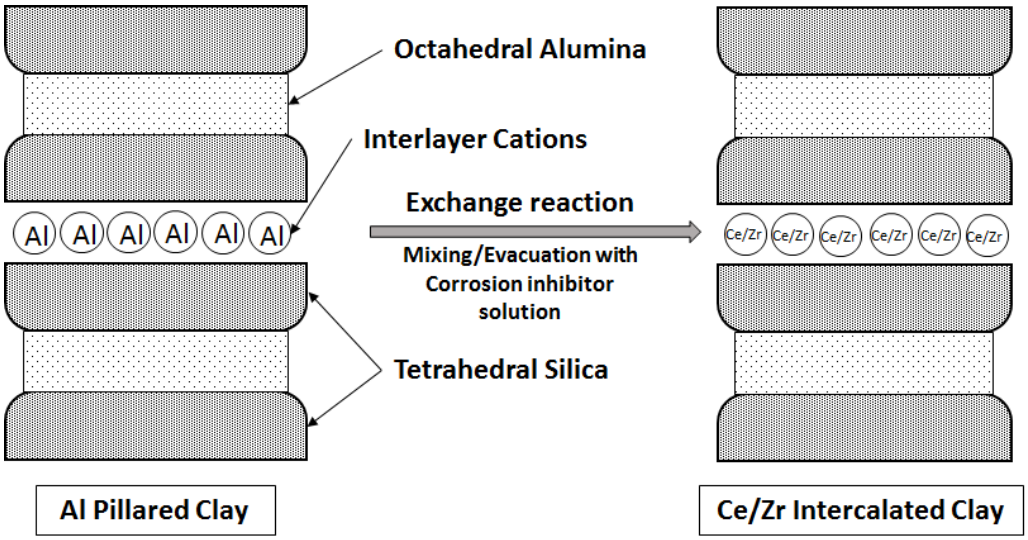

Figure 4.2: Schematic representation of intercalation of corrosion inhibitors into layers of MMT

4.2.2 Synthesis of sols and coating deposition

In order to examine the effect of the addition of MMT clay, 2 g of aluminum pillared MMT clay was dispersed in 98 g of hybrid MAT sol to obtain the clay matrix (CM) sol. 2 g of above mentioned inhibitor modified clays (IMM and IEM) were dispersed in MAT sol to synthesize IMM and IEM sols under constant stirring for 3 h. The substrate preparation and coatings generation was performed as mentioned in section 3.2 of chapter 3.

4.3 Characterization Techniques

4.3.1 MMT clay analysis

Field emission scanning electron microscopy (FESEM) and transmission electron microscopy (TEM) were used to examine the morphological properties of as-received and inhibitor modified MMT clay followed by elemental analysis using scanning electron microscope (SEM) fitted with EDS. X-ray diffraction (XRD) studies and small angle X-ray scattering (SAXS) analysis were performed to evaluate phase changes of as-received and inhibitor modified MMT clay.

Dual energy Mo-Cr SAXS system (Xeuss 1.0, Xenocs, France) was used to evaluate the inhibitor modified clays for the intercalation of corrosion inhibitors into the lamellar

spacing of clay. Mo as a source for X-rays with sample to detector distance of 550 mm was used to measure q-values in the range of 0.7-10 nm^{-1}, where, $q = \frac{4\pi}{\lambda} \sin(\frac{2\theta}{2})$ is the modulus of momentum transfer. λ and θ represent the wavelength of the incident X-ray and scattering angle, respectively. MMT clay was mounted in the scotch magic tape (3M, USA) for carrying out the measurements.

4.3.2 Coating characterization

The coatings were characterized for their adhesion strength using a cross-hatch cutter and tested according to ASTM B3359-17. The thickness of coatings was measured by using coating thickness gauge PosiTector® 6000 (DeFelsko Corporation, USA) and was found to be 5±1 µm for CM sol coatings, 7±1 µm for IMM sol coatings and 2.5±0.5 µm for IEM sol coatings. The anticorrosion properties of coatings were examined by using electrochemical measurements such as EIS and potentiodynamic polarization; weight loss experiments, whereas the self-healing ability of coatings was examined through scanning vibrating electrode technique (SVET) as mentioned in section 3.3 of chapter 3 and salt immersion test followed by SEM-EDS analysis.

Immersion tests were performed on MMT sol coated AZ91D substrates by exposing them to 0.6 M NaCl solution for 120 h. A scribe was made on the substrates at certain areas before exposing them to corrosive media. Nano-indenter was used to make the scribe as 'X' mark on the coated surface having width of 171±17 µm and depth of 20±1.0 µm. Surface morphology and elemental mapping of scribed substrates before and after exposure were then analyzed with SEM-EDS.

4.4 Results and Discussion

4.4.1 Morphological analysis of as-received and inhibitor modified MMT

The morphology of as-received MMT clay and corrosion inhibitor modified MMT clay examined using TEM and FESEM analyses is as shown in Fig. 4.3. SEM-EDS analysis was performed to examine the presence of corrosion inhibitors after modification of clay. FESEM analysis (Fig. 4.3a, 4.3b & 4.3c) revealed agglomerated flake like structure of as-received and IEM clay, whereas IMM clay was observed to be in the form of single lump. TEM images (Fig. 4.3d, 4.3e & 4.3f) clearly depicted layered structure in case of MMT and IEM, whereas IMM has shown some covering on the layers. SEM-EDS has revealed that, Al pillared MMT clay (Fig.4.3g) was primarily composed of silica and alumina with some traces of Mg, Na and Ca. Some traces of $Ce^{3+}$and Zr^{4+} were observed in IEM clay (Fig.4.3*i*),

whereas IMM clay (Fig.4.3h) has shown excessive amount of Zr^{4+}, which could be adsorbed on the surface of MMT. These results could be further corroborated with SAXS and XRD analyses.

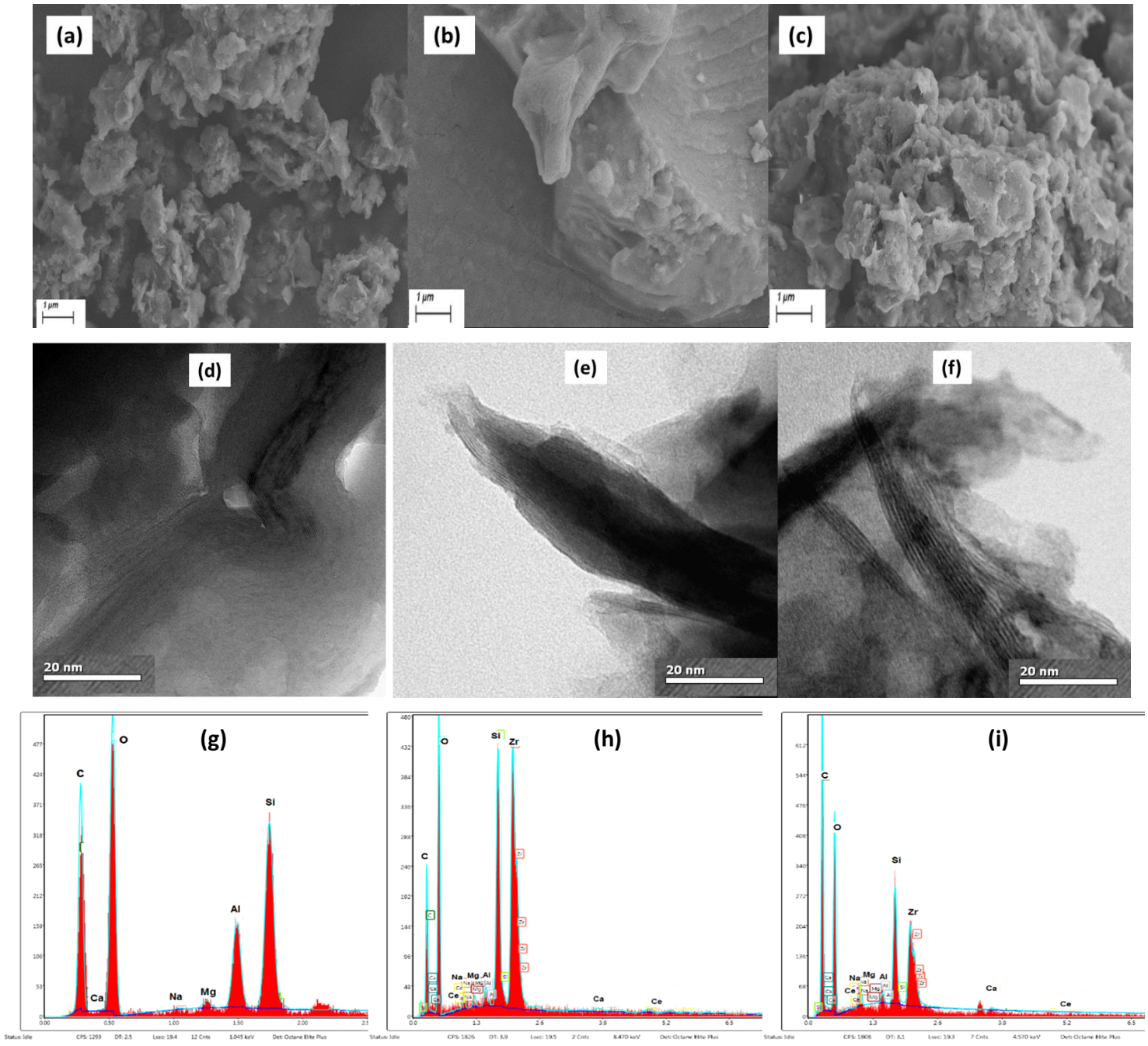

Figure 4.3: FESEM images (a), (b), (c); TEM images (d), (e), (f) and EDS spectra (g), (h), (i) of as-received MMT, IMM and IEM clays

4.4.2 XRD and SAXS analyses

XRD profiles of as-received MMT and cationic corrosion inhibitor exchanged MMT clay are depicted in Fig. 4.4 (a). In case of as-received MMT, the sharp peak at 4.80° indicated the crystalline phase. The inhibitor intercalated IEM clay also showed sharp peak

at 4.83°, which indicated that there is no change in lamellar crystal structure of MMT after intercalation of corrosion inhibitors with vacuum evacuation. However, IMM clay has shown broad peak at 6.10° with some shift in the peak position, which could occur due to delamination of the layered structure of clay because of adsorption of corrosion inhibitors. This could be further corroborated with SAXS analysis as described below.

SAXS analysis of as-received MMT and cationic corrosion inhibitor exchanged MMT clay with scattering intensity range of q = 0.3 nm^{-1} to q = 10 nm^{-1} are as shown in Fig. 4.4 (b). In case of as-received MMT, a well-defined peak (100) at q = 3.64 nm^{-1} (d = 1.73 nm) was corresponded to the lamellar structure of Al pillared MMT clay. IMM clay has shown weak and broad peak at q = 3.23 nm^{-1} (d = 1.95 nm) indicating that there is change in lamellar structure of MMT and the amorphous crystal structure. Matusewicz et al. [26] have shown that weak and broad peaks of MMT clay denote smaller crystallites and worse lamellar structure, whereas sharp and clear peak represent better lamellar order of stacks. In case of IEM clay, (100) peak has shown negligible shift in the position with q = 3.62 nm^{-1} (d=1.74 nm). Thus, it can be observed that there was no change in the layered structure of MMT clay after intercalation of corrosion inhibitor by vacuum evacuation approach.

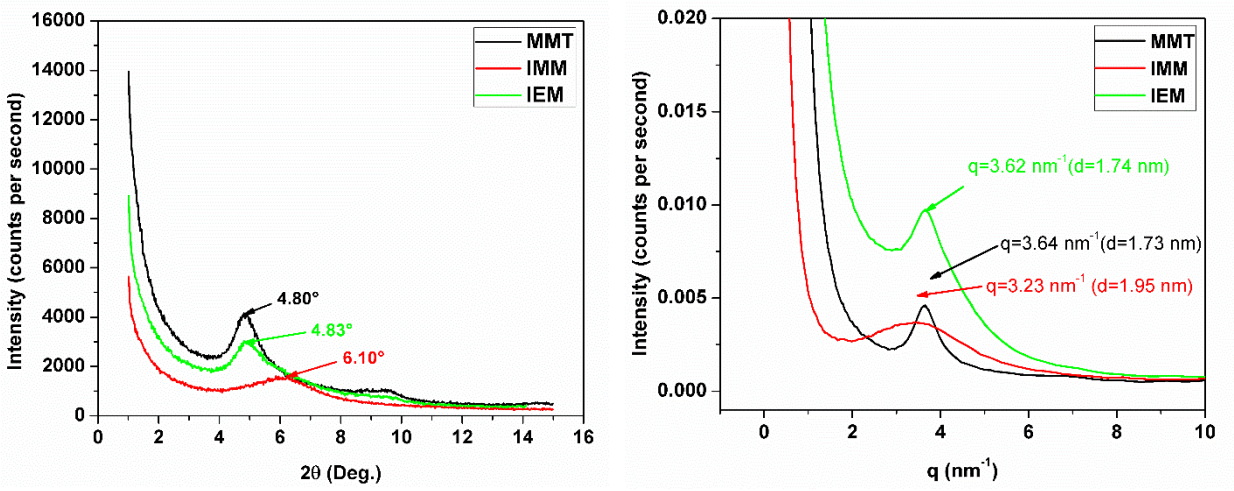

(a) **(b)**

Figure 4.4: (a) XRD patterns and (b) SAXS spectra as function of q for as-received MMT, IMM and IEM clays

4.4.3 Adhesion strength of coatings

The adhesion properties of coatings was measured using tape adhesion test according to ASTM D3359-17 and the results are classified as mentioned in Fig. 3.8 of chapter 3. Optical microscopic images for adhesion test of coated substrates carried out using cross-

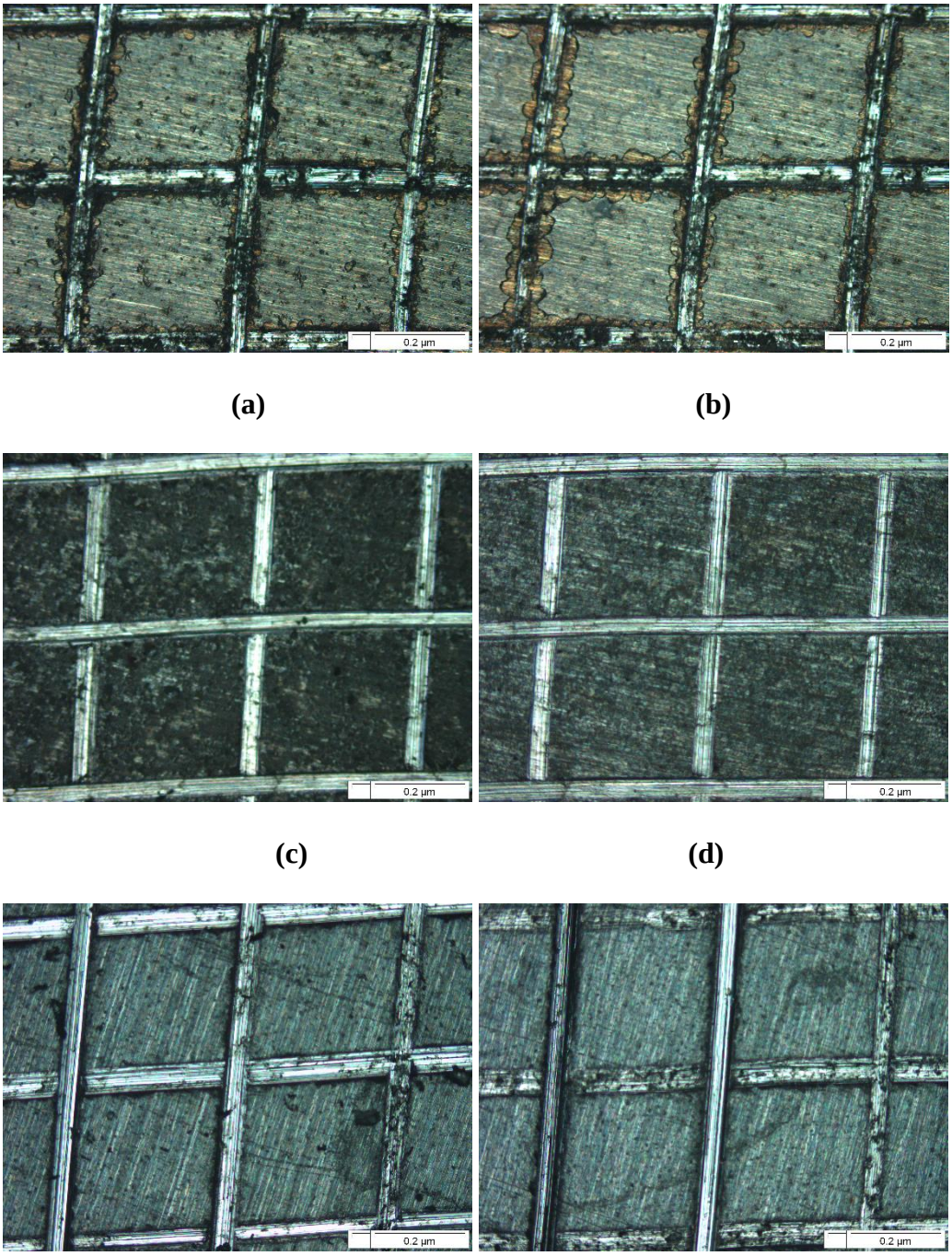

Figure 4.5: Optical microscopic images of adhesion test of CM sol coated (a, b), IMM sol coated (c, d) and IEM sol coated (e, f) substrates before putting on tape and after removal of tape

hatch cutter are as shown in Fig. 4.5. Very smooth edges of cut were observed with CM sol coatings on AZ91D (Fig. 4.5a, 4.5b) after peeling off the tape. Hence, the coating adhesion was considered as rank 4B, where less than 5 % of coating has got removed. In case of IMM and IEM sol coatings (Fig. 4.5c, 4.5d; 4.5e, 4.5f), very less amount of coating was

detached around the edges and the adhesion was ranked as 5B, which denoted best adhesion property as per ASTM D3359-17.

4.4.4 EIS and potentiodynamic polarization measurements

EIS and potentiodynamic polarization measurements were performed for evaluation of the anticorrosion properties of MMT sol based coatings (CM, IMM and IEM) on AZ91D samples after exposure to 0.6 M NaCl solution for various durations such as 24 h, 72 h and 120 h.

Electrochemical measurements were carried out as mentioned in section 3.3.6 of chapter 3. The Nyquist plots and Bode plots for MMT sol based coated substrates exposed to 0.6 M NaCl solution for different durations are depicted in Fig. 4.6 and Fig. 4.7, respectively. The fit data obtained by using two time constant equivalent electric circuit (Fig. 4.8) is shown in Table 4.1.

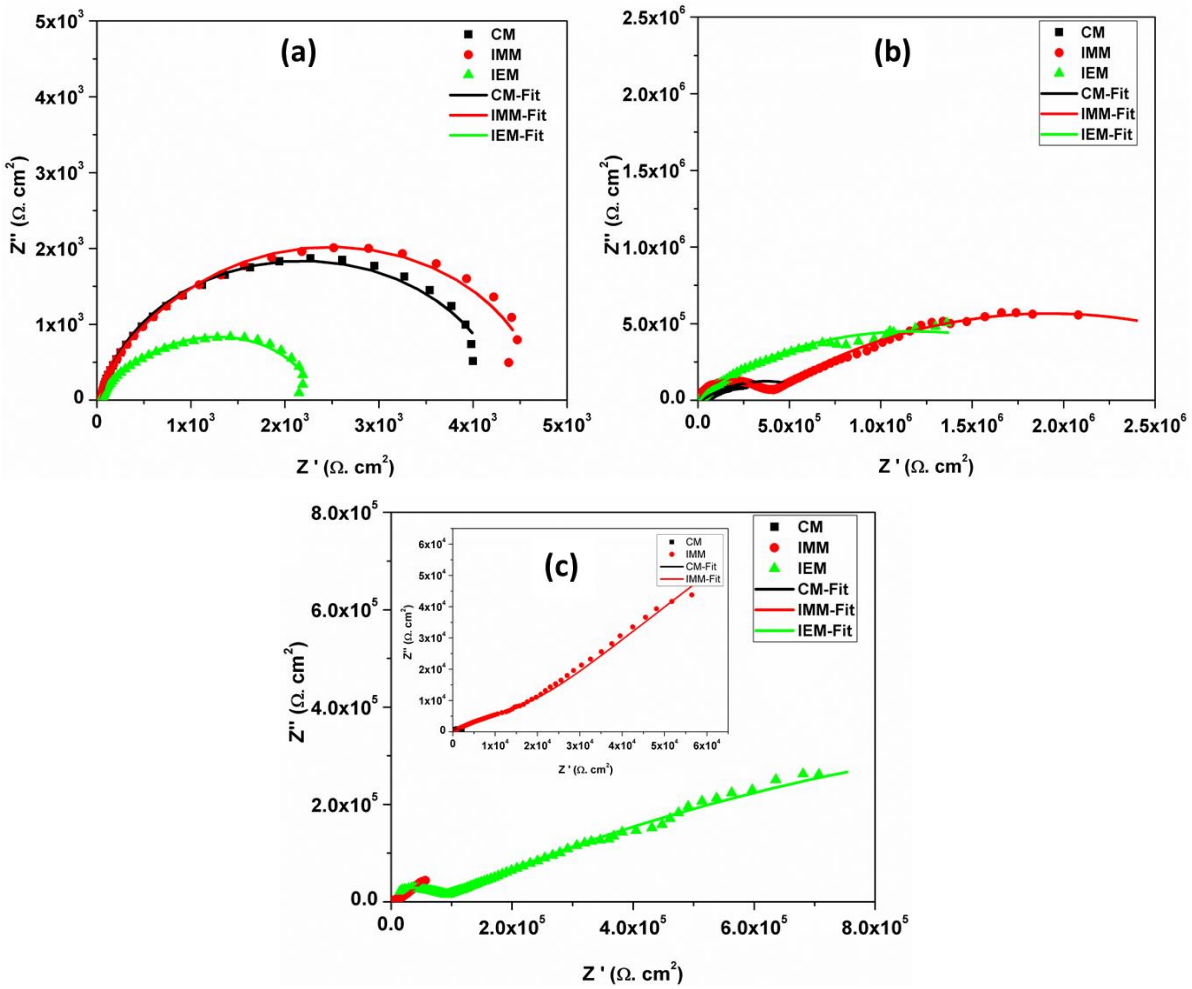

Figure 4.6: Nyquist plots for MMT sol coated AZ91D after (a) 24 h, (b) 72 h and (c) 120 h exposure to 0.6 M NaCl solution

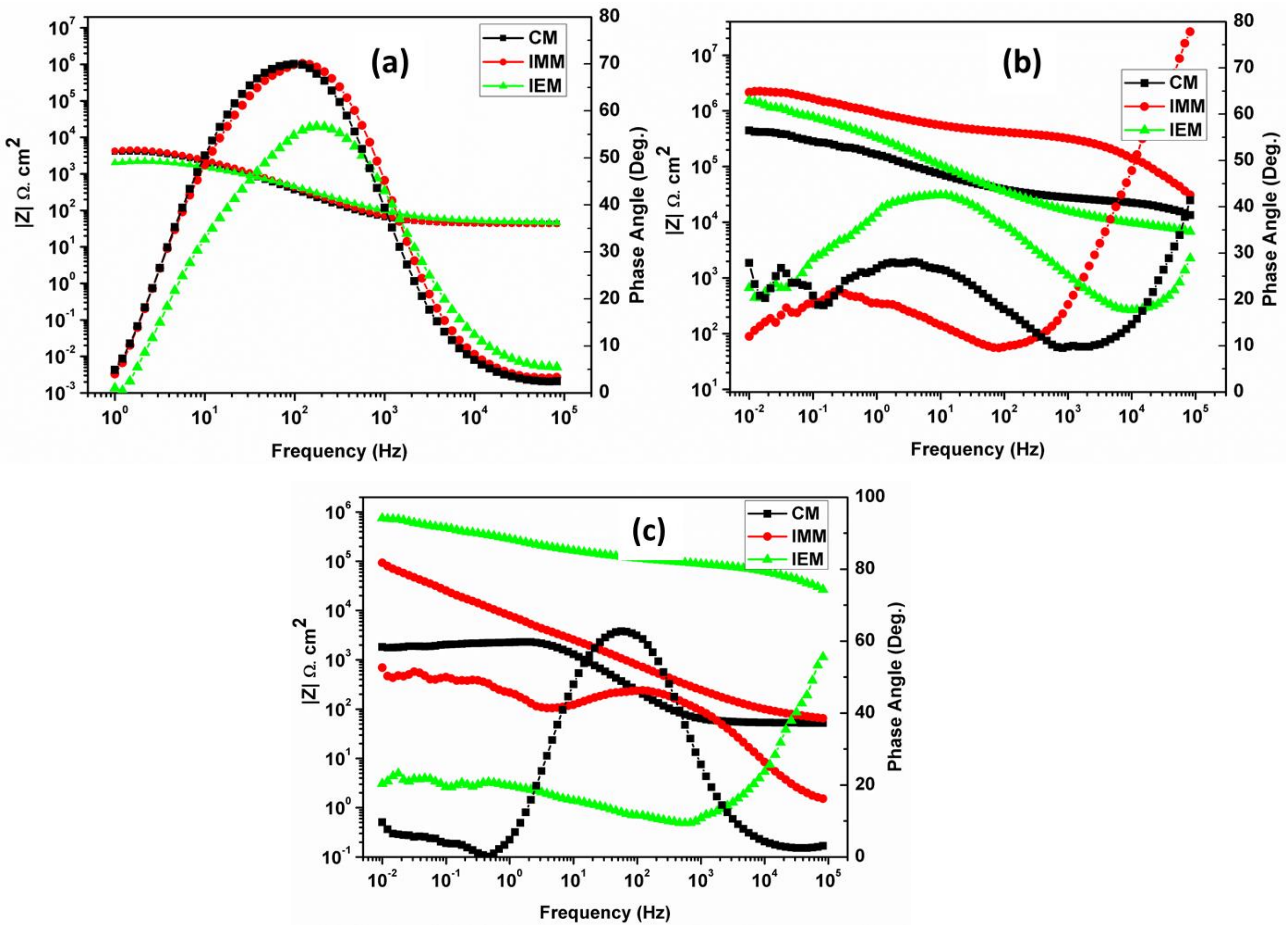

Figure 4.7: Bode plots for MMT sol coated AZ91D after (a) 24 h, (b) 72 h and (c) 120 h exposure to 0.6 M NaCl solution

After 24 h of exposure, CM sol coated substrates have shown better corrosion protection owing to the barrier properties of coatings. However, with the increase in exposure durations to the corrosion medium, the barrier properties were found to be deteriorating and the anticorrosion ability of the coatings decreased with time since, there are no corrosion inhibitors present in the coating. IMM sol coated substrates have shown higher corrosion resistance in low frequency region after 24 h exposure, which increases further after 72 h and could be attributed to adsorption of Zr-n-propoxide on MMT surface. In addition to this, IMM sol based coatings have shown lower double layer capacitance indicating the lower uptake of water. With the increase in exposure durations to corrosion medium, the corrosion resistance of coatings decreased drastically and coating capacitance also has increased, thereby showing more water uptake. After 24 h of exposure, IEM sol based coatings showed lower corrosion resistance owing to the lower coating thickness and high porosity because of which coatings have shown high double layer capacitance. After prolonged durations of exposure, the corrosion resistance of IEM sol based coatings

increased owing to the release of intercalated corrosion inhibitors with the change in local pH.

In case of EIS studies, best suited electrical equivalent circuit was preferred for analysing the impedance data of coated and bare substrates as depicted in Fig. 4.8.

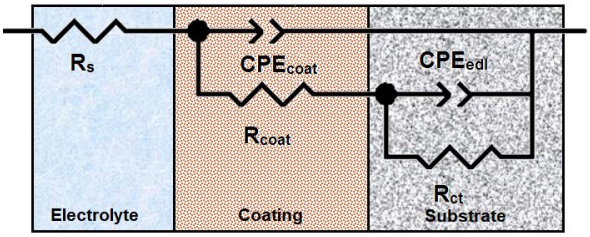

Figure 4.8: Equivalent electric circuits used to fit EIS data of coated substrates

For coated substrates, two-time constant circuit was used in which the charge transfer resistance (R_{ct}) is in parallel with electrical double layer capacitance (CPE_{edl}) which is in series with coating resistance (R_{coat}) with C_{coat} corresponding to coating capacitance. Here, constant phase element is preferred over pure capacitor as the Nyquist plots are deviating from ideal semi-circle behaviour. This non-ideal frequency response could be associated with the inhomogeneity of the surface of metal originating from interfacial phenomena or surface roughness. The magnitude of pseudo capacitance was evaluated using following expression:

$$C = (Q_0 \times R)^{(1\div n)} (1 \div R) \qquad (1)$$

Where, C is pseudo capacitance in F/cm^2; Q_0 is Constant Phase Element in $S\text{-}sec^n/cm^2$; n is frequency factor and R is resistance in **Ω**.

Table 4.1: EIS fit data for MMT sol coated substrates exposed to 0.6 M NaCl solution for various durations

Exposure Time	Substrate	R_s Ω.cm²	R_{coat} Ω.cm²	R_{ct} Ω.cm²	C_{coat}/ CPE F/cm²	C_{edl}/CPE F/cm²	χ^2
24 h	CM	44.39	2735	1783	4.2E-6	6.0E-6	0.0013
	IMM	42.86	54.68	4125	3.4E-6	4.2E-7	0.0013
	IEM	48.86	1743	566.8	4.6E-6	1.7E-5	0.0012
72 h	CM	1652	1.9E4	7.1E5	2.7E-8	7.3E-6	0.0044
	IMM	1251	3.4E5	3.2E6	9.6E-11	1.4E-6	0.0019

	IEM	1563	1.6E4	2.5E6	4.4E-10	5.0E-7	0.0016
120 h	**CM**	53.82	578.9	1494	6.2E-6	5.2E-6	0.0075
	IMM	52.65	5553	2. 3E5	1.6E-5	1.1E-3	0.0022
	IEM	52.34	6.8E4	2.8E6	7.4E-11	1.6E-4	8.8E-4

Tafel plots obtained from potentiodynamic polarization studies for MMT sol coated AZ91D after 24 h, 72 h and 120 h of exposure to 0.6 M NaCl solution are shown in Fig. 4.9 The corrosion currents and corrosion potentials obtained by Tafel extrapolation method are shown in Table 4.2. After 24 h of exposure, CM sol coated

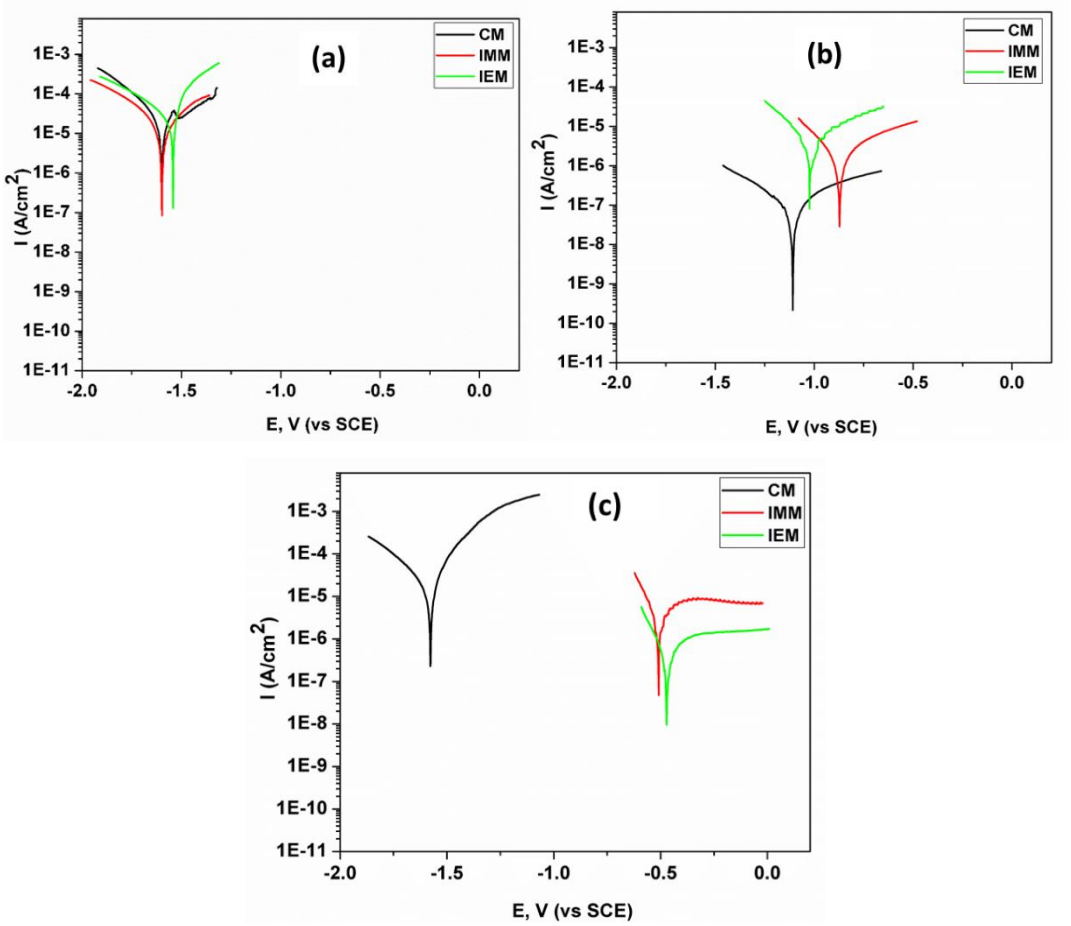

Figure 4.9: Polarization plots of MMT sol coated substrates exposed to 0.6 M NaCl solution after (a) 24 h, (b) 72 h and (c) 120 h

substrates and IEM sol coated substrates have shown very less difference in the magnitudes of corrosion current. This could indicate that, the barrier properties of CM sol based coatings and IEM sol based coatings are similar before the release of intercalated corrosion inhibitor from IEM clay. The magnitude of corrosion current of IMM sol based coatings

was observed to be least among all coated substrates after 24 h of exposure. After 72 h of exposure, CM sol coated substrates have shown enormous decrement in the corrosion current, which could be attributed to formation of passive thin film of oxides that might have improved the barrier properties of the coatings. IMM and IEM sol based coatings have shown gradual decrement in the corrosion current after 72 h owing to the release of adsorbed and intercalated corrosion inhibitors, respectively. After prolonged exposure of 120 h, IMM sol coated substrates showed small increment in the corrosion current, which could indicate that the inhibition activity of corrosion inhibitors adsorbed on MMT clay surface has reduced. In case of IEM sol coated substrates, drastic decrement in the corrosion current was observed owing to the consistent release of intercalated corrosion inhibitors, whereas CM sol based coatings have shown highest corrosion current because of depleted barrier properties of coatings. These results are further corroborated with weight loss measurements for evaluation of barrier properties of coatings.

Table 4.2: Tafel fitting parameters for MMT sol coated substrates exposed to 0.6 M NaCl solution for various durations

Exposure Time	Substrate	E_{corr}, V (vs SCE)	I_{corr}, A/cm^2	R_p, Ω.cm^2
24 h	**CM**	-1.598	3.8E-5	1619
	IMM	-1.598	1.4E-5	2825
	IEM	-1.542	4.2E-5	1022
72 h	**CM**	-1.108	8.3E-8	6.1E5
	IMM	-0.872	1.6E-6	2.5E4
	IEM	-1.024	5.9E-6	6.4E3
120 h	**CM**	-1.577	1.5E-5	2.1E3
	IMM	-0.569	3.1E-6	1.2E4
	IEM	-0.471	5.6E-7	5.9E4

4.4.5 Weight loss experiments

Weight loss measurements lend more practical data on the durability and corrosion resistance of MMT sol coated substrates. Here, rate of corrosion (Fig. 4.10) was evaluated for MMT sol coated AZ91D substrates after 24 h, 72 h and 120 h of exposure to 0.6 M NaCl solution. Due to lack of corrosion inhibitors, CM sol based substrates have shown higher corrosion rate after 24 h of exposure. However, with the increase in exposure

durations, the corrosion rate decreases, which could be attributed to the formation of corrosion products. Due to adsorbed corrosion inhibitors on the surface of MMT clay, IMM sol based coatings have shown lower rate of corrosion after 24 h and 72 h of exposure. IEM sol based coatings showed higher corrosion rate than IMM sol based coatings up to 72 h of exposure, owing to less adsorption of inhibitor on the surface of clay. However, once the intercalated corrosion inhibitor gets released after prolonged duration of exposure (120 h), the corrosion rate of IEM sol coated substrates decreased. The barrier property of IEM based coatings was found to be best among other coatings as observed from electrochemical studies and weight loss experiments. The self-healing ability of these coatings would be evaluated by salt immersion test and SVET analysis in upcoming sections.

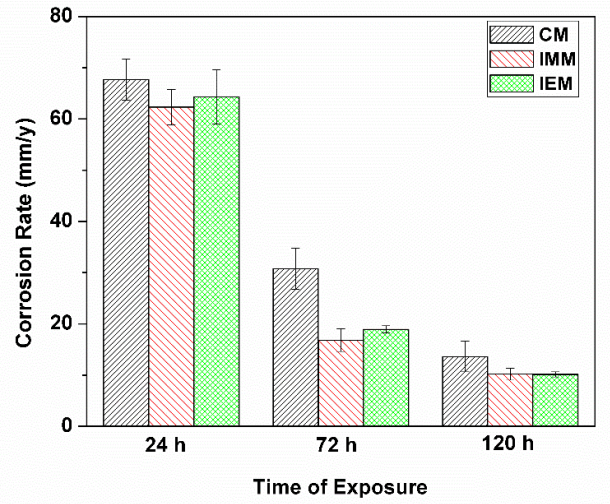

Figure 4.10: Comparison of corrosion rates of MMT clay based coated substrates after various durations of exposure to 0.6 M NaCl solution

4.4.6 Immersion test

In immersion test, coated and scribed substrates were exposed to 0.6 M NaCl solution for 120 h. The substrates were cleaned thoroughly with deionized (DI) water to remove any accumulated salt. The elemental distribution across coated surface and scribed area for CM sol, IMM sol and IEM sol coated substrates is shown in Fig. 4.11, whereas the change in the elemental composition for IMM and IEM sol coated substrates is mentioned in Table 4.3.

As shown in Fig. 4.11(a), negligible amount of oxides was observed on the scribed area of CM sol coated substrates, whereas the uniform distribution of Mg and Si as well as increase in oxide content on the coated surface and in the scribed area after 120 h of immersion (Fig. 4.11 (b)) indicated the deterioration of coating. This could reveal that coating will not be able to provide corrosion protection with further exposure to corrosive

medium. In case of IMM sol coated substrates, though amount of Zr^{4+} was observed to be increased on the scribed area after 120 h of exposure (Table 4.3), elemental mapping images (Fig. 4.11 (c) and 4.11 (d)), have shown that, Zr^{4+} has not been distributed evenly along the scribed and coated area, and some part of the coating has got removed after 120 h of exposure. The reason for this could be, the adsorption of more of Zr^{4+} on the surface of clay than getting intercalated, since the layer structure also was destroyed. Hence, the surface adsorbed Zr^{4+} could get released quickly within a very short period of time, without providing the slow and sustained release, which is normally required for realizing the self-healing effect. Due to this, it may be possible that Zr^{4+} appearing in scribed area was not enough to provide sufficient corrosion protection. Moreover, since the coating also was seen to have got removed, prolonged corrosion protection would not be possible.

After 120 h of exposure, IEM sol coated substrates showed increased amount of Ce^{3+} and Zr^{4+} in the scribed area, which could indicate that the passive film of oxides of inhibitors has formed, thereby providing the self-healing ability to the coatings. This Ce^{3+} and Zr^{4+} in the scribed area could be the one released from interlayers of IEM clay after prolonged exposure to the NaCl solution. Elemental mapping after 120 h in Fig. 4.11 (f) has revealed the presence of C and O on the coated surface, which could indicate that the coating is still intact. Further, it was observed that Ce^{3+} and Zr^{4+} have been uniformly distributed over scribed area, thereby indicating that the corrosion inhibitors have released from MMT clay owing to the change in localized pH and provide better anticorrosion properties even after 120 h exposure to NaCl solution. These results are further corroborated with SVET analysis.

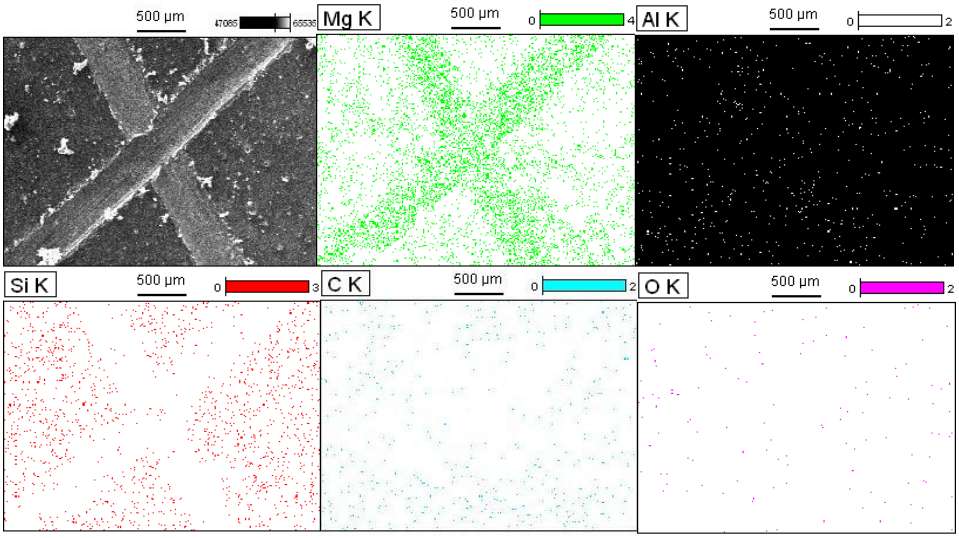

(a)

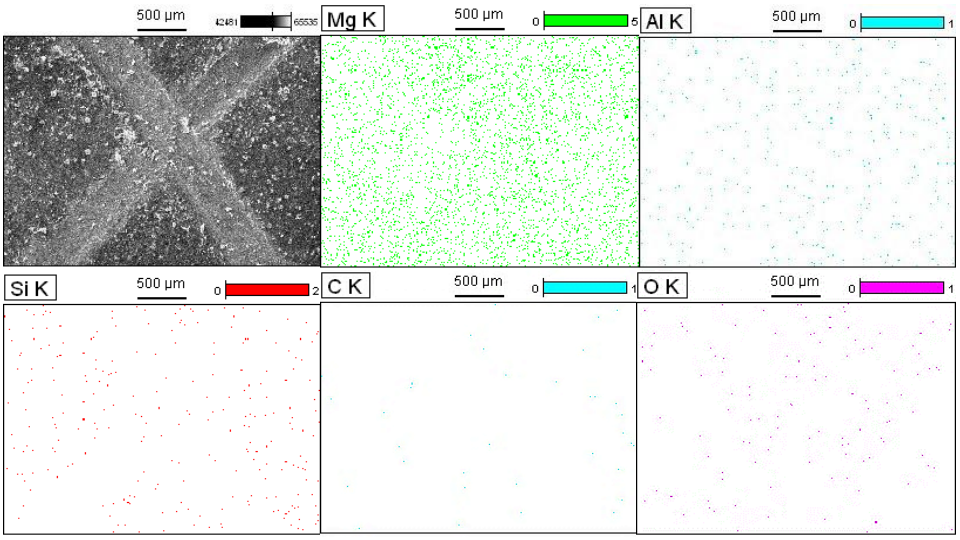
500 µm
Mg K
Al K
Si K
C K
O K

(b)

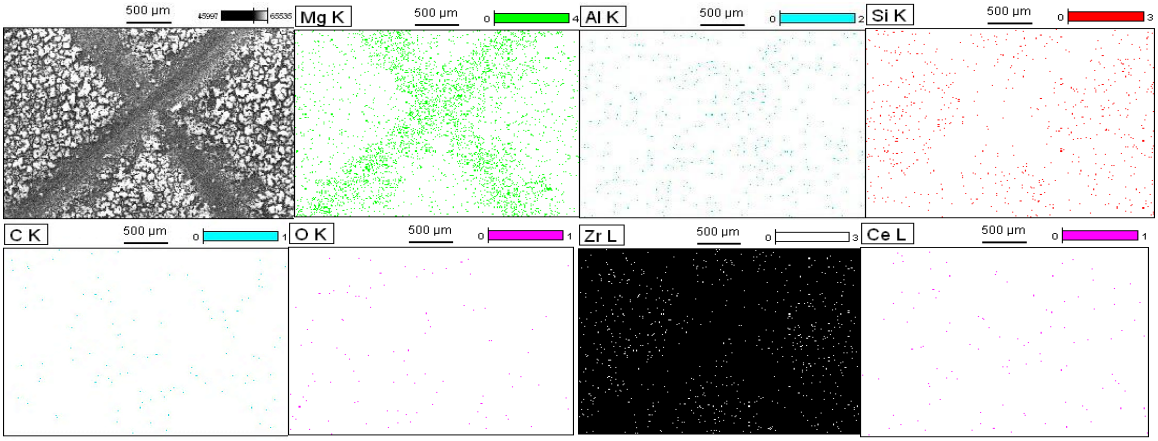
500 µm
Mg K
Al K
Si K
C K
O K
Zr L
Ce L

(c)

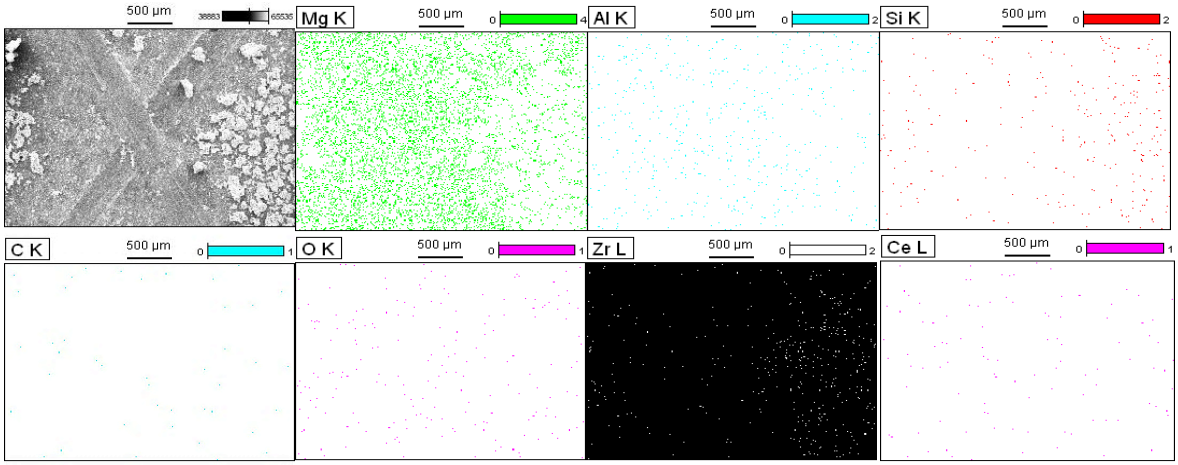
500 µm
Mg K
Al K
Si K
C K
O K
Zr L
Ce L

(d)

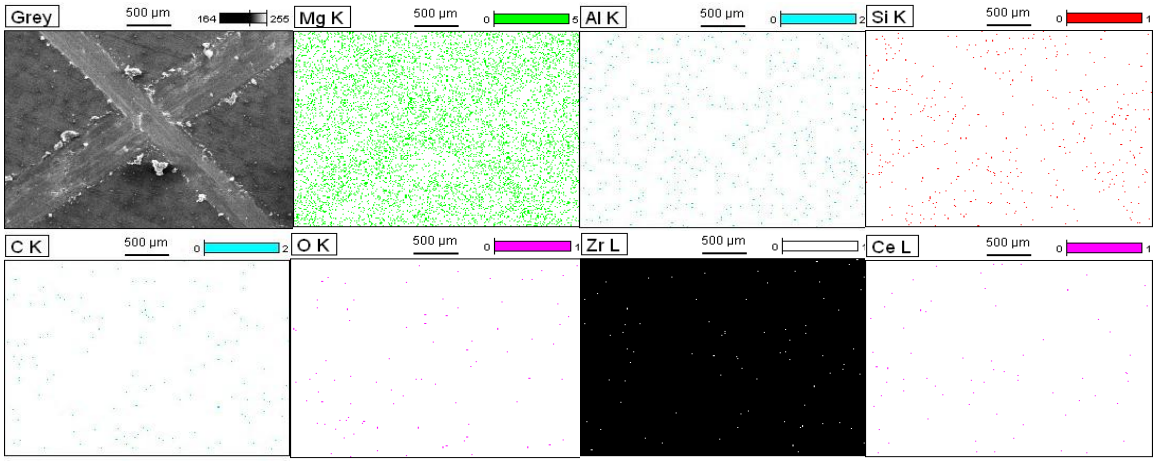

(e)

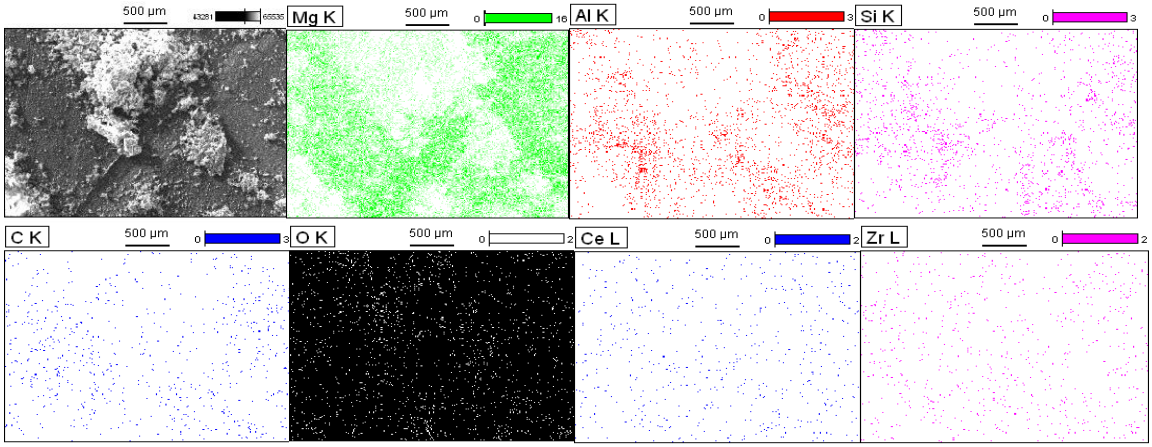

(f)

Figure 4.11: Elemental mapping of (a, b) CM sol coated, (c, d) IMM sol coated and (e, f) IEM sol coated AZ91D substrates before and after exposure to 0.6 M NaCl solution

Table 4.3: Elemental analysis (in wt %) of IMM and IEM sol coated AZ91D substrates before and after 120 h of exposure to 0.6 M NaCl solution

Substrate	**IMM**				**IEM**			
Elements	**Before exposure**		**After 120 h**		**Before exposure**		**After 120 h**	
	Surface	**Scratch**	**Surface**	**Scratch**	**Surface**	**Scratch**	**Surface**	**Scratch**
Mg	21.11	80.16	34.05	77.18	52.45	83.47	58.59	87.58
Al	3.12	13.64	4.54	10.98	6.14	8.52	5.11	7.01
Si	9.55	1.36	7.42	1.16	4.21	2.08	3.56	0.41
Zn	0.00	0.98	1.57	2.37	0.45	1.79	0.41	0.40
C	15.23	0.00	9.23	0.00	31.83	0.00	25.10	0.00

O	21.73	3.40	19.35	7.01	4.07	4.09	7.11	3.95
Ce	2.06	0.46	0.67	0.87	0.76	0.00	0.11	0.34
Zr	27.20	0.0	23.17	0.43	0.09	0.05	0.00	0.31

4.4.7 SVET measurements

The current density maps obtained from SVET analysis for coated substrates immersed in 0.6 M NaCl solution for various durations of time are depicted in Fig. 4.12. High anodic current flow depicted by red colour indicated the increased corrosion rate at the localised defect area because of small anode large cathode configuration. This revealed that the surface of substrate is disclosed to the corrosive medium due to the depletion of passive oxide film.

In case of CM sol coated substrates, gradual increase in the current density was observed after 1 h of exposure, which could reveal that the barrier property of coatings is not passive enough to restrict the diffusion of corrosive species. Initially, IMM sol coated substrates showed higher anodic current in the defect area, which decreases after 1 h of exposure owing to the release of corrosion inhibitor adsorbed on the surface of MMT clay. The anodic current was found decreasing thereafter, due to the deterioration of passive film of inhibitors and the barrier property of coatings could not remain longer as the inhibitors were not intercalated into the MMT clay. IEM sol coated substrates have shown high initial anodic current density in the scribed area in a similar manner to that of IMM sol coated substrates. However, with the increase in exposure durations, the current density of IEM sol coated substrates was decreased drastically owing to the formation of passive oxide film of corrosion inhibitors. The anodic current remains on the lower side even with prolonged exposure to the corrosive medium, thereby showing the self-healing ability of coatings due to release of intercalated corrosion inhibitor with the change in local pH.

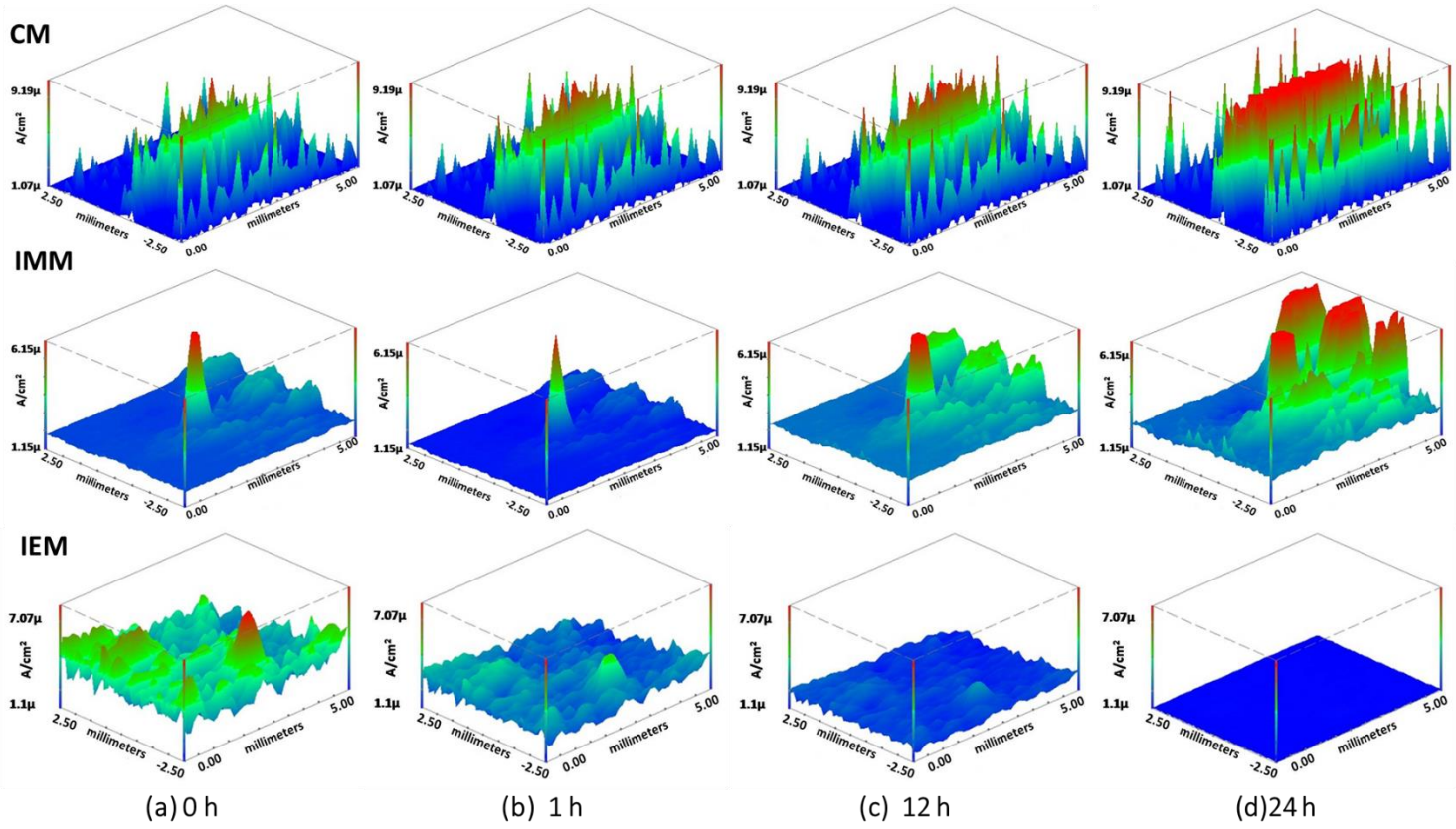

Figure 4.12: Current density maps for CM, IMM and IEM sol coated AZ91D after (a) 0 h, (b) 1 h, (c) 12 h and (d) 24 h of exposure to 0.6 M NaCl solution

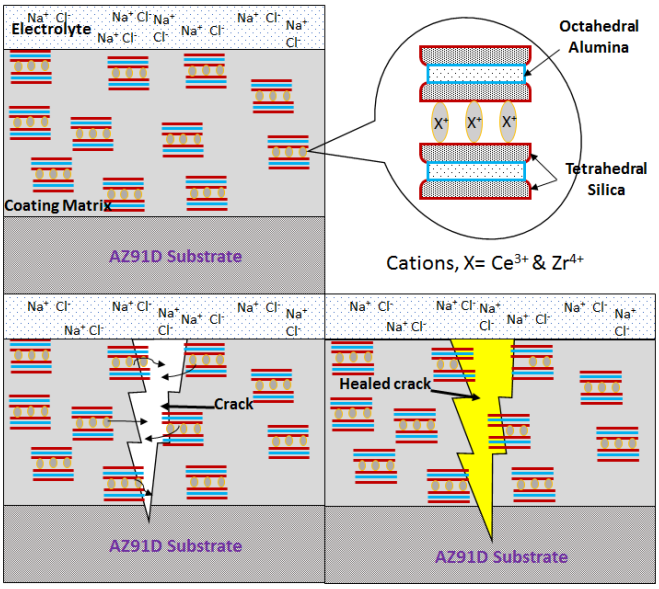

Figure 4.13: Schematic representation of self-healing mechanism by IEM clay-based coatings on AZ91D

SAXS and XRD analyses showed that lamellar structure of MMT clay remains unchanged after intercalation of corrosion inhibitor with evacuation method. Further, EIS

studies and weight loss experiments clearly stated that IEM sol coated substrates showed better barrier properties as compared to that for CM sol coated and IMM sol coated substrates for prolonged durations of exposure. The self-healing ability of coatings was further examined by immersion test and SVET analysis and it was observed that IEM sol based coatings could give better anticorrosion properties for longer durations of exposure to corrosive media. The schematic representation of self-healing mechanism of IEM sol based coatings is shown in Fig. 4.13.

4.5 References

[1] Yingjun Zhang, Yawei Shao, Tao Zhang, Guozhe Meng, Fuhui Wang, High corrosion protection of a polyaniline/organophilic montmorillonite coating for magnesium alloys, Prog. Org. Coat. 76 (2013) 804-811.

[2] Kenzi Suzuki, Masakazu Horio, Toshiaki Mori, Preparation of alumina-pillared montmorillonite with desired pillar population, Mat. Res. Bull. 23 (1988) 1711-1718.

[3] S. Ng, J. Plank, Interaction mechanisms between Na montmorillonite clay and MPEG-based polycarbonate superplasticizers, Cem. Concr. Res. 42 (2012) 847-854.

[4] I. Mohammadi, M. Izadi, T. Shahrabi, D. Fathi, A. Fateh, Enhanced epoxy coating based on cerium loaded Na-montmorillonite as active anti-corrosive nanoreservoirs for corrosion protection of mild steel: Synthesis, characterization, and electrochemical behaviour, Prog. Org. Coat. 131 (2019) 119-130.

[5] Habib Ashassi-Sorkhabi, Saleh Moradi-Alavian, Reza Jafari, Amir Kazempour, Elnaz Asghari, Effect of amino acids and montmorillonite nanoparticles on improving the corrosion protection characteristics of hybrid sol-gel coating applied on AZ91 Mg alloy, Mater. Chem. Phys. 225 (2019) 298-308.

[6] I. Danaee, E. Darmiani, G. R. Rashed, D. Zaarei, Self-healing and anticorrosive properties of Ce(III)/Ce(IV) in nanoclay-epoxy coatings, Iran. Polym. J. 23 (2014) 891-898.

[7] Ebrahim Darmiani , Gholam Reza Rashed , Davood Zaarei, Iman Danaee, Synergistic Effects of Montmorillonite/Cerium Nitrate Additives on the Corrosion Performance of Epoxy-Clay Nanocomposite Coatings, Polym. Plast. Technol. Eng. 52 (2013) 980-990.

[8] Ebrahim Darmiani , Gholam Reza Rashed , Davood Zaarei, Iman Danaee, Synergistic Effects of Montmorillonite/Cerium Nitrate Additives on the Corrosion Performance of Epoxy-Clay Nanocomposite Coatings, Polym. Plast. Technol. Eng. 52 (2013) 980-990.

[9] E. Darmiani, I. Danaee, G. R. Rashed, D. Zaarei, Formulation and study of corrosion prevention behaviour of epoxy cerium nitrate–montmorillonite nanocomposite coated carbon steel, J. Coat. Technol. Res. 10 (4) (2013) 493-502.

[10] Mazdak Izadi, Taghi Shahrabi, Iman Mohammadi, Bahram Ramezanzadeh, Synthesis of impregnated Na^{+}-montmorillonite as an eco-friendly inhibitive carrier and its subsequent protective effect on silane coated mild steel, Prog. Org. Coat. 135 (2019) 135-147

[11] Yu-Hong Zou, Jian Wang, Lan-Yue Cui, Rong-Chang Zeng, Qing-Zhao Wang, Qiu-Xia Han, Jun Qiu, Xiao-Bo Chen, Dong-Chu Chen, Shao-Kang Guan, Yu-Feng Zheng, Corrosion resistance and antibacterial activity of zinc-loaded montmorillonite coatings on biodegradable magnesium alloy AZ31, Acta Biomater. 98 (2019) 196-214.

[12] A. Ghazi, E. Ghasemi, M. Mahdavian, B. Ramezanzadeh, M. Rostami, The application of benzamidazole and zinc cations intercalated sodium montmorillonite as smart ion exchange inhibiting pigments in the epoxy ester coating, Corros. Sci. 94 (2015) 207-217.

[13] Thu Thuy Thai, Anh Truc Trinh, Marie-Georges Olivier, Hybrid sol-gel coatings doped with cerium nanocontainers for active corrosion protection of AA2024, Prog. Org. Coat. 138 (2020) 105428.

[14] Qiufeng Mo, Weizhou L, Haijuan Yang, Fengmei Gu, Quanzhi Chen, Ruixia Yang, Water resistance and corrosion protection properties of waterborne polyurethane coating enhanced by montmorillonite modified with Ce^{3+}, Prog. Org. Coat. 136 (2019) 105213.

[15] Trinh Anh Truc, Thai Thu Thuy, Vu Ke Oanh, To Thi Xuan Hang, Anh Son Nguyen, Nicolas Caussé, Nadine Pébère, 8-hydroxyquinoline-modified clay incorporated in an epoxy coating for the corrosion protection of carbon steel, Surf. Interfaces. 14 (2019) 26-33.

[16] Ianina Santana, Andrés Pepe, Wido Schreiner, Sergio Pellice, Silvia Ceré, Hybrid sol-gel coatings containing clay nanoparticles for corrosion protection of mild steel, Electrochim. Acta 203 (2016) 396-403.

[17] R. Naderi, M. Fedel, F. Deflorian, M. Poelman, M. Olivier, Synergistic effect of clay nanoparticles and cerium component on the corrosion behavior of eco-friendly silane sol–gel layer applied on pure aluminum, Surf. Coat. Technol. 224 (2013) 93-100.

[18] F. Deflorian, S. Rossi, M. Fedel, C. Motte, Electrochemical investigation of high-performance silane sol–gel films containing clay nanoparticles, Prog. Org. Coat. 69 (2010) 158-166.

[19] M. Fedel, E. Callone, S. Diré, F. Deflorian, M. G. Olivier, M. Poelman, Effect of Na-Montmorillonite sonication on the protective properties of hybrid silica coatings, Electrochim. Acta. 124 (2014) 90-99.

[20] To Thi Xuan Hang, Trinh Anh Truc, Truong Hoai Nam, Vu Ke Oanh, Jean-Baptiste Jorcin, Nadine Pébère, Corrosion protection of carbon steel by an epoxy resin containing organically modified clay, Surf. Coat. Technol. 201 (2007) 7408-7415.

[21] Kung-Chin Chang, Shih-Ting Chen, Hui-Fen Lin Chang-Yu Lin, Hsin-Hua Huang, Jui-Ming Yeh, Yuan-Hsiang Yu, Effect of clay on the corrosion protection efficiency of PMMA/Na+-MMT clay nanocomposite coatings evaluated by electrochemical measurements, Eur. Polym. J. 44 (2008) 13-23.

[22] Yuhua Dong, Liqin Ma, Qiong Zhou, Effect of the incorporation of montmorillonite-layered double hydroxide nanoclays on the corrosion protection of epoxy coatings, J. Coat. Technol. Res. 10 (6) (2013) 909-921.

[23] V. Dalmoro, J.H.Z. dos Santos, E. Armelin, C. Alemán, D.S. Azambuja, Sol–gel hybrid films based on organosilane and montmorillonite for corrosion inhibition of AA2024, J. Colloid Interface Sci. 426 (2014) 308-313.

[24] D. Seifzadeh, E. Golmoghani-Ebrahimi, Formation of novel and crack free nanocomposites based on sol gel process for corrosion protection of copper, Surf. Coat. Technol. 210 (2012) 103-112.

[25] G. Rapheal, S. Kumar, N. Scharnagl, C. Blawert, Effect of current density on the microstructure and corrosion properties of plasma electrolytic oxidation (PEO) coatings on AM50 Mg alloy produced in an electrolyte containing clay additives, Surf. Coat. Technol. 289 (2016) 150-164.

[26] International Atomic Energy Agency, NEA/RWMC/Clay Club 2013, www.iaea.org/inis/collection/NCLCollectionStore/_Public/46/109/46109585.pdf, (2013) (accessed February 5th, 2021).

Chapter 5

CORROSION RESISTANCE OF DIFFERENT CORROSION INHIBITOR LOADED IN AS-RECEIVED AND ETCHED HALLOYSITE NANOTUBES

Chapter-5

Corrosion resistance of different corrosion inhibitor loaded in as-received and etched halloysite nanotubes

5.1 Introduction

In chapter 1, the role of corrosion inhibitors in corrosion protection and how they can be used for preventing or reducing corrosion based on their different types was discussed. The literature for various corrosion inhibitors that have been used for corrosion protection of Mg alloys was reviewed in chapter 2. It was observed that, cationic Ce^{3+}-Zr^{4+} corrosion inhibitors encapsulated in nanocontainers like halloysite nanotube (HNT) and montmorillonite nanoclay (MMT) have not been evaluated for their corrosion inhibition ability on Mg alloy AZ91D. Hence, in chapters 3 and 4, prolonged corrosion protection and self-healing ability were evaluated by encapsulating Ce^{3+}-Zr^{4+} in naturally occurring nanoclays like HNTs and MMTs followed by dispersing them into hybrid matrix sol.

Various corrosion inhibitors have been reviewed for protecting Mg alloys from corrosion by dispersing them into coating matrix or encapsulated in microcapsules. Lamaka et al. [1], Umoren et al. [2], Liu et al. [3], Kartsonakis et al. [4], Sorkhabi et al. [5, 6], Gao et al. [7] and Ashraf et al. [8] have reviewed inhibition effect of different corrosion inhibitors on Mg alloys. Chen et al. [9] have intercalated aspartic acid as a corrosion inhibitor into Mg-Al layered double hydroxides (Mg-Al-LDH), which were deposited on AZ31 substrates by using a one-step hydrothermal method. Aspartic acid intercalated Mg-Al-LDH have exhibited better corrosion resistance and self-healing ability as observed from electrochemical measurements and salt immersion tests for 0.6 M NaCl solution for 20 days due to the inhibiting ability of aspartic acid ions, their larger specific surface area to entrap aggressive corrosive Cl^- ions and synergistic effect between aspartic acid and laminate structure of LDH. Plasma Electrolytic Oxidation (PEO) coatings were generated by Qian et al. [10] using alkaline sodium silicate solution on AZ91D substrates followed by post-sealing treatment with sodium phosphate solution dispersed with sodium fumarate as a corrosion inhibitor for 15 min, 30 min and 60 min. H_2 evolution tests revealed that volume of H_2 released for inhibitor based sealing was much lower (0.01 ml/cm^2) than that for only sealing (0.08 ml/cm^2) and only PEO coating without sealing (0.11 ml/cm^2) after 48 h of exposure to 0.6 M NaCl solution. EIS studies for 120 h in 0.6 M NaCl solution showed that inhibitor based sealing treatment for 15 min gave best corrosion resistance,

whereas salt spray tests for 30 days in 0.85 M NaCl solution revealed that inhibitor based sealing treatment for 60 min showed much lower corrosion product accumulation as compared to other sealing treatments. Solimann et al. [11] dispersed nano-graphene oxide (GO) as a corrosion inhibitor in 8-hydroxyquinoline sodium solution prepared by mixing diluted NaOH into aqueous 8-hydroxyquinoline (HQ) followed by immersion of untreated, oxidized and phosphated AZ31 samples. An artificial scribe was made on coated substrates for evaluation of self-healing ability. Electrochemical measurements in simulated body fluid (SBF) showed that AZ31 substrates with oxide pretreatment followed by immersion in HQ sodium solution dispersed with GO have shown highest corrosion resistance and lowest corrosion current, whereas immersion test in SBF for 3 days revealed that the pretreated substrates have shown less damaged surface and healed scribed area as observed from optical microscopic images. Yan et al. [12] have intercalated a green corrosion inhibitor, methionine in Mg-Al LDH nanocontainers which are dispersed in epoxy coatings deposited on Mg alloy AZ91D. Electrochemical measurements of AZ91D substrates (coated and immersed in supernatant solution of methionine released from LDH at different pH conditions) in 0.6 M NaCl for different durations of exposure revealed that the substrates showed better corrosion resistance at pH 9 as compared to that under pH 5 and 7 conditions. Liu et al. [13] have synthesized dodecyltrimethoxysilane modified magnesium silicate nanotubes (MS-TNs/DTMS) by hydrothermal method, whereas in other case MS-TNs were encapsulated with 2-mercaptobenzimidazole (MBI) which are then dispersed into epoxy matrix followed by generating first layer of MBI loaded MS-TNs dispersed epoxy film and second layer of MS-TNs/DTMS dispersed epoxy film on AZ31B substrates. Electrochemical measurements and scratch tests revealed that the corrosion resistance of AZ31B substrates was greatly enhanced after exposure to 0.6 M NaCl solution for 21 days along with retention of superhydrophobicity as observed from contact angle and sliding angle measurements. Zhang et al. [14] have reviewed number of surface modification techniques under the categories, physical barrier coatings and smart self-healing coatings for Mg alloys. A number of coating systems have been reviewed in aforementioned categories like metal-based coatings, sol-gel coatings, encapsulation coatings, etc.by using different corrosion inhibitors.

Halloysite nanotubes (HNT) has been widely considered as an eco-friendly nanocontainer for encapsulating corrosion inhibitors, due to its wide availability, low cost and capability of providing a loading capacity of up to 20 % [15]. Further, selective etching of inner lumen of HNT using H_2SO_4 can result in increase of the lumen diameter, which is

expected to enhance the inhibitor loading by up to 60 % [16]. Hence, it would be of great interest to investigate the effect of etching on the corrosion protection properties of coatings based on etched and corrosion inhibitor loaded HNTs.

In addition, it would be appropriate to investigate the release properties of different corrosion inhibitors from HNTs in order to understand the conditions under which the optimum release occurs to render the self-healing effect. Few studies have been reported on the release rate of corrosion inhibitors like 2-mercaptobenzothiazole (MBT), benzotriazole (BTA) and L-valine from HNTs [17-19]. The release kinetics of corrosion inhibitor from nanocontainers was described by theoretical models like zero order, first order, Higuchi, Hixson-Crowell and Korsmeyer-Peppas models [20]. These models can correlate corrosion inhibitor release with respect to time. More information regarding diffusion mechanism and matrix degradation can be evaluated by using kinetic study of corrosion inhibitor release. Bhanvase et al. [21] and Tyagi et al. [22] have reported the kinetic property evaluation of corrosion inhibitor release from cerium zinc molybdate nanocontainers and silica nanocontainers, respectively.

Although a lot of studies have been reported using different corrosion inhibitor/nanocontainer combinations, a comparative study of inhibition ability of different corrosion inhibitors like cationic Ce^{3+}-Zr^{4+} and organic inhibitors such as HQ and MBT loaded in HNT or etched HNT (EHNT) has not been carried out so far. In addition to this, release rate and its kinetic studies for aforementioned cationic and organic corrosion inhibitors loaded in HNT and EHNT has also not been reported so far. Hence, in this chapter, the corrosion protection ability of coatings based on Ce^{3+}-Zr^{4+}, HQ and MBT loaded in HNT and EHNT was studied in addition to percentage release of these three corrosion inhibitors loaded in HNT and EHNT under different pH conditions. The release data was fitted with various kinetic models to understand the factors affecting the release of inhibitors.

5.2 Materials and Methods

5.2.1 Etching of HNT lumen

The selective etching of inner alumina layer of HNT lumen was carried out by using 1 M H_2SO_4 as shown in Fig. 5.1. 5 g of HNTs having lumen diameter in the range of 10-15 nm were added to 500 ml H_2SO_4 with 1 M concentration followed by heat treatment under water bath at 50 ^oC for 72 h with continuous stirring conditions. EHNTs were separated from acid solution by centrifugation at 5000 rpm for 10 min followed by multiple washing

with deionized water until pH of solution increases in the range of 6-7 and dried overnight in hot air oven at 50 ^{o}C [16, 23].

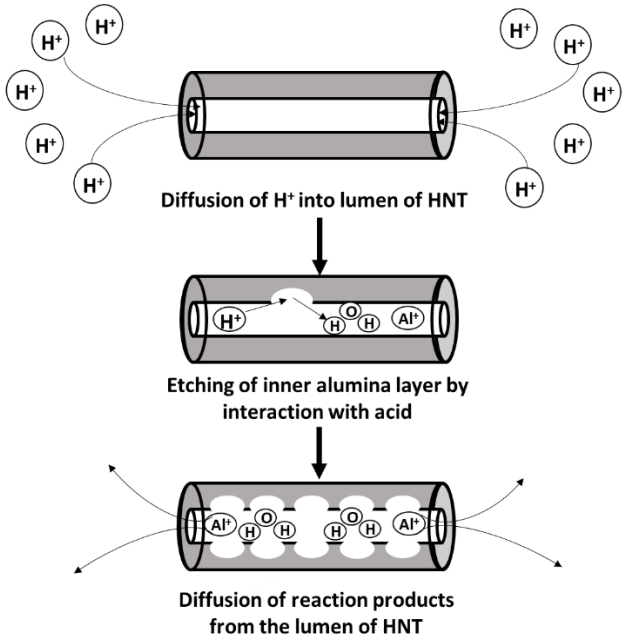

Figure 5.1: Schematic representation of etching the lumen of HNTs using sulfuric acid

5.2.2 Release rate studies

Corrosion inhibitor encapsulated HNT and EHNT were dispersed in 100 ml of 0.6 M NaCl solution with pH values of 3, 7, 8.5 and 10.2 for evaluating the pH dependent release properties. The external trigger for the release of corrosion inhibitor was provided by keeping the solution under constant stirring conditions. 10 ml aliquots of the supernatant was withdrawn for measuring absorbance at specified time intervals (every 10 min duration for first hour and thereafter, 60 min duration up to 420 min and then at 1440 min) and same amount of fresh NaCl solution was added to maintain a constant volume. The absorbance of the solution was measured over the wavelength range of 200-900 nm by using UV-VIS-NIR spectrophotometer (Shimadzu UV-3600 Plus). The release behaviour of Ce^{3+}-Zr^{4+}, HQ and MBT encapsulated in HNT and EHNT was examined by measuring absorbance at 209 nm (for Ce^{3+}-Zr^{4+}), at 249 nm (for HQ) and at 325 nm (for MBT). Absorbance as a function of concentration data and corresponding equations for fitting the data were obtained for pure corrosion inhibitor solutions as control for calculation of release data. The detailed procedure for obtaining standard concentration-absorbance curves and release rate has been reported by Yu et al. [17].

In addition, the release percentage was also evaluated for Ce^{3+}-Zr^{4+} loaded HNTs with stoppered ends of polymeric microcapsules, where the capping procedure is performed as

mentioned in section 3.2 of chapter 3 and the evaluation of percentage release was carried out as mentioned above.

5.2.3 Synthesis of sols and coating deposition

Synthesis of hybrid matrix sol, synthesis of polymeric microcapsules and loading of corrosion inhibitors (Ce^{3+}-Zr^{4+}, HQ and MBT) in HNT and EHNT were carried out as mentioned in section 3.2 of chapter 3. The polymeric microcapsules and 2 wt % of inhibitor loaded HNTs and EHNTs were dispersed in hybrid matrix sol to prepare the self-healing sol. Dip coating technique was used to deposit the coatings on AZ91D substrates with 1 mm/s withdrawal speed followed by heat treatment at 130 ^{o}C for 1 h. The substrate preparation and coatings generation was performed as mentioned in section 3.2 of chapter 3.

5.3 Characterization Techniques

5.3.1 HNT and EHNT clay analysis

Field emission scanning electron microscopy (FESEM) and transmission electron microscopy (TEM) were used to examine the morphological properties of inhibitor loaded/unloaded HNTs and EHNTs followed by elemental analysis using scanning electron microscope (SEM-Hitachi S3400N) fitted with energy dispersive spectroscopy (EDS) attachment. X-ray diffraction (XRD) studies were performed to evaluate phase changes of HNTs and EHNTs. BET surface area and pore volume measurements were carried out for confirmation of inhibitor loading in HNTs and EHNTs.

5.3.2 Coating characterization

The thickness of coatings was measured using thickness gauge PosiTector® 6000 (DelFelsko Corporation, USA) and by cross sectional analysis using SEM. The corrosion protection ability of coatings based on HNT and EHNT encapsulated with different corrosion inhibitors was evaluated by using electrochemical measurements such as EIS and potentiodynamic polarization as mentioned in section 3.3 of chapter 3.

5.4 Results and Discussion

5.4.1 Morphological analysis of EHNT and inhibitor loaded HNT and EHNT

The morphology of EHNT and inhibitor loaded EHNT examined using FESEM and TEM analyses is as shown in Fig. 5.2. SEM-EDS analysis was performed to examine the presence of corrosion inhibitors after loading of modified clay. The lumen diameter of

HNTs was observed to be varying in the range of 10-15 nm (Fig. 3.3), whereas that of EHNTs was in the range of 35-45 nm as shown in Fig. 5.2. The elemental analysis of inhibitor loaded and unloaded EHNT confirmed presence of alumina and silica and the appearance of Zr^{4+} that was loaded into the lumen. Though Ce^{3+} was also loaded into the lumen, peaks of Ce^{3+} did not show up in EDS analysis, since it was present in an amount lower than the detection limit of the instrument.

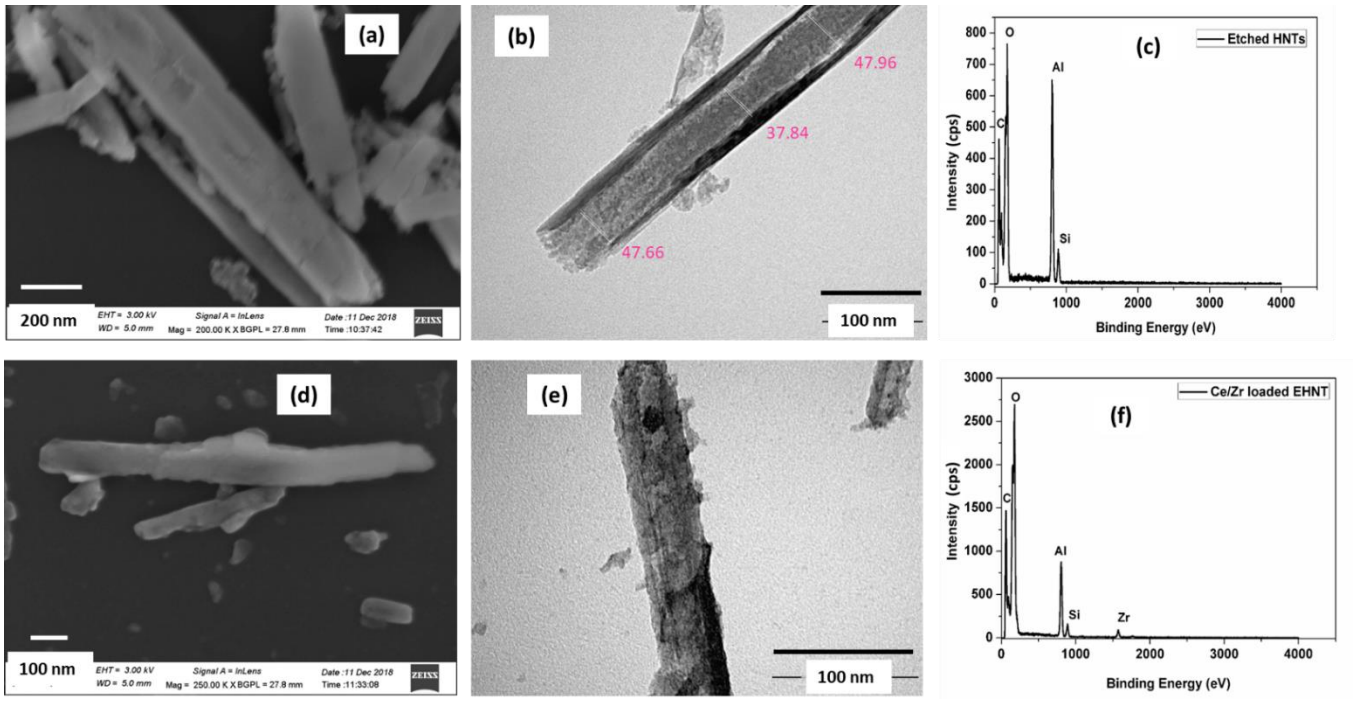

Figure 5.2: FESEM images (a), (d); TEM images (b), (e) and EDS spectra (c), (f) of etched HNTs and Ce^{3+}- Zr^{4+} loaded etched HNTs

In addition, FESEM analysis was performed to examine the morphology of different corrosion inhibitor (HQ and MBT) loaded HNTs and the presence of corrosion inhibitors was confirmed by SEM-EDS analysis as shown in Fig. 5.3 and Table 5.1 respectively. Some traces of N were observed in HQ loaded HNT whereas presence of N and S in MBT loaded HNT confirmed the appearance of corrosion inhibitors with the HNTs, either adsorbed on the surface or loaded into the lumen.

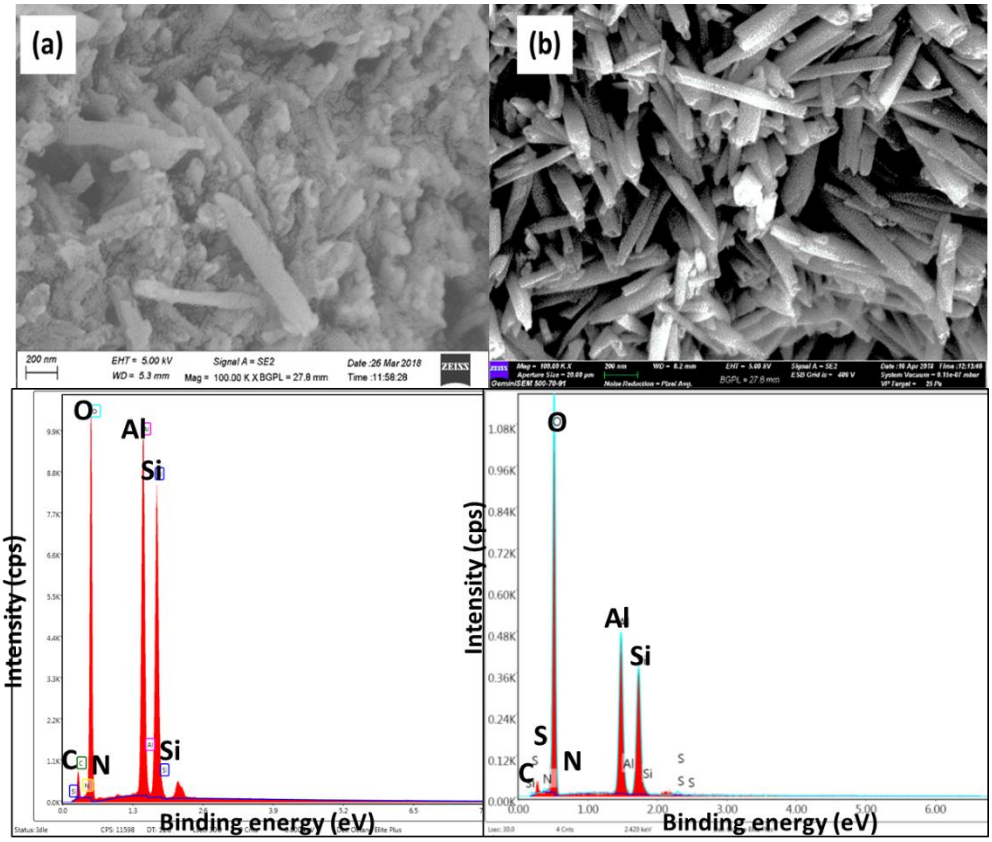

Figure 5.3: FESEM images and EDS spectra of (a) HQ and (b) MBT loaded HNTs

Table 5.1: Elemental analysis of HQ and MBT loaded HNTs using SEM-EDS

Clay Type	Elements (wt %)					
	Al	**Si**	**C**	**O**	**N**	**S**
HQ-HNT	1.32	29.56	19.28	48.83	1.01	-
MBT-HNT	21.97	21.09	9.16	46.23	0.78	0.77

5.4.2 XRD Analysis

XRD profiles of inhibitor loaded and unloaded HNTs and EHNTs are as shown in Fig. 5.4. (001) peak at 7.3 Å represents multilayer wall packing structure of HNTs, which did not show any decrement in the relative intensity after etching, thereby indicating zero loss of the crystallinity of tube wall. Also, (001) peak does not show any shift to lower angles , thereby indicating that there is no intercalation of H_2SO_4 into the interlayer spacing. This revealed that the etching of HNT lumen takes place from the innermost layer to the outermost layer, thereby removal of alumina in a layer-by-layer manner. Further, the (020) peak at 4.5 Å corresponding to tubular nature of HNTs, did not show any change in relative intensity or shift in 2θ values, which indicated that corrosion inhibitors were not encapsulated in the interlayer spacing but only inside the lumen of HNTs [16,24].

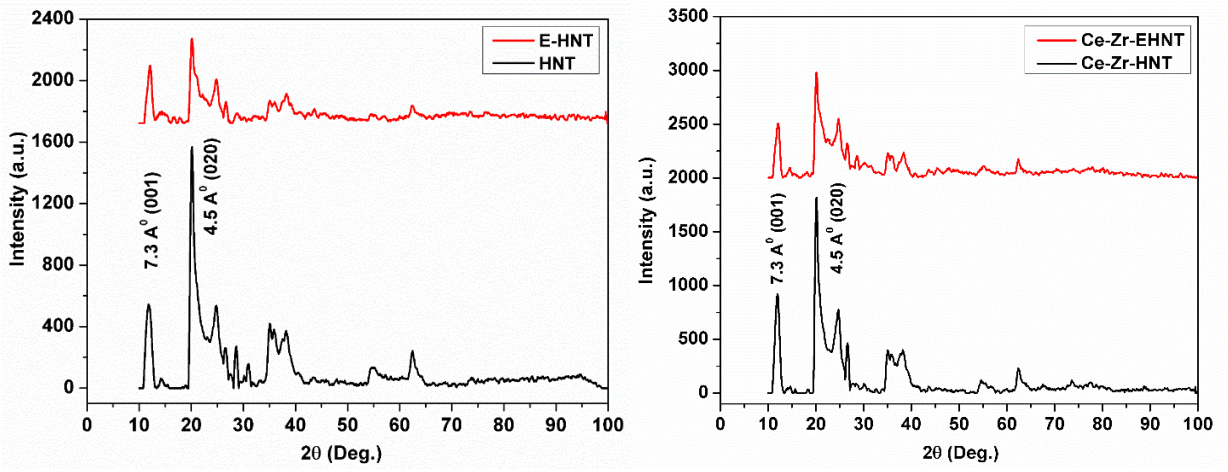

(a) **(b)**

Figure 5.4: XRD patterns of (a) HNTs and EHNTs and (b) Ce^{3+}- Zr^{4+} loaded HNTs and EHNTs

5.4.3 BET surface area and pore volume analysis

The encapsulation of corrosion inhibitors into the HNT lumen was ascertained with BET pore volume and surface area analysis. The comparison of surface areas and pore volumes of inhibitor loaded and unloaded HNTs and EHNTs are shown in Fig. 5.5. The enhanced surface area and pore volume of HNTs after treatment with H_2SO_4 confirmed the

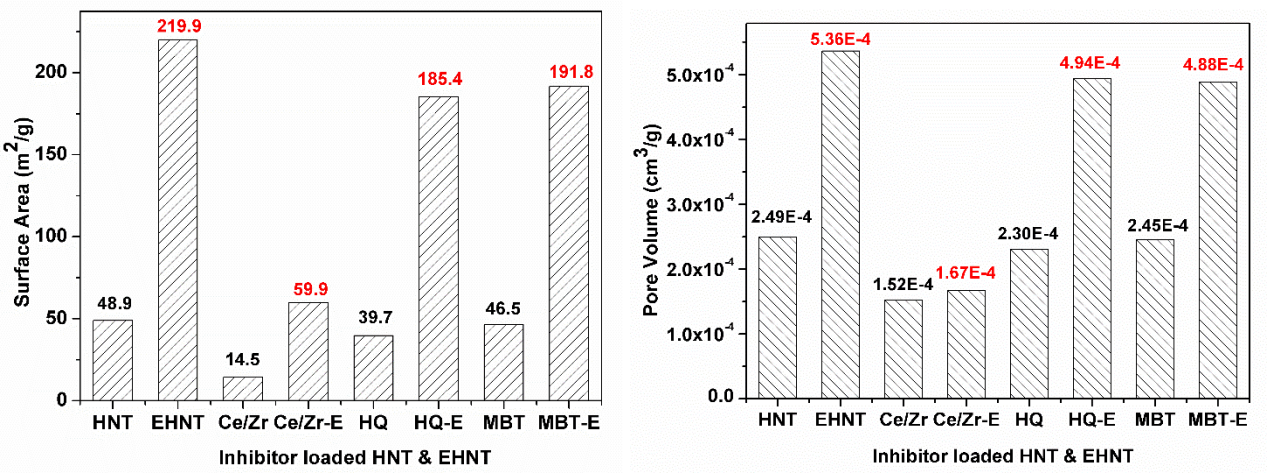

(a) **(b)**

Figure: 5.5: Comparison of (a) surface areas and (b) pore volumes of inhibitor loaded and unloaded HNTs and EHNTs

dealumination of lumen of HNTs. Further, the decrement in the surface area of HNTs and EHNTs after encapsulation of corrosion inhibitor indicated that the corrosion inhibitor may have either got loaded into the lumen and/or adsorbed on the surface. However, the

decrement in the pore volume of corrosion inhibitor loaded HNTs and EHNTs unequivocally confirmed the encapsulation of inhibitor into the lumen only.

5.4.4 Percentage release studies of different corrosion inhibitors from HNTs and EHNTs

The percentage release profiles of Ce^{3+}-Zr^{4+}, HQ and MBT encapsulated in HNT and EHNT at different pH values are depicted in Fig. 5.6. The objective of these measurements was to explore the effect of pH of aqueous NaCl solution (pH 3, 7, 8.5 and 10.2) on the percentage release of the corrosion inhibitors with respect to time. The percentage release of the corrosion inhibitors was found to increase with respect to time initially and then attained the steady state. The higher initial release corresponded to the inhibitor adsorbed on the surface of HNTs, whereas the slow and steady release was attributed to the inhibitor loaded into the lumen of HNTs. The release rate attains steady state after 420 min, which could be attributed to decrease in diffusion rate of inhibitor when the solution reaches its equilibrium, thereby decreasing the concentration gradient. It can be seen that the release for MBT, HQ and Ce^{3+}-Zr^{4+} at any particular pH are higher for EHNT when compared to HNT. The higher release for inhibitors loaded in EHNT could be due to the higher amount of inhibitor loaded inside lumen as expected, which was already confirmed with BET surface area and pore volume analysis. It can also be seen that there was a drastic increase in release rate during the first one hour of stirring (that simulated the conditions of an external damage), after which time, the values attained a steady state.

It was found that, percentage release of Ce^{3+}-Zr^{4+} was highest at pH 7 followed by pH 8.5, pH 10.2 and pH 3. In case of HQ, the percentage release was highest at pH 3, followed by 10.2, 8.5 and 7. MBT has shown highest percentage release at pH 10.2, followed by 3, 8.5 and 7. Yendluri et al [25] found that at higher pH values, the MAA complex is not stable and hinders the release of encapsulated drug. In this case, Ce^{3+}-Zr^{4+} were loaded in HNT and EHNT along with MAA as the complex forming stabilizing agent for Ce^{3+} and Zr^{4+}. Hence, the reason for very low release of Ce^{3+}-Zr^{4+} in pH 3 could be due to the presence of complex of MAA that restricts the release of loaded compound in HNT. In case of HQ and MBT loaded HNTs, similar conclusions were reported earlier [18, 26] for the release of HQ and MBT from HNTs at acidic and basic pH values. HQ has shown higher

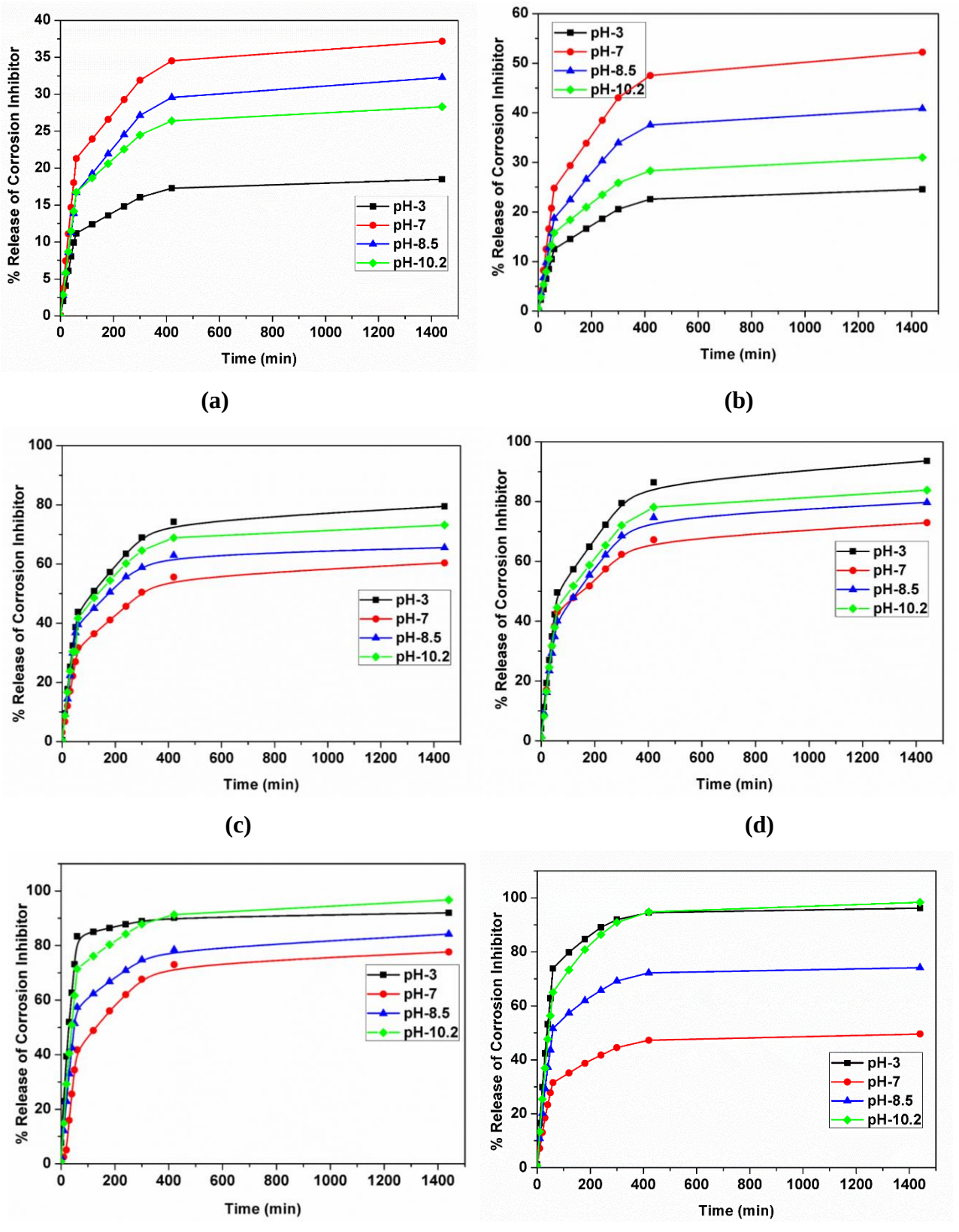

Figure 5.6: Percentage release profiles of (a), (b) Ce^{3+}-Zr^{4+}; (c), (d) HQ and (e), (f) MBT loaded in HNT and EHNT

release at acidic pH owing to the formation of ions of HQ under acidic conditions, thereby accelerating the rate of HQ release. In case of MBT loaded HNTs, during 1 h of exposure, the release of MBT adsorbed on the HNTs is more under acidic conditions as compared to the one under alkaline conditions. However, the release is more under alkaline conditions when MBT is released from lumen of HNT, which later attains the equilibrium slowly.

The percentage release profiles of Ce^{3+}-Zr^{4+} encapsulated in HNT with and without end stoppers at different pH values are depicted in Fig. 5.7. The objective of these measurements was to explore the effect of closing ends of HNTs (capped HNT, CHNT) at different pH conditions of aqueous NaCl solution (pH 3, 7, 8.5 and 10.2) on the percentage release of the corrosion inhibitors with respect to time. It could be observed that, the percentage release has decreased after closing the ends of inhibitor loaded HNTs with polymeric microcapsules at different pH values. This could be attributed to the slow release of inhibitors from HNTs due to the covering of microcapsules and at particular pH environment, the end cappings get separated from the ends of HNTs, thereby facilitating the release of inhibitor. As observed earlier, the release profiles of Ce^{3+}-Zr^{4+}, HQ and MBT from CHNT have been found similar to that of uncapped HNTs at different pH.

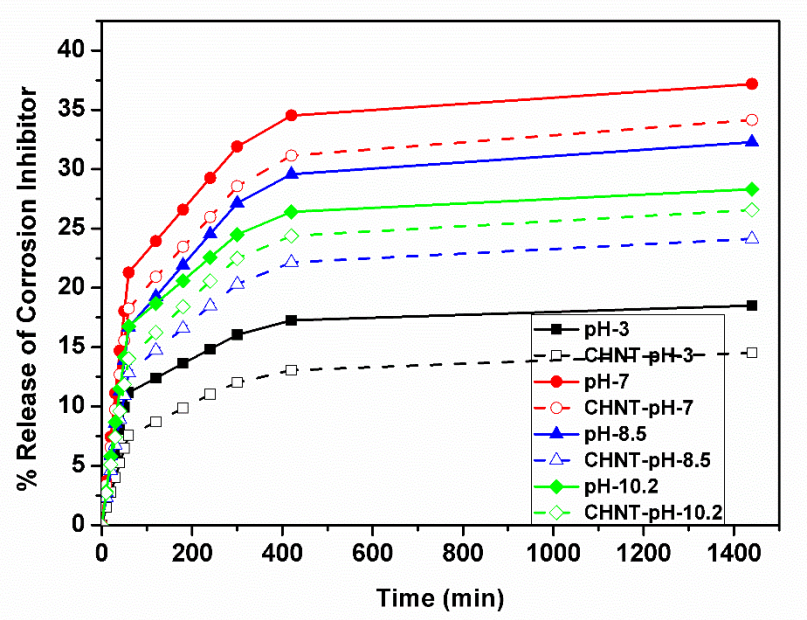

Figure 5.7: Comparison of percentage corrosion inhibitor release profiles of Ce^{3+}-Zr^{4+} loaded HNTs with and without end stoppers

Since the percentage release for the initial one hour was the maximum, the kinetics of the release was further studied using the data obtained for the first one hour duration, only for the Ce^{3+}-Zr^{4+} inhibitor from uncapped HNTs. Various kinetic models were analyzed for release of corrosion inhibitor Ce^{3+}-Zr^{4+} from HNT and EHNT to correlate the data and

increased understanding of the release mechanism. The models used are the ones that have been reported to understand the release of drugs from controlled drug delivery systems [27]. Assuming that the self-healing mechanism is similar to the controlled release of drugs from drug delivery systems, these models were used to study the release data. The Korsmeyer-Peppas model assumes release for cylindrical shaped matrices. Since, the HNTs have a cylindrical shape, this model was also included for analysing the release data. Accordingly, the Ce^{3+}-Zr^{4+} release data from HNT and EHNT at various pH values as a function of time was fitted to zero-order (Eq.1), first-order (Eq.2), Higuchi (Eq.3), Hixson-Crowell (Eq.4) and Korsmeyer-Peppas (Eq.5) models.

$$Q_t = Q_0 + k_0 t \quad (1)$$

Q_t = amount of Ce^{3+}-Zr^{4+} released after time t, Q_0 = Initial amount of Ce^{3+}-Zr^{4+} in the solution (in this case, $Q_0 = 0$), k_0 = Zero order release constant (concentration/time)

$$ln\ (M_t/M_\infty) = - kt \quad (2)$$

M_t = Concentration of Ce^{3+}-Zr^{4+} present in HNT at time t, M_∞ = Initial concentration of Ce^{3+}-Zr^{4+} in HNT, k = First order rate constant ($time^{-1}$)

$$Q_t = K_H\, t^{1/2} \quad (3)$$

Q_t = amount of Ce^{3+}-Zr^{4+} released after time t, K_H = Higuchi dissolution constant

$$W_0^{1/3} - W_t^{1/3} = K_s\, t \quad (4)$$

W_t = Remaining amount of Ce^{3+}-Zr^{4+} in HNT at time t, W_0 = Initial amount of Ce^{3+}-Zr^{4+} in HNT, K_s = Constant incorporating the surface-volume relation

$$Q_t / Q_0 = k_t\, t^n \quad (5)$$

Q_t = amount of Ce^{3+}-Zr^{4+} released after time t, Q_0 = Initial amount of Ce^{3+}-Zr^{4+} in the solution,

k_t = Release rate constant, n = Release exponent

Figures 5.8 and 5.9 depicted the use of zero-order, first-order, Higuchi, Korsmeyer-Peppas and Hixson-Crowell model for fitting Ce^{3+}-Zr^{4+} release profile from HNT and EHNT up to 1 h, respectively. The respective rate constants and R^2 values are mentioned in Tables 5.2 and 5.3. The rate constant values have shown the rate of diffusivity of corrosion inhibitor and could be correlated with corrosion inhibition ability of coatings. The preferred mechanism of release of the inhibitor is a zero-order one, since it is time-independent release. It could be observed from Tables 5.2 and 5.3 that zero order and Korsmeyer-Peppas models have shown better fit as compared to other models and of the two, the Korsmeyer-Peppas model was seen to be the best fit for the data obtained. Korsmeyer-Peppas model gave information about diffusion mechanism of corrosion

inhibitors in NaCl solution. As mentioned in Tables 5.2 and 5.3, diffusional release coefficient, n ≈ 1 indicated that the diffusion mechanism followed zero order time independent release. The release profile was also fitted for the duration from 2 h to 24 h. It was observed that, all the models fitted the release profile in the similar manner for both durations. Hence, it could be concluded that there is no change in reaction order after the release rate attained the steady state.

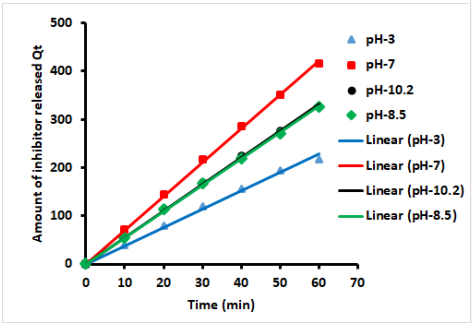

(a)

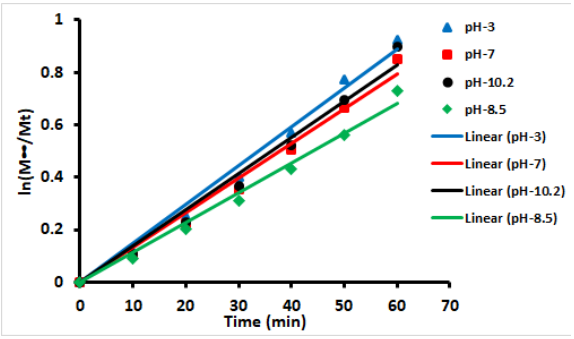

(b)

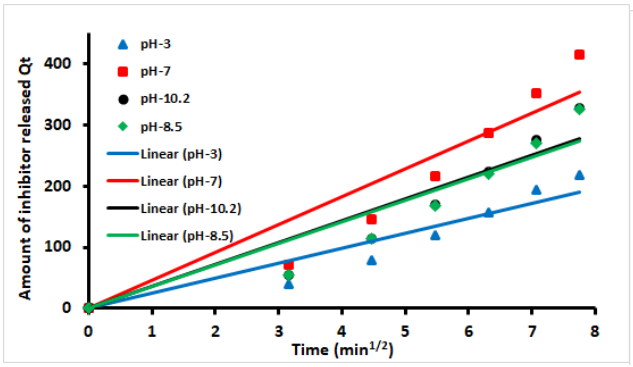

(c)

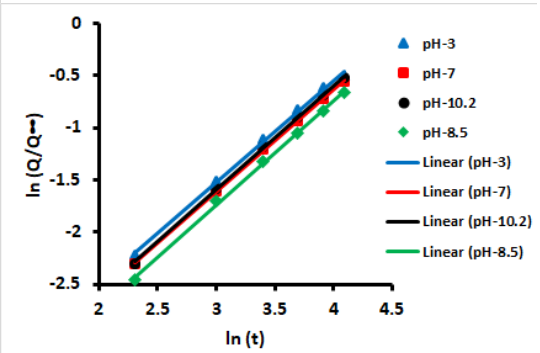

(d)

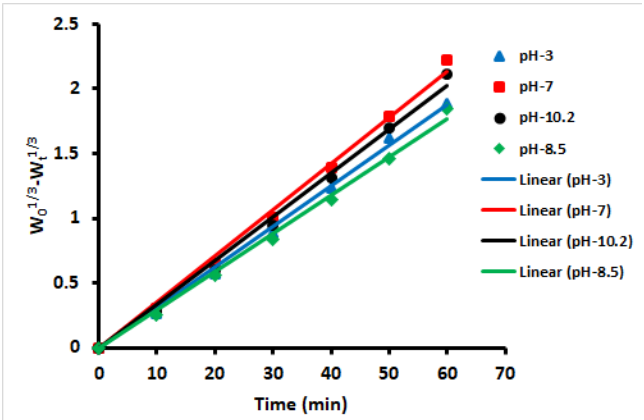

(e)

Figure 5.8: Linear fit plots for Ce^{3+}-Zr^{4+} release from HNT at different pH, (a) Zero order, (b) First order, (c) Higuchi model, (d) Korsmeyer-Peppas model and (e) Hixson-Crowell model

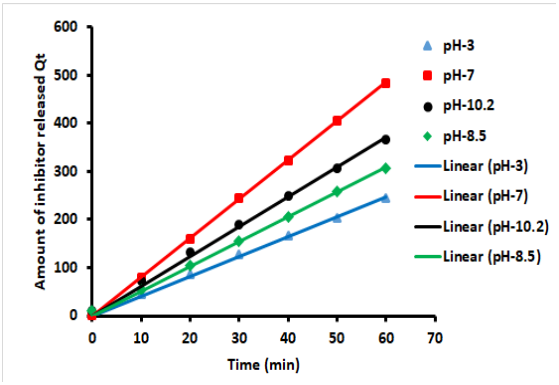

(a)

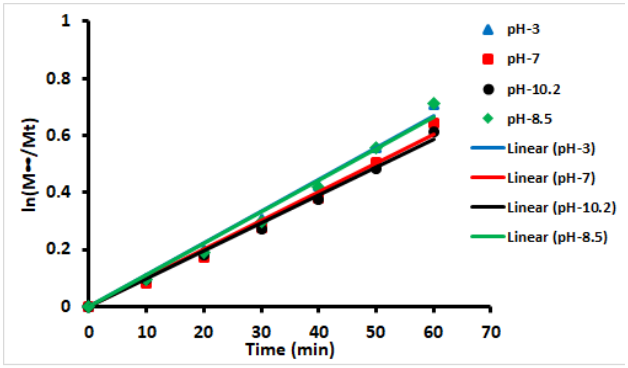

(b)

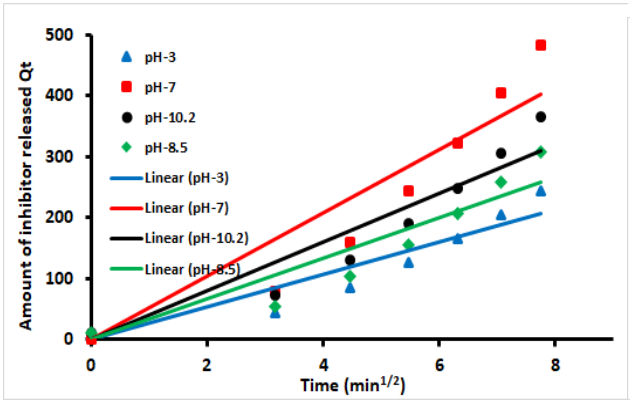

(c)

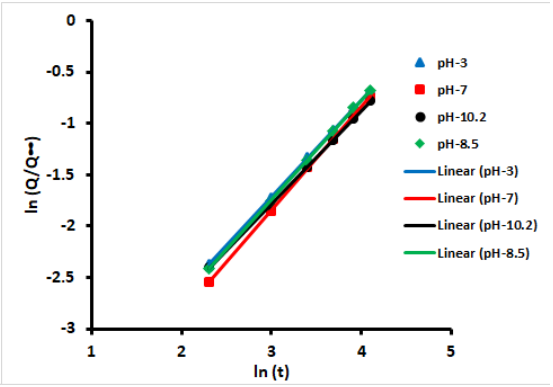

(d)

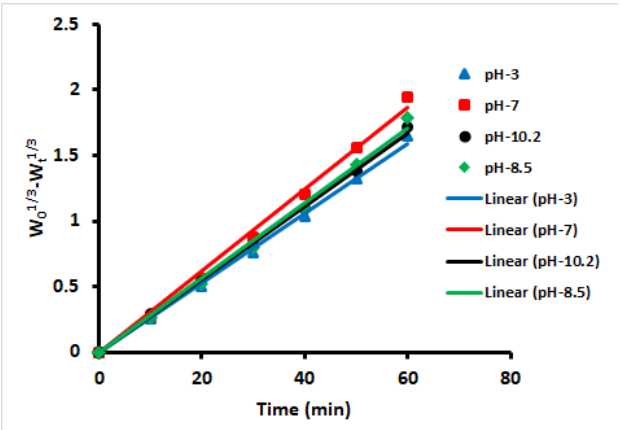

(e)

Figure 5.9: Linear fit plots for Ce^{3+}-Zr^{4+} release from EHNT at different pH, (a) Zero order, (b) First order, (c) Higuchi model, (d) Korsmeyer-Peppas model and (e) Hixson-Crowell model

Table 5.2: Comparison of parameters of various models for release of corrosion inhibitor from HNT

pH	Zero Order		First Order		Higuchi model		Korsmeyer-Peppas model			Hixson-Crowell model	
	k_0 (mg/g. min)	R^2	K (min^{-1})	R^2	K_H (mg/g. $min^{1/2}$)	R^2	k_t (min^{-n})	N	R^2	κ ($mg^{1/3}$/g $^{1/3}$.min)	R^2
3	3.8007	0.9953	0.0148	0.9884	24.669	0.9013	0.01177	0.9732	0.9981	0.0312	0.9962
7	7.0436	0.9990	0.0132	0.9856	45.625	0.8929	0.01053	0.9800	0.9996	0.0356	0.9950
8.5	5.461	0.9993	0.0113	0.9874	35.349	0.8891	0.00891	0.9943	0.9987	0.0295	0.9952
10.2	5.5263	0.9994	0.0138	0.9823	35.773	0.8900	0.01038	0.9916	0.9996	0.0338	0.9934

Table 5.3: Comparison of parameters of various models for release of corrosion inhibitor from EHNT

pH	Zero Order		First Order		Higuchi model		Korsmeyer-Peppas model			Hixson-Crowell model	
	k_0 (mg/g. min)	R^2	K (min^{-1})	R^2	K_H (mg/g. $min^{1/2}$)	R^2	k_t (min^{-n})	N	R^2	κ ($mg^{1/3}$/g $^{1/3}$.min)	R^2
3	4.1142	0.9985	0.0112	0.9903	26.672	0.8944	0.010588	0.9451	1	0.0266	0.9969
7	8.0752	1	0.0101	0.9872	52.166	0.8798	0.007762	1.0058	1	0.0311	0.9943
8.5	5.156	0.998	0.0111	0.9863	33.356	0.8797	0.0096	0.9684	0.9999	0.0285	0.9943
10.2	6.1838	0.9962	0.0098	0.9942	40.155	0.8996	0.011146	0.9047	0.9997	0.0279	0.9983

5.4.5 EIS and potentiodynamic polarization measurements

EIS and potentiodynamic polarization measurements were performed for evaluation of the anticorrosion properties of different corrosion inhibitor based coatings on AZ91D samples after exposure to 0.6 M NaCl solution for various durations like 24 h, 72 h and 120 h. Electrochemical measurements were carried out as mentioned in section 3.3.6 of chapter 3. The Nyquist plots and bode plots for uncoated and different corrosion inhibitor loaded

HNT and EHNT based sol coated AZ91D substrates exposed to 0.6 M NaCl solution for different durations are depicted in Fig. 5.10; Fig. 5.12and Fig. 5.11; Fig. 5.13, respectively. The corresponding fit data obtained by using two time constant equivalent electric circuit (Fig. 5.14) is shown in Tables 5.4 and 5.5.

MgO and $Mg(OH)_2$ are considered as unstable under acidic conditions and dissolve to form Mg^{2+} whereas they are more stable and generate passive layer under alkaline conditions. Uncoated AZ91D substrates showed higher corrosion resistance in 0.6 M NaCl solution after 24 h of exposure owing to the formation of thin passive films of corrosion products. After 72 h of exposure, the corrosion resistance of uncoated substrates gets increased because of accumulation of thick and porous film of corrosion products on the substrate surface. However, this porous film allows diffusion of corrosive medium and with prolonged exposure of 120 h, the corrosion resistance decreased because of deterioration of film.

In case of Ce^{3+}-Zr^{4+} loaded HNT based coatings, the corrosion resistance was least after 24 h of exposure due to the porous nature of coatings. However, with the increase in exposure durations the corrosion resistance was found to be increasing and has shown highest value after 120 h of exposure. This could indicate that, due to release of cationic Ce^{3+}-Zr^{4+} corrosion inhibitors with the change in local pH, the coatings have regained their barrier property and showed better corrosion resistance after prolonged duration. HQ loaded HNT based coatings showed highest corrosion resistance among all corrosion inhibitors after 24 h of exposure owing to the formation of complex chelate of HQ on the surface of Mg like bis (8-hydroxyquinoline) magnesium (MgQ_2), which may inhibit the active sites and prevent the permeability of the corrosive species [28, 29]. The corrosion resistance of HQ loaded HNT based coatings decreased drastically after 72 h exposure, may be due to the degradation of chelate film. After prolonged durations of exposure, when HQ based coatings lose their barrier properties, anions of HQ and free Mg^{2+} recrystallize to MgQ_2 at the damaged area and inhibits the progress of localized corrosion. After 24 h of exposure, MBT based coatings showed higher corrosion resistance than Ce^{3+}-Zr^{4+} based

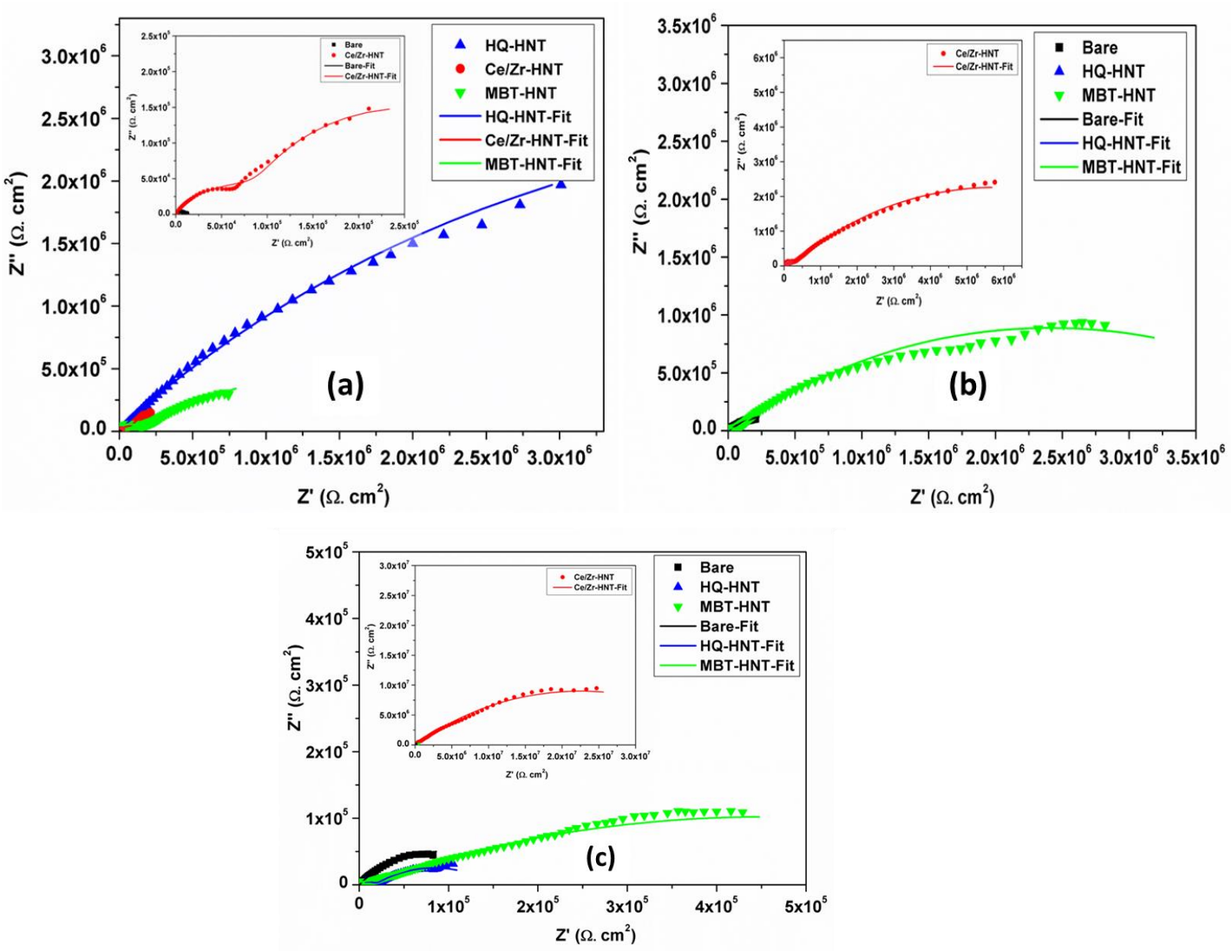

Figure 5.10: Nyquist plots for bare and different corrosion inhibitor loaded HNT based sols coated AZ91D substrates after (a) 24 h, (b) 72 h and (c) 120 h of exposure to 0.6 M solution

coatings and lower than that of HQ based coatings. This could be attributed to inhibitory action of O, N and S atoms present in the organic ring which gets attached to Mg substrate and block active corrosion sites. These atoms are active centers for the adsorption of inhibitor molecules on the substrate surface by replacing the water molecules owing to their high basicity and electron density [30]. The corrosion resistance of MBT based coatings decreased after prolonged exposure of 120 h before showing increment after 72 h of exposure to corrosive medium.

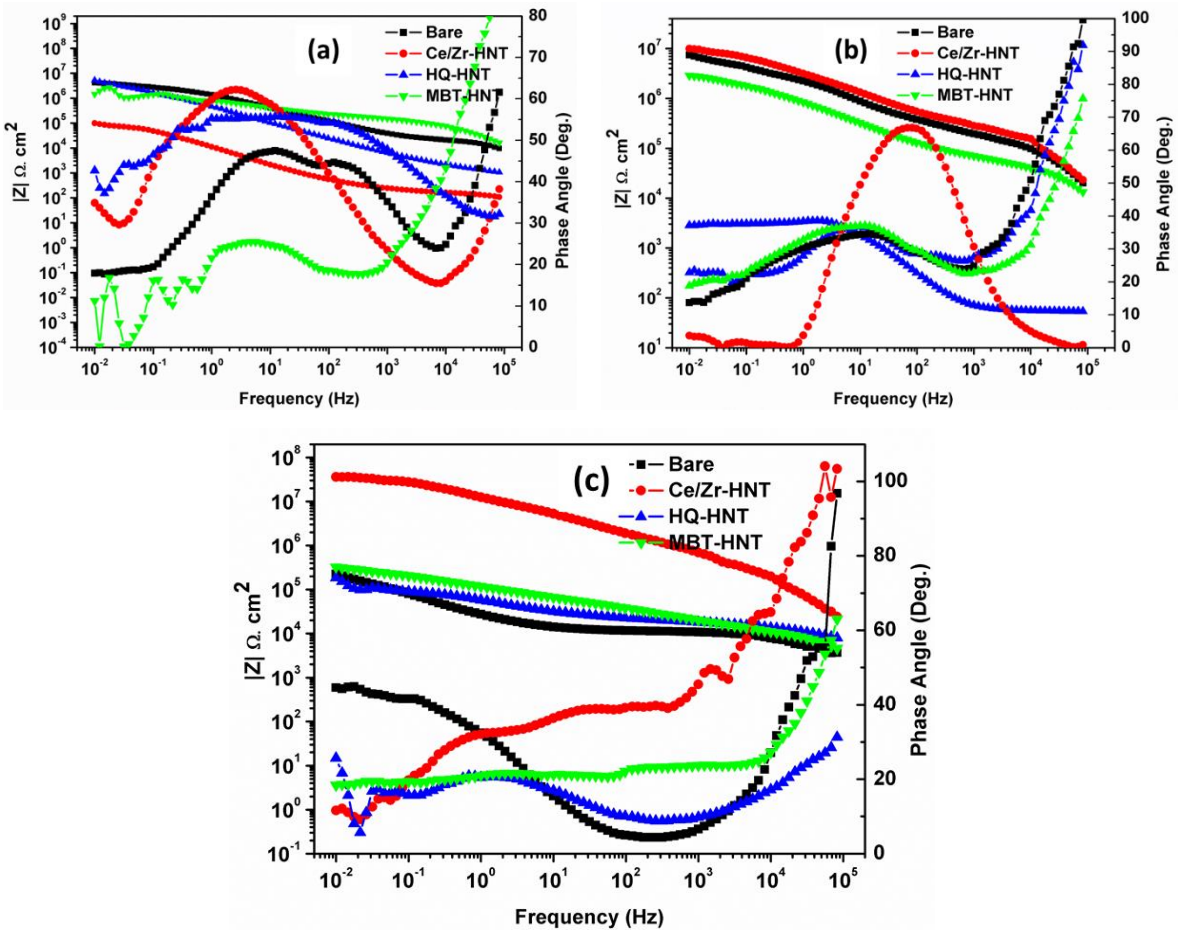

Figure 5.11: Bode plots for bare and different corrosion inhibitor loaded HNT based sols coated AZ91D substrates after (a) 24 h, (b) 72 h and (c) 120 h of exposure to 0.6 M solution

Table 5.4: EIS fit data for bare and different corrosion inhibitor loaded HNT based sol coated AZ91D substrates after exposure to 0.6 M NaCl solution

Sl. No.	Exposure Time	Substrate	R_s $\Omega.cm^2$	R_{coat} $\Omega.cm^2$	R_{ct} $\Omega.cm^2$	C_{coat}/ CPE F/cm^2	C_{edl}/CPE F/cm^2	χ^2
01	24 h	Bare	291.5	-	3.7E6	-	1.5E-8	0.001
		Ce-Zr-HNT	159.3	1.3E5	3. 2E5	4.1E-6	4.5E-5	0.028
		HQ-HNT	810.5	1.9E5	1.1E7	8.4E-8	1.1E-8	0.0035
		MBT-HNT	996.4	7. E4	4.4E6	1.2E-11	4.9E-7	0.0032

02	**72 h**	**Bare**	632.4	-	1. 5E7	-	5.6E-8	0.0037
		Ce-Zr-HNT	230.1	2.0E5	1.1E7	8.3E-12	3.4E-8	0.0038
		HQ-HNT	558.2	1040	1654	5.2E-6	2.6E-6	0.0015
		MBT-HNT	110.4	3.7E4	4.7E6	1.4E-11	1.3E-7	0.0040
03	**120 h**	**Bare**	731.6	-	1.9E5	-	2.2E-6	0.0016
		Ce-Zr-HNT	307.0	3.5E5	4.5E7	7.3E-12	2.7E-9	0.0061
		HQ-HNT	281.5	1.9E4	1.3E5	2.5E-10	8.6E-6	9.4E-4
		MBT-HNT	316.1	3291	9.0E5	2.8E-11	1.6E-5	0.0012

It is expected that the etched HNTs should accommodate more amount of inhibitors and their release also should be high giving rise to higher corrosion protection during coating damage. However, Ce^{3+}-Zr^{4+} loaded EHNT based coatings have shown higher corrosion resistance due to higher amount of loading after 24 h of exposure which gets decreased with the increase in exposure durations. There could be the possibility that, with higher release of cationic inhibitor, the oxide film formed became more porous, allowing diffusion of corrosive medium, thereby showing higher capacitance for Ce^{3+}-Zr^{4+} loaded EHNT based coatings after 120 h of exposure. Similar case was examined with MBT loaded EHNT based coatings, where coatings showed better corrosion resistance after 24 h owing to the inhibitory action of O, S and N by adsorption of inhibitor on the substrate surface by displacing molecules of corrosive medium. However, the increase in exposure durations and higher release of inhibitor from EHNT might have resulted in weak adsorption and, thereby indicated poor corrosion resistance with higher capacitance after 120 h of exposure. In case of HQ, due to lower amount of HQ loaded in HNT, the chelate film that has formed after its release from the HNT might have depleted easily with longer durations of exposure. In another way, the minimum amount required to generate the chelate film could be higher in case of HQ and since the amount of inhibitor loaded inside the HNT is less in case of as-received HNT, the active corrosion protection may not be effective. However, in the case of HQ loaded inside EHNT, the required amount of HQ

could have been released and hence, the corrosion protection is highest after 120 h of exposure, when compared to the coatings based on HQ loaded in as-received HNT. These results are further corroborated with potentiodynamic polarization studies.

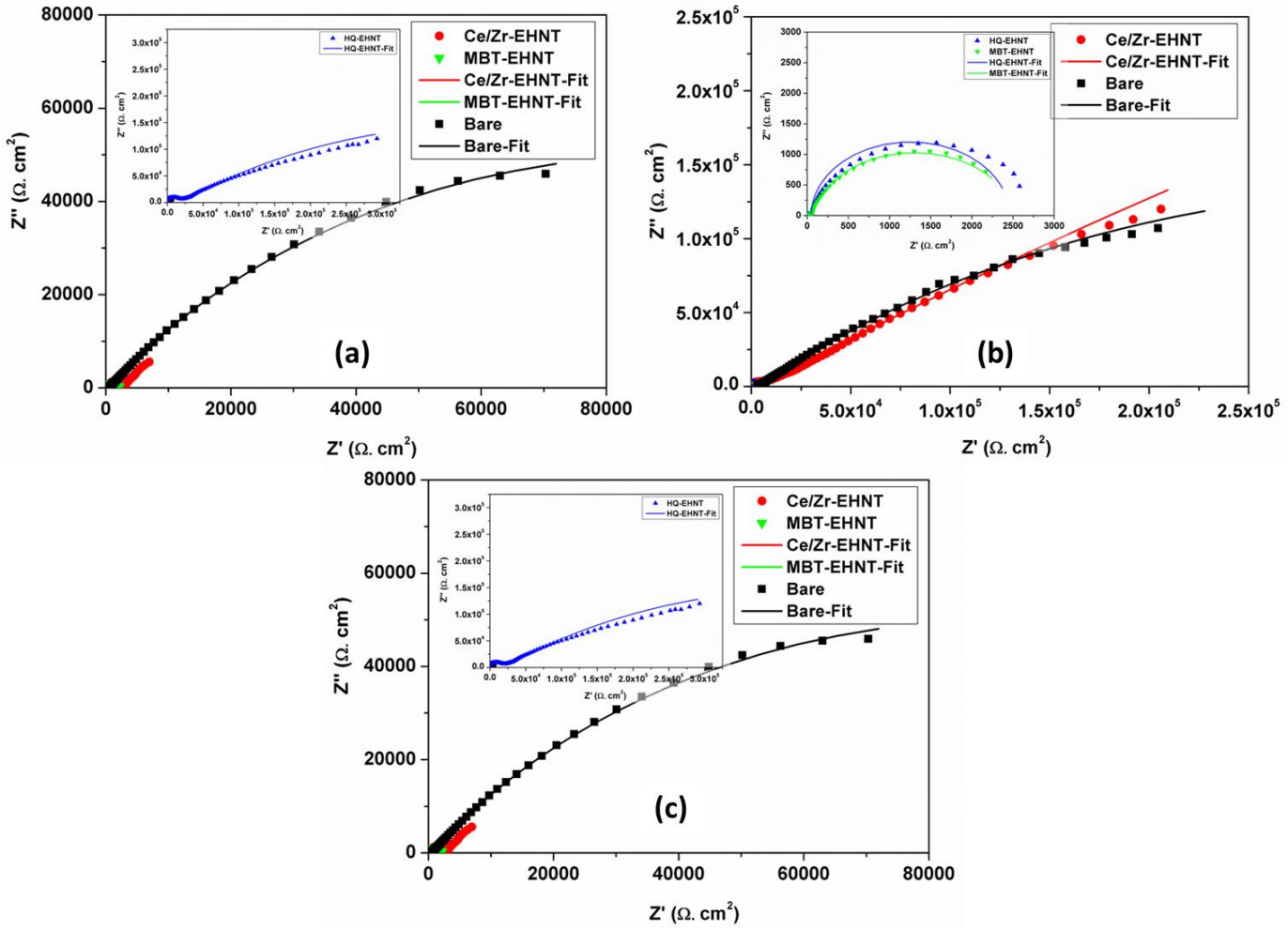

Figure 5.12: Nyquist plots for bare and different corrosion inhibitor loaded EHNT based sols coated AZ91D substrates after (a) 24 h, (b) 72 h and (c) 120 h of exposure to 0.6 M NaCl solution

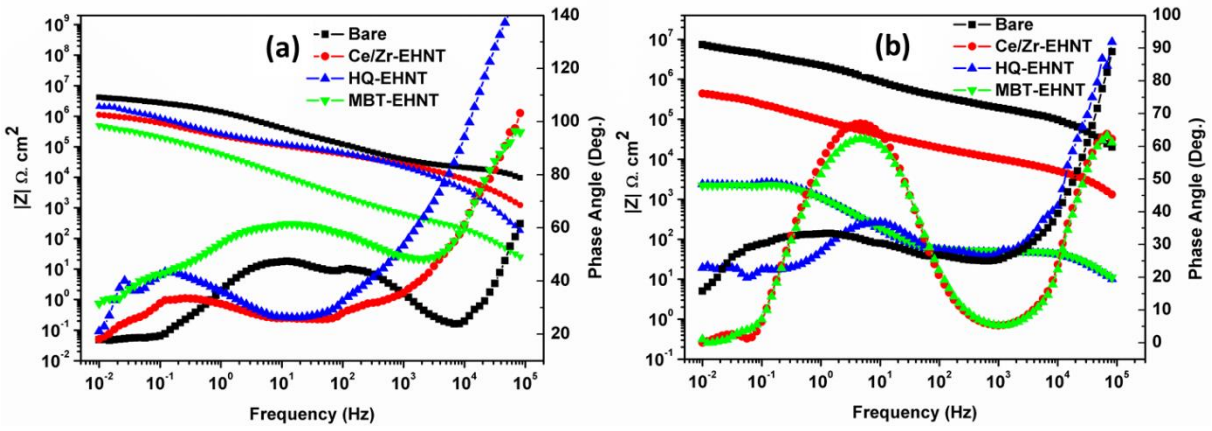

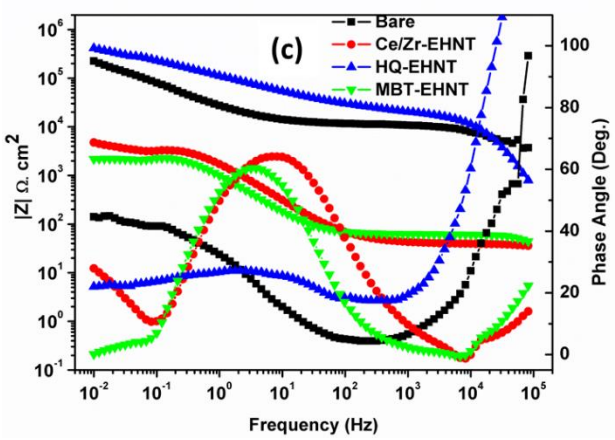

Figure 5.13: Bode plots for bare and different corrosion inhibitor loaded EHNT based sols coated AZ91D substrates after (a) 24 h, (b) 72 h and (c) 120 h of exposure to 0.6 M NaCl solution

In case of EIS studies, best suited electrical equivalent circuit was preferred for analysing the impedance data of coated and bare substrates as depicted in Fig. 5.14.

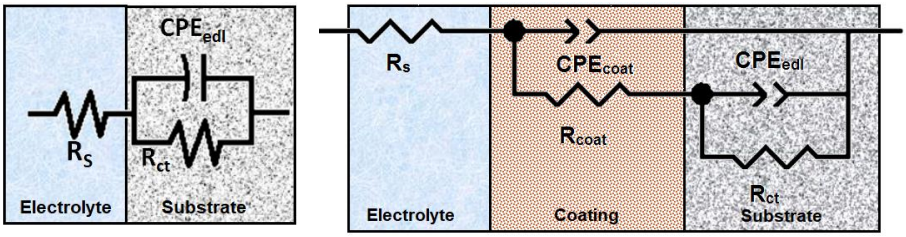

(a) (b)

Figure 5.14: Equivalent electric circuits used to fit EIS data of (a) bare and (b) coated substrates

In case of bare substrates (Fig. 5.14a), very thin porous oxide/hydroxide film is formed after exposure to corrosive medium which provides negligible corrosion resistance. Further, this thin film was removed during pretreatment of substrates. Hence, the results were fitted with one-time constant circuit for bare substrates where, the charge transfer resistance (R_{ct}) is in parallel with electrical double layer capacitance (CPE_{edl}) which is in series with solution resistance. For coated substrates, two-time constant circuit was used in which the charge transfer resistance (R_{ct}) is in parallel with electrical double layer capacitance (CPE_{edl}) which is in series with coating resistance (R_{coat}) with C_{coat} corresponding to coating capacitance. Here, constant phase element is preferred over pure capacitor as the Nyquist plots are deviating from ideal semi-circle behaviour. This non-ideal frequency response could be associated with the inhomogeneity of the surface of metal originating from interfacial phenomena or surface roughness. The magnitude of pseudo capacitance was evaluated using following expression:

$$C = (Q_0 \times R)^{(1 \div n)} (1 \div R) \quad (1)$$

Where, C is pseudo capacitance in F/cm^2; Q_0 is Constant Phase Element in S-sec^n/cm^2; n is frequency factor and R is resistance in **Ω**.

Table 5.5: EIS fit data for bare and different corrosion inhibitor loaded EHNT based sol coated AZ91D substrates after exposure to 0.6 M NaCl solution

Sl. No.	Exposure Time	Substrate	R_s Ω.cm^2	R_{coat} Ω.cm^2	R_{ct} Ω.cm^2	C_{coat}/ CPE F/cm^2	C_{edl}/CPE F/cm^2	χ^2
01	24 h	Bare	291.5	-	3.7E6	-	1.5E-8	0.001
		Ce-Zr-EHNT	294.3	1.9E4	2.9E6	1.6E-10	2.3E-5	0.0074
		HQ-EHNT	100	4.3E4	3.7E6	4.4E-10	5.4E-7	0.069
		MBT-EHNT	207.6	351.5	7.0E5	6.5E-9	1.0E-6	0.0087
02	72 h	Bare	632.4	-	1. 5E7	-	5.6E-8	0.0037
		Ce-Zr-EHNT	143.1	4849	2.8E6	1.4E-10	2.6E-5	0.0029
		HQ-EHNT	264.6	46.58	2409	2E-8	1.0E-5	0.0089
		MBT-EHNT	312.0	47.15	2505	1.8E-8	1.3E-5	0.0012
03	120 h	Bare	731.6	-	1.8E5	-	2.2E-6	0.0016
		Ce-Zr-EHNT	40.1	3585	1.6E4	8.1E-6	9.6E-4	0.0053
		HQ-EHNT	124.6	1.8E4	8. 7E5	1.2E-10	3.2E-6	0.043
		MBT-EHNT	295.1	32.27	2.5E3	6. 8E-9	1.5E-5	0.001

Tafel plots obtained from potentiodynamic polarization studies for uncoated and ;different corrosion inhibitor loaded HNT and EHNT based sol coated AZ91D substrates exposed to 0.6 M NaCl solution for different durations are shown in Fig. 5.15 and Fig. 5.16, respectively. The corrosion currents and corrosion potentials obtained by Tafel extrapolation method are shown in Tables 5.6 and 5.7.

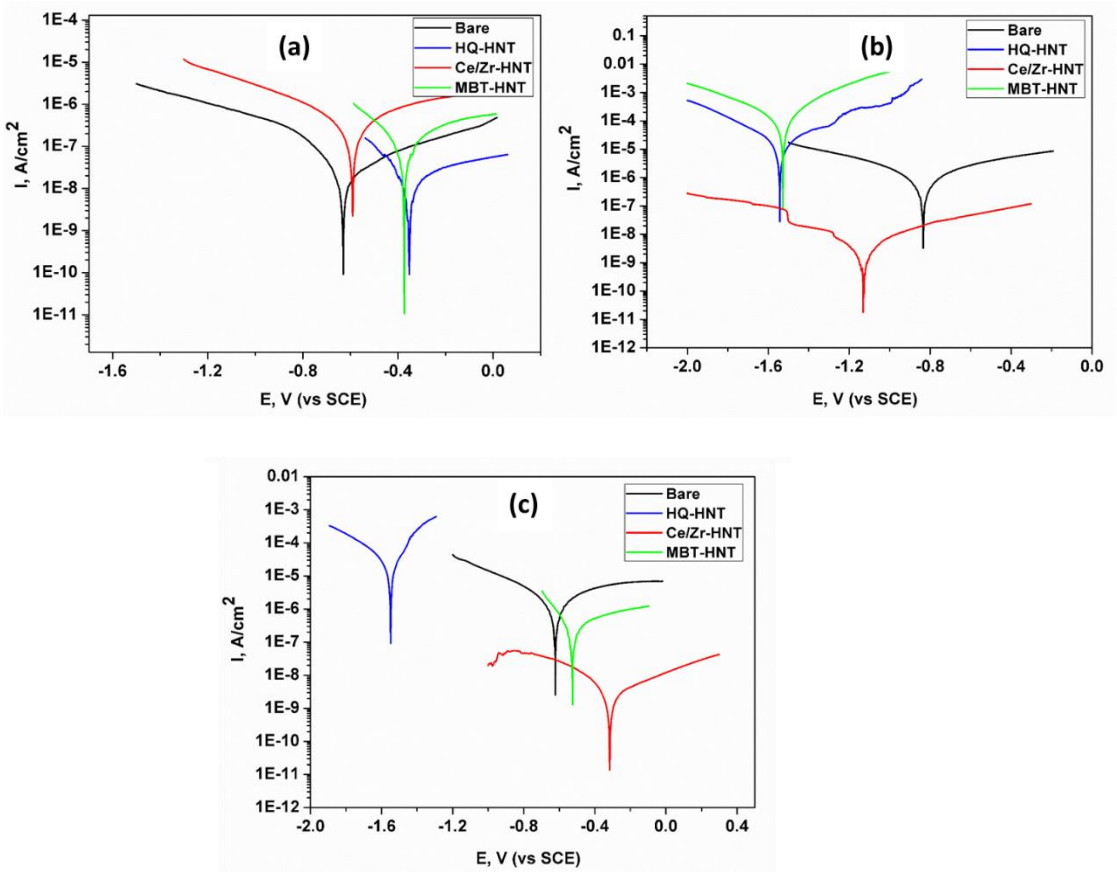

Figure 5.15: Polarization curves for bare and different corrosion inhibitor loaded HNT based sols coated AZ91D substrates after exposure to 0.6 M NaCl solution

The lower corrosion current of bare substrates after 24 h of exposure could be referred to the generation of MgO and Mg $(OH)_2$ films that provide corrosion protection for shorter durations. Further, with prolonged exposure these layers gets depleted and do not provide barrier properties anymore. HQ based coatings showed least corrosion current owing to the formation of complex chelate of MgQ_2. The drastic increase in the corrosion current was observed with the depletion of barrier properties of this complex after longer durations of exposure, which could indicate that higher concentrations of HQ may be required to inhibit the corrosion process. This could be observed when HQ was loaded into EHNT, where coatings have shown least corrosion current after 120 h of exposure. Ce^{3+}-Zr^{4+} based coatings showed sudden decrement in the corrosion current values after 72 h of exposure

with 24 h exposure showing higher corrosion current values. This could reveal that the release of Ce^{3+}-Zr^{4+} from HNTs has provided effective corrosion protection with the increase in exposure durations. When higher amount of Ce^{3+}-Zr^{4+} is loaded in EHNT, it is expected to give higher corrosion protection. However, the coatings have shown better anticorrosion properties (lower corrosion current) only up to 24 h of exposure and then the corrosion current gets increased with increase in exposure durations due to depletion of porous film of oxides of corrosion inhibitor. In case of MBT based coatings, the corrosion current was lower after 24 h of exposure current due to adsorption of inhibiting species on the substrate surface. Further, with the depletion of these barrier properties after 72 h, the corrosion current decreases with prolonged exposure of 120 h owing to the release of inhibitor from HNTs. However, loading higher amount of MBT in EHNTs has shown detrimental effect on anticorrosion properties and the protection was on the lower side during all durations of exposure.

Table 5.6: Tafel fitting parameters for bare and different corrosion inhibitor loaded HNT based sols coated AZ91D substrates

Sl. No.	Exposure Time	Substrate	E_{corr}, V (vs SCE)	I_{corr}, A/cm^2	R_p Ω.cm^2
01	24 h	**Bare**	-0.613	2.3E-8	1.9E6
		Ce-Zr-HNT	-0.590	2.0E-7	2.1E5
		HQ-HNT	-0.352	1.6E-8	2.9E6
		MBT-HNT	-0.373	9.4E-8	4.4E5
02	72 h	**Bare**	-0.834	5.2E-7	8.2E4
		Ce-Zr-HNT	-1.131	2.5E-9	1.6E7
		HQ-HNT	-1.543	1.5E-5	3.1E3
		MBT-HNT	-1.527	7.4E-5	5.1E4
03	120 h	**Bare**	-0.662	1.0E-6	1.1E5
		Ce-Zr-HNT	-0.316	2.7E-9	1.8E7
		HQ-HNT	-1.549	1.6E-5	1.7E3

		MBT-HNT	-0.525	2.7E-7	1.5E5

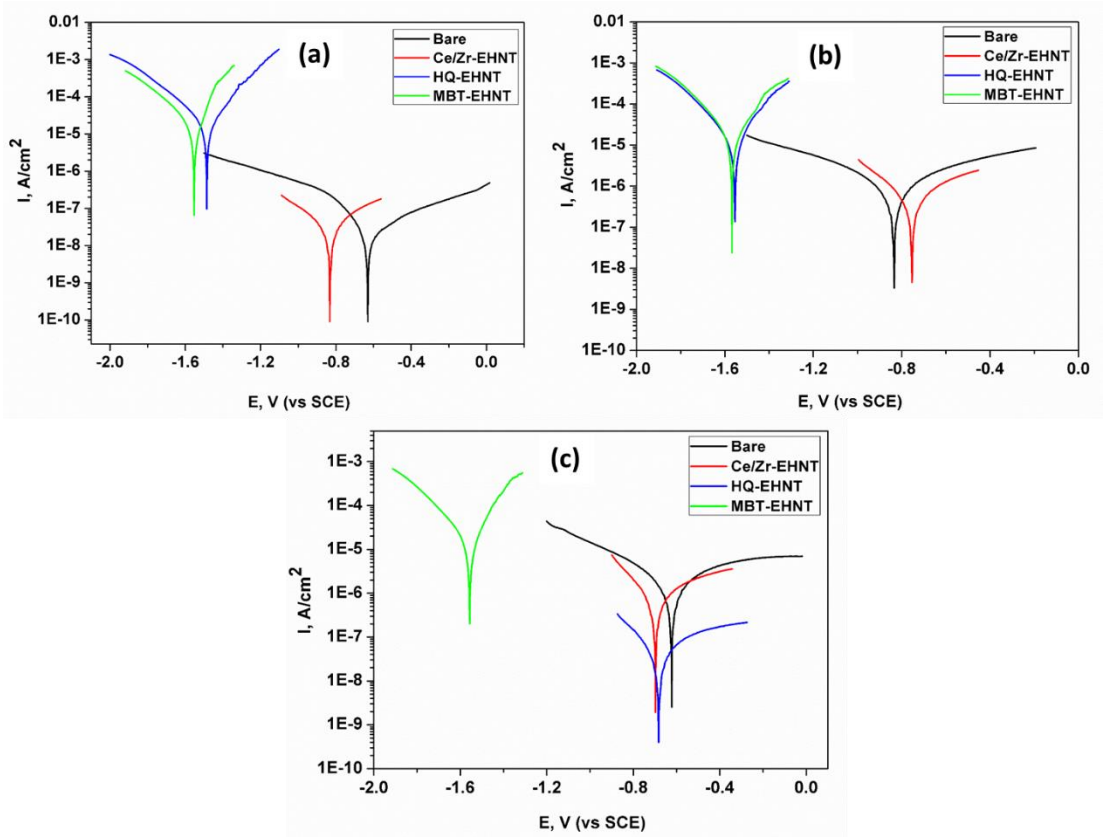

Figure 5.16: Polarization curves for bare and different corrosion inhibitor loaded EHNT based sols coated AZ91D substrates after exposure to 0.6 M NaCl solution

Table 5.7: Tafel fitting parameters for bare and different corrosion inhibitor loaded EHNT based sols coated AZ91D substrates

Sl. No.	**Exposure Time**	**Substrate**	**E_{corr}, V (vs SCE)**	**I_{corr}, A/cm^2**	**R_p Ω.cm^2**
01	**24 h**	**Bare**	-0.613	2.3E-8	1.9E6
		Ce-Zr-EHNT	-0.833	2.7E-8	1.6E6
		HQ-EHNT	-1.486	1.8E-5	2.0E3
		MBT-EHNT	-1.553	9.1E-6	5.1E5
02	**72 h**	**Bare**	-0.834	5.2E-7	8.2E4
		Ce-Zr-EHNT	-0.753	4.2E-7	9.9E4

		HQ-EHNT	-1.554	1.1E-5	2.8E3
		MBT-EHNT	-1.568	1.5E-5	2.1E3
03	**120 h**	**Bare**	-0.662	1.0E-6	1.1E5
		Ce-Zr-EHNT	-0.611	5.5E-6	7.6E4
		HQ-EHNT	-0.682	3.7E-8	1.1E6
		MBT-EHNT	-1.556	1.2E-5	2.3E3

TEM analysis has shown that the acid treatment resulted in the increased lumen diameter of HNT without disturbing the crystal structure. The loading of different corrosion inhibitors like Ce^{3+}-Zr^{4+}, HQ and MBT into lumen of HNTs and EHNTs was confirmed using SEM-EDS and BET analyses. The release studies of these inhibitors were carried out at different pH values in 0.6 M NaCl solution in order to simulate actual release of corrosion inhibitor, when localised change in pH takes place after the initialization of corrosion process. Ce^{3+}-Zr^{4+} has shown higher release under neutral pH conditions which are similar to that of 0.6 M NaCl solution, whereas HQ and MBT have shown higher release under acidic and alkaline conditions respectively. The corrosion protection ability of different corrosion inhibitors was evaluated by using EIS and polarization measurements in 0.6 M NaCl solution for different durations of exposure. It was observed that, Ce^{3+}-Zr^{4+} and HQ have shown better corrosion protection after 120 h of exposure when loaded in HNTs and EHNTs, respectively.

5.5 References

[1] S. V. Lamaka, B. Vaghefinazari, Di Mei, R. P. Petrauskas, D. Höche, M. L. Zheludkevich, Comprehensive screening of Mg corrosion inhibitors, Corros, Sci. 128 (2017) 224-240.

[2] Saviour A. Umoren, Moses M. Solomon, A. Madhankumar, Ime B. Obot, Exploration of natural polymers for use as green corrosion inhibitors for AZ31 magnesium alloy in saline environment, Carbohydr. Polym. 230 (2020) 115466.

[3] Dan Liu, Yingwei Song, Dayong Shan, En-Hou Han, Comparison of inhibition effect of four inhibitors on the corrosion behaviour of AM60 magnesium alloy, Int. J. Electrochem. Sci. 13 (2018) 2219-2235.

[4] I. A. Kartsonakis, S. G. Stanciu, A. A. Matei, E. K. Karaxi, R. Hristu, A. Karantonis, C. A. Charitidis, Evaluation of the protective ability of typical corrosion inhibitors for magnesium alloys towards the Mg ZK30 variant, Corros. Sci. 100 (2015) 194-208.

[5] Habib Ashassi-Sorkhabi, Saleh Moradi-Alavian, Mehdi D. Esrafili, Amir Kazempour, Hybrid sol-gel coatings based on silanes-amino acids for corrosion protection of AZ91 magnesium alloy: Electrochemical and DFT insights, Prog. Org. Coat. 131 (2019) 191-202.

[6] Habib Ashassi-Sorkhabi, Saleh Moradi-Alavian, Amir Kazempour, Salt-nanoparticle systems incorporated into sol-gel coatings for corrosion protection of AZ91 magnesium alloy, Prog. Org. Coat. 135 (2019) 475-482.

[7] H. Gao, Q. Li, Y. Dai, F. Luo, H. X. Zhang, High efficiency corrosion inhibitor 8-hydroxyquinoline and its synergistic effect with sodium dodecylbenzenesulphonate on AZ91D magnesium alloy, Corros. Sci. 52 (2010) 1603-1609.

[8] M. A. Ashraf, Z. Liu, W. X. Peng, N. Yoysefi, Amino acid and TiO2 nanoparticles mixture inserted into sol-gel coatings: An efficient corrosion protection system for AZ91 magnesium alloy, Prog. Org. Coat. 136 (2019) 105296.

[9] Jialing Chen, Liang Fang, Fang Wu, Jiao Xie, Jia Hu, Bin Jiang, Haijun Luo, Corrosion resistance of a self-healing rose-like MgAl-LDH coating intercalated with aspartic acid on AZ31 Mg alloy, Prog. Org. Coat. 136 (2019) 105234.

[10] Kun Qian, Weizhou Li, Xiaopeng Lu, Xinxin Han, Yong Jin, Tao Zhang, Fuhui Wang, Effect of phosphate-based sealing treatment on the corrosion performance of a PEO coated AZ91D Mg alloy, J. Magnesium Alloys 8 (2020) 1328-1340.

[11] Hanaa Soliman, Junyu Qian, Shuai Tang, Peng Xian, Yingqi Chen, Abdel-Salam Makhlouf, Guojiang Wan, Hydroxyquinoline/nano-graphene oxide composite coating of self-healing functionality on treated Mg alloy AZ31, Surf. Coat. Technol. 385 (2020) 125395.

[12] Dashuai Yan, Yanli Wang, Jialing Liu, Dalei Song, Tao Zhang, Jingyuan Liu, Fei He, Meng Zhang, Jun Wang, Self-healing system adapted to different pH environments for active corrosion protection of magnesium alloy, J. Alloys. Compd. 824 (2020) 153918.

[13] Xiang Liu, Huaqiang He, Tian C. Zhang, Like Ouyang, Yu-Xin Zhang, Shaojun Yuan, Superhydrophobic and self-healing dual-function coatings based on mercaptabenzimidazole inhibitor-loaded magnesium silicate nanotubes for corrosion protection of AZ31B magnesium alloys, Chem. Eng. J. 404 (2021) 127106.

[14] Dongdong Zhang, Feng Peng, Xuanyong Liu, Protection of magnesium alloys: From physical barrier coatings to smart self-healing coating, J. Alloys. Compd. 853 (2021) 157010.

[15] E. Joussein, S. Petit, J. Churchman, B. Theng, D. Righi, B. Delvaux, Halloysite clay minerals- a review, Clay Miner. 40 (2005) 383-426.

[16] Elshad Abdullayev, Anupam Joshi, Wenbo Wei, Yafei Zhao, Yuri Lvov, Enlargement of halloysite clay nanotube lumen by selective etching of aluminum oxide, ACS Nano 6 (8) (2012) 7216-7226.

[17] D. Yu, J. Wang, W. Hu, R. Guo, Preparation and controlled release behaviour of halloysite/2-mercaptobenzothiazole nanocomposite with calcined halloysite as nanocontainer, Mater. Des. 129 (2017) 103-110.

[18] Chundong Dong, Manxin Zhang, Tengfei Xiang, Ling Yang, Wenming Chan, and Cheng Li, Novel self-healing anticorrosion coating based on L-valine and MBT-loaded halloysite nanotubes, J. Mater. Sci. 53 (2018) 7793-7808.

[19] Xuteng Xing, Xiaoyang Xu, Jihui Wang, Wenbin Hu, Preparation, release and anticorrosion behavior of a multi-corrosion inhibitors-halloysite nanocomposite, Chem. Phys. Lett. 718 (2019) 69-73.

[20] D. Suvakanta, P. Murthy, L. Nath, P. Chowdhury, Kinetic modeling on drug release from controlled drug delivery systems, Acta Pol. Pharm. Drug Res. 67 (2010) 217–223.

[21] B. A. Bhanvase, M. A. Patel, S. H. Sonawane, Kinetic properties of layer-by-layer assembled cerium zinc molybdate nanocontainers during corrosion inhibition, Corros. Sci. 88 (2014) 170-177.

[22] Megha Tyagi, Bharat A. Bhanvase, Shekhar L. Pandharipande, Computational studies on release of corrosion inhibitor from layer-by-layer assembled silica nanocontainer, Ind. Eng. Chem. Res. 53 (2014) 9764-9771.

[23] Ao-Bo Zhang, Li Pan, Hai-Yan Zhang, Shu-Ting Liu, Ying Ye, Mei-Sheng Xia, Xue-Gang Chen, Effects of acid treatment on the physico-chemical and pore characteristics of halloysite, Colloids Surf., A 396 (2012) 182-188.

[24] A. Joshi, E. Abdullayev, A. Vasiliev, O. Volkova, Y. Lvov, Interfacial modification of clay nanotubes for the sustained release of corrosion inhibitors, Langmuir 29 (2013) 7439–7448.

[25] R. Yendluri, Y. Lvov, M. M. de Villiers, V. Vinokurov, E. Naumenko, E. Tarasova, R. Fakhrullin, Paclitaxel encapsulated in halloysite clay nanotubes for intestinal and intracellular delivery, J. Pharm. Sci. 106 (2017) 3131–3139.

[26] Mei Wang, Jihui Wang, Wenbin Hu, Preparation and corrosion behaviour of Cu-8-HQ@HNTs/epoxy coating, Prog. Org. Coat. 139 (2020) 105434.

[27] D. Suvakanta, P. Murthy, L. Nath, P. Chowdhury, Kinetic modeling on drug release from controlled drug delivery systems, Acta Pol. Pharm. Drug Res. 67 (2010) 217–223.

[28] Shangyi Shen, Yu Zuo, Xuhui Zhao, The effects of 8-hydroxyquinoline on corrosion performance of a Mg-rich coating on AZ91D magnesium alloy, Corros. Sci. 76 (2013) 275-283.

[29] Qiufeng Zong, Lida Wang, Wen Sun, Guichang Liu, Active deposition of bis (8-hydroxyquinoline) magnesium coating for enhanced corrosion resistance of AZ91D alloy, Corros. Sci. 89 (2014) 127-136.

[30] E. Roussi, A. Tsetsekou, A. Skarmoutsou, C.A. Charitidis, A. Karantonis, Anticorrosion and nanomechanical performance of hybrid organo-silicate coatings integrating corrosion inhibitors, Surf. Coat. Technol. 232 (2013) 131-141.

Chapter 6

EVALUATION OF EFFECT OF COATING TECHNIQUE ON ANTICORROSION PROPERTIES

Chapter-6

Evaluation of effect of coating technique on anticorrosion properties

6.1 Introduction

There are several reports on the development of self-healing coatings on Mg alloys [1-4] and it was observed from the literature search that, dip coating technique has been widely used for coating deposition, since uniform coatings on complex shaped components can also be generated efficiently by adjusting the thickness using varying withdrawal speeds. Hence, our earlier studies of generation of coatings based on different corrosion inhibitor loaded halloysite nanotubes and Ce^{3+}-Zr^{4+} intercalated montmorillonite nanoclay were carried out with dip coating technique. However, different components in automobile and aerospace industries have different requirement of finishing touch, which could not be obtained by dip coating alone. Another most commonly and commercially used coating technique is spray coating. Spray coating uses an atomized cloud or spray of the coating material and compressed air to evenly coat the surfaces. In terms of actual application of the coatings to components on industrial scale, spray coating would be an appropriate coating deposition method having an ability to give high quality finishes for large components. However, dip coating and spray coating techniques have their own distinct differences in terms of appearance and performance. Very few studies were carried out earlier for comparison of dip and spray coating techniques, which are discussed below.

Covalo et al. [5] have compared corrosion protection ability of hybrid sol-gel coatings developed using dip, spin coating and brush, spray painting techniques on aluminum alloy AA2024. Scanning electron microscope (SEM) and Atomic force microscope (AFM) analyses showed that spin coating generated more homogeneous coatings than dip coating technique. EIS studies in 0.1 M NaCl solution for 240 h revealed that coatings with spin coating technique have shown higher corrosion resistance than the coatings with other techniques due to low degree of porosity and better adhesion strength. A double layered sol-gel coating was prepared by Hwang et al. [6] by using both spray and dip coating technique on SS 304 substrates. Here, spray coated layer having rough and cracked morphology was further covered with a dip coated layer to obtain homogeneous and crack-free surface as observed from SEM and AFM analyses. Electrochemical measurements showed that the double layered coating provided better corrosion protection as compared to that of only the spray coated layer owing to the reduced diffusion pathways of corrosive

medium through the coating. Garcia et al. [7] developed Si/Zr sol-gel coating on Al alloy AA2024 using single layer; multilayer dip coating and spray coating techniques and compared the corrosion protection ability of coatings using polarization studies. They observed that spray coated substrates showed 57 % polarization resistance as that of 27 % and 14 % for multilayer and single layer dip coatings due to less generation of defects after solvent evaporation. Tan et al. [8] generated anodized layer on Mg alloy AZ91D followed by deposition of single and double sol-gel layers using spray coating technique with number of spray passes. Electrochemical studies have revealed that the barrier properties of coatings got enhanced with the increased number of layers and passes due to elimination of diffusion pathways of corrosive medium. Wei et al. [9] generated epoxy coatings on AZ31B substrates using spray coating technique followed by deposition of hydroxydecyl silane or perfluorodecyl silane. The contact angle and sliding angle studies have shown that bilayer coating exhibited better superhydrophobicity which remained intact even after 70 days of immersion test and 35 days of neutral salt spray test. Due to reduced contact between corrosive medium and substrate, the coatings could effectively provide long lasting corrosion protection to AZ31B. Zhao et al. [10] deposited polyethyleneimine solution on AZ31 substrates by spin coating followed by spin-spray layer-by-layer assembly of silica and ceria nanoparticles. Electrochemical studies and hydrogen evolution rates have revealed that coated substrates showed much lower corrosion current density and lower hydrogen evolution as compared to bare substrates due to barrier properties of silica and inhibitory action of ceria nanoparticles. Rosero-Navarro et al. [11] generated cerium-based coatings synthesized form alcoholic sol-gel sols on aluminum (AA2024 and AA3105) and magnesium alloys (AZ31 and AZ91) by dip coating and spray coating. Electrochemical studies (196 h for both Al and Mg alloys) and salt spray tests (312 h for Mg alloys and 960 h for Al alloys) have shown that cerium based coating systems were more promising owing to the inhibition ability showed by cerium species. Number of articles are available [12-14], where spray coating has been used for developing coatings with different functionalities. However, to the best of our knowledge, there are no studies reported for development of self-healing coatings based on sol-gel process on Mg alloys using spray coating technique and its comparison with dip coating technique.

In our earlier investigations, only dip coating has been employed to generate the coatings. Hence, it would be highly appropriate to compare and evaluate the performance of dip coated and spray coated samples with respect to their corrosion resistance, keeping in mind the feasibility of using these coatings for industrial applicability. Moreover, in all

our previous experiments, the anticorrosion properties of the dip coated AZ91D substrates were evaluated only by electrochemical experiments such as potentiodynamic polarization and electrochemical impedance spectroscopic (EIS) analysis using aqueous corrosive medium and not using accelerated tests. Therefore, in this chapter, in order to evaluate the effect of coating techniques, the matrix (MAT) sol, clay matrix (CM) sol and Ce^{3+}-Zr^{4+} loaded HNT based coatings generated by dip coating technique were compared with the ones generated by spray coating technique and were evaluated for their long term corrosion protection ability by employing accelerated tests like neutral salt spray test. Further, coatings generated with dip coating technique was having thickness similar to that generated by spray coating technique and properties compared for Ce^{3+}-Zr^{4+} loaded HNT based coatings.

6.2 Materials and Methods

6.2.1 Synthesis of sols

Synthesis of hybrid matrix sol and CM sol, synthesis of polymeric microcapsules and loading of corrosion inhibitors, Ce^{3+}-Zr^{4+} in HNT were carried out as mentioned in section 3.2 of chapter 3. The polymeric microcapsules and 2 wt % of inhibitor loaded HNTs and EHNTs were dispersed in hybrid matrix sol to prepare the self-healing sol.

6.2.2 Generation of coatings with spray coating and multilayer dip coating technique

The substrate preparation was carried out as mentioned in section 3.2 of chapter 3. Coatings were generated by using spray coating technique with spray gun (DeVilbiss SRiPro TS1-08, Scottsdale, US) having orifice diameter of 0.8 mm at a pressure of 2.5 bar and a distance of 200 mm. 3 layers of dip coating deposition at 1 mm/s withdrawal speed was carried out to generate the coatings with thickness equivalent to that of spray coating. The coatings on AZ91D substrates were cured by heat treatment in hot air oven at 130 ^{o}C for 1 h.

6.3 Characterization Techniques

6.3.1 Coating characterization

The surface morphology of both spray and multilayer dip coated substrates was observed by using scanning electron microscope (SEM- Hitachi S3400N). The thickness of coatings (spray and multilayer dip coated) as measured using Eddy Current PosiTector® (DelFelsko Corporation, USA) was found to be around 14-20 µm and confirmed using by

SEM cross-sectional analysis. The corrosion protection ability of coatings based on HNT encapsulated with different corrosion inhibitors was evaluated by using electrochemical measurements such as EIS and potentiodynamic polarization as mentioned in section 3.3 of chapter 3.

6.3.2 Salt Spray tests (SST)

Salt spray tests were performed on bare and coated substrates according to ASTM B117 standard in NaCl solution of 0.85 M concentration for 168 h at 35 ℃. In order to check the consistency, two substrates for each corrosion inhibitor based coating were taken into the consideration. The edges and back surface of the substrates were covered by using a transparent adhesive tape. The substrates were vertically placed into the sample holder at an angle of 15^0 as shown in Fig. 6.1. After removal from the chamber, the coupons were rinsed with deionized water, dried and examined within 30 mins.

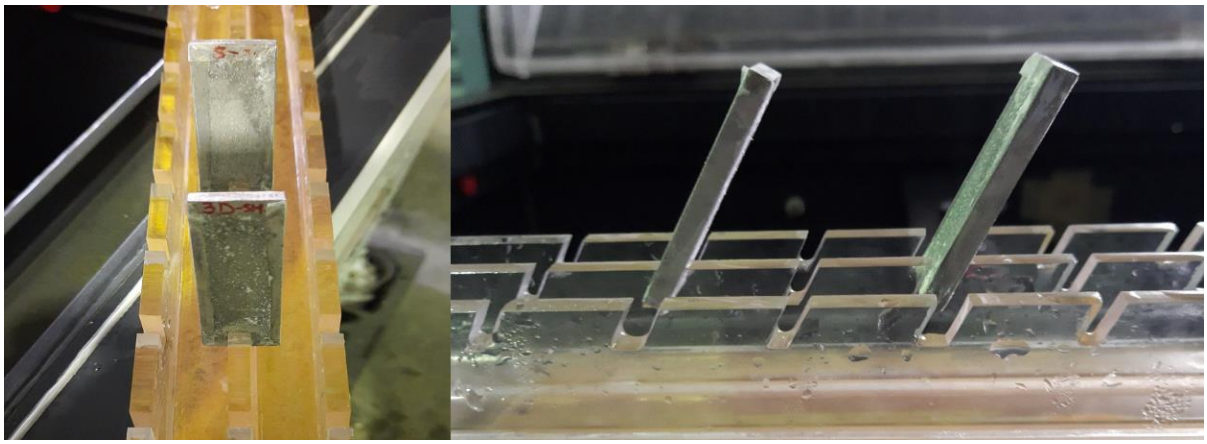

Figure 6.1: Arrangement of substrates with sample holder for SST

6.4 Results and Discussion

6.4.1 Morphology and thickness of coatings

Morphology of Ce^{3+}-Zr^{4+} loaded HNT based coatings generated by spray coating and multilayer dip coating technique was observed by SEM as shown in Fig. 6.2 (a) and (b). Spray coated substrates were observed to have random and agglomerated distribution of microcapsule capped HNTs, whereas in case of dip coated substrates capped HNTs were uniformly distributed all over the coated area with less agglomerates. The thickness of spray and multilayer dip coatings was found to be around 14 to 20 µm as observed from SEM cross sectional analysis is shown in Fig. 6.2 (c) & (d). The cross section of spray coated substrates has shown non-uniform thickness and irregular distribution of coating as compared to that of multilayer dip coated substrate. Elemental analysis obtained from

SEM-EDS analysis revealed the presence of Si, C and O as coating compositions; Al and Si as HNT compositions; and Ce and Zr as corrosion inhibitors loaded in HNT. Higher coating thickness in case of spray coated and 3 layer dip coated can also be verified from the wt % of substrate elements (Mg, Al and Zn) that are less when compared to that of single layer dip coated substrates. Very less difference was observed in the weight % of coating compositions (spray and multilayer dip coating), which could confirm that nearly the same amount of mass has been deposited on substrates, using two different coating techniques. Hence, effect of the coating morphology achieved from the two coating techniques will be the parameter affecting the corrosion resistance.

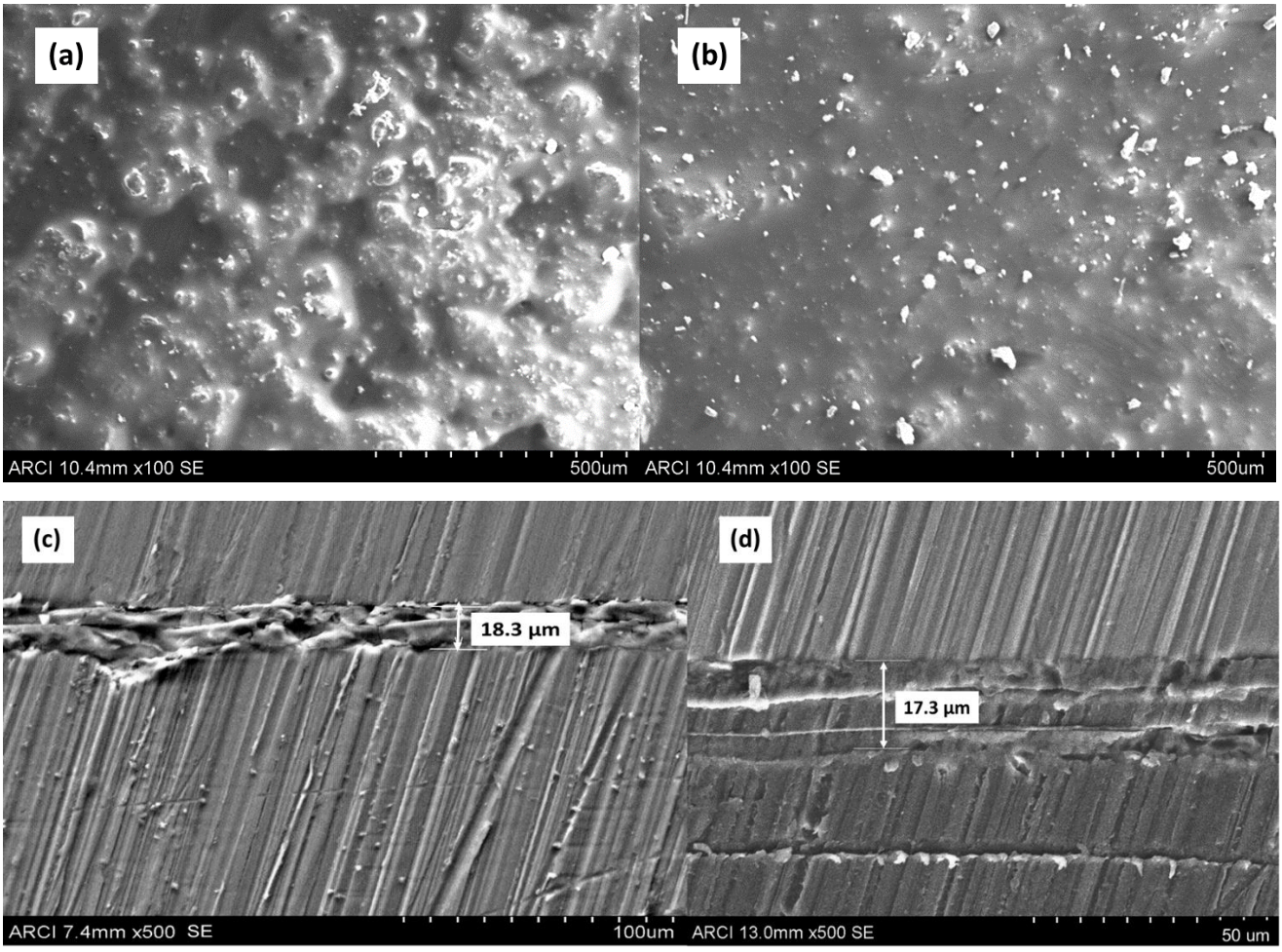

Figure 6.2: Surface morphology (a) & (b) and SEM cross-sectional images (c) & (d) of spray coated and multilayer dip coated AZ91D substrates

Table 6.1: Elemental analysis (wt %) of dip coated, spray coated, 3 layer dip coated and cross sections of spray coating and 3 layer dip coating obtained by SEM-EDS analysis

Elements (Wt %)	Dip Coated substrate	Spray Coated substrate	3 layer dip coated substrate	Cross section of spray coating	Cross section of 3 layer dip coating		
					1	2	3
Mg	53.47	9.89	3.01	-	-	-	-
Al	4.72	1.46	1.26	2.31	1.40	1.23	1.12
Si	5.85	20.98	39.83	33.70	21.93	31.99	24.95
Zn	0.49	0.16	0.25	-	-	-	-
C	26.63	55.02	38.34	32.01	56.95	35.51	46.93
O	8.63	11.78	16.31	29.74	18.68	28.78	25.23
Ce	0.0	0.07	0.08	0.21	0.12	0.06	0.09
Zr	0.21	0.64	0.92	2.03	0.92	2.43	1.68

6.4.2 EIS studies

EIS measurements were performed for evaluation of the anticorrosion properties of spray coated (MAT, CM and Ce^{3+}-Zr^{4+}-HNT) and 3 layer dip coated (Ce^{3+}-Zr^{4+}-HNT) AZ91D samples after exposure to 0.6 M NaCl solution for various durations like 24 h, 72 h and 120 h. Electrochemical measurements were carried out as mentioned in section 3.3 of chapter 3.

The Nyquist plots for single layer dip coated; spray coated and 3 layer dip coated AZ91D substrates exposed to 0.6 M NaCl solution for different durations are depicted in Fig. 6.3 and Fig. 6.4 respectively, whereas the bode plots for spray coated and 3 layer dip coated AZ91D substrates are depicted in Fig. 6.5. The corresponding fit data obtained by using two time constant equivalent electric circuit (Fig. 6.7) are shown in Tables 6.2 and 6.3.

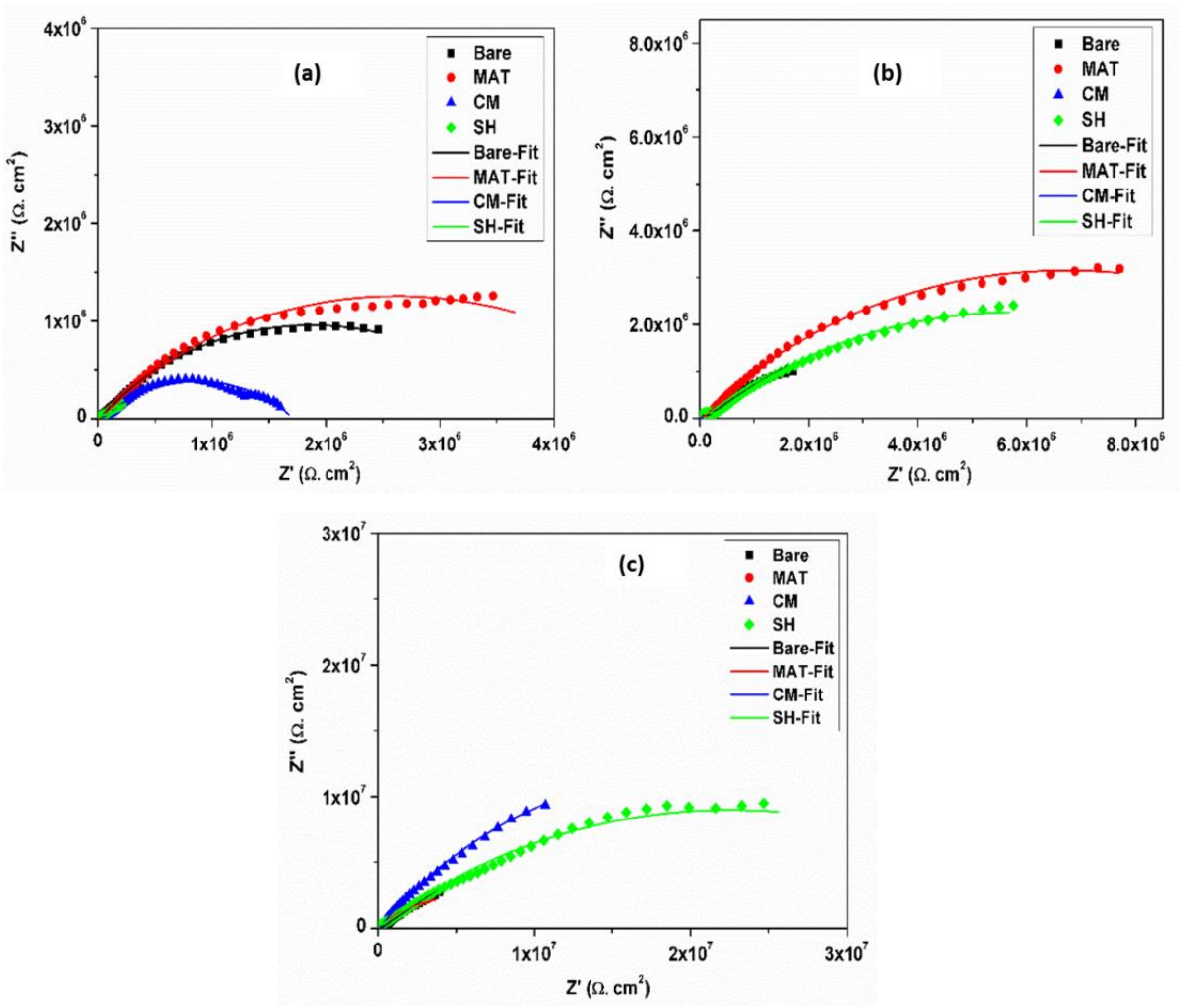

Figure 6.3: Nyquist plots for uncoated and single layer dip coated AZ91D substrates after (a) 24 h, (b) 72 h and (c) 120 h exposure to 0.6 M NaCl solution

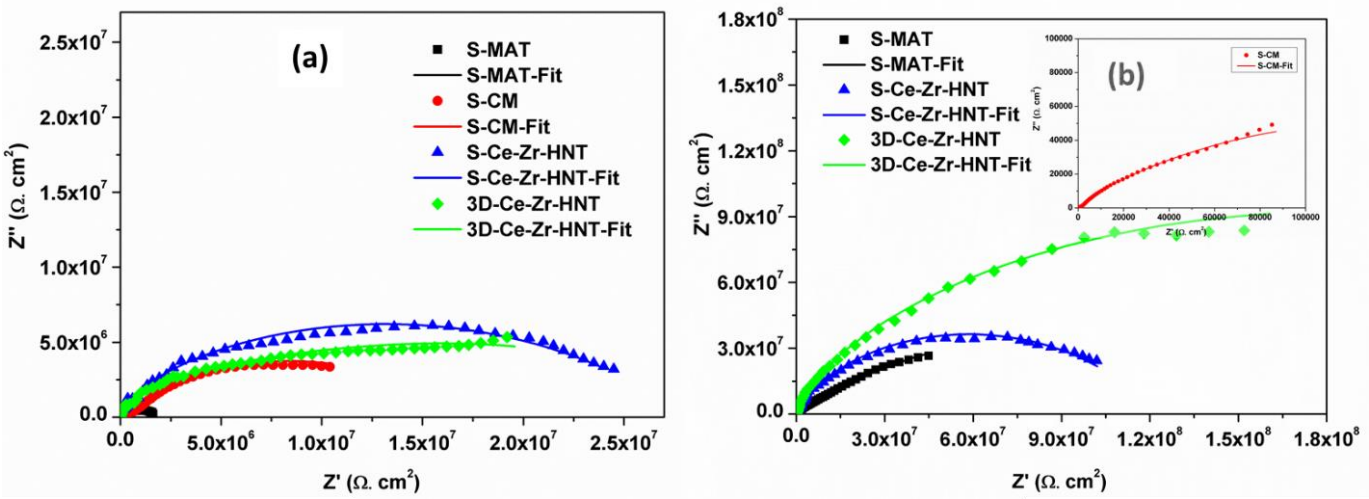

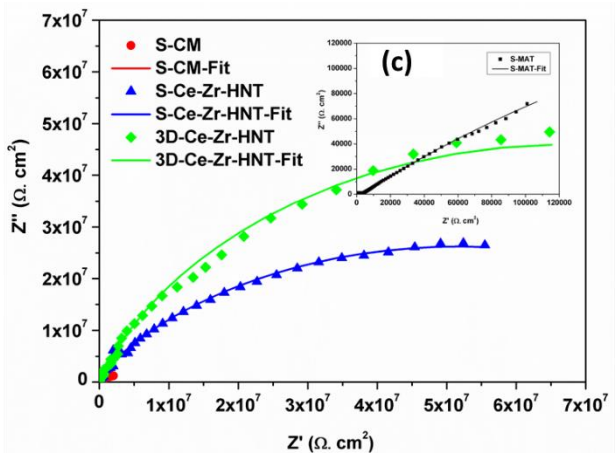

Figure 6.4: Nyquist plots for spray coated and 3 layer dip coated AZ91D substrates after (a) 24 h, (b) 72 h and (c) 120 h of exposure to 0.6 M solution

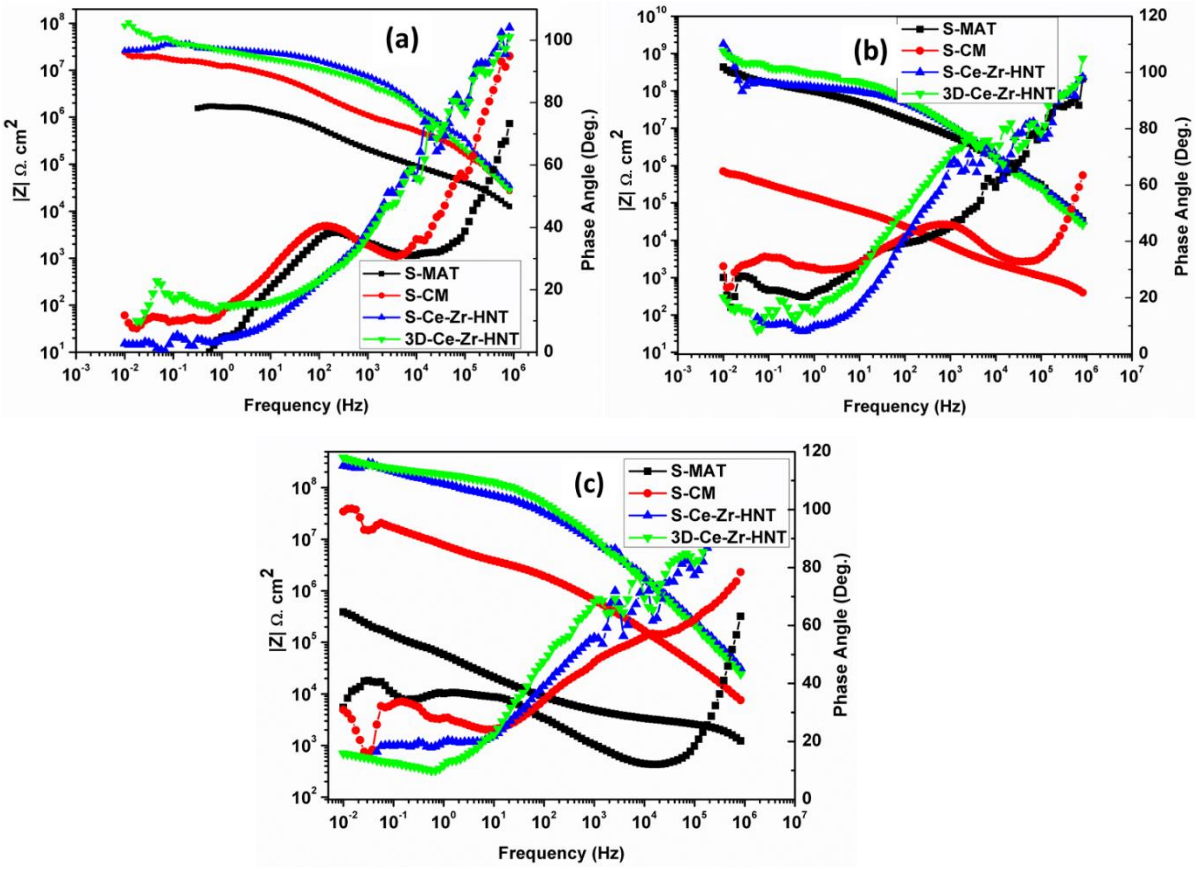

Figure 6.5: Bode plots for spray coated and 3 layer dip coated AZ91D substrates after (a) 24 h, (b) 72 h and (c) 120 h of exposure to 0.6 M solution

As discussed in section 3.4.6 of chapter 3, MAT sol dip coated substrates have shown better barrier properties till 72 h of exposure owing to the strong covalent bond between AZ91D substrate and silane in the coating. However, with the prolonged durations of exposure, the coating gets deteriorated and corrosion protection ability gets decreased. After 24 h of exposure, spray coated MAT sol coatings have shown lower corrosion

resistance as compared to that of dip coated substrates. This could be attributed to the fact that in dip coating technique, coating wets the substrate uniformly, whereas in spray coating technique, the sol droplets are sprayed on the substrate under the influence of compressed air as shown in Fig. 6.6. Hence, in spray coated substrates, there may be some areas where coating has deposited in the form of a very thin film, which gets deteriorated or can be susceptible to corrosion in shorter time span.

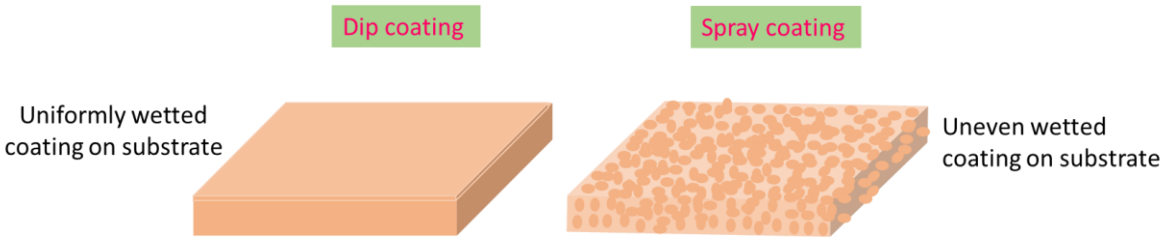

Figure 6.6: Schematic view of dip and spray coated substrates

The corrosion protection ability of MAT sol spray coated substrates increased after 72 h of exposure, thereby indicating that the corrosive medium has penetrated at the coating-substrate interface and formed a thin film of corrosion products which provided short term corrosion protection. Spray coated CM sol based substrates showed similar corrosion resistance behaviour as that of dip coated one. CM sol coated substrates have shown least corrosion resistance after 72 h of exposure due to random distribution of HNTs within coating matrix, as examined by Huttunen-Saarivirta et al. [15].

After 120 h of exposure, the corrosion resistance of CM sol coated substrates was increased, which could be attributed to the formation of corrosion products underneath the coatings due to the diffusion of corrosive medium through porous coatings. Dip coated Ce^{3+}-Zr^{4+} loaded HNT based coatings (self-healing, SH) showed increase in the corrosion resistance with increase in exposure durations due to sustained release of Ce^{3+}-Zr^{4+} as denoted in Table 6.2. In case of spray coated Ce^{3+}-Zr^{4+} loaded HNT based coatings, the corrosion resistance was found to be lower than that of multilayer dip coatings after 24 h, which got increased with prolonged exposure of 120 h as mentioned in Table 6.3. In case of multilayer dip coated substrates, the corrosion resistance was found to increase till 72 h of exposure and then decreased slightly after 120 h. This could be attributed to sealing of pores in each layer by the subsequent layer, thereby providing a good barrier. However, very less difference in the magnitudes of corrosion resistance of spray and multilayer dip coating was observed. These results are further corroborated with salt spray tests.

In case of EIS studies, best suited electrical equivalent circuit was preferred for analysing the impedance data of coated and bare substrates as depicted in Fig. 6.7.

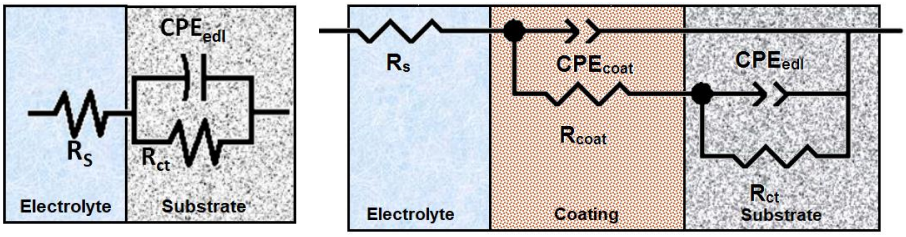

(a) (b)

Figure 6.7: Equivalent electric circuits used to fit EIS data of (a) bare and (b) coated substrates

In case of bare substrates (Fig. 6.7a), very thin porous oxide/hydroxide film is formed after exposure to corrosive medium which provides negligible corrosion resistance. Further, this thin film was removed during pretreatment of substrates. Hence, the results were fitted with one-time constant circuit for bare substrates where, the charge transfer resistance (R_{ct}) is in parallel with electrical double layer capacitance (CPE_{edl}) which is in series with solution resistance. For coated substrates, two-time constant circuit was used in which the charge transfer resistance (R_{ct}) is in parallel with electrical double layer capacitance (CPE_{edl}) which is in series with coating resistance (R_{coat}) with C_{coat} corresponding to coating capacitance. Here, constant phase element is preferred over pure capacitor as the Nyquist plots are deviating from ideal semi-circle behaviour. This non-ideal frequency response could be associated with the inhomogeneity of the surface of metal originating from interfacial phenomena or surface roughness. The magnitude of pseudo capacitance was evaluated using following expression:

$$C = (Q_0 \times R)^{(1\div n)}(1 \div R) \qquad (1)$$

Where, C is pseudo capacitance in F/cm^2; Q_0 is Constant Phase Element in S-sec^n/cm^2; n is frequency factor and R is resistance in **Ω**.

Table 6.2: EIS fit data for bare and single layer dip coated substrates exposed to 0.6 M NaCl solution for various durations

Sl. No.	Exposure Time	Substrate	R_s Ω.cm^2	R_{coat} Ω.cm^2	R_{ct} Ω.cm^2	C_{coat}/ CPE F/cm^2	C_{edl}/CPE F/cm^2	χ^2
01	**24 h**	**Bare**	291.5	-	3.7E6	-	1.5E-8	0.001
		MAT	234.9	2.6E4	5.2E6	1.5E-11	3.5E-8	0.0023
		CM	106	4.3E4	1.7E6	1.4E-11	2.4E-8	0.0072

		SH	159.3	1.3E5	3.2E5	4.1E-6	4.5E-5	0.028
02	**72 h**	**Bare**	632.4	-	1.5E7	-	5.6E-8	0.0037
		MAT	765.6	7.3E4	1.3E7	9.8E-12	7.8E-9	0.0038
		CM	269.3	351.3	7.6E4	5. 7E-10	4.3E-6	0.0012
		SH	230.1	2.0E5	1.1E7	8.3E-12	3.4E-8	0.0038
03	**120 h**	**Bare**	731.6	-	1.9E5	-	2.2E-10	0.0016
		MAT	645.7	4.4E4	9.5E6	2.5E-11	2.3E-7	0.0027
		CM	458.9	7.4E4	4.8E7	9.9E-12	2.1E-8	0.0023
		SH	307.0	3.5E5	4.5E7	7.3E-12	2.7E-9	0.0061

Table 6.3: EIS fit data for spray coated and 3 layer dip coated AZ91D substrates after exposure to 0.6 M NaCl solution

Sl. No.	**Exposure Time**	**Substrate**	**R_s $\Omega.cm^2$**	**R_{coat} $\Omega.cm^2$**	**R_{ct} $\Omega.cm^2$**	**C_{coat}/ CPE F/cm^2**	**C_{edl}/CPE F/cm^2**	χ^2
01	**24 h**	**S-MAT**	63.6	5.4E4	2.0E6	1.8E-11	5.5E-9	0.002
		S-CM	99.9	3.4E5	1.6E7	7.1E-12	1.7E-9	0.005
		S-Ce-Zr-HNT	27.6	1.2E6	2.7E7	5.2E-12	5.2E-11	0.011
		3D-Ce-Zr-HNT	68.7	2.9E5	3.3E7	6.9E-12	4.3E-10	0.0064
02	**72 h**	**S-MAT**	25.1	6.1E5	1.8E8	5.3E-12	9.2E-10	0.004
		S-CM	96.9	8415	2.6E5	1.4E-8	6.5E-9	0.001
		S- Ce-Zr-HNT	38.1	1.1E6	1.2E8	5.5E-12	2.6E-11	0.006

		3D-Ce-Zr-HNT	40.1	1.4E6	4.1E8	8.4E-12	7.7E-11	0.014
03	**120 h**	**S-MAT**	38.1	2654	8.7E5	1.4E-10	8.0E-5	0.001
		S-CM	15.8	1.9E4	4.8E6	2.2E-11	8.2E-10	0.0004
		S-Ce-Zr-HNT	10.1	1.2E6	1.1E8	5.8E-12	7.1E-11	0.01
		3D-Ce-Zr-HNT	45.8	2.3E6	1.4E8	7.3E-12	2.6E-11	0.0069

6.4.3 Salt spray tests

Atmospheric corrosion tests that are usually performed in automobile, aerospace and other metallurgical industries were carried out to evaluate the anticorrosion properties of bare and coated AZ91D substrates, as atmospheric corrosion can lead to serious damage due to rain, fog and dew. SST of bare, dip and spray coated AZ91D substrates was carried out according to ASTM B117 in 0.85 M NaCl solution for 168 h as shown in Fig. 6.8.

After 72 h of exposure, bare substrates were completely covered with the corrosion products. MAT sol and CM sol dip coated substrates were corroded completely after 120 h and hence are not displayed here. MAT sol and CM sol spray coated substrates showed filiform type of corrosion and accumulation of corrosion products due to pitting in some areas of substrate, respectively. Dip coated Ce^{3+}-Zr^{4+} loaded HNT based coatings were observed to have some pits on the surface, where coating might have deteriorated after exposure to corrosive medium for longer durations. In case of spray coated substrates, very few corroded areas were observed after 168 h due to penetration of corrosive medium through micropores developed after solvent evaporation during spray coating. Further, in case of multilayer dip coated substrates, negligible pits were observed and there wasn't any visible accumulation of corrosion product on the surface. Hence, Ce^{3+}-Zr^{4+}-HNT based 3 layer dip coated substrates have shown better anticorrosion properties as compared to single layer dip coated and spray coated substrates from the salt spray tests and EIS measurements.

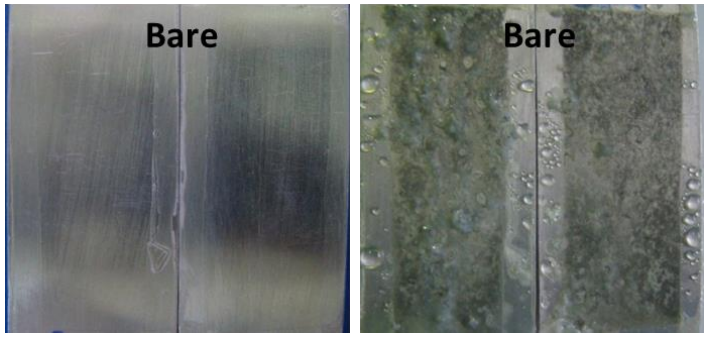

(a)

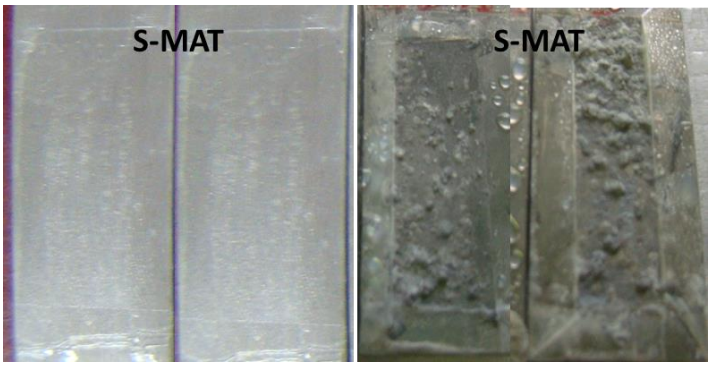

(b)

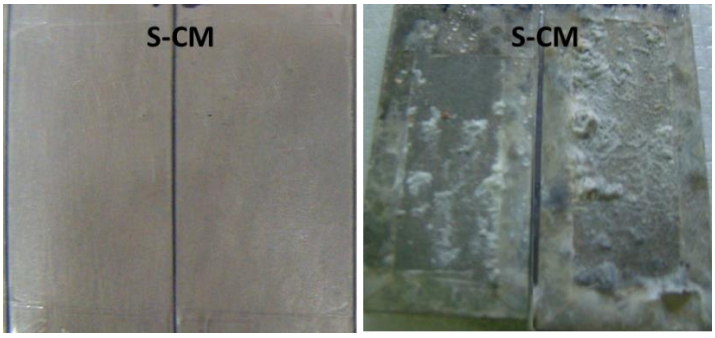

(c)

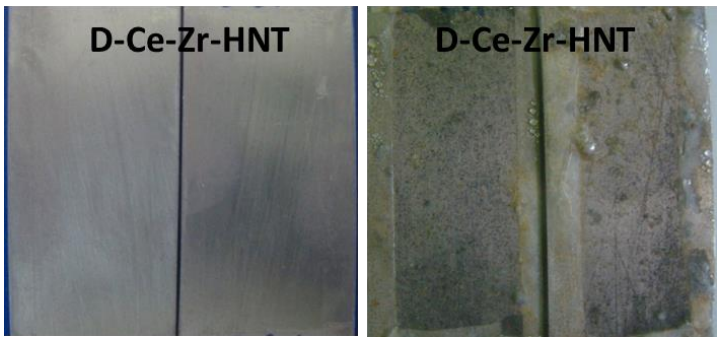

(d)

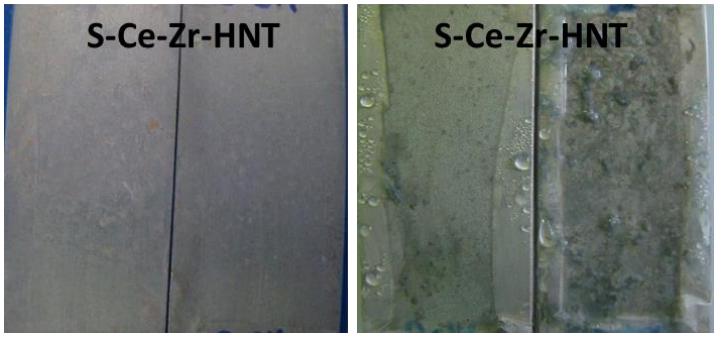

(e)

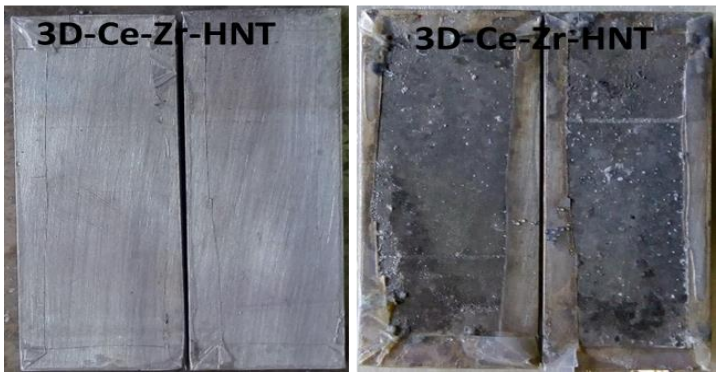

(f)

Figure 6.8: Salt spray images of (a) uncoated, (b) MAT sol spray coated, (c) CM sol spray coated, (d) Ce^{3+}-Zr^{4+} loaded HNT based sol dip coated, (e) Ce^{3+}-Zr^{4+} loaded HNT based sol spray coated and (f) Ce^{3+}-Zr^{4+} loaded HNT based sol 3 layer dip coated AZ91D coupons before and after 168 h of exposure to 0.85 M NaCl solution

Electrochemical studies and accelerated corrosion tests have revealed that, spray coated substrates (MAT and CM sols) have shown better barrier properties as compared to dip coated substrates up to 72 h of exposures, which could be attributed to higher thickness of spray coatings and consequently the barrier properties. In case of Ce^{3+}-Zr^{4+} loaded HNT sol based coatings, single layer dip coated substrates have shown increase in the corrosion resistance with the increase in exposure durations. Spray coated substrates were found to give corrosion protection when corrosive medium diffuses through the micropores and changes the localized pH, thereby leading to release of corrosion inhibitors and then inhibition of corrosion. In case of multilayer dip coated substrates, the micropores of each layer are covered by another layer, so that the corrosive medium cannot penetrate and reach the substrate within shorter durations of exposure.

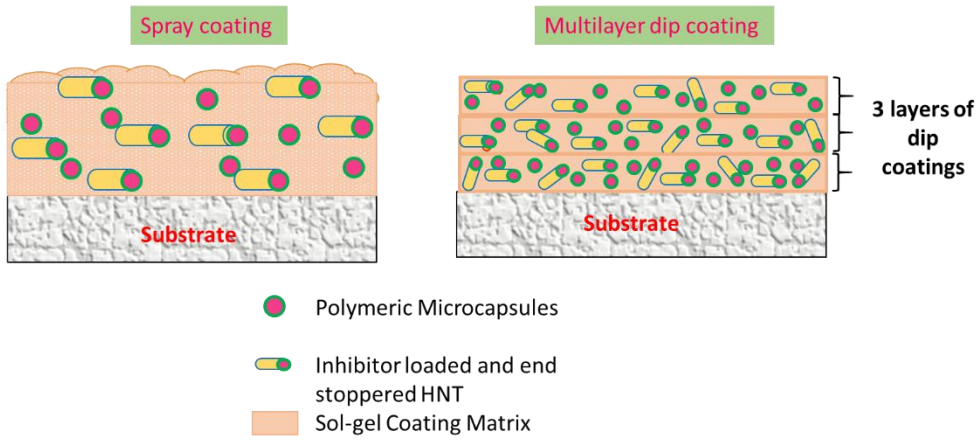

Figure 6.9: Schematic representation of spray coating and multilayer dip coating on AZ91D substrates

This could be elaborated through the schematic representation of spray coating and 3 layer dip coated substrates as depicted in Fig. 6.9. There could be micropores developed after the evaporation of solvent in the coating matrix dispersed with inhibitor loaded HNTs. In case of multilayer dip coated substrates the porosity in one layer could be covered by another one, thereby restricting or reducing the diffusion of corrosive species to the substrate. The spray coated substrates have shown non-uniform surface morphology with some areas having higher thickness (peaks) and some having lower thickness (valleys) along with the micropores. The spray coated substrates could provide some barrier property at the regions having higher thickness for less amount of time. However, when the low thickness region gets exposed to the corrosive medium, the corrosive species penetrates through the micropores and initiates the corrosion. At such areas, the corrosion inhibitor releases from HNTs due to change in localised pH upon corrosion initiation. Hence, it could be concluded that multilayer dip coated substrates could give better corrosion protection as compared to that of spray coated substrates owing to the restricted diffusion of corrosive species through micropores. These coatings are further evaluated for their barrier property when the corrosion is forced to take place by applying the external voltage in polarization studies.

6.4.4 Potentiodynamic polarization measurements

Tafel plots obtained from potentiodynamic polarization studies for single layer dip coated; spray coated and 3 layer dip coated AZ91D after 24 h, 72 h and 120 h of exposure to 0.6 M NaCl solution are shown in Fig. 6.10 and Fig. 6.11 respectively. Lower corrosion current of MAT sol spray coated substrates after 24 h of exposure could be attributed to the

barrier properties of hybrid sol-gel matrix, which gets deteriorated with increase in the exposure durations and showed highest corrosion current after 120 h. Polarization studies of CM sol spray coated substrates have shown similar behaviour as that of EIS studies. The coatings showed lower corrosion current after 24 h of immersion owing to the better barrier properties of coatings. However, due to random distribution of HNTs in the coating matrix, the corrosion current increases after 72 h and because of the formation of corrosion products underneath the coatings as mentioned earlier, the corrosion current decreases after prolonged exposure of 120 h as shown in Tables 6.4 and 6.5. After

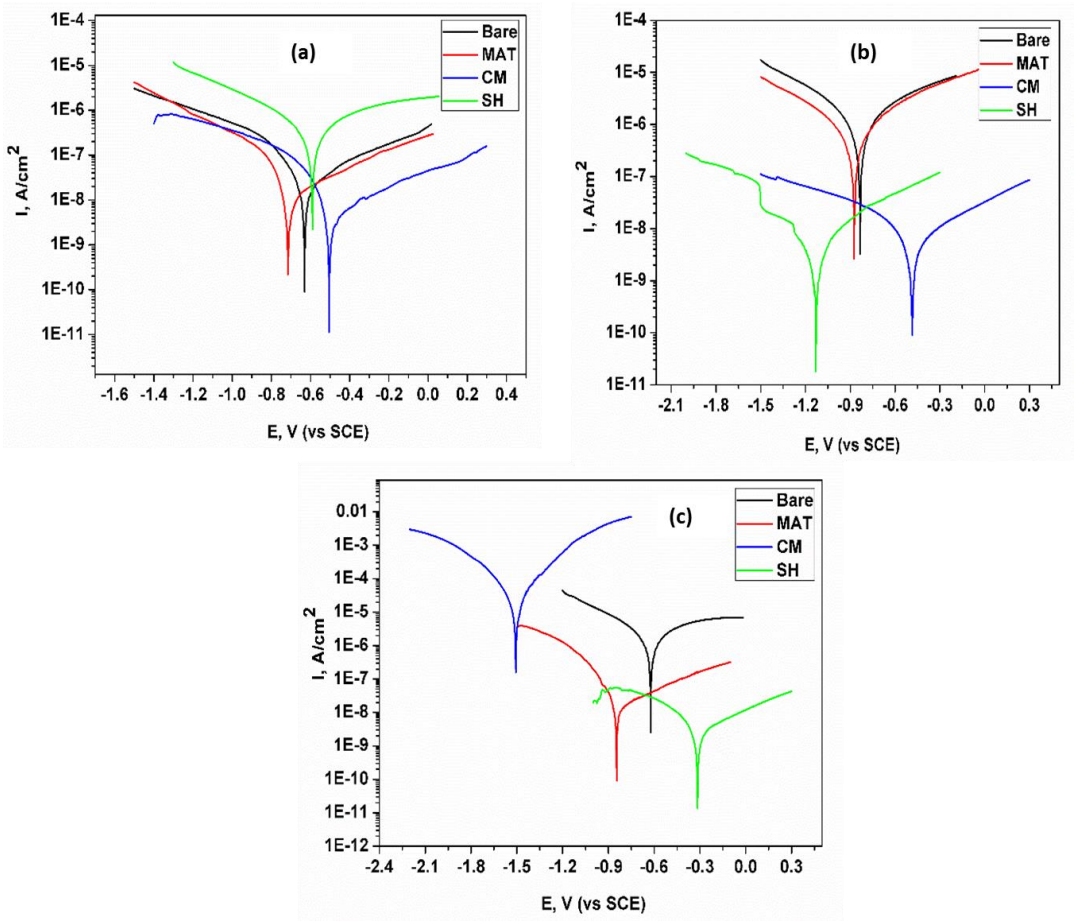

Figure 6.10: Polarization plots of uncoated and single layer dip coated substrates exposed to 0.6 M NaCl solution after (a) 24 h, (b) 72 h and (c) 120 h

24 h of exposure, very less difference in the magnitudes of corrosion current for spray coatings and multilayer dip coatings was observed, which could indicate that the initial barrier properties of both coatings are similar before the diffusion of corrosive species through the coatings. However, when corrosive species diffuses through the micropores of spray coated substrates after 72 h and 120 h, corrosion initiates and release of inhibitors from HNTs takes place due to change in localised pH. In case of multilayer dip coated

substrates, as observed from Fig. 6 (a) & (b), the corrosive species could get diffused easily through the uniform thin film having micropores as compared that of spray coated film and hence multilayer films have shown higher corrosion current after prolonged exposure of 120 h.

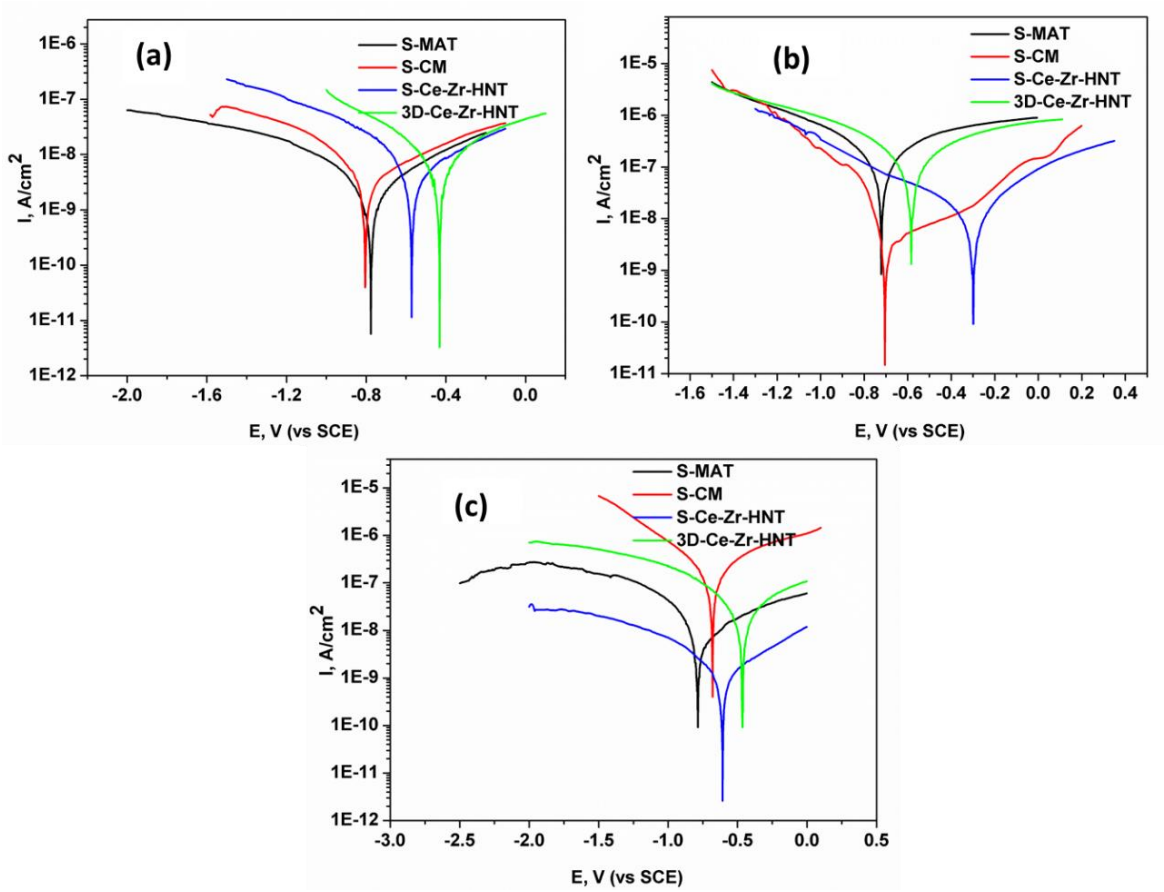

Figure 6.11: Polarization curves for spray coated and 3 layer dip coated AZ91D substrates after exposure to 0.6 M NaCl solution

Table 6.4: Tafel fitting parameters for uncoated and single layer dip coated substrates exposed to 0.6 M NaCl solution for various durations

Sl. No.	Exposure Time	Substrate	E_{corr}, V (vs SCE)	I_{corr}, A/cm^2	R_p Ω.cm^2
01	24 h	**Bare**	-0.613	2.3E-8	1.9E6
		MAT	-0.715	1.5E-8	2.9E6
		CM	-0.505	6.3E-9	7.8E6
		SH	-0.590	2.1E-7	2.1E5

02	**72 h**	**Bare**	-0.834	5.2E-7	8.2E4
		MAT	-0.875	3.3E-7	1.4E5
		CM	-0.486	3.9E-9	1.2E7
		SH	-1.131	2.5E-9	1.6E7
03	**120 h**	**Bare**	-0.662	1.0E-6	1.1E5
		MAT	-0.846	2.5E-8	1.7E6
		CM	-1.506	1.2E-5	2.6E3
		SH	-0.316	2.7E-9	1.8E7

Table 6.5: Tafel fitting parameters for spray coated and 3 layer dip coated AZ91D substrates

Sl. No.	**Exposure Time**	**Substrate**	**E_{corr}, V (vs SCE)**	**I_{corr}, A/cm^2**	**R_p Ω.cm^2**
01	**24 h**	**S-MAT**	-0.777	1.4E-9	3.2E7
		S-CM	-0.805	3.9E-9	1.5E7
		S-Ce-Zr-HNT	-0.572	3.0E-9	2.8E6
		3D-Ce-Zr-HNT	-0.431	4.6E-9	9.2E6
02	**72 h**	**S-MAT**	-0.785	5.7E-9	8.5E6
		S-CM	-0.681	8.8E-8	5.1E5
		S-Ce-Zr-HNT	-0.608	1.0E-9	5.4E7
		3D-Ce-Zr-HNT	-0.466	1.1E-8	3.9E6
03	**120 h**	**S-MAT**	-0.722	1.1E-7	4.3E5
		S-CM	-0.705	4.3E-9	7.9E6

		S-Ce-Zr-HNT	-0.299	8.0E-9	5.3E6
		3D-Ce-Zr-HNT	-0.584	8.1E-8	5.5E5

It could be observed that potentiodynamic polarization studies have shown different results than that of EIS and salt spray tests, where spray coated substrates have shown lower corrosion current than multilayer dip coated substrates after prolonged exposure of 120 h. This could be attributed to the corrosion inhibition provided by corrosion inhibitors released from HNTs due to change in localized pH, when the corrosive medium diffuses through the micropores or the region where coating is thin as shown in Fig. 6.12. In polarization measurements, the potential is applied in order to evaluate the corrosion protection ability of coatings when the corrosion is initiated due to anodic reaction after corrosive medium diffuses through the coating and reaches the substrate. In case of EIS and salt spray tests (without artificial defect), the adhesion of coating and diffusional characteristics of coatings with respect to corrosive medium are evaluated. Hence, the actual corrosion protection ability of coatings is evaluated by using polarization studies when any external defect occurs in the coating or after initialization of corrosion with diffusion of corrosive species.

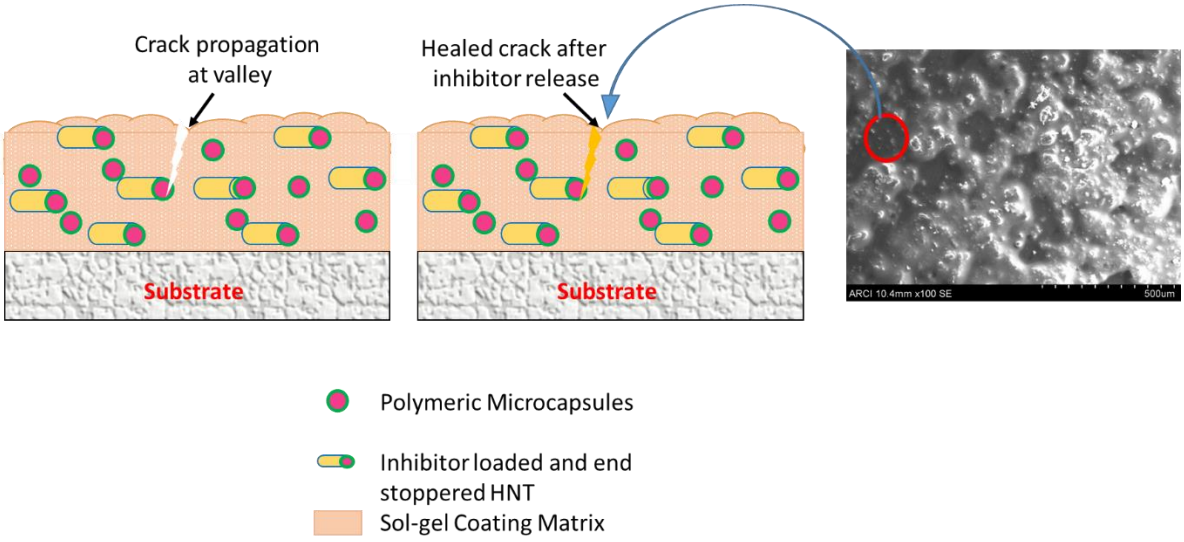

Figure 6.12: Schematic representation of corrosion inhibition at the site of micropores in spray coated substrate

Table 6.6 compares the corrosion resistance obtained from EIS studies and corrosion current evaluated from polarization measurements after 120 h of exposure to 0.6 M NaCl solution for different coating compositions based on type of nanoclay (HNT, EHNT and MMT), corrosion inhibitors (Ce^{3+}-Zr^{4+},HQ and MBT) and coating techniques (dip and spray). It could be observed that among the dip coated substrates, single layer Ce^{3+}-Zr^{4+} loaded HNT based coatings have shown better corrosion protection (highest corrosion resistance and lowest corrosion current), which is one order lower than spray coated and multilayer dip coated substrates. Since cationic Ce^{3+}-Zr^{4+} encapsulated in HNTs have not been used earlier as corrosion inhibitors for corrosion protection of Mg alloys, the results of Ce^{3+}-Zr^{4+} directly dispersed into the coating matrix earlier reported by Phani et al. [16] are compared with the results of this work. They have examined the effect of ceria-zirconia (15 wt % each) dispersed in 2-propanol based sol-gel coatings on corrosion protection ability of Mg alloys AZ91D and AZ31 using salt spray test for 96 h. It was found that as casted AZ91D has shown least number of pits and damage to the coatings as compared to other substrates. Han et al. [17] have developed ceria based conversion coatings on AZ91D substrates under different conditions. The corrosion current after exposure to 0.6 M NaCl solution was 7.5E-4 which is three orders higher than that mentioned in this work. Li et al. [18] have developed zirconia based sol-gel conversion coating on AZ91D substrates. The magnitude of the corrosion current obtained from polarization studies after 96 h in 0.6 M NaCl (3.5 E-6) is higher than that obtained in present work (2.7E-9). Barranco et al. [19] have developed sol-gel coatings containing Ce^{3+} and Zr^{4+} ions on AZ91 substrates. It was observed that hybrid sol-gel coatings doped with Ce^{3+} gave highest corrosion resistance after 7 days in 0.5 M Na_2SO_4 as compared to only hybrid coatings and Zr^{4+} doped organic coating and the magnitude of corrosion resistance of hybrid sol-gel coatings doped with Ce^{3+} (3.1E4) is lower to that examined in this study (3.5E5).

Hence, from the aforementioned comparison of literature with present study, it could be concluded that loading of cationic Ce^{3+} and Zr^{4+} into the lumen of HNTs is giving best anticorrosion properties to the AZ91D substrates without any pretreatment or any additional topcoat layer.

Table 6.6: Comparison of corrosion resistance and corrosion current values of different coating compositions on AZ91D substrates after 120 h of exposure to 0.6 M NaCl solution

Corrosion Measurement Entity	**Bare**	**Coating Composition**									
		HNT			**EHNT**			**MMT**		**3D-HNT**	**S-HNT**
		Ce^{3+}-Zr^{4+}	HQ	MBT	Ce^{3+}-Zr^{4+}	HQ	MBT	Ce^{3+}-Zr^{4+} (IMM)	Ce^{3+}-Zr^{4+} (IEM)	Ce^{3+}-Zr^{4+}	Ce^{3+}-Zr^{4+}
R_{ct} ($\Omega.cm^2$)	1.9E5	4.5 E7	1.3 E5	9.0 E5	1.6 E4	8.7 E5	2.5 E3	2. 3E5	2.8E6	1.4 E8	1.1 E8
I_{corr} (A/cm^2)	1.0E-6	2.7 E-9	1.6 E-5	2.7 E-7	5.5 E-6	3.7 E-8	1.2 E-5	3.1E-6	5.6E-7	8.1 E-8	8.0 E-9

6.5 References

[1] I.A. Kartsonakis, A.C. Balaskas, E.P. Koumoulos, C.A. Charitidis, G. Kordas, Evaluation of corrosion resistance of magnesium alloy ZK10 coated with hybrid organic–inorganic film including containers, Corros. Sci. 65 (2012) 481-493.

[2] Xiao Jiang, Ruiguang Guo, Shuqin Jiang, Evaluation of self-healing ability of Ce-V conversion coating on AZ31 magnesium alloy, J. Magnesium Alloys. 4 (3) (2016) 230-241.

[3] Zhi-Hui Xie, Shiyao Shan, Nanocontainers-enhanced self-healing Ni coating for corrosion protection of Mg alloy, J. Mater. Sci. 53 (2018) 3744-3755.

[4] M. F. Montemor, M. G. S. Ferreira, Analytical characterisation and corrosion behaviour of bis-aminosilane coatings modified with carbon nanotubes activated with rare-earth salts applied on AZ31 magnesium alloy, Surf. Coat. Technol. 202 (2008) 4766-4774.

[5] A. Covelo, Ivan Puente-Lee, J. Uruchurtu, C. Menchaca, José-Guadalupe Bañuelos, M. Hernandez, Effect of coating deposition technique on the protective properties of hybrid sol-gel coatings on AA2024, ECS Trans. 64 (27) (2015) 45-54.

[6] Taejin Hwang, Heung Yeol Lee, Hohyeong Kim, Gyun Tak Kim, Two layered silica protective film made by a spray-and-dip coating method on 304 stainless steel, J. Sol-Gel Sci. Technol. 55 (2010) 207-212.

[7] R. B. R. Garcia, F. S. Silva, E. Y. Kawachi, Evaluation of dip and spray coating techniques in corrosion inhibition of AA2024 alloy using a silicon/zirconium sol-gel film as coating, AIP Conference Proceedings 1809 (2017) 020017.

[8] A. L. K. Tan, A. M. Soutar, I. F. Annergren, Y. N. Liu, Multilayer sol-gel coatings for corrosion protection of magnesium, Surf. Coat. Technol. 198 (2005) 478-482.

[9] Jinfei Wei, Bucheng Li, Lingyun Jing, Ning Tian, Xia Zhao, Junping Zhang, Efficient protection of Mg alloy enabled by combination of a conventional anti-corrosion coating and a superamphiphobic coating, Chem. Eng. J. 390 (2020) 124562.

[10] Yanbin Zhao, Zhao Zhang, Liqian Shi, Fen Zhang, Shuoqi Li, Rongchang Zeng, Corrosion resistance of a self-healing multilayer film based on SiO_2 and CeO_2 nanoparticles layer-by-layer assembly on Mg alloys, Mater. Lett. 237 (2019) 14-18.

[11] N.C. Rosero-Navarro, M. Curioni, Y. Castro, M. Aparicio, G. E. Thompson, A. Duran, Surf. Coat. Technol. 206 (2011) 257-264.

[12] Zhi Geng, Junhui He, Lin Yao, Fabrication of robust high-transmittance superamphiphobic coatings through dip-coating followed by spray-coating, RSC Adv. 5 (2015) 89262.

[13] Keqin Zheng, Jinde Zhang, Erin Keaney, Hanna Dodiuk, Samuel Kenig, Carol Barry, Joey Mead, The effect of superhydrophobic surface topography on underwater corrosion resistance of steel, J. Coat. Technol. Res. (2021) https://doi.org/10.1007/s11998-020-00433-1.

[14] Xu Wu, Ian Wyman, Ganwei Zhang, Jing Lin, Zhaoqing Liu, Yu Wang, Heng Hu, Preparation of superamphiphobic polymer-based coatings via spray-and dip-coating strategies, Prog. Org. Coat. 90 (2016) 463-471.

[15] E. Huttunen-Saarivirta, G.V. Vaganov, V. E. Yudin, J. Vuorinen, Characterization and corrosion protection properties of epoxy powder coatings containing nanoclays, Prog. Org. Coat. 76 (2013) 757-767.

[16] A. R. Phani, F. J. Gammel, T. Hack, H. haefke, Enhanced corrosion resistance by sol-gel-based ZrO_2-CeO_2 coatings on magnesium alloys, Mater. Corros. 56(2) (2005) 77-82.

[17] Huimin Han, Dantong Wang, Huaqian Yu, min Zuo, Lihong Wang, Degang Zhao, Ceria coatings prepared by sol-gel approach on AZ91 magnesium alloy, Mater. Sci. For. 898 (2017) 1369-1380.

[18] Q. Li, B. Chen, S. Q. Xu, H. Gao, L. Zhang, C. Liu, Structural and electrochemical behaviour of sol-gel ZrO_2 ceramic film on chemically pre-treated AZ91D magnesium alloy, J. Alloys Compd. 478 (2009) 544–553.

[19] V. Barranco, N. Carmona, J. C. Galván, M. Grobelny, L. Kwiatkowski, M. A. Villegas, Electrochemical study of tailored sol–gel thin films as pre-treatment prior to organic coating for AZ91 magnesium alloy, Prog. Org. Coat. 68 (2010) 347-355.

Chapter 7

CONCLUSIONS AND FUTURE SCOPE

Chapter-7
Conclusions and Future Scope

7.1 Overall Conclusions

Although sol-gel coatings have been widely used to provide enhanced barrier properties and better adhesion to the substrates and top coats, these coatings are not able to provide corrosion protection when a damage occurs due to mechanical impact or exposure to the corrosive medium. Dispersion of inhibitor loaded/intercalated halloysite (HNT) and montmorillonite (MMT) clay into sol-gel coatings was found to exhibit self-healing ability and enhance their durability for prolonged corrosion protection of AZ91D. Following are the summary and overall conclusions drawn from each studies.

Coatings based on HNT loaded with Ce^{3+}-Zr^{4+}

Cationic corrosion inhibitors, Ce^{3+}-Zr^{4+} were successfully loaded into the lumen of HNTs, which could be confirmed from transmission electron microscopy (TEM), scanning electron microscopy (SEM) in conjunction with energy dispersive spectroscopy (SEM-EDS) and BET analysis. Hybrid matrix sol-based coatings could exhibit better barrier properties (higher charge transfer resistance) of one order higher magnitude than HNT dispersed matrix sol based coatings for shorter durations of exposure to 0.6 M NaCl solution as observed from results of EIS and potentiodynamic polarization studies. Coatings consisting of HNTs without any loaded corrosion inhibitor showed one order lower corrosion resistance (charge transfer resistance) than self-healing (SH) coatings, which may be due to porous nature of coatings resulting in the diffusion of corrosive medium through coatings. Ce^{3+}-Zr^{4+} loaded HNT based coatings could render improved barrier properties for prolonged durations of exposure as observed from weight loss studies and electrochemical measurements. The SH coatings have shown two orders higher corrosion resistance and three orders lower corrosion current than bare substrates after prolonged durations of exposure. Micro-Raman analysis confirmed the formation of passive film of corrosion inhibitors released in the scribed area, thereby showing the self-healing ability. Scanning vibrating electrode technique (SVET) analysis was used to measure the localized change in anodic current density to confirm the self-healing ability of coatings. It was observed that the scribed area of SH sol coated substrates has shown progressive healing of defect (change of red color into green) after exposure to NaCl solution thereby decreasing the anodic current density after 24 h, whereas, increase in

anodic current of bare and matrix sol based substrates showed progressive corrosion of substrates depicted by red color in current density maps.

Ce^{3+}-Zr^{4+} intercalated MMT based coatings

Ce^{3+}-Zr^{4+} as cationic corrosion inhibitors were intercalated into the interlayer spacing of aluminum pillared MMT clay without affecting the layered structure. As-received MMT dispersed matrix sol coatings showed better barrier properties during initial periods of exposure to corrosive medium. Modification of the pillared clay by evacuation of corrosion inhibitors mixture could provide better anticorrosion properties for prolonged durations of exposure as observed from electrochemical measurements and weight loss experiments. Corrosion inhibitor mixed MMT could provide corrosion protection up to some extent, but the barrier property and corrosion inhibition activity of the coatings was found to deplete with the increase in exposure time to corrosive medium. Electrochemical results showed that inhibitor evacuated MMT (IEM) based coatings exhibited one order and three orders higher corrosion resistance (with respect to charge transfer resistance) than inhibitor mixed MMT (IMM) and MMT dispersed matrix sol based coatings, respectively. SVET measurements confirmed that IEM sol coatings were able to provide autonomous healing for prolonged exposures to corrosive medium showing lowest corrosion current density at the defect site. SVET analysis showed drastic change in anodic current density (indicated by change of red into blue color at defect area) of IEM based coatings after 1 h in the scribed area after exposure to NaCl solution. After comparing the magnitudes of charge transfer resistances of HNT (4.5E7) and MMT (2.8E6) based coatings, it was observed that HNT based coatings are providing better prolonged corrosion protection than MMT based coatings.

Corrosion resistance of different corrosion inhibitor loaded in HNT and EHNT

Acid treatment for etching the lumen of HNTs, increased the inhibitor loading capacity without affecting the crystal structure of HNTs. TEM analysis confirmed the increase in lumen diameter of etched HNTs (EHNT) by 40% - 60% and BET analysis confirmed that higher amount of different corrosion inhibitors such as cationic Ce^{3+}-Zr^{4+}, 8-hydroxyquinoline (HQ) and 2-mercaptobenzothiazole (MBT) were loaded into the EHNTs. The quantitative analysis of release of corrosion inhibitor from HNT and EHNT was carried out using various semi-empirical kinetic models, and the Korsmeyer-Peppas model was confirmed to be the best fit. Under conditions of neutral pH, electrochemical measurements have shown that after prolonged duration of exposure, Ce^{3+}-Zr^{4+} based coatings have

revealed better corrosion protection ability (two order higher corrosion resistance in terms of charge transfer resistance than other two inhibitors) when loaded in HNT, whereas HQ shown better corrosion protection properties (one order higher charge transfer resistance than Ce^{3+}-Zr^{4+} and two orders higher than MBT) when loaded in EHNT owing to higher amount of loading. Polarization results followed the results obtained from EIS measurements wherein Ce^{3+}-Zr^{4+} loaded in HNT showed four orders and two orders lower corrosion current than HQ and MBT, respectively. HQ loaded in EHNT showed two orders and three orders lower corrosion current than Ce^{3+}-Zr^{4+} and MBT, respectively

Effect of coating technique on anticorrosion properties

In order to evaluate the effect of coating technique, comparison of the corrosion protection abilities of dip coated and spray coated substrates was carried out. Multilayer dip coatings (3 layers) were carried out in order to generate the coating thickness similar to that of spray coated samples. Multilayer dip coatings have shown better corrosion resistance (one order higher charge transfer resistance for Ce^{3+}-Zr^{4+} loaded HNTs) as compared to that of spray coatings as observed from electrochemical measurements. Salt spray tests according to ASTM B117 for 168 h have shown that multilayer dip coatings have better barrier properties than that of spray coatings.

7.2 Future Scope

The developed environment friendly self-healing coatings can be efficiently used as a drop-in replacement to carcinogenic chromate based coatings for corrosion protection of structural parts made using Mg alloys in automobile and aerospace industries. The coatings could be further investigated for other metals/alloys in addition to varying the matrix coating compositions, using other corrosion inhibitors, micro/nanocontainers, etc. The efficiency of the coatings can be examined in actual environmental conditions by developing commercial coating system (multilayer coating system) on AZ91D substrates. Another functionality called superhydrophobicity can be generated in the coatings by incorporating silica nanoparticles and fluorosilane precursors, which will decrease the contact time of coatings with corrosive medium and enhance the efficiency of coatings.

Research Output

1) **List of Publications**

   i. **Swapnil H. Adsul,** T. Siva, S. Sathiyanarayanan, Shirish H. Sonawane, R. Subasri, Self-healing ability of nanoclay-based hybrid sol-gel coatings on magnesium alloy AZ91D, **Surf. Coat. Technol. 309 (2017) 609-620** (SCI impact factor: 3.784)**.**

   ii. **Swapnil H. Adsul,** K. R. C. Soma Raju, B. V. Sarada, Shirish H. Sonawane, R. Subasri, Evaluation of self-healing properties of inhibitor loaded nanoclay-based anticorrosive coatings on magnesium alloy AZ91D, **J. Magnesium Alloys. 6 (2018) 299-308** (SCI impact factor: 10.088)**.**

   iii. **Swapnil H. Adsul,** T. Siva, S. Sathiyanarayanan, Shirish H. Sonawane, R. Subasri, Aluminum pillared montmorillonite clay-based self-healing coatings for corrosion protection of magnesium alloy AZ91D, **Surf. Coat. Technol. 352 (2018) 445-461** (SCI impact factor: 3.784)**.**

   iv. **Swapnil H. Adsul,** Uday D. Bagale, Shirish H. Sonawane, R. Subasri, Release rate kinetics of corrosion inhibitor loaded halloysite nanotube-based anticorrosion coatings on magnesium alloy AZ91D, **J. Magnesium Alloys 9 (2021) 202-215** (SCI impact factor: 10.088)**.**

   v. **Swapnil H. Adsul,** Shirish H. Sonawane, R. Subasri, Active protection of Mg alloy AZ91D using corrosion inhibitor encapsulated halloysite nanoclay based smart sol-gel coatings, ASTM Mater. Perform. Charact. (Accepted) (SCI impact factor: 0.72).

2) **International and National Conferences attended**

   i. **Poster Presentation: Swapnil H. Adsul,** Shirish H. Sonawane, R. Subasri, Corrosion behaviour study of nanoclay-based sol-gel coatings on Mg alloy AZ91D, **International Conference on Emerging Trends in Materials and Manufacturing Engineering (iMME 17)**, Department of Metallurgical and Materials Engineering, NIT, Trichy, March 10-12, 2017 and awarded as best poster.

   ii. **Poster Presentation: Swapnil H. Adsul,** Shirish H. Sonawane, R. Subasri, Investigations on anticorrosion properties of montmorillonite clay-based sol-gel coatings on Mg alloy AZ91D, **International Conference on Electrochemical**

Science and Technology (ICONEST-2017), IISc, Bengaluru, August 10-12, 2017.

iii. **Oral presentation: Swapnil H. Adsul,** A. Srinivasan, Shirish H. Sonawane, R. Subasri, Effect of inhibitor loaded halloysite nanoclay on corrosion protection properties of sol-gel coatings on Mg alloy AM50, **Frontiers in Corrosion Control of Materials (FCCM),** Department of Metallurgical and Materials Engineering, NIT, Warangal, July 28-29, 2018.

iv. **Oral Presentation: Swapnil H. Adsul,** Shirish H. Sonawane, R. Subasri, Evaluation of corrosion protection ability of different corrosion inhibitor loaded halloysite nanoclay based sol-gel coatings on magnesium alloy AZ91D, **National Conference on Industrial Coatings (NCIC-2019)**, CSIR-IMMT, January 24-25, 2019.

v. **Oral Presentation: Swapnil H. Adsul,** Shirish H. Sonawane, R. Subasri, Different corrosion inhibitor loaded smart halloysite nanocontainer based sol-gel coatings for corrosion protection of Mg alloy AZ91D, **International Conference on Advanced Materials and Processes for Defence Applications (ADMAT 2019)**, DMRL, Hyderabad, September 23-25, 2019.

3) Book Chapter

i. "**Corrosion protection of metals/alloys through multifunctional sol-gel nanocomposite coatings**" authored by **Swapnil H. Adsul**, K. Pradeep Prem Kumar, S. Manasa, Aarti Gautam, K.V. Gobi, Shirish H. Sonawane, R. Subasri in: Handbook on Corrosion Science and Technology, edited by T. Subba Rao, et al., Springer Nature (2021), In press.
